Ollscoil Chathair Bhaile Átha Cliath
Dublin City University

The Development of Hybrid Antigene Therapeutics using Nucleic Acid Click Chemistry

Teresa Lauria M.Sc.

PhD Thesis

Associate Prof. Andrew Kellett
School of Chemical Sciences
Dublin City University

December 2019

DECLARATION

I hereby certify that this material, which I now submit for assessment on the programme of study leading to the award of PhD is entirely my own work, and that I have exercised reasonable care to ensure that the work is original, and does not to the best of my knowledge breach any law of copyright, and has not been taken from the work of others save and to the extent that such work has been cited and acknowledged within the text of my work.

Signed: ID No.: 15211324 Date

ACKNOWLEDGEMENTS

I would like to express my sincere gratitude to my supervisor Ass. Prof. Andrew Kellett for the opportunity to work in his group and to collaborate with international and multidisciplinary network characterised by the presence of the leading exponents of the areas covered in my project.

This thesis is part of the Marie Skłodowska-Curie ITN project, ClickGene [H2020-MSCA_ITN-2014-642023] and was conducted in particular in collaboration with the research group of Prof Thomas Carell at Ludwig Maximilian University of Munich (LMU).

I would like to acknowledge the Prof. Thomas Carell for permitting me to conduct my secondment in his research group, where I could develop the in-house procedure for the generation of TFO-hybrids and the method for the visualisation of triplex formation using PAGE electrophoresis. In particular, I would like to thank Antony Crisp and Samuele Stazzoni in training me in the use of the solid-phase oligo-synthesiser, HPLC and MALDI for the generation and characterisation of modified TFOs and for the further MALDI analysis of the hybrid materials I synthesised after my return in Dublin and, Dr. Markus Müller for the design of the experiments with fluorophore-tagged sequences for the site-selectivity cleavage study. I would like also to thank Prof. Vickie Mckee for supporting and assisting me with ESI mass analysis and crystallographic structures of my samples, but especially for helping me with PyMOL.

Lastly but more important I would to thank my parents and my twin-sisters for their unconditional love and support also from distance and my friends, the “Clickgeners” and my partner with who among hard times and smiles we became a family and went through together this fascinating and challenging period of our life, better known as PhD.

PUBLICATIONS

- Lauria T., Slator C., McKee V., Müller M., Stazzoni S., Crisp A. L., Carell T., Kellett A. A Click Chemistry Approach to Developing Molecularly Targeted DNA Scissors *Chem. Eur. J.*, accepted https://doi.org/10.1002/chem.202002860.
- Fantoni N.; Lauria T., Kellett, A. Genome Engineering with Synthetic Copper Nucleases *Synlett* ***2015****,* 26 (19), 2623-2626.

POSTER AND SCIENTIFIC TALKS

Poster Titles:

- Fantoni, N., Lauria, T., Avella, G., Barron, N., Kellett, A. *'ClickGene: Click Chemistry for Future Gene Therapies to Benefit Citizens, Researchers and Industry'.*68th Irish Universities Chemistry Research Colloquium (23-24 June 2016, Cork).
- Fantoni, N., Lauria, T., Avella, G., Barron, N., Kellett, A. *'ClickGene: Click Chemistry for Future Gene Therapies to Benefit Citizens, Researchers and Industry'.* Medicinal Chemistry Ireland Conference (1 June 2016, Dublin).
- Teresa Lauria, Creina Slator, Zara Molphy, Vickie McKee, Andrew Kellett *'Therapeutic and Biochemical Applications of Oxidative Chemical Nucleases'.* Colloquium, (21-22 June 2018, Belfast).
- Teresa Lauria, Creina Slator, Zara Molphy, Vickie McKee, Andrew Kellett *'Therapeutic and Biochemical Applications of Oxidative Chemical Nucleases'.* Medicinal Chemistry, Dublin City University, (29 June 2018, Dublin).

Scientific Talks:

- *'N,N-intercalator bearing the azido group: first step for the synthesis of new artificial nucleases'.* COST Action CM1201: Biomimetic Radical Chemistry & ClickGene Meeting (25-27 April 2016, Grenoble).
- *'Molecular scissors and oncogene knockout in human cells'.* ClickGene Meeting-Lecture/Mini- Symposium (EU Grant Writing and Industry/Laboratory visit) in Oxford, UK (19-21 March 2018, Oxford, UK).
- *'The Development of Hybrid Antigene Therapeutics using Nucleic Acid Click'.* Chemistry Chemistry Day, Dublin City University, Ireland (4 May 2018, Dublin).

TABLE OF CONTENTS

DECLARATION i

ACKNOWLEDGEMENTS ii

PUBLICATIONS iii

POSTER AND SCIENTIFIC TALKS iii

Poster Titles: iii

Scientific Talks: iii

ABBREVIATIONS xv

ABSTRACT xvii

CHAPTER 1: GENE EDITING AND NUCLEIC ACID CLICK CHEMISTRY 1

1.1 An introduction to artificial DNA cutters 2

1.2 Selective ssDNA and dsDNA damage 5

1.3 ZNFs, TALENs and CRISPR/Cas 8

1.4.1 Click Chemistry 10

1.4.2 Nucleic acid click chemistry 15

1.5.1 Triple-stranded DNA 20

1.5.2 Stabilising triplexes 22

1.6.1 Ruthenium complexes 30

1.6.2 Ruthenium-DNA interaction 35

1.6.3 Ruthenium modified oligonucleotides 39

References 43

CHAPTER 2: SYNTHESIS AND CHARACTERISATION OF NEW COPPER(II)- AND RUTHENIUM(II)-COORDINATING AZIDE LIGANDS AND THEIR HYBRIDISATION TO OLIGONUCLEOTIDES 71

2.1 Introduction 72

2.2 Materials and methods 72

2.3 Synthetic routes of azide-functionalised ligands 73

2.3.1 Preparation of 5-azido-1,10-phenanthroline (A, Route I) 73

2.3.2 Preparation of 2-(4-azidophenyl)-1H-imidazo[4,5-f]-1,10-phenanthroline (B, Route II) 73

2.3.4 Preparation of 5-amino-1,10-phenanthroline (7, Route III) 78

2.3.5 Preparation of 5-azido-*N*-(1,10-phenanthrolin-5-yl)-pentanamide (D, Route IV) 79

2.3.6 Preparation of *N*-(4-azidobenzyl)-1,10-phenanthrolin-5-amine (E, Route V) 80

2.3.7 Preparation of 4-azido-*N*-(dipyrido[3,2-a:2',3'-c]phenazin-11-yl)butanamide (F, Route VI) 82

2.4 Preparation of *N*,*N*'-(1,3-phenylenebis(methylene))bis(1,10-phenanthrolin-5-amine) (G_R) 85

2.4.1 Preparation of $[Cu_2(N,N'\text{-phenanthrene})_2(G_R)](NO_3)_4$ (where N,N'-phenanthrene= Phen, DPQ and DPPZ) 86

2.5 Preparation of ruthenium(II) complexes 88
2.5.1 Preparation of [Ru(1,10-phenanthroline)$_2$(5-azido-1,10-phenanthroline)](PF$_6$)$_2$ 88
2.5.2 Preparation of of [Ru(1,10-phenanthroline)$_2$(2-(4-azidophenyl)-1-H-imidazo[4,5-f][1,10]-phenanthroline)](PF$_6$)$_2$ 89
2.5.3 Preparation of [Ru)(1,10-phenanthroline)$_2$(11-azidodipyrido[3,2-a:2',3'-c]phenazine)](PF$_6$)$_2$ 90
2.5.4 Preparation of [Ru(5-azido-N-(1,10-phenanthrolin-5yl)pentanamide)(1,10-phenanthroline)$_2$](PF$_6$)$_2$ 92
2.6 UV-vis analysis of G_R and [Cu$_2$(N,N'-phenanthrene)$_2$(G_R)](NO$_3$)$_4$ 93
2.7 Crystallography 95
2.8 Oligonucleotide synthesis 95
2.9 Generation of TFO-hybrid materials *via* click chemistry 96
2.10 Molecular biological and biophysical techniques 97
2.10.1 Thermal melting experiments 97
2.10.2 Triplex formation and nuclease activity 97
2.10.3 Site-selective cleavage with fluorescently labelled DNA 98
2.10.4 Photophysical properties of Ru(II) complexes 98
2.10.5 Data analysis 99
References 100

CHAPTER 3: PHENANTHRENE-MODIFIED TFOS STABILISE PARALLEL DNA TRIPLEXES AND PROMOTE TARGETED OXIDATIVE CLEAVAGE 102

3.1 Introduction 103
3.2 Results and discussion 105
3.2.1 Design of hybrid AMN-TFO systems 105
3.2.2 Preparation of N,N-intercalators 106
3.2.3 Preparation of AMN-TFO hybrids 111
3.2.4 Triplex formation 111
3.2.5 PAGE analysis 114
3.2.6 Chemical nuclease activity 115
3.2.7 Cleavage specificity 117
3.2.8 *Di*-copper AMN-TFO systems 119
3.3 Conclusions 123
References 125

CHAPTER 4: GENERATION OF RUTHENIUM-LABELLED TRIPLEX FORMING OLIGONUCLEOTIDES *VIA* CLICK CHEMISTRY 130

4.1 Introduction 131
4.2 Results and discussion 133
4.2.1 Design of ruthenium complexes bearing azide-functionality 133
4.2.2 TFO design and triplex formation 136

4.2.3 Preliminary photophysical analysis....139
4.3 Conclusion 142
References 144
CHAPTER 5: FUTURE WORK 147
5.0 Future work 148
5.1 Cell validation Experiments 148
5.2 Mono-nuclear AMN-hybrids:.... 148
5.3 Di-nuclear AMN-hybrids:.... 150
5.4 Ruthenium hybrids: 151
CONCLUSION....153
APPENDICES 155
APPENDIX A 156
APPENDIX B....186
APPENDIX C 188
APPENDIX D 200
APPENDIX E....202
APPENDIX F....213
APPENDIX G 226
APPENDIX H 228
APPENDIX I....234
APPENDIX L....236

TABLE OF FIGURES

Figure 1.1 Mechanism of hydrolytic DNA damage through phosphodiester hydrolysis (**A**) and oxidative DNA cleavage promoted by ROS species through the abstraction C1' hydrogen from deoxyribose (**B**).[4] . 2

Figure 1.2 Molecular structures of **A**) Cu-Phen-DPQ, **B**) Cu-Phen-DPPZ, **C**) Cu-Phen-DPPN, **D**) [Cu(o-phthalate)(Phen)], **E**) Cu-Oda, **F**) Cu-Terph and **G**) Cu_2TPNap. 3

Figure 1.3 Molecular structures of EDTA-ON conjugate at **A**) 5′-position and **B**) internal position for Fe(II)-based nucleases. **C**) Zr(IV)-based and **D**) Ce(IV)-based AMNs. 5

Figure 1.4 A) Double strand DNA cleavage mechanism of Ce(IV)/EDTA complex assisted by pcPNA. Molecular structures copper-hybrids developed by **B**) Sigman and **C**) Hélène. 7

Figure 1.5 Schematic representation of the most widely recognised known programmable targeted nucleases employed in gene editing: **A**) Zinc Finger Nucleases (ZFNs), **B**) transcription activator-like effectors nucleases (TALENs) and **C**) clustered regularly interspaced short palindromic repeats (CRISPR/Cas9). 8

Figure 1.6 Regioselectivity of Click chemistry depending on the reaction conditions: mixture of the 1,4- and 1,5-stereoisomers in the absence of a metal catalyst, 1,4-stereoisomer in the presence of copper-catalyst (Cu-catalyst) and 1,5-stereoisomer in the presence of ruthenium-catalyst (Ru-catalyst). 12

Figure 1.7 Reaction mechanisms of Click chemistry in the presence of **A**) copper (CuAAC) and **B**) ruthenium (RuAAC). 12

Figure 1.8 Molecular structures of tris(2-carboxyethyl)phosphine (TCEP), tris(benzyltriazolylmethyl)-amine (TBTA) and tris(3-hydroxypropryltriazolylmethyl)amine (THPTA). 13

Figure 1.9 A) Ring strain-promoted azide-alkyne cycloaddition reaction (SPAAC). **B)** Alkyne-cyclootyne derivatives (DIFO, DIBO, BCN, DIMAC and BARAC). 14

Figure 1.10 Schematic representation of biolabeling using SPAAC in situ cultured cell. 15

Figure 1.11 Sites of DNA modification for the insertion of alkyne group. 17

Figure 1.12 Selective multi-labeling of single DNA strand using post-synthetic strategy using TMS- and TIPS-protected alkyne (TMS = trimethysilyl; TIPS = triisopropylsilyl). 18

Figure 1.13 A) DNA analog with clicked backbone. **B)** Structural comparison of peptide-nucleic acid (PNA), locked DNA (LNA) and morpholino-oligo (MO) with DNA. 19

Figure 1.14 Secondary structures of DNA. **A)** Duplex (PDB code: 2M2C**). B)** G-quadruplex (PDB code: 1K8P). **C)** 4-way Holliday junction (PDB code: 1DCW). **D)** Triplex (PDB code: 1D3X). 20

Figure 1.15 A) Schematic representation of Watson-Crick and Hoogsteen interactions in a triple helix. **B**) Parallel and antiparallel triplex formation of the TFO indicated by the green arrow. **C**) Illustration of triplets involved in parallel (TA-T, CG-C^+) and antiparallel triplexes (TA-T, CG-G, TA-A)**.** 22

Figure 1.16 Molecular structure of **A**) 5-methylcytosine, **B**) 6-oxocytosine, **C**) 5-methyl derivative of 6-oxocytosine, **D**) 2′-O-methylpseudoisocytidine, **E**) 5-methylcytosine functionalised with spermine group, **F**) uracil functionalised with spermine group (U^S), **G**) uracil functionalised with spermine 5-propargylamino group (APdU). 23

Figure 1.17 A) N- and S-sugar conformation. **B**) Molecular structure of LNA/BNA, ENA, BNA^{NC}, 3′-amino-2′,4′-BNA, bicycle-DNA, tricycle-DNA, phosphate residue with N,N-diethyl-ethylenediamine

linkage (DEED), sugar moieties with amine group at 2′- or 4′- position (2′-AE, 4′-AE), and pyrrolidine-DNA. 25
Figure 1.18 Uridine with 4′-AE and APdU modifications—BAU (**A**) or DMAPdU (**B**). 26
Figure 1.19 Structures of INA, AMANY, para-TINA and orto-TINA. 27
Figure 1.20 Structures of two psoralen molecule-modified TFOs (5-MOP-TFO and HMT-TFO) and schematic representation of ICs. 28
Figure 1.21 Molecular structures of **A**) $[Ru(bpy)_3]^{2+}$, **B**) $[Ru(phen)_3]^{2+}$, **C**) $[Ru(phen)_2(DPPZ)]^{2+}$, **D**) $[Ru(DIP)_2(PIP)]^{2+}$, **E**) $[Ru_2(bpy)_2(N,N'\text{-(pyridine-2,6-diylbis(methylene))bis(1,10-phenanthrolin-5-amine))}]^{4+}$, **F**) $[Ru_2(bpy)_2(N,N'\text{-((1,8-naphthyridine-2,7-diyl)bis(methylene))bis(1,10-phN,N'-((1,8-naphthyridine-2,7-diyl)bis(methylene))bis(1,10-phenanthrolin-5-amine))}]^{4+}$ and **G**) $[Ru_2(bpy)_2(tatpp))]^{4+}$. 32
Figure 1.22 Molecular structures of NAMI-A, NK1339, and TDL1433. 34
Figure 1.23 Schematic illustration of photodynamic therapy (PDT): excitation by light irradiation of the photosensitiser (PS) to the singlet excited state (^{1}PS*), converted by intersystem crossing (ISC) into the triplet excited state (^{3}PS*) which interacting with molecular oxygen can bring to the development ROS species (Type I) or with ground triplet state oxygen ($^3O_2$) can generate the highly reactive singlet oxygen species, $^1O_2$. 35
Figure 1.24 Non-covalent binding. **A)** external electrostatic binding with K^+ (PDB code: 1FQ2). **B)** Minor groove binding with DAPI (PDB code: 2B0K). **C)** Intercalation with 1R-trans-anti-Benzo[c]phenanthrene (PDB code: 2ROU). 36
Figure 1.25 A) Molecular structure of Λ- and Δ-$[Ru(phen)_2(DPPZ)]^{2+}$. **B)** Crystal structures of the two enantiomers (Λ-$[Ru(phen)_2(DPPZ)]^{2+}$ PDB code: 4E7Y and Δ-$[Ru(phen)_2(DPPZ)]^{2+}$ PBD code: 5JEU). **C)** Λ-$[Ru(phen)_2(DPPZ)]^{2+}$ bounds to a short substitute DNA sequence (PDB code: 5LFW). **D)** DNA binding with a racemic mixture of $[Ru(phen)_2(DPPZ)]^{2+}$ (PDB code: 4JD8). **E)** Intercalation of Δ-$[Ru(phen)_2(DPPZ)]^{2+}$ at T/A site (PDB code: 5JEU). 38
Figure 1.26 Schematic illustration of Ru-modified ON targeting the complementary strand and/or the relative duplex. 39
Figure 1.27 Molecular structures of ON functionalised with $[Ru(TAP)_2(phen)]^{2+}$ (left) and schematic representation of cross-linking reaction (right). 40
Figure 1.28 A) Schematic representing experiments conducted for long-range ET with a Ru- and Rh-complex modified 15 mer duplex , **B**) with two different ruthenium complexes acting as donor and acceptor (8-14 mer duplex, and **C**) Os and Ru- modified 19 mer duplexes. 41
Figure 1.29 Schematic representation of **A**) cis-$[Ru(bpy)_2(imidazo)]^{2+}$ connected to two dT_{10} sequences via two hexyl spacers, **B**) cis-$[Ru(bpy)_3]^{2+}$ attached to DNA squences with short linkers **C**) ruthenium bis(terpyridine) complexes linked to two identical 20-mer DNA sequences through triethylene glycol linkers. 42
Figure 2.1 I UV study of $\mathbf{G_R}$ 25 μM with and without complexation in situ with 2 eq of Cu(II) and ancillary ligands in ACN and H_2O (solid line) in comparison to the solutions of Cu-Phen, Cu-DPQ and Cu-DPPZ 50 μM in ACN and H_2O (dotted line). **II** d-d transition of $\mathbf{G_R}$(Cu-Phen)$_2$, $\mathbf{G_R}$(Cu-DPQ)$_2$ and $\mathbf{G_R}$(Cu-DPPZ)$_2$ 5 mM in DMF compared to the solutions of Cu-Phen, Cu-DPQ and Cu-DPPZ 10 mM in DMF. 94

Figure 3.1 I Generation of phenanthrene-functionalised TFOs using 'click' chemistry. Coordination of copper to TFO hybrids induces targeted DNA cleavage. **II** Library of azide-functionalised phenanthroline and phenazine derivatives: **A**-**F**. **III** Alkyne-modified nucleobase inserted at 5′-terminal or internal position of the TFO. **IV** Library of alkyne-modified TFOs of various lengths showing modification position (X) with corresponding duplex targets designed from the GFP cloning vector..... 106
Figure 3.2 Synthetic routes to phenanthrene derivatives bearing an azide group (ligands **A**-**F**). **Route I**: azidation of epoxy-1,10-phenanthroline to generate ligand **A** (q.y.=quantitative yield). **Route II**: Diazotization for the generation of ligands **B** and **C**. **Route III**: Synthesis of the 5-amino-1,10-phenanthroline (**7**) allowed subsequent formation of ligands **D** and **E** via **Routes IV and V**, respectively. **Route VI**: Treatment of amino-DPPZ (**5**) with an acyl chloride followed by azidation provided ligand **F**. 109
Figure 3.3 I Thermal melting (T_M) values of TFO-hybrids containing ligands **A-F** in TFO2, 3, 5 and 6 along with non-clicked alkyne-modified TFO (TFO 1 and 4 omitted as $T_M < 20$ °C). Tm values for duplex D2 (TFO 2 and 5) = 73.2 ± 0.2 °C and duplex D3 (TFO 3 and 6) = 79.0 ± 0.7 °C. Samples were prepared in 10 mM phosphate buffer with 150 mM NaCl and 2 mM $MgCl_2$ (pH = 6.0). **II** Direct comparison of ΔT_M with ligand modification of TFO-hybrids. 113
Figure 3.4 I Triplex formation with varying amounts of non-clicked TFO–≡ and hybrid **TFO3C**. The duplex GFP target D3 (1.25 pmol, lane 2) was treated with increasing equivalents of TFO for 6 h. **II** Triplex formation of **TFO3B** examined across various incubation times. **TFO3C** showed full triplex formation in the incubation of 6 hours at 37 °C already at the ratio D:TFO=1:10. **III** Triplex formation of TFO3 (T3) and TFO3 hybrids **IV**, in the presence of titrated Cu^{2+} (12.5 pmol) and **V**, with Na-L-ascorbate (12.5 nmol). The results of triplex formation of TFO3 hybrids are in agreement with the thermal melting data with the exception of the TFO3B, which showed slower kinetic at this D:TFO ratio. Negligible effect of Cu^{2+} and Na-L-ascorbate on triplex formation apart for **TFO3B** and **TFO3E**, which are slightly perturbated. All samples were prepared in 10 mM phosphate buffer, 150 mM NaCl, 2 mM $MgCl_2$ (pH 6.0) in a total volume of 5.5 µL. Reactions were incubated at 37 °C for 6 h (**I-III-IV-V**), loaded onto 22% PAGE gel and subjected to electrophoresis for 14 h at 50 V in 50 mM tris-acetate running buffer (pH 6.0). 115
Figure 3.5 I Optimisation of cleavage conditions with varying amounts of ascorbate reductant. Target duplex (1.25 pmol, lane 1) was treated with TFO3A (12.5 pmol, lane 2), Cu^{2+} (12.5 pmol) and increasing amounts of ascorbate with TFO:Cu:Asc = 1:1:X where X = 10-500 equivalents (0.125 nmol, lane 3; 0.312 nmol, lane 4; 0.625 nmol, lane 5; 1.25 nmol, lane 6; 1.87 nmol, lane 7; 2.5 nmol, lane 8; 3.12 nmol, lane 9; 5 nmol, lane 10). **II** Cleavage reactions of TFO 3 hybrids. Target duplex (1.25 pmol, lane 1) was treated with unclicked TFO (TFO–≡, 12.5 pmol, lane 2) or TFO hybrids (A - F, lane 3 - 8) with Na-L-ascorbate (1.25 nmol) and Cu^{2+} (12.5 pmol). All samples were prepared in 10 mM phosphate buffer, 150 mM NaCl, 2 mM $MgCl_2$ (pH 6.0) in a total volume of 5.5 µL. Reactions were incubated at 37 °C for 6 h, loaded onto 22% PAGE gel and subjected to electrophoresis for 14 h at 50 V in 50 mM tris-acetate running buffer (pH 6.0). **III** Band densitometry of cleavage reactions of TFO3 hybrids. The target duplex band (D) was normalised to lane 1 (D_{nor}) and used to calculate the corresponding theoretical values of triplex formed (100% - D_{nor} = T_{tot}, lanes 2-8 in **II**). T_{tot} was then compared with triplex observed (T_{obs}) to provide the

extent of DNA cleavage ($T_{tot} - T_{obs}$ = % cleaved). The hybrids functionalised with the organic azides **B** and **C** showed higher cleaving activity in the incubation of 6 hours. 116
Figure 3.6 I Targeting experiment design: Cu(II) coordinated TFO-hybrids were co-treated with a target duplex (on-target, D_{ON}) and a non-target duplex (off-target, D_{OFF}). In the presence of excess Asc, cleavage specificity can be measured. **II** Triplex formation with non-clicked TFO3 and TFO6 was monitored in the presence of D_{ON} and D_{OFF}. **III** Cleavage activity towards D_{ON} and D_{OFF} by **TFO3A** and **TFO6B** was identified in the presence of $Cu(NO3)_2$ (TFO:Cu^{2+} = 1:1) and Asc (1.25 nmol). 117
Figure 3.7 I Cleavage experiments were designed using fluorescently-tagged complementary single strands of the target duplex (S1 labelled with FAM and S2 labelled with Cy3) and proposed cleavage-site probes (F1 and F2). **II** Denaturing PAGE experiments with the S1:S2 target treated with varying amounts of TFO in lanes 5-7 (D:TFO:Cu:Asc = 1:X:2X:1500X, where X = 1, 10 or 25 equivalents). S1 and S2 are shown in lane 1 and 2 while F1 and F2 are shown in lane 3 and 4. 118
Figure 3.8 I Synthetic route of ligand **G**, N,N'-((5-azido-1,3-phenylene)bis(methylene))bis(1,10-phenanthrolin-5-amine). **II** Alkyne-modified TFO3 and TFO6 for CuAAC (X = C8-dU) or TFO7 for SPAAC (**Y** = BCN-dC). **III** TFO7G-hybrid with copper chelating and phenazine ancillary ligands Phen, DPQ and DPPZ. **IV** Thermal melting values of TFO-hybrids containing ligand **G** in TFO3, TFO6 and TFO7 along with non-clicked alkyne-modified TFO in the presence of Cu^{2+}, Cu-Phen, Cu-DPQ and Cu-DPPZ (D:TFO:Cu^{2+} = 1:1.25:2.5). Samples were prepared in 10 mM phosphate buffer with 150 mM NaCl and 2 mM $MgCl_2$ (pH = 6.0). The marginal stabilisation induced by the presence of the dinuclear system was observed, but Increased triplex stability was detectedupon the introduction of copper(II) ions or coordinated ancillary ligands. **V** Targeting experiment design: Cu(II) coordinated **G**-TFO hybrids were co-treated with a target duplex (on-target, D_{ON}) and a non-target duplex (off-target, D_{OFF}). Selective on-target cleavage was identified at D:TFO:Cu^{2+}:Asc = 1:10:20:1000. All samples were prepared in 10 mM phosphate buffer, 150 mM NaCl, 2 mM $MgCl_2$ (pH 6.0) in a total volume of 5.5 μL. Reactions were incubated at 37 °C for 6 h, loaded onto 22% PAGE gel and subjected to electrophoresis for 14 h at 50 V in 50 mM tris-acetate running buffer (pH 6.0). The damage of the on-target was remarkably enhanced by the addition of the ancillary ligands with the target selectivity fully preserved. 120
Figure 3.9 Optimisation of triplex formation and cleavage conditions. **I-II** Triplex formation with varying amounts of unclicked TFO–≡, TFO7G (**I**) and TFO3G (**II**), compared to the unclicked triplex interacting with the Cu_2(N,N'-phenanthrene)$_2$(G)]$^{2+}$. Duplex D3 (1.25 pmol, lane 1) was treated with increasing amount of D:TFO = 1:X, where X = 2.5-25 equivalents (3.12 pmol, lane 2,6; 12.5 pmol, lane 3,7; 31.2 pmol, lane 4,8) for 6 h; compared to the unclicked triplex interacting with $\mathbf{G^R}$ previously coordinated in situ with Cu^{2+} and ancillary ligands (A.L., line 9-12). **III** Triplex formation of all the hybrids in presence and in absence of the ancillary ligands and Cu^{2+} (D:TFO:Cu(A.L.) = 1:10:20, incubation time of 6 hours at 37°C). **IV** Competitive study of triplex formation using TFO3E and TFO3G at different ratios: TFO3E:TFO3G = 100:0, 85:15; 70:30; 50:50; 30:70; 15:85; 0:100 (D:TFO=TFO3E+TFO3G) = 1:10). All reactions were carried out in 10 mM phosphate buffer, 150 mM NaCl, 2 mM $MgCl_2$ (pH 6.0) in a total volume of 5.5 μL and incubated at 37 °C. Samples were loaded onto 22% PAGE and subjected to electrophoresis for 14 h at 50 V in 50 mM tris-acetate running buffer (pH 6.0).....122

Figure 4.1 I Azide-modifed Ru(II) complexes [Ru(Phen)$_2$(N_3-Phenanthrene)](PF_6)$_2$ were conjugated to alkyne-modified triplex forming oligonucleotide (TFOs) through copper-catalysed azide-alkyne cycloaddition (CuAAC) reactions. **II** The alkyne-modified nucleobase C8-Alkyne-dU was positioned at either 5′-termini or at internal position within the TFO probe. **III** Ru(II) complexes were designed with either 5-azido-1,10-phenanthroline (**A**), 2-(4-azidophenyl)-1H-imidazo[4,5-f][1,10]-phenanthroline (**B**), 11-azidodipyrido[3,2-a:2′,3′-c]phenazine (**C**), or 5-azido-N-(1,10-phenanthrolin-5-yl)pentanamide (**D**) ligands. **iv)** Alkyne-modified TFOs with GFP sequence recognition contain modification sites highlighted in red (X). 133

Figure 4.2 Synthetic routes for azide-modified Ru(II) complexes. Route i) Epoxy-1,10-phenanthroline was complexed and followed thereafter by the azidation to release the desired product [Ru(Phen)$_2$(**A**)](PF_6)$_2$. Route ii) Complexation of the amino-derivates of dipyrido[3,2-a:2',3'-c]phenazine and 2-phenyl-1H-imidazo[4,5-f]-1,10-phenanthroline provided intermediates for products [Ru(Phen)$_2$(**B**)](PF_6)$_2$ and [Ru(Phen)$_2$(**C**)](PF_6)$_2$. Route iii) [Ru(Phen)$_2$(**D**)](PF_6)$_2$ was prepared by directly coordinating 5-azido-N-(1,10-phenanthrolin-5-yl)pentanamide to [Ru(Phen)$_2$$Cl_2$]. 135

Figure 4.3 Synthesis of Ru(II)-hybrids using the in-house method of 'click chemistry' **I** Control (TBE) PAGE gel for the CuAAC chemistry for the Ru(II) complexes with TFO3 and TFO6. Samples were loaded onto 22% PAGE and subjected to electrophoresis for 2 h at 80 V TBE (1X) running buffer. **II** Schematic representation of Ru(II)-TFO hybrids. 136

Figure 4.4 I Stabilisation of triplex and duplex thermal melting induced by the Ru(II) complexes in TFO3 and TFO6 compared to control TFOs. **II** Direct comparison of ΔT_m of the triple and double helixes of TFO3 (blue) and TFO6 (green) prompted by the presence of the Ru(II) complexes. **III** Triplex formation of Ru(II)-hybrids (Duplex:TFO = 1:10) incubated for 6 hours at 37 °C in 10 mM phosphate buffer, 150 mM NaCl, 2 mM $MgCl_2$ (pH 6.0) in a total volume of 5 µL. The samples were loaded onto 22% PAGE and subjected to electrophoresis for 14 h at 50 V in 50 mM tris-acetate running buffer (pH 6.0). 137

Figure 4.5 I UV (dotted line) and fluorescent (solid line) analysis of [Ru(phen)$_2$(**A**)](PF_6)$_2$, [Ru(phen)$_2$(**B**)](PF_6)$_2$ and [Ru(phen)$_2$(**D**)](PF_6)$_2$ 25 µM in ACN, H_2O, PBS (pH=7.4) and 10 mM phosphate 150 mM NaCl and 2 mM $MgCl_2$ buffer (pH=6). Emission slit: 2.5 nm/excitation slit: 5 nm. **II** Table of λ_{max}, ε and λ_{em} of [Ru(phen)$_2$(**A**)](PF_6)$_2$, [Ru(phen)$_2$(**B**)](PF_6)$_2$ and [Ru(phen)$_2$(**D**)](PF_6)$_2$. 139

Figure 4.6 Comparison of the emission spectra of [Ru(Phen)$_2$(**B**)](PF_6)$_2$ (5 µM) and [Ru(Phen)$_2$(**D**)](PF_6)$_2$ complexes (1 µM) and equivalent TFO-hybrids clicked to TFO3 in 10 mM phosphate buffer 150 mM NaCl 2 mM $MgCl_2$ (pH=6). l_{ex} of [Ru(Phen)$_2$(**B**)](PF_6)$_2$: 457 nm and l_{ex} of [Ru(Phen)$_2$(**D**)](PF_6)$_2$: 447 nm. Emission slit: 2.5 nm/excitation slit: 5 nm. 140

Figure 4.7 I Titration of [Ru(phen)$_2$(**D**)](PF_6)$_2$ and TFO3-Ru**D** at the concentration of 1 µM with the target D3. **II** [Ru(phen)$_2$(**B**)](PF_6)$_2$ and TFO3-Ru**B** at the concentration of 5 µM with the target D3. **III** Direct comparison of variation of luminescence intensity (FI) and normalised luminescence intensity (ΔFI) of the titration of [Ru(phen)$_2$(**B**)](PF_6)$_2$, TFO3-Ru**B**, [Ru(phen)$_2$(**D**)](PF_6)$_2$and TFO3-Ru**D** with D3 and TFO3-Ru**B** with D_{OFF} detected at 600 nm. The titration was conducted with the loading ratio R=0.00 - 1.00 in 10 mM phosphate buffer 150 mM NaCl and 2 mM $MgCl_2$ (pH=6). λ_{ex} of [Ru(Phen)$_2$(**B**)](PF_6)$_2$: 457 nm and λ_{ex} of [Ru(Phen)$_2$(**D**)](PF_6)$_2$: 447 nm. Emission slit: 2.5 nm/excitation slit: 5 nm. 141

Figure 5.1 I Library of azide-functionalised phenanthroline and phenazine derivatives: **A**-**F**. **II** Structures of alkyne-modified TFO1 and TFO4 and single-strand antisense target. **III** Thermal stability of hybrid duplexes TFO1(A-F) and TFO4(A-F) compared to unclicked hybridisation probes. Samples were prepared at the concentration of 4 μM in PBS. **IV** Double-sigmoidal profile of TFO1F and TFO4F. 149
Figure 5.2 Schematic representation of the experiment to investigate the "light switch" properties of G and its complexes. 150
Figure 5.3 Left: hypothesis for the same trend of luminescence activity observed performing D_{ON} and D_{OFF} titration. Right: Possible strategy for further elucidations of the fluorescent properties of Ru-TFOs. 151

TABLE OF TABLES

Table 3.1. Crystal data and structure refinement data (100 K, CuKα radiation). Figures show 50% displacement ellipsoids for non-hydrogen atoms. 110

Table 5.1 λmax, ε and λem of $\mathbf{G_R}$ and $[Cu(\mathbf{G_R})(N,N\text{-phennthrene})_2]^{2+}$ in ACN..……..……..... 150

TABLE OF SCHEMES

Scheme 2.1 Synthetic route for the generation of the ligand **A (Route I)**. 73
Scheme 2.2 Synthetic route for the generation of the ligand **B** (**Route II**)..... 73
Scheme 2.3 Synthetic route for the generation of the ligand **C** (**Route II**). 76
Scheme 2.4 Synthetic route for the generation of the ligand **D** (**Route IV**). 79
Scheme 2.5 Synthetic route for the generation of the ligand **E** (**Route V**)..... 80
Scheme 2.6 Synthetic route for the generation of the ligand **F (Route VI)**. 82
Scheme 2.7 Synthesis of $[Cu(\mathbf{A})_2](NO_3)_2$. 83
Scheme 2.8 Synthetic route for the generation of the ligand **G**. 83
Scheme 2.9 Synthetic route for the generation of the ligand $\mathbf{G_R}$. 85
Scheme 2.10 Synthetic route for the generation of the complexes $[Cu_2(N,N'\text{-phenanthrene})_2(\mathbf{G_R})](NO_3)_4$. 87
Scheme 2.11 Synthetic route for the generation of the complex $[Ru(phen)_2(\mathbf{A})](PF_6)_2$. 88
Scheme 2.12 Synthetic route for the generation of the complex $[Ru\ (phen)_2(\mathbf{B})](PF_6)_2$..... 89
Scheme 2.13 Synthetic route for the generation of the complex $[Ru(phen)_2(\mathbf{C})](PF_6)_2$. 90
Scheme 2.14 Synthetic route for the generation of the complex $[Ru(phen)_2(\mathbf{D})](PF_6)_2$. 92

Abbreviations

A	Adenine
ACN	Acetonitrile
AMN	Artificial metallo-nucleases
AMANY	(*S*)-4-(4-(1H-Phenanthro[9,10- d]imidazol-2-yl)phenoxy)butane-1,2-diol
Asc	Na-L-ascorbate
ATR	Attenuated total reflectance
Bpy	2,2'-Bipyridine
C	Cytosine
CCDC	Cambridge Crystallographic Data Centre
$CDCl_3$	Deuterated chloroform
^{13}C-NMR	Carbon-13 nuclear magnetic resonance
COSY	Correlation spectroscopy
CuAAC	Copper promoted alkyne-azide cycloaddition
dA	Deoxyadenine
dC	Deoxycytosine
dG	Deoxyguanine
dI	Deoxyinosine
DIPEA	*N*,*N*-Diisopropylethylamine
DMSO	Dimethylsulfoxide
DMF	Dimethylformamide
DNA	Deoxyribose nucleic acid
dsDNA	Double stranded DNA
DPPN	Benzo[*i*]dipyrido[3,2-a:2′,3′-c]phenazine
DPPZ	Dipyrido[3,2-a:2′,3′-c]phenazine
DPQ	Dipyrido[3,2-f:2′,3′-h]quinoxaline
dU	Deoxyuracil
dT	Deoxythymine
EDTA	Ethylenediaminetetraacetic acid
ESE	Electron spin echo
ESI-MS	Electrospray ionisation mass spectrometry
Et_2O	Diethyl ether
EtOH	Ethanol
FT	Fourier transform
G	Guanine
GFP	Green fluorescent protein
^{1}H-NMR	Proton nuclear magnetic resonance
HPLC	High performance liquid chromatography
HSQC	Heteronuclear single quantum correlation

IL	Ionic liquids
IR	Infrared spectroscopy
MeOD	Deuterated methanol
$^1O_2$	Singlet oxygen
Oda	Octanedione
$^{\bullet}OH$	Hydroxyl radical
$O_2^{\bullet-}$	Superoxide radical
PD	1,10-Phenanthroline-5,6-dione
Ph	*o*-Phthalate
Phen	1,10-Phenanthroline
PPA	Polypycolylamine
Pu	Purine
Py	Pyrimidine
ROS	Reactive oxygen species
SPAAC	Strain promoted alkyne-azide cycloaddition
T	Thymine
TBE	Tris/Borate/EDTA
TBTA	Tris[(1-benzyl-1H-1,2,3-triazol-4-yl)methyl]amine
TEAA	Triethylammonium acetate
TFO	Triplex forming oligonucleotide
THF	Tetrahydrofuran
TINA	Twisting Intercalant Nucleic Acid
T_M	Thermal melting
TPNap	*tetra*-(2-pyridyl)-NMe-naphthalene
Terph	Terephthalate
U	Uracil
WC	Watson-Crick

ABSTRACT

Teresa Lauria M.Sc.

The Development of Hybrid Antigene Therapeutics using Nucleic Acid Click Chemistry

Given their ability to break single- and double-strand DNA with high selectivity, the design of restriction endonuclease mimics has become an area of considerable research interest. One class of mimetics are copper artificial metallo-nucleases (AMNs) that prompt direct strand scission by oxidatively damaging duplex DNA. Therefore, the formation of metal-catalysed free radicals in the vicinity of nucleic acids provides a viable route to developing artificial gene editing tools. The aim of this research was to develop new copper-based AMNs for selective knockdown of the green fluorescent protein (GFP) gene. To achieve this, a novel pool of gene-targeted biomaterials was developed by hybridising intercalating azide-modified phenanthrene AMNs to triplex formation oligonucleotides (TFOs) using copper-catalysed alkyne-azide cycloaddition (CuAAC) 'click' chemistry. Upon isolating the family of AMN-TFO hybrids, the project focused on their triplex formation and stabilisation properties. In the presence of coordinated copper(II) ions and a reductant, AMN-TFOs selectively cleaved the GFP gene fragment and site-specific fragmentation patterns were identified using fluorophore-tagged sequences. Building on this first generation of hybrid AMNs, second generation hybrids were developed by clicking *di*-copper binding *bis*-phenanthroline ligands to alkyne-TFOs. These *di*-copper(II) AMN-TFOs were prepared using both CuAAC and strain-promoted azide-alkyne cycloaddition (SPAAC) reactions and cleavage reactions with a GFP gene fragment were compared to first generation mononuclear AMN-TFO hybrids. The final aspect of this work focused on extending this technology to develop a novel class of luminescent probes. To achieve this, polypyridyl ruthenium(II) complexes bearing an azide-phenanthroline handle were prepared and conjugated to alkyne TFOs and their preliminary GFP-targeting and luminescence properties were identified.

CHAPTER 1

Gene editing and nucleic acid click chemistry

1.1 An introduction to artificial DNA cutters

Artificial DNA cutters are mimics of type II restriction enzymes and are useful tools for the cutting of single-strand (ssDNA) and double-strand DNA (dsDNA) that aim to provide higher selectivity than naturally occurring enzymes.[1] An emerging approach allows investigators to perform direct modification of any gene in a diverse range of cell types and organisms. This powerful method is known as 'genome editing' and is characterised by the fusion of two domains: a sequence-specific DNA-binding site and a non-specific DNA cleavage module. The genetic modifications induced by double-strand breaks with these artificial scissors stimulate the cellular DNA repair mechanisms, including error-prone non-homologous end joining (NHEJ) and homology-directed repair (HDR).

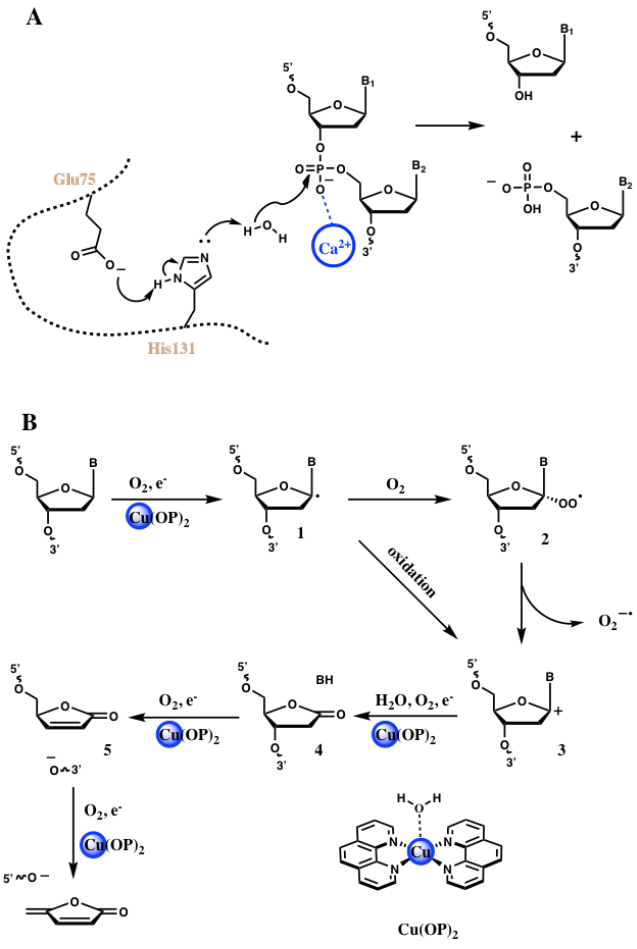

Figure 1.1 Mechanism of hydrolytic DNA damage through phosphodiester hydrolysis (**A**) and oxidative DNA cleavage promoted by ROS species through the abstraction C1' hydrogen from deoxyribose (**B**).[4]

Based on their mechanism of DNA damage, artificial nucleases can be classified into two categories: oxidative and hydrolytic cleavage agents.[2,3] Oxidative nucleases promote deoxyribose cleavage by redox chemistry[4,5] and are applied to probe DNA structures and as footprinting agents. Hydrolytic nucleases induce the hydrolysis of phosphodiester bonds[6] and provide a more compatible approach for biological systems *in vivo* and *in vitro*. The commonly accepted mechanism for hydrolytic damage involves the nucleophilic attack of hydroxyl ion from water to phosphate backbone, resulting in the hydrolysis of the phosphate esters at the 3'-OH (**Figure 1.1 A**). This type of mechanism has been found in

several biological process including expression, duplication, repair and elimination of foreign DNA, catalysed by metal-dependent enzymes, such as nucleases and topoisomerases. Metal ions involved in catalysing DNA cleavage are primarily Ca^{2+}, Mg^{2+} and Zn^{2+}.

Regarding oxidative DNA cleavage, the first synthetic chemical nuclease $[Cu(Phen)_2]^{2+}$ (where Phen = 1,10-phenanthroline) was discovered by Sigman during the course of experiments to identify if phenanthroline could inhibit *Escherichia coli* DNA polymerase I *via* sequestering zinc from the active site.[7,8] $[Cu(Phen)_2]^{2+}$ cleaves DNA using a predominant two-step mechanism: in the first step Cu(II) is reduced to Cu(I) using biological or exogenous reducing agent[9,10] such as Na-L-ascorbate or 3-mercaptopropionic acid and in the presence of trace amount of exogenous oxidant (H_2O_2 or O_2), reactive oxygen species (ROS) are generated. [11] In the second step, there is semi-intercalation into the minor groove of DNA (slow) followed by DNA degradation (fast) through the abstraction of a C1′ hydrogen atom from deoxyribose (**Figure 1.1 B**).[12,13,14]

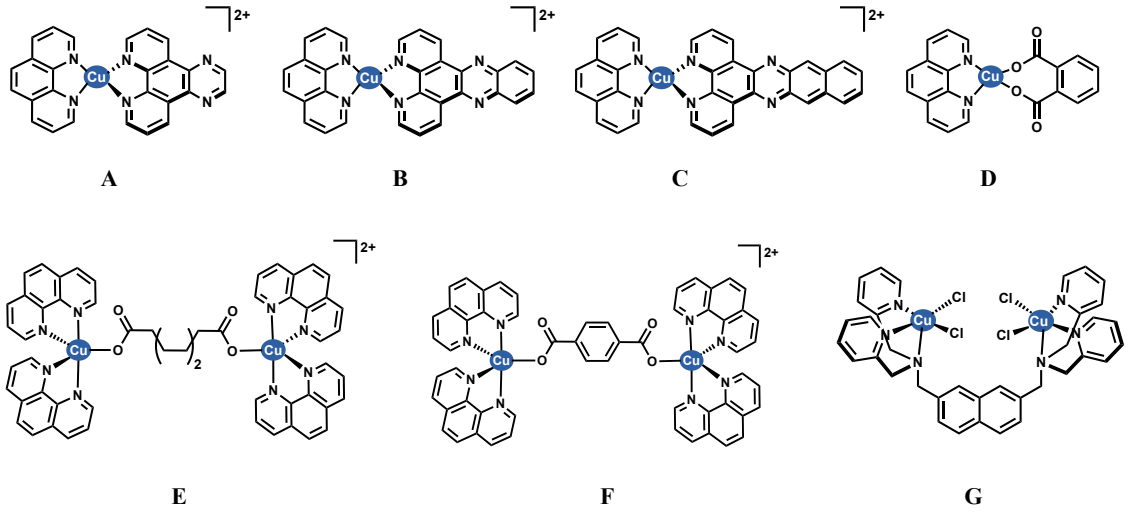

Figure 1.2 Molecular structures of **A**) Cu-Phen-DPQ, **B**) Cu-Phen-DPPZ, **C**) Cu-Phen-DPPN, **D**) [Cu(o-phthalate)(Phen)], **E**) Cu-Oda, **F**) Cu-Terph and **G**) Cu_2TPNap.

An important discovery in determining the cleavage mechanism by $[Cu(Phen)_2]^{2+}$ (**Figure 1.1**) was provided by the Greenberg group.[12] They identified that direct strand breakage proceeds *via* β-elimination with the formation of 5-methylene furanone.[13] In the increasingly complex design of appropriate and improved artificial DNA nucleases, the Kellett group developed copper complexes with systematic extensions of phenanzine derivatives, $[Cu(Phen)(DPQ)]^{2+}$ (**Figure 1.2 A**), $[Cu(Phen)(DPPZ)]^{2+}$ (**Figure 1.2 B**), and

[Cu(Phen)(DPPN)]$^{2+}$(**Figure 1.2 C**), which displayed a clear enhancement in DNA binding affinity and oxidative damage when compared to [Cu(Phen)$_2$]$^{2+}$.[11] The quantification of DNA damage with an ELISA protocol analysing 8-oxo-2′-deoxyguanosine (8-oxo-dG) lesion formation by the interaction of DNA with some of these Cu(II) complexes showed an overall trend following Cu-DPQ-Phen > Cu-Phen > Cu-DPPZ. Moreover, this family of copper complexes was expanded with the development of a phthalate complex [Cu(*o*-phthalate)(1,10-phenanthroline)] (**Figure 1.2 D**) which is characterised by pronounced generation of ROS species both *in vitro* and intracellularly.[15] This complex showed dual targeting properties, inducing double strand breaks in the genomic DNA of ovarian cancer cells and large-scale mitochondrial dysfunction in the form of depolarisation.

Over time, the design of metallo-artificial nucleases (AMN) was expanded with the introduction of two (or more) metal centres enhancing DNA cleavage sensitivity together with high sequence selectivity. For example, Karlin and Rokita reported a *di*-copper artificial nuclease containing a dinucleating ligand with two *tris*-(2-pyridylmethyl)-amine units covalently linked in their 5-pyridyl positions by a -CH_2CH_2-bridge that cleaved with higher nucleolytic effects when compared to [Cu(Phen)$_2$]$^{2+}$ with selective scission at junctions between single- and double-stranded DNA.[16] Recent efforts have been made in the optimisation of *di*-nuclear copper complexes by changing the oxidation target sensitivity from deoxyribose to guanine[17] and tuning intermetal distances.[18] This led to the generation of two *di*-copper complexes: [Cu$_2$(μ-octanedioate)(Phen)$_4$]$^{2+}$ (Cu-Oda, **Figure 1.2 E**),[19] [{Cu(Phen)2}2(μ-Terph)]$^{2+}$ (Cu-Terph, **Figure 1.2 F)**[19] and [Cu$_2$(*tetra*-(2-pyridyl)-NMe-naphthalene)Cl$_4$] (Cu$_2$TPNap, **Figure 1.2 G)**.[20] The long bridging dicarboxylate ligand allowed Cu-Oda to discriminate TA/TA from AT/AT steps and induce damage through a combination of singlet oxygen ($^1O_2$) and superoxide ($O_2^{\bullet-}$) ROS production. Alternatively, a rigid aromatic naphthalene linker in Cu$_2$TPNap improved DNA binding affinity with exclusive major groove targeting properties. In addition, both Cu-Oda and Cu$_2$TPNap present 'self-activating' properties which facilitates DNA damage induction without the presence of a reducing agent.

Artificial nucleases can be combined with sequence-recognising molecules using a covalent or non-covalent approach.[21] In the covalent approach a DNA cleaving agent is directly bound to a sequence-recognising molecule through a covalent bond. In the

second approach a DNA cutting agent is not directly bound to a sequence-recognising reagent, but the target site is activated by a secondary interaction whereby the artificial nuclease recognises this binding event and induces selective DNA damage. Recently, peptide nucleic acid (PNA)-based artificial nucleases have gained considerable traction as non-covalent sequence-directed cleaving agents.[22,23] For example, Kramer and co-workers recently described a family of PNA-metal chelating conjugates whose Zr(IV) complexes could selectively hydrolyse single stranded DNA (ssDNA).[24]

1.2 Selective ssDNA and dsDNA damage

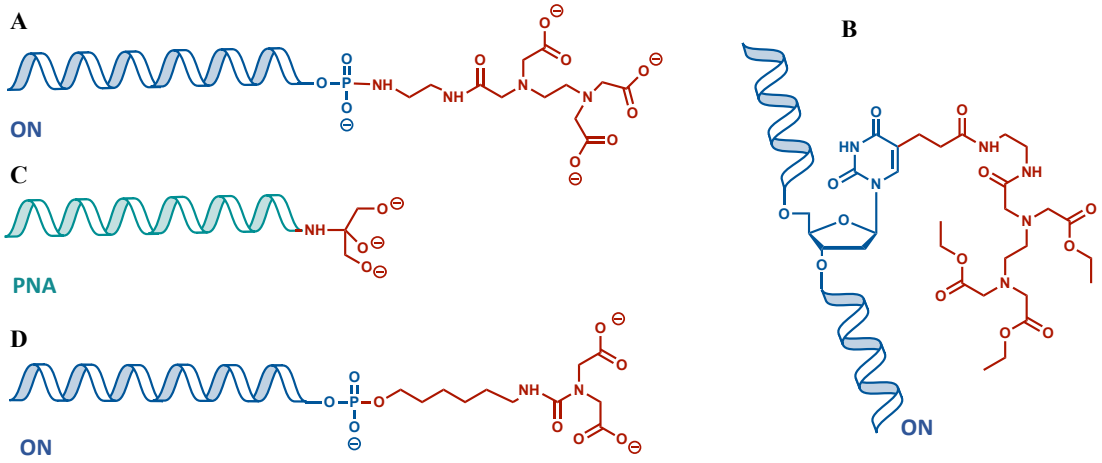

Figure 1.3 Molecular structures of EDTA-ON conjugate at **A**) 5′-position and **B**) internal position for Fe(II)-based nucleases. **C**) Zr(IV)-based and **D**) Ce(IV)-based AMNs.

It is possible to target ssDNA and dsDNA using careful hybrid design that exploits the oxidative or the hydrolytic cleaving mechanisms to induce selective damage. Initially, oxidative ssDNA cleavage was performed using a hybrid system consisting of Fe(II) attached to an oligonucleotide (ON). Two synthetic methods were attempted in developing these hybrids: post-synthetic conjugation of an Fe(II) ethylenediaminetetraacetic acid (EDTA) complex to the 5′-terminus of a 16 mer ON was reported by Chu and Orgel (**Figure 1. 3 A**)[25] and the incorporation of EDTA-modified thymidine into a 19-mer ON was later reported by Dervan and Dreyer (**Figure 1.3 B**).[26] In both cases a ssDNA target was cleaved upon DNA hybridisation and the reduction of Fe(III) to Fe(II) *in situ* by the addition of a reductant (dithiothreitol). Hydrolytic cleavage of ssDNA can be also achieved using covalent and non-covalent approaches. For example, conjugates of Zr(IV)/PNA (peptide nucleic acid, **Figure 1.3 C**)[27] and Ce(IV)/ONs (**Figure 1.3 D**) provided promising results when the ligand was directly (covalently) bound to the probe strand.[28,29,30] However, Ce(IV)/EDTA complexes can

also provide targeted cleavage using a non-covalent approach since the free complex can catalyse phosphodiester hydrolysis in gap sites (*i.e.* ssDNA sites of non-hybridised regions),[28] however, undesired off-targeting effects can arise using this approach.[30] To overcome this drawback, scientists hybridised an ON to EDTP (ethylenediaminetetrakis(methylenephosphonic acid)), which strongly binds Ce(IV) thereby reducing off-targeting effects.[2] One other hybrid class worth mentioning here is PNA-neocuproine which act as artificial restriction enzymes of RNA.[31] These hybrids do not damage ssDNA and rely on a mechanism whereby the PNA sequence is designed to form a bulge around the cleaving site, which is selectively cleaved by Cu(II).[32]

Although covalently bound hydrolytic artificial nucleases have not been reported to directly cleave dsDNA, a Ce(IV)/EDTA complex with pseudo-complementary peptide nucleic acid (pcPNA) has provided cleavage of two ssDNA sequences (**Figure 1.4 A**).[33,34] The cleavage of dsDNA involves two pcPNA strands forming double-duplex invasion, followed thereafter by single strand hydrolysis catalysed by the Ce(IV) complex.[34] Another strategy involves the combination of the enzymatic nuclease S1 with a homopyrimidine PNA sequence, which is designed to form a PNA-DNA-PNA triplex.[35] Later, the design of this nuclease was changed to involve two pcPNA sequences, which perform double-duplex invasion and the cleavage is induced by the enzyme S1.[36] Regarding oxidative dsDNA cleavage, significant efforts were made by Sigman (**Figure 1.4 B**)[37] and Hélène (**Figure 1.4 C**).[38] In particular, they identified that Cu-Phen hybrids of short (7-11 mer) homopyrimidine oligomers were effective targeting triplexes. However, the presence of a cationic adjuvant (spermine) was required to stabilise the triple-helical structure. Another oxidative nuclease identified was a non-covalent conjugate of Ni(II) acetate combined with bis-PNA-GGH chimera (two PNA sequences connected by an aliphatic spacer with one end functionalised with a Gly-Gly-His tripeptide).[39] However, the level of DNA damage induced by this nuclease was not higher than 20% as a result of the strict stereospecific orientation of the tripeptide-nickel complex and the short radical half-life. The cleavage efficiency was also affected by self-cleavage effects. Other types of oxidative chemical nuclease include Mn(II) porphyrin and Cu(II)/Co(III) metallodesferal complexes linked to ONs. Both hybrids provide reasonable cleavage effects with good efficiency but some triplex destabilisation was found to accompany hybrid binding.[40,41,42] A non-covalent approach involving benzoquinoquinoxaline (BQQ) has also provided promising results for dsDNA damage.

BQQ is known to selectively intercalate and stabilise triple helices[43] and the first BQQ-based artificial nuclease involved conjugation with Fe(II)/EDTA,[44] which stabilises triplex formation *via* the BQQ moiety and locates Fe(II)/EDTA in proximity of the cleaving site. The state-of-the-art in BQQ hybrids is now recognised as a Phen compound (BQQ-OP)[45,46] assisted by bis-LNA (containing a clamp-type locked nucleic acid), which performs duplex-invasion and forms a stable triplex.[47]

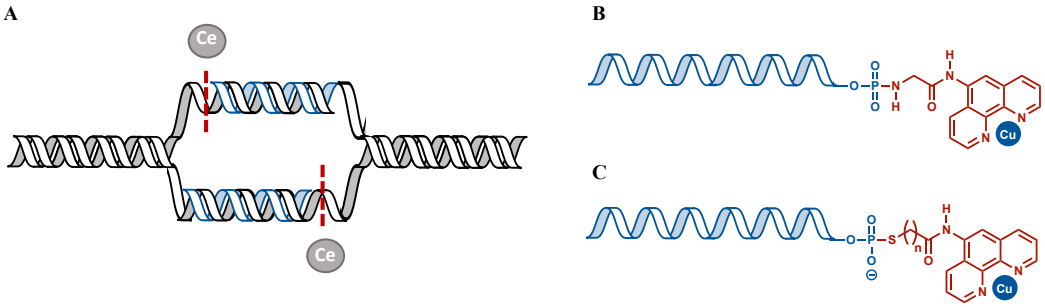

Figure 1.4 A) Double strand DNA cleavage mechanism of Ce(IV)/EDTA complex assisted by pcPNA. Molecular structures copper-hybrids developed by **B**) Sigman and **C**) Hélène.

1.3 ZNFs, TALENs and CRISPR/Cas

Another class of programmable targeted nucleases are protein-based hybrids, which originated from combining two naturally occurring systems. This class of nucleases induce highly selective double-stranded DNA cleavage and comprise a DNA-cleaving moiety from a natural nuclease (e.g. *Fok* I) and a proteolytic moiety with an affinity for the target scission site. Among the best known and most widely applied, are zinc finger nucleases (ZFNs, **Figure 1.5 A**)[48] and transcription activator-like effectors nucleases (TALENs, **Figure 1.5 B**).[49]

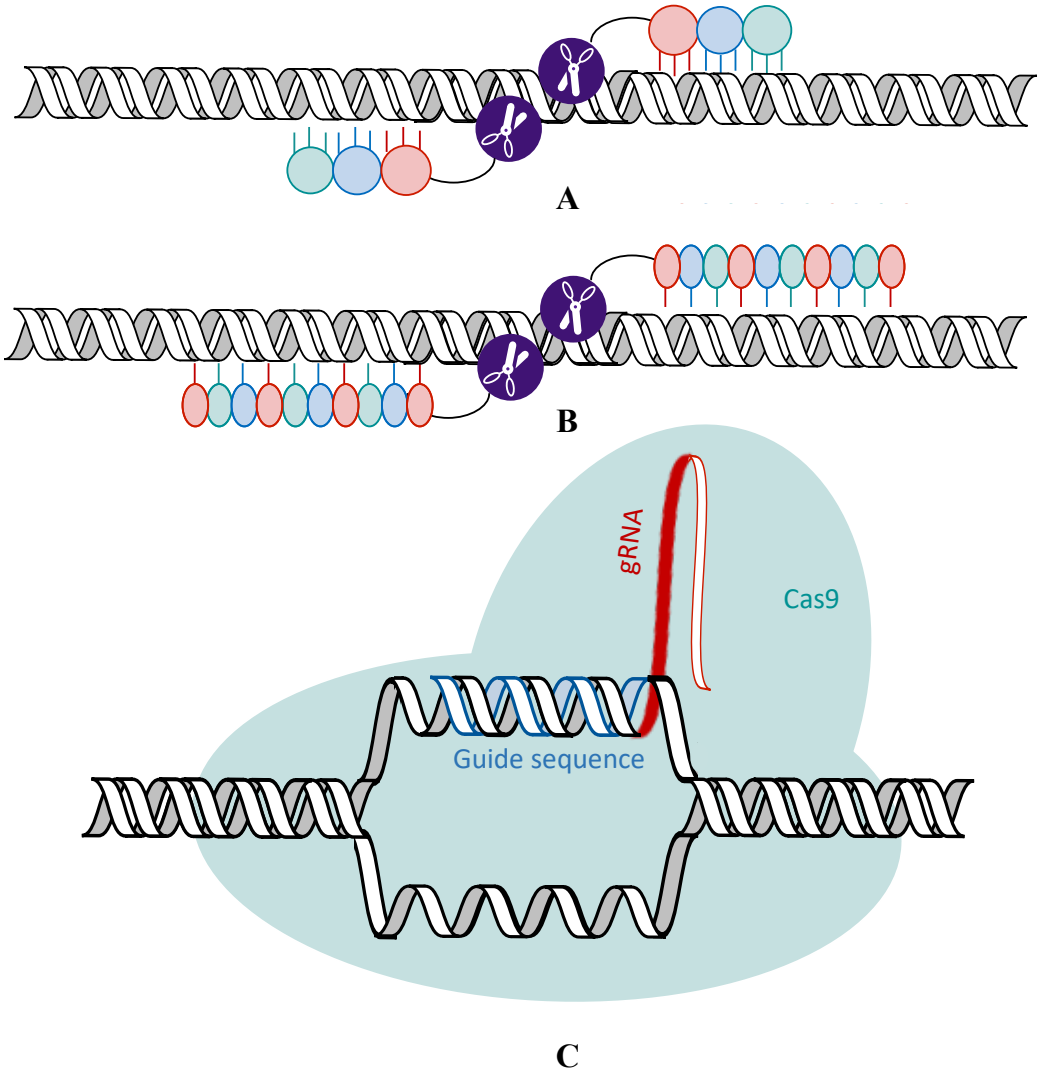

Figure 1.5 Schematic representation of the most widely recognised known programmable targeted nucleases employed in gene editing: **A**) Zinc Finger Nucleases (ZFNs), **B**) transcription activator-like effectors nucleases (TALENs) and **C**) clustered regulatory interspaced short palindromic repeats (CRISPR/Cas9).

ZFNs consist of an *N*-terminal DNA-binding domain, which corresponds to a zinc finger protein, and a DNA-cutting domain of naturally occurring *Fok* I restriction

endonucleases at the *C*-terminal.[50] The DNA-cutting domain is non-sequence specific and the cleavage selectivity is determined by the zinc finger proteins which bind in the major groove of dsDNA. However, the DNA cleavage requires the simultaneous binding of the two moieties to the substrate. To improve the affinity for long DNA sequences, it is possible to use a tandem track of several zinc-finger protein units.[51] For the first time ZFNs entered clinic trial for the treatment of HIV.[52] The method involves the extraction of T-cells and the disruption of the CCR5 gene by a ZNF,[53] followed therefore by the reintroduction of the modified gene into the patient. ZFNs have been employed for the treatment of Hunter Syndrome (SB-913)[54] and haemophilia B (SB-FIX).[55,56]

ZFNs were the first tools generated for genomic-editing but had some limitations correlated to gene targeting and cleavage efficiency. These limitations were addressed with transcription activator-like effectors nucleases (TALENs). TALENs were generated by plant pathogens in the genus *Xanthomonas*, which deliver the proteins to plant cells during an infection. In plant cell, TALEs bind effector-specific DNA sequences in the nucleus and transcriptionally activates the expression of the gene. Normally, the target gene activation increased plant sensitivity to pathogen colonisation, but occasionally it prompted the plant defence.[49] TALE bind DNA through a protein central region which includes 30 tandem repeats of a 33- to 35-amino acid sequence motif. The peptide sequence of each repeat is practically invariant with exception of two adjacent amino acids—known as the repeat variable di-residues or RVD,[57] which recognise the base pairs in DNA target sequence with one-to-one correspondence, corresponding to a straightforward code. RVD are essentially located in positions 12 and 13 and are affected by polymorphism.[58] The structure of TALEs presents an *N*-terminal translocation domain, which mediates sequence-specific DNA binding; a *C*-terminal segment which includes nuclear localisation signals (NLS) and a domain for the transcriptional activation. Currently TALENs are used for the generation of off-the-shelf chimeric antigen receptor (CAR) for T-cell therapy (CAR-T).[59]

The current state-of-the-art in genome editing is represented by clustered regulatory interspaced short palindromic repeats (CRISPR)/Cas-based RNA-guided DNA endonucleases (CRISPR/Cas, **Figure 1.5 C**),[60] which are restriction nucleases characterised by easier design than ZFNs and TALENs.[61] The cleaving moiety of CRISPR/Cas is the enzymatic system Cas9, an endonuclease that induces a double-stranded break (DSB) in DNA. Sequence-specific binding, however, is driven by guide

RNA (gRNA) which central to CRISPR activity.[61] The target binding proceeds *via* RNA strand invasion inducing local DNA unwinding to generate an R-loop.[62,63] CRISPR/Cas-associated nucleases suffer from sequence limitations because the site-specific cleavage occurs at target sites 3′ downstream of the target protospacer DNA and a short motif (protospacer adjacent motif-PAM-sequence requirement).[64,65] Another problem is off-targeting effects due to the imperfect single guide RNA hybridisation and prolonged activity of Cas9.[66] To overcome these obstacles, novel enzymatic systems Cas12 and Cas13 were generated. Cas12 presents DNA targeting and affinity for T-rich PAM sequences (G-rich PAM sequence for Cas9), which leads to the instauration of weaker binding interactions decreasing off-target events.[67,68] Interesting, the target of Cas13 is mRNA but still present PAM sequence dependence.[64] Despite the advancement of Cas design, Cas12 and Cas13 have shown off-targeting effects, especially Cas13 which provides non-selective cleavage of RNA and DNA sequences.[64] To further expand the applicability of CRISPR/Cas as gene editing tools, Brown and El-Sagheer established a novel 'split-and-click' method for generating libraries (of pool) of single modified gRNAs.[69] The method involves the splitting of the gRNA sequence into two components, crRNA and tracrRNA, then reassembled using click chemistry for the development of individual or pools of gRNA libraries with distinctive modifications. Despite the necessity of further optimisation of CRISPR/Cas design, some systems are already being tested as promising anticancer, anti-viral and anti-bacterial agents.[67] For example CRISPRs are under clinical trials for the treatment of sickle cell disease, multiple myeloma, sarcoma and melanoma[67] and the Cas9 system has provided interesting results against the hepatitis B virus (HBV)[70] and HIV.[71] Interesting activities were also detected in the treatment of antibiotic resistant *E.coli*[72] and *Staphylococcus Aureus.*[73]

1.4.1 Click Chemistry

The term click chemistry was devised in 2001 by K. B. Sharpless and defines a set of powerful, highly reliable, and selective reactions for the conjugation of small units with carbon-heteroatom bonds.[74] Synthetic approaches are classified as 'click chemistry' with the accomplishment of the following criteria: *modularity*, *wide in scope* and *stereospecificity*, *high yields* and only *inoffensive byproducts* and normally used for the synthesis of novel, useful and easily-obtainable compounds and combinatorial libraries.[75] Furthermore, the synthetic route has to be *simple*, involves the

use of *readily available starting materials* and *reagents*, works in *an environmentally friendly* or *easily removable* solvent or in its *absence*, in case of microwave-assistance. The final product has to be *stable under physiological conditions* and *easily purifiable* exploiting recrystallisation or distillation and avoiding the use of chromatographic methodologies.[76] Because of its high versatility and applicability, click chemistry attracts the interest of chemists working in different research areas, consequently it is widely employed in molecular biology, drug-design, biotechnology, and materials science. Click reactions are commonly divided into four main classifications:

- Non-aldol reactions on carbonyl groups
- Carbon multiple bond additions
- Nucleophilic ring-openings
- Cycloadditions.

Among these four classifications of click reactions, the most widely used is Cu(I)-catalysed Huisgen 1,3-dipolar cycloadditions of organic azides and molecules with alkyne-functionality to form 1,2,3-triazoles. Azide-alkyne cycloaddition was known for more than 100 years and rediscovered in the 1960s by Rolf Huisgen.[77,78] However, the initial conditions for the azide-alkyne cycloaddition required high temperatures for the reaction to proceed, the kinetic was slow and provided a mixture of 1,4- and 1,5-regioisomers (**Figure 1.6**).

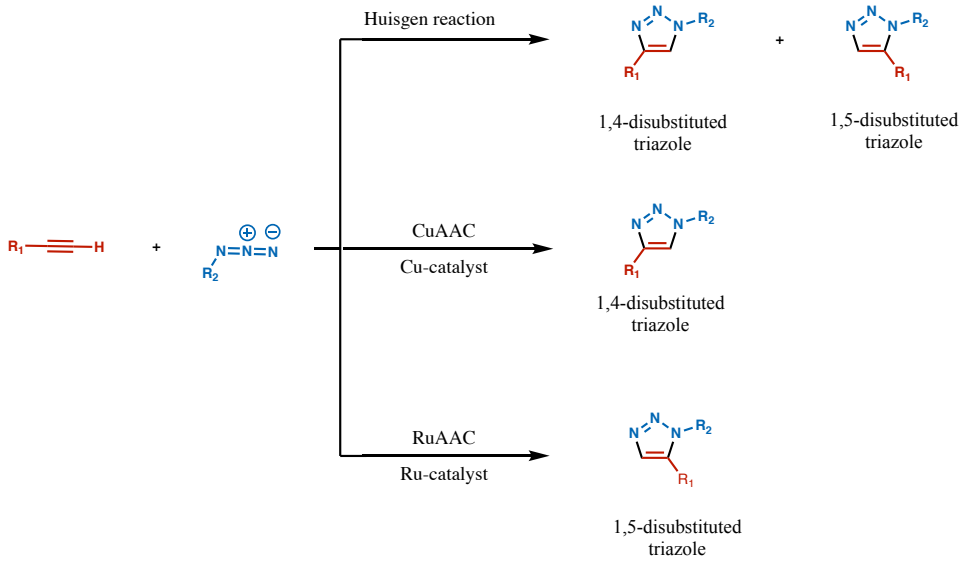

Figure 1.6 Regioselectivity of Click chemistry depending on the reaction conditions: mixture of the 1,4- and 1,5-stereoisomers in the absence of a metal catalyst, 1,4-stereoisomer in the presence of copper-catalyst (Cu-catalyst) and 1,5-stereoisomer in the presence of ruthenium-catalyst (Ru-catalyst).

Safety concerns regarding the handling of organic azides[79] and the lack of regioselectivity had an unfavourable effect on the full exploitation of the azide-alkyne cycloaddition. It was found that the high reactivity of organic azides is disguised unless a good dipolarophile is added to the mixture of reaction.[80] The issue concerning the regioselectivity were solved by the groups of Sharpless and Meldal with the introduction of Cu(I) as catalyst for the promotion of the 1,4-disubstituted triazole product (mechanism in **Figure 1.7 A**).[80,81]

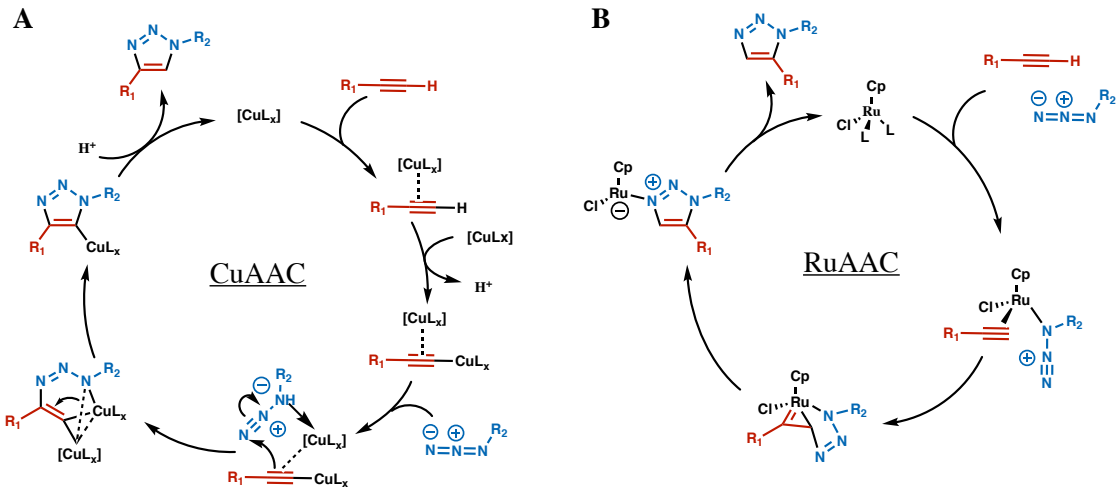

Figure 1.7 Reaction mechanisms of Click chemistry in the presence of **A**) copper (CuAAC) and **B**) ruthenium (RuAAC).

From here on, many changes and optimisations of the click reaction were conducted. For example, ruthenium-based catalysts were employed to promote the

formation of the 1,5-disubstituted triazole product (mechanism in **Figure 1.7 B**). Particular attention was focused on the selection of an alternative catalyst to Cu(I), owing to the instability of the metal salts in aqueous solution. There are a variety of pre-catalysts and synthetic strategies adopted to generate the active form of the metal, as such the reduction of Cu(II) to the active species Cu(I) *in situ* or Cu(0) as wire, powder or nanoparticles.[82] The reduction of Cu(II) is usually assisted by reducing agents such as ascorbate or TCEP (tris(2-carboxy-ethyl)phosphine, **Figure 1.8**). The chemoselectivity of azide-alkyne reaction and regioselectivity provided by Cu(I) allowed expansion of click chemistry also for the functionalisation of biomolecules. However, bio-functionalisation demanded the selection of more biocompatible conditions and consequently stabilising chelating agents with polytriazole ligands, such as tris(benzyltriazolylmethyl)amine (TBTA, **Figure 1.8**)[83] or tris(hydroxypropyltriazolylmethyl)amine (THPTA, **Figure 1.8**) were developed.[84] TBTA and THPTA were shown to stabilise the metal and protect biomolecules from oxidative damage. In addition, the polytriazole ligands were found to be capable of autocatalysing the cycloaddition reaction.[83] Copper-catalysed azide-alkyne cycloaddition (CuAAC) reactions were further optimised using microwave dielectric heating or ionic liquids (IL), which allow shorter reaction times along with increased yields and make the click chemistry more environmentally friendly.[85] An interesting pre-catalyst is the cupric complex $[Cu(OAc)_2]^{2+}$ (OAc=acetate) because a reducing agent is not required due to complex being reduced to an active Cu(I) form by alkynes.[86]

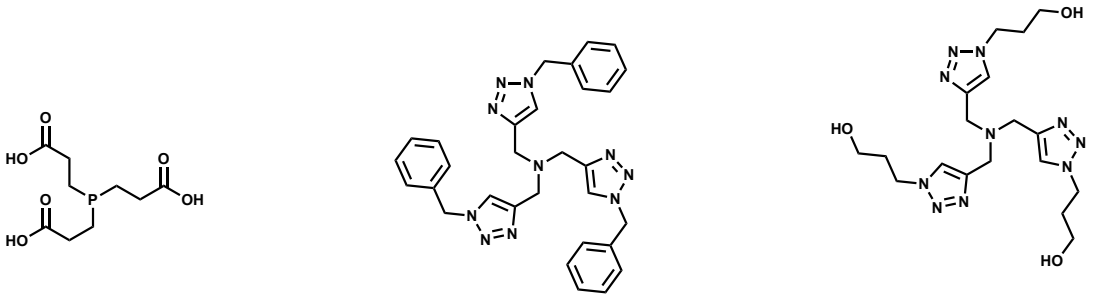

TCEP **TBTA** **THPTA**

Figure 1.8 Molecular structures of tris(2-carboxyethyl)phosphine (TCEP), tris(benzyltriazolylmethyl)-amine (TBTA) and tris(3-hydroxypropryltriazolylmethyl)amine (THPTA).

Finally, attention was recently focused on possible alternative types of click reaction because Cu(I) is known to have undesirable toxicity properties.[87] On this basis, a more biocompatible method was developed based on a ring strain-promoted azide-

alkyne cycloaddition reaction (SPAAC, **Figure 1.9 A**)[88] where the alkyne derivative is a cyclooctyne substituted in α-position by an electron-withdrawing group.[89] The most commonly used is strained difluorooctyne (DIFO),[90,91] in which the electron-withdrawing group work together with the ring strain to destabilise the alkyne without the assistance of a copper catalyst. Other successful cyclootyne derivatives ordinarily employed are: dibenzylcyclooctyne (DIBO),[92] due to the presence of additional benzene rings provides very high strain and improved reactivity; biarylazacyclooctynone (BARAC),[93] due to the higher pharmacokinetic; and dimethoxyazacyclooctyne (DIMAC)[94] because of the water solubility despite of the lower reactivity (**Figure 1.9 B**).

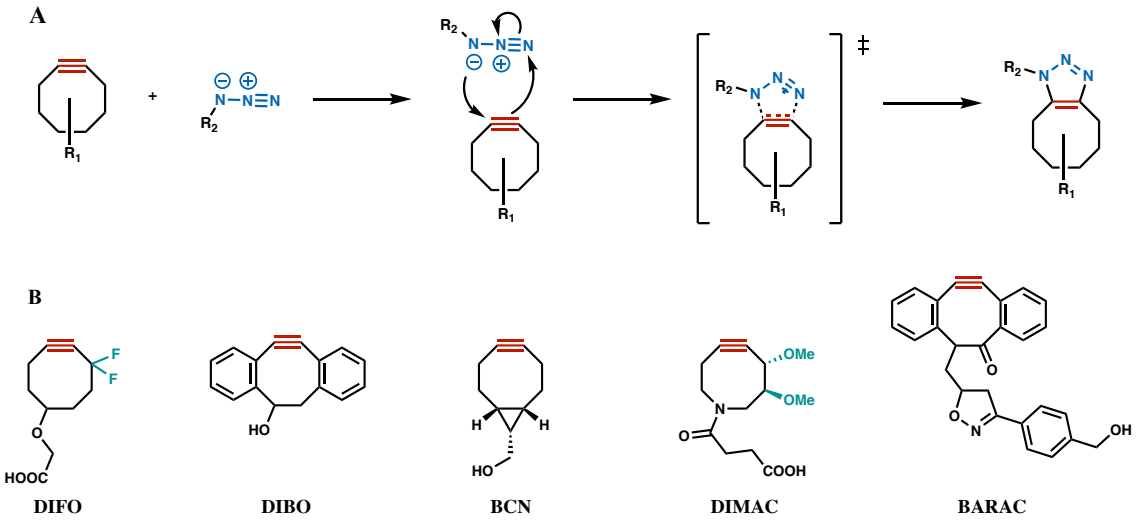

Figure 1.9 A) Ring strain-promoted azide-alkyne cycloaddition reaction (SPAAC). **B)** Alkyne-cyclootyne derivatives (DIFO, DIBO, BCN, DIMAC and BARAC).

The absence of copper also allows click chemistry to be performed within a living system without interfering with the native biochemical processes.[95] In 2003 the concept of bioorthogonality was introduced by Betozzi to indicate biocompatible chemical reaction characterised by chemoselectivity, fast kinetics, biological and chemical inertia that can be inserted into naturally occurring biomolecules *via* metabolic pathways or biomolecular engineering.[95,96] The bioorthogonality of the Cu-free click reaction also consents to perform the bioconjugation of biomolecules properly with fluorophores *in situ* cultured cells, live zebrafish, and mice, paving the way to novel diagnostic methodologies and imaging applications (**Figure 1.10**).[97–100] Although the aforementioned cyclootynes are not highly regioselective, this is not a limitation for imaging applications, but can have some influence in fields such as drug design. This

issue was settled with the development of bicyclo[6.1.0]nonyne (BCN), form a single regioisomer upon cycloaddition.[101] In contrast to the wide applicability of metal-free click chemistry, this method is still slower than CuAAC and another drawback of SPAAC is the low yield in the synthesis of cyclootyne derivatives. In addition, the key properties that play a dramatic role in the *in-vivo* functionalisation and limit the exploitation of the majority of the cyclooctyne derivatives are the low water-solubility and the sensitivity to the large amount of nucleophiles in cells (e.g. thiols, amines and hydroxy groups). The hydrophobicity of the cyclooctene can also affect the progress of click reaction altering the biodistribution, circulation and secretion. Consequently, CuAAC is still the preferred method of click chemistry widely adopted.

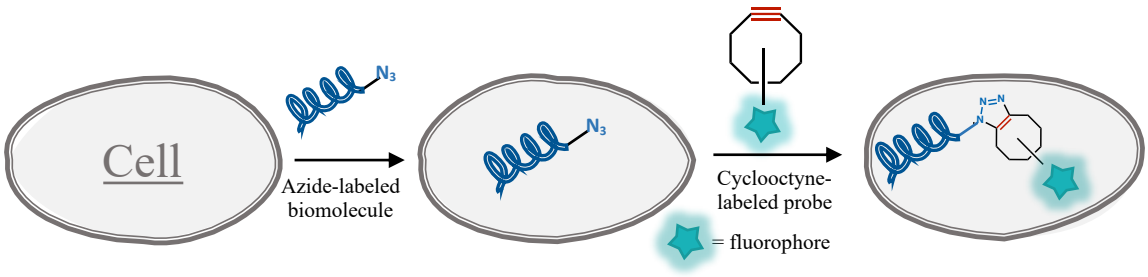

Figure 1.10 Schematic representation of biolabeling using SPAAC in situ cultured cell.

1.4.2 Nucleic acid click chemistry

Biolabeling makes click chemistry of high importance in the area of biomedical research.[85] The azide-alkyne cycloaddition is adopted for the synthesis and functionalisation of biomolecules for the development of varied series of biomaterials, such as stationary phases for bioseparation, site-specific modified proteins, delivery carriers, ON or protein microarrays, and modified cell surfaces.[102] The high versatility and the wide range of applicability of click chemistry are due to the following reasons:[103]

- The azide group and alkyne group can be incorporated into nucleic acids or any other biomolecules without significantly affecting their biophysical properties;
- Azides and alkynes react selectively without interfering with other functional groups found in nature;
- The triazole ring does not present toxic properties and also characterised by very high stability.

In particular, CuAAC has significantly affected the functionalisation of oligonucleotides. There are two available strategies for the attachment of labels to DNA:

pre- and post-synthetic modification.[104] The second, post-synthetic, method was identified as the best strategy for manipulation of nucleic acids. It is possible to label short oligonucleotides using alkyne-modified phosphoramidites in solid-phase synthesis because the azide-modified DNA is reduced by P(III) of the phosphoramidite group.[104,105] The first example of successful modification of DNA with Huisgen azide-alkyne cycloaddition was a 5′-alkylamino-modified DNA sequence that was treated with succinimidyl-5-azidovalerate to obtain an azide group at the 5′-terminus.[103,106]

An alternative approach for the functionalisation of nucleic acids is a two-step method involving the incorporation of the azide group into a ssDNA followed by the attachment to a glass surface *via* CuAAC for a sequencing-by-synthesis procedure. [104,107,108] Another method for DNA surface-immobilisation of DNA involves the use of alkyne-modifed ONs at the 5′-OH group and a gold surface functionalised with the azide-groups.[109] The Reinhoudt group developed another procedure involving a polydimethylsiloxane stamp covered with alkyne-modified ONs imposed onto an azide-functionalised glass performing the click chemistry under pressure without the assistance of Cu(I).[110]

CuAAC can be exploited for the preparation of complex DNA-protein conjugates. For example, Di Stefano *et al.* tethered the tetrapeptide CVIA green fluorescent protein (GFP) using the enzyme farnesyltransferase for the development of the azide-modified isoprenoid diphosphate, followed by treatment with ssDNA bearing an alkyne-group.[111] An interesting strategy of doubly labelled DNA strand has been developed by Brown and El-Sagheer. The method involved the solid-phase synthesis of 5'-alkyne modified ssDNA, followed by the coupling with succiminidyl-4-azidobutyrate for the conversion of the amino-linker at the 3'-terminal into an azido-group.[112] Click chemistry can be employed also for the labelling of oligonucleotides with fluorescent dyes, sugars, peptides and other groups, or for the generation of cyclised DNA, hybrid structures oligonucleotides-PNA and analogues of ssDNA with modified nucleobases and backbones (*cf.* **Figure 1.11**).[113]

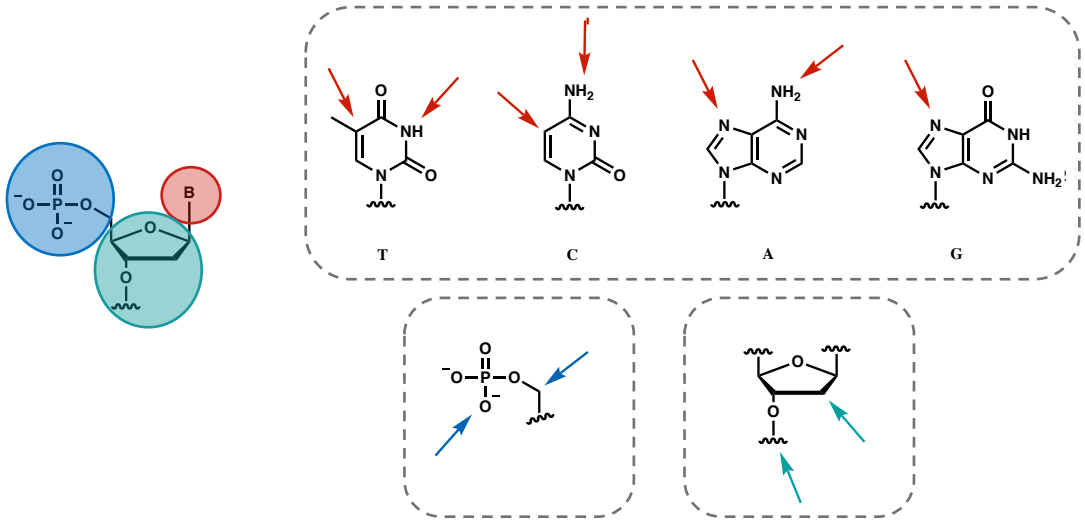

Figure 1.11 Sites of DNA modification for the insertion of alkyne group.

The selection of alkyne group is important to achieve an efficient click reaction. An alkyne functional group can be attached to different locations on DNA (**Figure 1.11**), but in a study using modified dU conducted by the Carell group, it was found that functionalising an alkyne group with a hexynyl spacer provides better results than when the group is directly incorporated to the nucleobase.[114] To introduce alkyne functionality, it is possible to exploit appropriately modified non-natural nucleobases. In this area, an important contribution was provided by the Seela group, specifically concerning oligonucleotides containing alkyne-labelled 7-deazapurines.[115] From this study it was found that non-nucleoside post-synthetic click-conjugation to a non-fluorescent 3-azido-7-hydroxycoumarin gives strong pH-dependent fluorescence. Moreover, Seela also employed click chemistry to introduce two fluorescent labels into a single thymidine unit generating a bis-coumarin oligonucleotide that was less fluorescent than a singly labelled derivate.[116] Another example of multi- and sequential labelling is provided by the Carell group with the generation of DNA strands containing TMS- and TIPS-protected alkyne 5-alkyne-2'-deoxycytidine analogues for the conjugation of two or three fluorophores (**Figure 1.12**).[117] Similarly, the Morvan group performed multilabelling of oligonucleotides with carbohydrates using microwave-assisted click chemistry.[118]

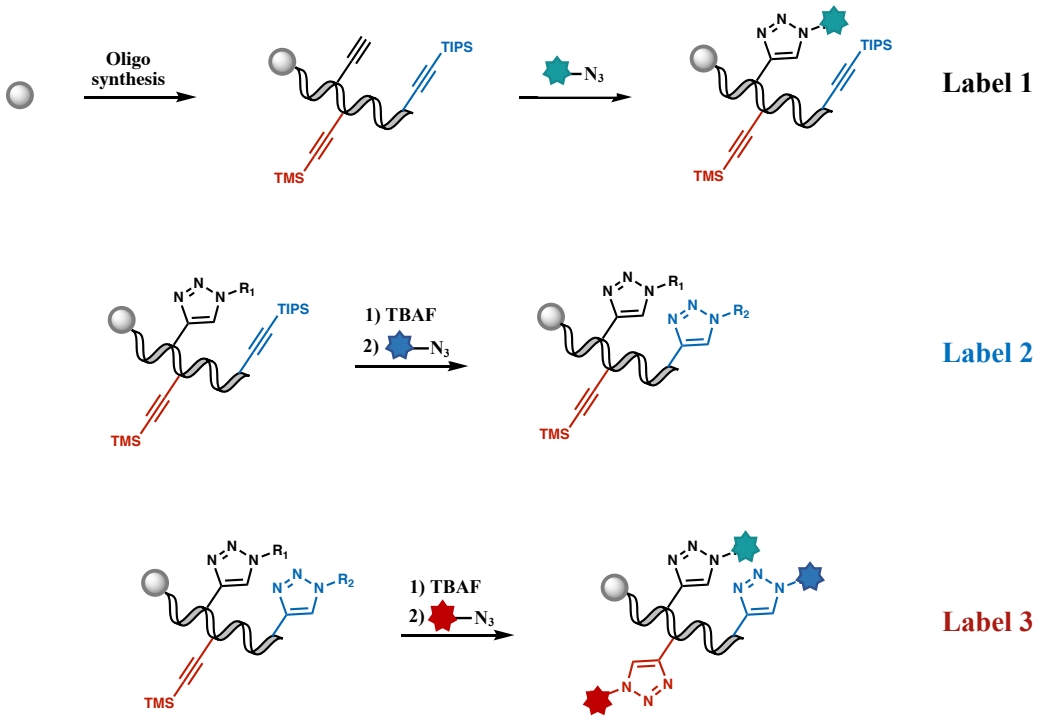

Figure 1.12 Selective multi-labeling of single DNA strand using post-synthetic strategy using TMS- and TIPS-protected alkyne (TMS = trimethysilyl; TIPS = triisopropylsilyl).

Click chemistry was also employed for the generation of DNA analogues with backbone modifications due to the incorporation of triazole units. For example, nucleobase analogues containing a triazole ring between the 2′-deoxyribose and the nucleobase have been reported.[119] Here, the presence of the triazole ring as substitute of the N-glycoside bond was found to provide a duplex destabilising contribution with A and T derivatives. The exploitation of click chemistry was expanded to generate ODN analogues with phosphate-backbones fully replaced by clicked triazole-moieties (**Figure 1.13 A**).[120,103] The triazole-backbone significantly increased the duplex stability which arose from the rigidness of the π-rich triazole-rings and the removal of the charge repulsion. The triazole-backbone DNA was generated in a one-pot reaction using nucleosides with 5′-azide and 3′-alkyne groups. Another significant result is that the clicked triazole-moieties were successfully recognised and replicated by DNA polymerases. The versatility of click chemistry also allowed for the synthesis of oligonucleotide catenanes of pseudo-hexagonal geometry with each side consisting of a single turn of B-DNA[112] and cyclic mini-duplexes generated by a hairpin with a loop region consisting of hexaethylene glycol units.[121] Both artificial systems are characterised by very high thermal stability after the intramolecular click ligation. Furthermore, the cross-linked oligonucleotides were prepared using the one-step synthesis 'bis-click'[122]

protocol and the two-step 'stepwise click' method,[123] which allow the cross-linking to non-identical sequences with different length linkers. The influence of the triazole ring on duplex stability was investigated and it was found that the stacking of the triazole in the major groove induces a stabilising effect and the presence of mismatches promotes slight destabilisation.[124] Therefore, the Hrdlicka group investigated C2′-pyrene-functionalised triazole-linked DNA using the approach of 'universal bases'.[125] Here, it was demonstrated that this modified ON presented somewhat lower affinity for DNA and RNA targets but compensation was provided *via* pyrene intercalation.

The development of modified oligonucleotides is interesting because it can be employed for antigene and antisense therapy and to increase cellular uptake in comparison to other commonly modified oligos such as peptide nucleic acid (PNA),[126] locked DNA (LNA)[127–129] or morpholino oligonucleotide (MO)[130,131] (**Figure 1.13 B**).

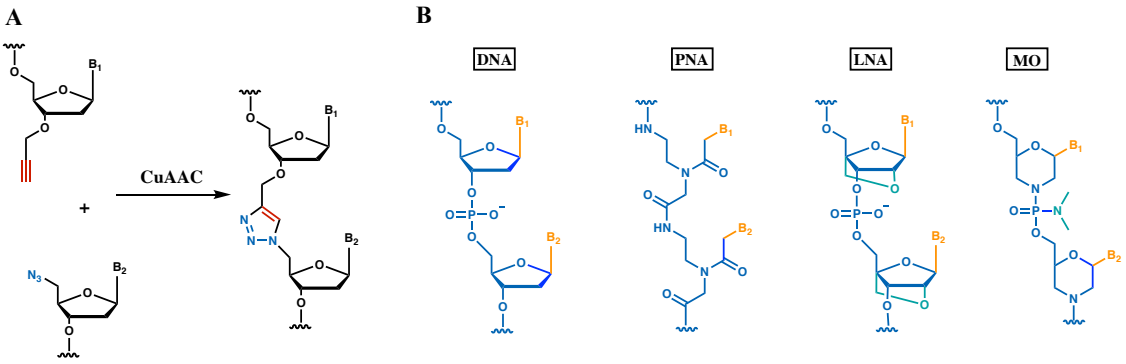

Figure 1.13 A) DNA analog with clicked backbone. **B)** Structural comparison of peptide-nucleic acid (PNA), locked DNA (LNA) and morpholino-oligo (MO) with DNA.

Finally, alkyne bearing nucleobases and also some azide bearing nucleobases were found to be compatible with phosphoramidite DNA synthesis and can be incorporated into PCR sequencing using type B thermostable polymerase, Deep *Vent exo*-DNA and KOD XL polymerase.[132] Type A polymerase such as Taq failed to recognise modified ONs.[103] A number of DNA analogues were synthesised using click chemistry, for example, artificial duplex and oligonucleotide catenanes endowed with a triazole-ring modified backbone, or systems bearing alkyne-functionality for the conjugation with fluorescent dyes, sugars and peptides.[104]

1.5.1 Triple-stranded DNA

DNA is present predominantly as a right-handed B-form duplex (**Figure 1.14 A**), but it is possible to find a wide variety of secondary structures. Other forms include A-DNA and Z-DNA, and more complex structures including G-quadruplexes[133] and Holliday junctions.[134] G-quadruplexes are formed by G-rich sequences and can be generated by the interaction of one, two or four DNA sequences (**Figure 1.14 B**).[135] Monomolecular G-quadruplexes are possible to find in telomeric regions, located at the ends of chromosomes, and in the transcriptional regulatory section of multiple genes and oncogenes.[136] The Holliday junction is a cross-shaped DNA structure containing four double-stranded arms joined together (**Figure 1.14 C**).[137] This secondary structure plays a key role in the process of genetic recombination, in particular for the repair of double-strand break (DSB).[138] Recently attention was focused on another secondary structure—triple-strand DNA due to its most promising therapeutic and antigene properties (**Figure 1.14 D**).[129]

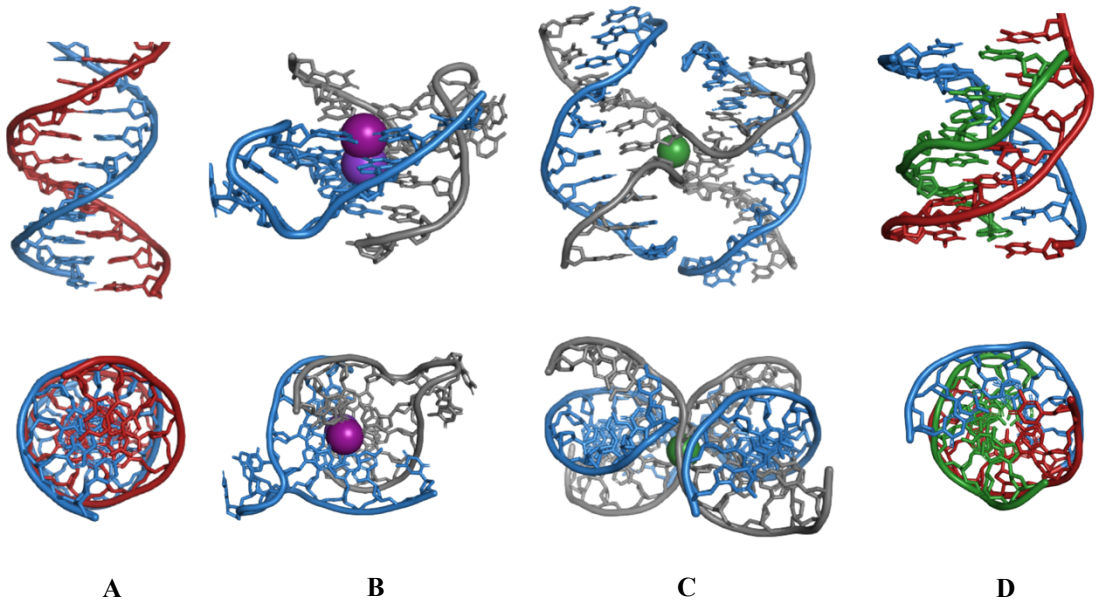

Figure 1.14 Secondary structures of DNA. **A)** Duplex (PDB code: 2M2C**). B)** G-quadruplex (PDB code: 1K8P). **C)** 4-way Holliday junction (PDB code: 1DCW). **D)** Triplex (PDB code: 1D3X).

In previous studies, 97.8% of all human genes were identified to have at least one potential triple helix forming nucleotide sequence in the promoter or gene sequence and 86.5% have a unique sequences for potential triplex formation[139,140] Triple-stranded DNA forms intermolecularly between three nucleic acid strands or intramolecularly between an antiparallel duplex DNA helix and a third strand. Triplex forming oligonucleotides

(TFO) are usually polypyrimidine strands that interact with polypurine-rich duplexes, specifically in the major groove at the Hoogsteen face of base-pairs through H-bonds (**Figure 1.15 A**). Based on the orientation of the third strand it is possible to identify two categories of triplexes: *(i)* parallel and *(ii)* anti-parallel triplexes (**Figure 1.15 B**). The triads in parallel triplexes form the following motifs; (TA-T), (CG-C^+) (the cytosine is protonated in the third strand) where Hoogsteen bonds stabilise the duplex-TFO interaction (**Figure 1.15 C**). Less common triads (CG-G) have been found to form in supercoiled plasmids, where TFOs are particular sensitive to salt concentrations.[141] Switching (CG-C^+) with (CG-G) can be promoted in the presence of magnesium.[142,143] In the antiparallel triplexes, the third strand forms a reverse Hoogsteen pair with the duplex generating the triplets: (TA-T), (CG-G) and (TA-A) (**Figure 1.15 C**). Hoogsteen triplexes are more stable than reverse-Hoogsteen because the triplets formed are structurally isomorphic leading to the superimposition of the anomeric carbons involved in the Watson-Crick base pair.[144] Since the positions of the anomeric carbons of the third strand are almost identical, the backbone distortions between adjacent triplets are minimised and the formation of the triplex provides just a slight perturbation of the overall duplex structure.[144] Parallel TFOs can discriminate single base duplex mismatches. For example, it is known that centrally placed mismatches have higher destabilising effects in comparison to terminal mismatches.[145,146,144] In contrast to that, nucleobase mismatches increase the dissociation speed without any influence on the annealing of parallel triplexes. Inversion sites on the third strand do not prevent the formation of triple helices and the affinity can be improved adjusting its length, incorporating stabilising nucleoside analogues, adding triplex-stabilising molecules, such as triazole orange (TO)[147] or benzoquinoquinoxaline (BQQ),[43] or increasing the concentration of Mg^{2+}.[142] The kinetics of triplex formation and duplex formation are significantly different. For example, it is known that the rate of triplex formation is about three orders of magnitude slower than duplex formation and the hybridisation to the Hoogsteen face of DNA is likely promoted by a nucleation-zipper mechanism.[144,145,148] At first instance there is the formation of a quasi-stable intermediate with a limited number of triplets, followed by the 'zippering' of the remaining of the strand around the duplex [145] TFOs introduce limitations to the flexibility of the DNA, affecting the recognition for specific proteins along the major groove and altering the mechanisms controlling DNA function. Overall, the specificity of the recognition process and ease of

sequence design makes TFOs excellent candidates for gene-therapy and diagnostics applications.

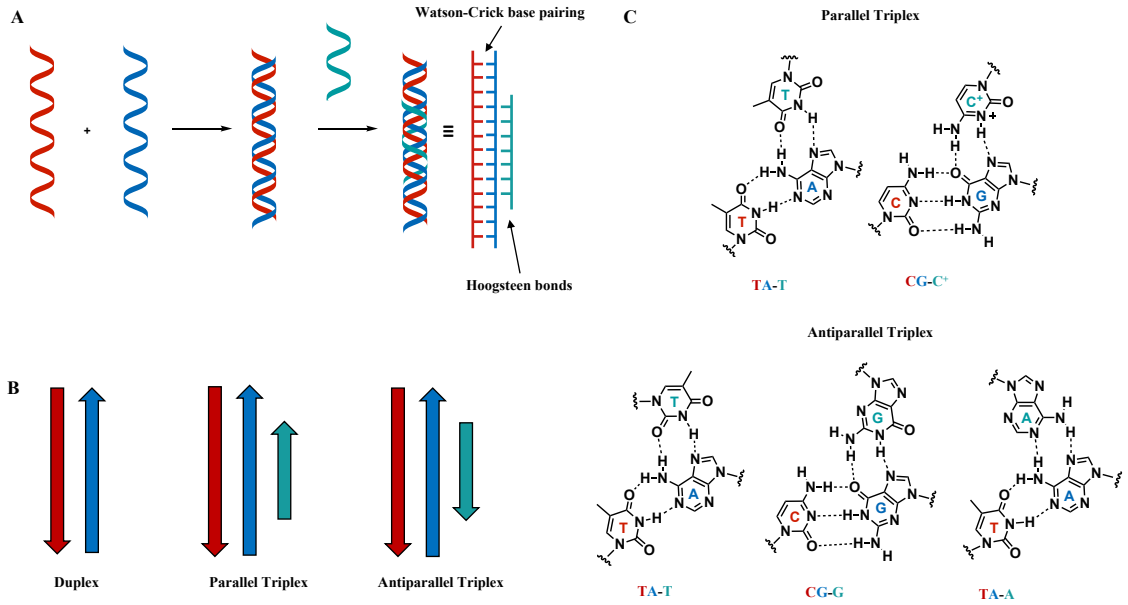

Figure 1.15 A) Schematic representation of Watson-Crick and Hoogsteen interactions in a triple helix. **B**) Parallel and antiparallel triplex formation of the TFO indicated by the green arrow. **C**) Illustration of triplets involved in parallel (TA-T, CG-C^+) and antiparallel triplexes (TA-T, CG-G, TA-A)**.**

1.5.2 Stabilising triplexes

Despite their remarkable potential, parallel triplex technology presents some limitations mostly related to pH-dependence, due to the necessity of protonated cytosines and reduced stability at physiological pH, sequence restrictions limited to polypurine tracks in the duplex-target, sensitivity to nucleases and intracellular delivery to nuclei.

Recently, several methods were successfully established using a variety of novel base, sugar and phosphate modifications to improve the stability of triplexes. To generate pH-independent parallel triplexes and consequently to improve the thermal stability it is possible to directly modify the cytosine or the sugar-phosphate backbone. For the first method, several molecules were employed such as 5-methylcytosine (**Figure 1.16 A**),[149] 6-oxocytosine[150] and its methyl derivative (**Figure 1.16 B** and **C**),[150] or 2′-O-methylpseudoisocytidine (**Figure 1.16 D**). In particular, 5-methylcytosine was the first molecule reported for the elimination of pH dependence in parallel triplexes and is frequently used.[149] In addition, parallel triplexes modified by 5-methylcytosines are more stable than antiparallel triplexes at physiological concentrations of K^+.[151]

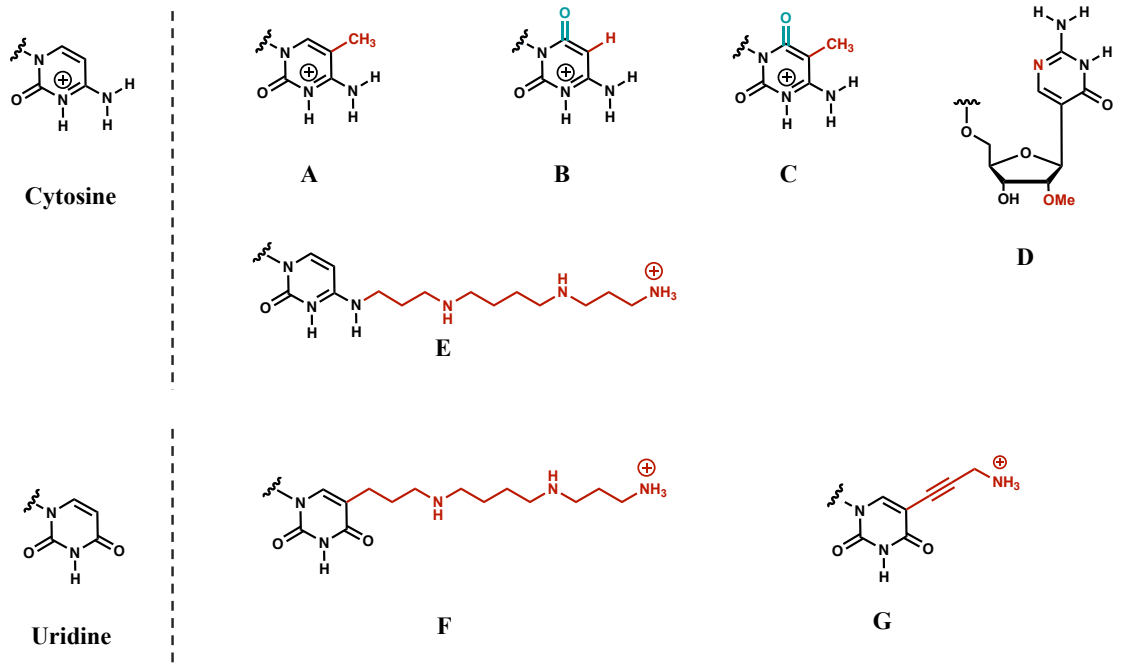

Figure 1.16 Molecular structure of **A**) 5-methylcytosine, **B**) 6-oxocytosine, **C**) 5-methyl derivative of 6-oxocytosine, **D**) 2′-O-methylpseudoisocytidine, **E**) 5-methylcytosine functionalised with spermine group, **F**) uracil functionalised with spermine group (U^S), **G**) uracil functionalised with spermine 5-propargylamino group (APdU).

Another strategy to enhance thermal stability is the introduction of positive charges as the negative charge density from the phosphate moieties is increased by 50% after triplex formation, thereby amplifying the charge repulsion.[129] In view of this, the methylcytosine and uracil were functionalised with a spermine group (**Figure 1.16 E** and **F**).[152,153] This modification provided enhanced triplex stability under physiological pH but lower sequence-selectivity. Another strategy was aimed at optimising the stability of the triplet TA-T introducing a 5-propargylamino group to uracil (APdU, **Figure 1.16 G**) by locating a positive charge at the 5-position of dU which avoids the positive charge interfering with the nucleobase-stacking.[154] Triplexes functionalised with multiple substitutions of APdU still present pH dependence, but its denaturation temperature is higher than the unmodified triplex analogue, indicating that in the π-stacking there is higher stabilisation due to the presence of the charge in the major groove.

The design of TFOs may also be optimised by introducing modifications on the backbone of the nucleic acid. Here, the phosphate diester bonds were initially substituted with a 3′→5′-methylphosphonate group. TFOs fully substituted with methylphosphonate groups were destabilised by the modification,[155] but interestingly oligonucleotides

alternating methylphosphonate groups and unmodified phosphates displayed higher stability. Consequently, the O3′–P bond was replaced with N3′–P constraining the N-type sugar conformation and increasing the binding by two orders of magnitude at neutral pH.[156]

Another approach involved the full replacement of the sugar-phosphate motif using morpholino-ring moieties and PNA. In the first example, the sugar moiety and the phosphodiester linkage are substituted respectively by a six-membered morpholino ring (**Figure 1.13 B**) and a phosphorodiamidate.[130,131] The second example of modified backbone was abovementioned and consists of the full replacement of the sugar-phosphate backbone with an uncharged peptidic structure composed of repeating (2-aminoethyl)glycine units linked by methylene bridges to the nucleobases.[126] PNA interacts with DNA differently from an unmodified ON and is highly dependent on the ratio of PNA:DNA. In the presence of two molecules of PNA, the peptide nucleic acid strands interact with the target *via* duplex invasion displacing a strand of the target and providing double-invasion. A clear example is provided by the non-covalent hybrid Ce(IV)/EDTA with pcPNA, that performs the cleavage of two ssDNA strands due to the double duplex invasion. If the ratio of PNA:DNA is 1:2 the modified oligonucleotide can still perform duplex invasion or provides simple triplex formation. Despite the low solubility of PNA sequences, the resulting triplexes are extremely more stable than the relative unmodified triplex due to the absence of negative charges.

The most common backbone modification involves the insertion of an additional two carbon bridge connecting the 2' oxygen and 4' carbon or 5' carbon of the ribose moiety. The sugar moieties of nucleic acids can adopt N- or S-type configurations (**Figure 1.17 A)** and the bridge restricts the sugar to an N-type configuration inducing the formation of a more stable triple helix.[157] Oligonucleotides with this type of backbone modification are known as locked nucleic acid (LNA or bridged nucleic acid—BNA, **Figure 1.17 B**).[130,158] Remarkable stabilisation was observed in LNA modified TFOs, but only when every 2-3 nucleotides were replaced by an LNA.[159,160,129] To overcome this restriction, LNA analogues were developed by introducing an ethylene bridge (ENA, **Figure 1.17 B**),[161] an O-N bond (BNA^{NC}, **Figure 1.7 B**), which provides higher nuclease resistance,[162] or replacing the O-P bond with an N-P bond (3′-amino-2′,4′- BNA, **Figure 1.17 B**).[163,164] Leumann *et al.* generated locked nucleic acids with a 2′-O, 5′-C bridge to constrain the sugar moiety in S-type conformation with bicyclo-DNA (**Figure 1.17 B**) or

in N-type conformation with tricyclo-DNA (**Figure 1.17 B**).[165] Other backbone modifications have employed two strands with inverted sequence directions (3'-5' → 5'-3') connected by intercalating linker to generate a 5′–5′-linked alternate Hoogsteen triplex with high thermal stability at physiological pH.[166,167]

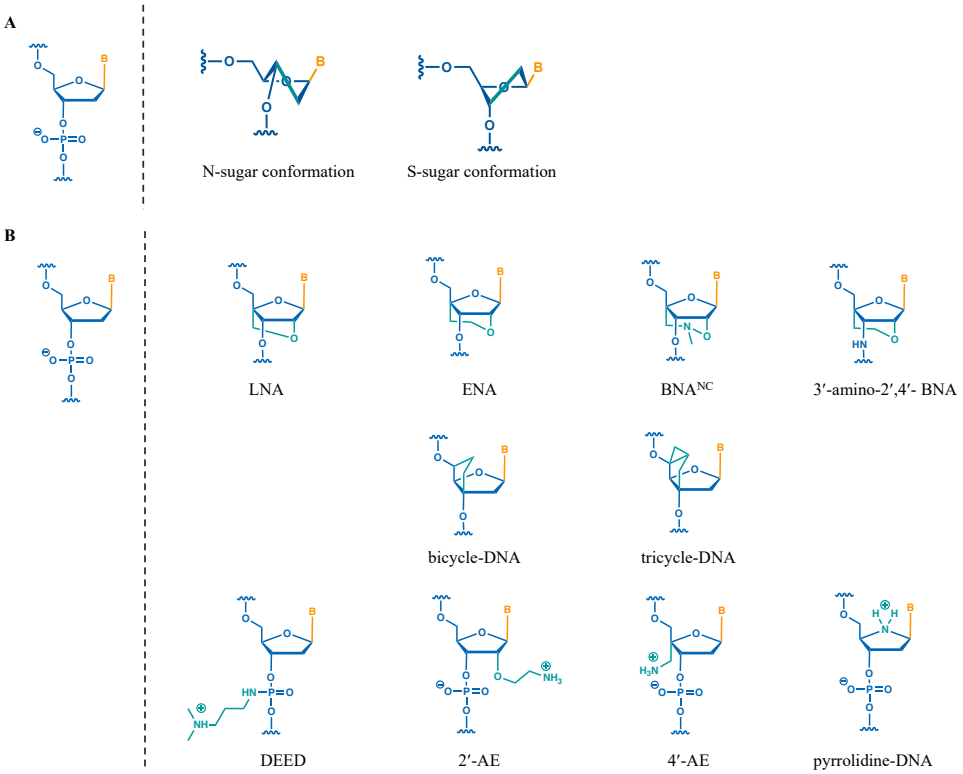

Figure 1.17 A) N- and S-sugar conformation. **B**) Molecular structure of LNA/BNA, ENA, BNA^{NC}, 3′-amino-2′,4′-BNA, bicycle-DNA, tricycle-DNA, phosphate residue with *N,N*-diethyl-ethylenediamine linkage (DEED), sugar moieties with amine group at 2′- or 4′- position (2′-AE, 4′-AE), and pyrrolidine-DNA.

Cationic groups can also be incorporated in the phosphate, sugar or base moieties of TFOs to partially alleviate charge repulsion. The addition of the positively charged guanidinium linkages[168] or the replacement of a phosphate residue with *N,N*-diethyl-ethylenediamine linkage (DEED, **Figure 1.17 B**) showed noticeable stabilising effects[169] and were found to be more stable than the relative duplex.[170] Sugar moieties can be further modified by introducing a positively charged primary amine to the 2′- or 4′-position (**Figure 1.17 B**), which provided an enhanced stability at pH 7.[171] Another approach involved the replacement of the furanose oxygen with nitrogen producing pyrrolidine oligonucleotides (**Figure 1.17 B**), which showed varying stabilisation properties depending on the base.[172,173]

In an attempt to combine the stabilising properties of APdU with a sugar modification, a *bis*-amino nucleoside (BAU, **Figure 1.18 A**) was generated.[174] In the presence of duplex mismatches and GC inversion (GC-T), BAU did not show stabilisation effects but exhibited a great base pair selectivity for TA (TA-BAU) producing very stable TA triplets.[175] The enhanced sequence-selectivity is explained by the slow dissociation kinetics for TA compared with other base pairs.[176] The disadvantage of employing positively-charged nucleoside analogues in modified TFOs are side-reactions of the amine-groups in the oligonucleotide synthesis and deprotection reactions. Compensating for this limitation, 5-dimethylaminopropargyl-dU (DMAPdU, **Figure 1.18 B**) was prepared.[177] This modification contains dimethylamines in place of the amine groups providing the triplex with higher stability than those containing T but lower stability than those containing the equivalent amine modification. This destabilisation is probably due to the interference of the TFO-interaction by the steric hindrance of the methyl groups and the removal of hydrogen bond donor interactions. However, the main issue of using positively charged TFOs is their propensity for off-target binding.

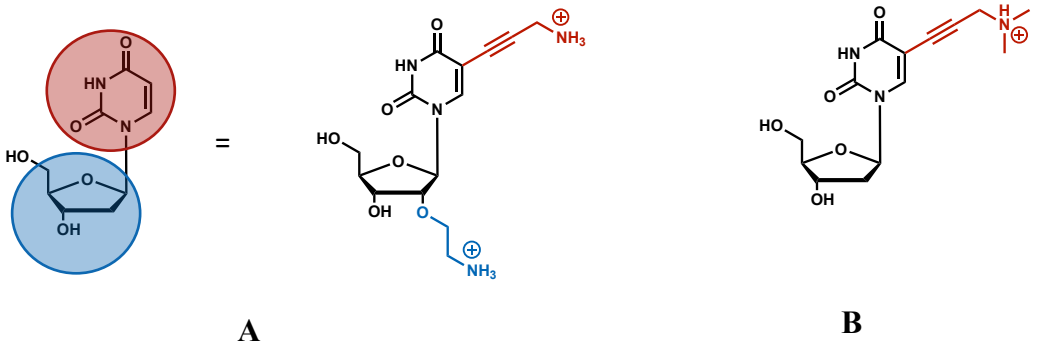

Figure 1.18 Uridine with 4′-AE and APdU modifications—BAU (**A**) or DMAPdU (**B**).

Another promising approach is the insertion of DNA intercalators into TFOs as this provides a noticeable contribution to the stabilisation of parallel triplexes. Pyrenyl-based intercalators are well known to be capable of inducing stabilisation in nucleic acid and worked as a starting point for the design of intercalator-modified ONs. In particular, intercalating nucleic acid (INA, (*S*)-1-O-(1-pyrenylmethyl)glycerol, **Figure 1.19**) displayed triplex-stabilisation, but was mainly employed for DNA duplexes. INAs stabilise DNA but not RNA and can be inserted as a bulge into the phosphate backbone of nucleotide sequences or preferentially in terminal positions of oligonucleotides as it induces higher stabilisation.[178] It is also possible to insert two INA molecules for an enhanced effect however they should be placed with at least one nucleotide apart.

Increasing the distance between the two DNA intercalators in the sequence results in noticeably higher thermal stability of the triplex.[178]

If an INA molecule is designed to be directly in proximity of a nucleotide mismatch, it can cancel the destabilising effect of this nucleotide mismatch.[179] However, if the INA molecule is introduced one or more nucleotides away from the mismatch site in the same sequences, the mismatch discriminative effect is reinstated. Two INA molecules can also provide a negative contribution to the thermal stability of an antiparallel duplex if they are inserted into the two nucleotide sequences directly opposite each other.[180] The design of DNA intercalators which act as stabilisers of Hoogsteen type parallel triplexes are called twisted intercalating nucleic acids (TINA, **Figure 1.19**).[181] In particular, (*R*)-1-O-[4-(1-pyrenylethynyl)phenyl-methyl]glycerol (*para*-TINA) and (*S*)-4-(4-(1H-Phenanthro[9,10-d]imidazol-2-yl)phenoxy)butane-1,2-diol (AMANY)[182] were generated to thermally stabilise parallel double and triple helices (**Figure 1.19**).[183]

A study involving the thermal stability of double helixes revealed that changing the attachment of ethynylpyrene functional group from *para* to *ortho*-TINA ((*R*)-1-O-[2-(1-pyrenylethynyl)phenylmethyl]glycerol) provided higher stabilising properties (**Figure 1.19**).[184] The use of *para*-TINA molecules has been extended to other DNA structures, such as antiparallel triple helices and G-quadruplexes.[182] The stabilising effect of DNA intercalators can also overcome some limitations associated with TFO design. As such, the incorporation of TINA monomers in G-rich oligonucleotides interferes with quadruplex formation thereby releasing the ON for antiparallel triplex formation.[185,186] Overall, the pH-independent stabilising contribution of these DNA intercalators and their preferential discrimination for the antiparallel triplex over the G-quadruplex structures make these TFOs potential tools for antigene therapy.

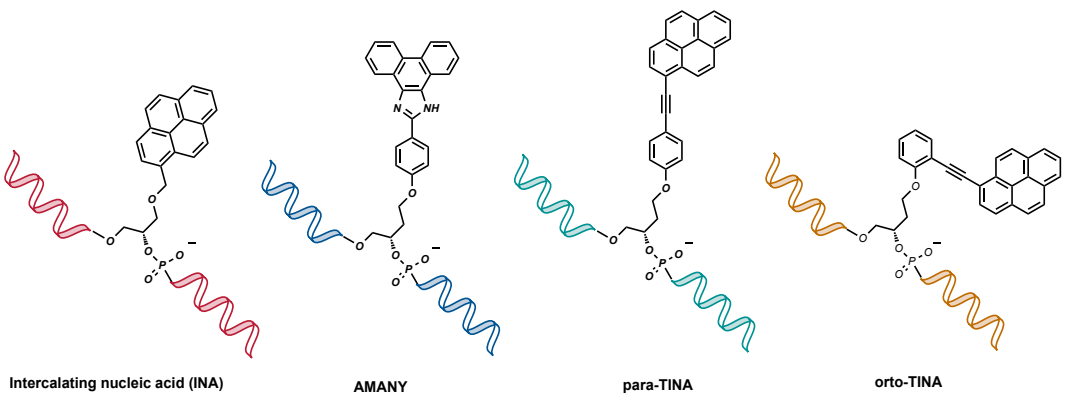

Figure 1.19 Structures of INA, AMANY, para-TINA and orto-TINA**.**

One other approach to modify TFO probes involves the use of DNA cross-linking agents. The most widely exploited is the photoactivated cross-linking agent 4,5,8-trimethylpsoralen (psoralen)[42] and when conjugated to ODNs, improves binding to the target site (although with a lower efficiency to DNA intercalating agents).[187] The advantage of using psoralen is the ability to form covalent bonds with pyrimidine bases when irradiated with UV light, covalently linking the TFO to the duplex target. 5-methoxypsoralen (5-MOP) and 4'-hydroxymethyl-4,5',8-trimethylpsoralen (HMT) (**Figure 1.20)** are two psoralen-based molecules predominantly used for coupling to TFOs and are capable of forming interstrand crosslinks (ICs, **Figure 1.20**) between opposite pyrimidines. The formation of crosslinking involves a two-step mechanism: firstly, the 4',5'-double bond of the furan ring forms covalent interactions with an adjacent pyrimidine; secondly, the adduct formed with the opposite pyrimidine using the 3,4-double bond of the pyrone ring. The coupling of psoralen to TFOs does not impede intercalation of the psoralen between bases and consequently the crosslinking. On the contrary, triplex formation is enhanced by the crosslinking and at the same time promotes IC activity to the vicinity of the triplex binding site.[188] Due to the targeting effects of TFOs, psoralen can adopt only one conformation where the furan ring is linked to a thymine in a predominantly polypurine-rich strand and the pyrone ring is linked to the thymine of the polypyrimidine-rich strand.[188,189,190] Regarding triplex stabilisation, 5-MOP with a C6-linker was observed to increase thermal stabilisation by 10 °C when conjugated to a 15 mer TFO.[191]

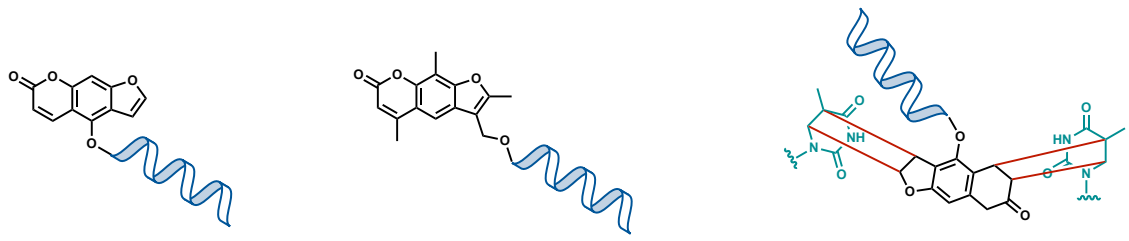

Figure 1.20 Structures of two psoralen molecule-modified TFOs (5-MOP-TFO and HMT-TFO) and schematic representation of ICs.

Crosslinking can be exploited for genotoxic, recombinagenic and mutagenic activities, and when combined with TFOs, selectivity can be introduced. Significantly, when attached to TFOs, psoralen showed no genotoxicity.[42] Recombinagenic activities of psoralen-TFO targeted adducts were also investigated but where it inhibited

homologous recombination very low levels of intermolecular recombination induced by psoralen-adduct were detected.[192] Interesting findings were furnished by the a mutagenicity study of psoralen-modified TFOs which showed up to 10% of induced mutagenesis when an SV40 *E. coli* shuttle vector carrying the SupF reporter gene was treated *in vitro* with the modified TFOs and transfected in COS or human cells.[189,193] Similar experiments were conducted confirming site-directed mutagenic activity and demonstrating that triplex formation could occur within cells.[194] Theoretically, photoactivated crosslinking with near-UV light should be irreversible, but studies of the psoralen-adduct repair mechanism supported that the repair of the lesion goes through NER (nucleotide excision repair) and EPR (error-prone repair) mechanisms.[42] Despite this, *in vivo* studies demonstrated the presence of a TFO seems to stop some steps of repair.[42]

1.6.1 Ruthenium complexes

Interest in ruthenium(II) polypyridyl complexes largely stems from photophysical and photochemical properties of these complexes towards luminescent imaging agents, therapeutics and theranostic agents. Ruthenium complexes can absorb visible light (700–400 nm) and emit at longer wavelengths within the red and near-infrared spectral regions and, in many cases, exhibit long luminescent lifetimes.[195,196] Additionally, ruthenium complexes can adopt different geometries that are easily tuned by the ligand design thereby allowing for the generation of suitable compounds for specific cellular targeting.[197–199] These ligands are typically σ donor, π donor and π* acceptor in nature. $[Ru(bpy)_3]^{2+}$ is the most widely studied Ru(II) polypyridyl complex and used as a template to explain the photophysical behaviour of ruthenium complexes.[200,201] This model involves the excitation of an electron leads to the metal-to-ligand-charge transfer (MLCT) followed by deactivation of the luminescent state by radiative and non-radiative decay to the ground state in competition with thermal population to the metal-centred antibonding state (MC) excited state. The MC excited state can repopulate the MLCT state, deactivate to the ground state or undergo a series of chemical reactions producing photo-adducts.[202]

Another widely studied ruthenium complex is $[Ru(Phen)_3]^{2+}$ (**Figure 1.21 B**) which presents binding affinity for duplex DNA with enhanced fluorescence upon semi-intercalation.[203] In addition, it was found by NMR and CD studies that both enantiomers, Δ-$[Ru(Phen)_3]^{2+}$ and Λ-$[Ru(Phen)_3]^{2+}$, bind duplex DNA in the minor groove with different binding modes and affinity.[204] Actually, Δ-$[Ru(Phen)_3]^{2+}$ binds using a semi-intercalative mode involving two phenanthrolines and with a higher binding constant than Λ-$[Ru(Phen)_3]^{2+}$, which interacts with DNA using only one phenanthroline. Despite the simplicity of the structure, $[Ru(Phen)_3]^{2+}$ found application as electrochemiolumiscent (ECL) biosensor owing to the higher stability and lower toxicity than the commonly use ethidium bromide.[205] For example, it was added to an oligo-sequence and combined with tetrahedron-structured DNA for the development of ECL biosensor of ATP.[206] Similar approach it was employed for the generation Hg^{2+} sensor.[207] Also ruthenium complexes with 2-phenylazopyridine or *o*-tolylazopyridine were initially investigated, but they only displayed modest antiproliferative properties.[208,209] Over time, numerous ruthenium complexes have been synthesised, but DPPZ- (DPPZ = Dipyrido[3,2-a:2′,3′-

c]phenazine, **Figure 1.21 C**) and imidazo-phenanthroline derivates ruthenium complexes attracted significantly the attention of scientists.

A peculiar property of DPPZ-ruthenium complexes is the exhibition of 'light switch' behaviour when interacting with nucleic acids making them optimal candidates for DNA probe development. In the presence of water, the luminescent properties of ruthenium complexes are attenuated or quenched but in hydrophobic environments its emissive abilities are restored. By interacting with DNA, complexes are protected by collisional quenchers (such as water) while DNA itself catalyses electronic transfer (ET) thereby leading to an enhancement of the photophysical properties. Solvent effects also have an impact on the photophysical properties of ruthenium complexes since luminescent activity is enhanced in hydrophobic solvents and quenched in aqueous or protic solvents. Ruthenium complexes are also affected by the pH of its microenvironment since protonation of nitrogen atoms of phenazine ligands likely deactivates ET.[210] The 'light switch' behaviour can also be considered as a result of the formation of a 'dark' excited state and 'bright' species[211,212] whereby the 'dark' excited state forms in water, is non-luminescent and rapidly deactivates while the 'bright' species is luminescent and found in non-aqueous environments. Exploiting the 'light switch' property of DPPZ ligand, the Barton group introduced -CO_2H, acetylene, -Br, and phenyl groups onto DPPZ ligand with the aim to generate $[Ru(bpy)_2(\text{DPPZ derivatives})]^{2+}$ more extended and/or laterally bulkier DPPZ in the attempt of optimising the DNA mismatch discrimination.[213] It was found that the luminescent response were not particularly affected by the presence of the functional groups. In addition, ruthenium complexes of DPPZ laterally modified simple groups (*e.g.* Br) did not enhance mismatch targeting. On the contrary, the introduction of bulkier modifications (e.g. chrysene- and pyrene-groups) did not allow mismatch discrimination probably due to the formation of aggregates. The derivative that provided interesting results was DPPN (benzo[*i*]dipyrido[3,2-*a*:2′,3′-c]phenazine), which displayed a relatively high discriminating properties at mismatch sites, which is indicative of a stronger DNA affinity and more efficient solvent-shield. In general, DPPZ is incorporated into ruthenium complexes in order to endorse DNA binding and to exploit the related selective emission. For example, the Keyes group developed Ru(II) DPPZ complexes linked to a nuclear localisation transcription factor NF-κB (NLS) for targeting the nucleus of HeLa cells for determining delivery to the nucleus.[214] DPPZ also displayed noteworthy

targeting properties when coordinated to the photo-reactive complex $[Ru(TAP)_2(DPPZ)]^{2+}$ (and derivatives) linked to ON sequences.[215] Whether DPPZ was directly connected to the sequence or acted as an ancillary ligand, the properties of the complexes were unchanged, but different DNA binding modes were found. In the first case DPPZ intercalated the target and in the second, the complex provided DNA-interaction *via* one of the TAP ligands. The different binding mode was aimed at bringing the metal center in proximity to the nucleobase target in both hybrids.

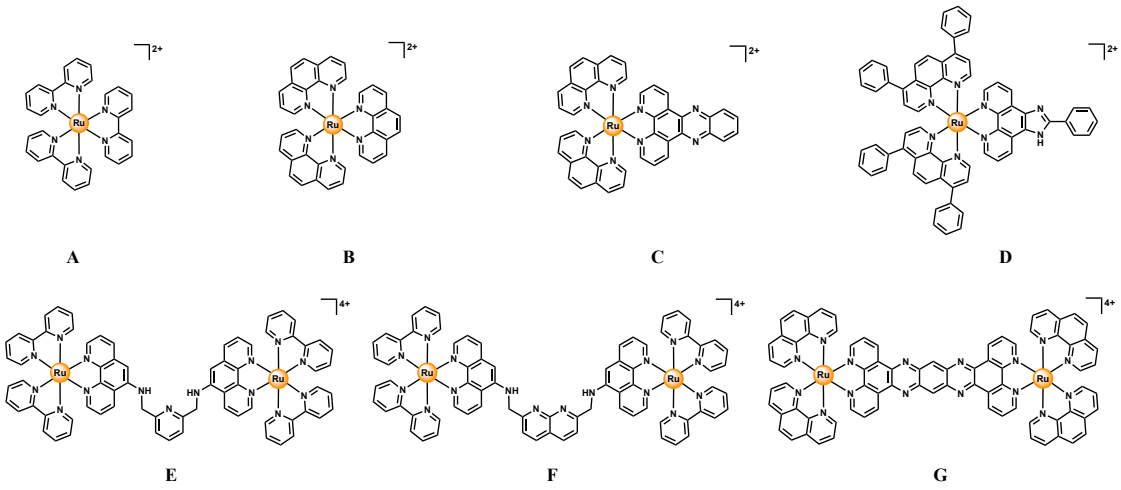

Figure 1.21 Molecular structures of **A**) $[Ru(bpy)_3]^{2+}$, **B**) $[Ru(phen)_3]^{2+}$, **C**) $[Ru(phen)_2(DPPZ)]^{2+}$, **D**) $[Ru(DIP)_2(PIP)]^{2+}$, **E**) $[Ru_2(bpy)_2(N,N'$-(pyridine-2,6-diylbis(methylene))bis(1,10-phenanthrolin-5-amine))$]^{4+}$, **F**) $[Ru_2(bpy)_2(N,N'$-((1,8-naphthyridine-2,7-diyl)bis(methylene))bis(1,10-phN,N'-((1,8-naphthyridine-2,7-diyl)bis(methylene))bis(1,10-phenanthrolin-5-amine))$]^{4+}$ and **G**) $[Ru_2(bpy)_2(tatpp))]^{4+}$.

Another class widely studied is ruthenium imidazo-phenanthroline complexes. They provide rapid responses to external stimulus and are particularly sensitive to variations in pH. Different analogs of imidazo-phenanthroline ruthenium complexes were employed for the generation of photo-synthesisers due to the tuneability of *on-off* emission switch by protonation of the imidazole-ring.[216] This property broadened the applicability of this class of complex into medicinal chemistry for the development of switchable molecular machines. For example, derivates $[Ru(DIP)_2(PIP)]^{2+}$ (DIP = 4,7-diphenyl-1,10-phenanthroline and PIP = 2-phenylimidazo[4,5-f][1,10]phenanthroline, **Figure 1.21 D**) displayed potential activity as mitochondrial anticancer agents.[217] The design of class of ruthenium complexes underwent to structural modifications, such as the introduction of fluorine and/or *t*-butyl-benzene-groups to increase the lipophilicity in order to improve bioavailability and membrane permeability.[218] Similarly to DPPZ analogues, PIP ruthenium complexes were modified replacing the phenyl-ring with

naphthyl-, anthryl- and pyrenyl-groups to enhance DNA binding.[219] This work showed that the derivatives with naphthyl- and pyrenyl-groups provided an increasing of MLCT signal along with the decreasing of DNA secondary structure due to DNA condensation.[219] Another strategy involved the increment of the nuclearity nuclear generating $[(bpy)_2Ru(bpibp)Ru(bpy)_2](ClO_4)_4$ and $[(phen)_2Ru(bpibp)Ru(bpy)_2](ClO_4)_4$ (bpibp = 4,4′-bis (1, 10-phenanthroline-[5, 6-d] imidazole- 2-yl)-biphenyl and bpy = 2,2-bipyridine), which were found to target c-MYC G-quadruplex DNA and have anti-proliferative activity against cancer cells.[220] To improve the targeting properties of this class of complex, they were conjugated to cell penetrating peptides (CPPs) in order to selectively target specific organelles in living cells.[198,221] In addition, the targeting properties were found to be tuneable also changing the ancillary ligands, for he $[Ru(LL)_2PIC]ClO_4$ system (where PIC = 2-(4-carboxyphenyl)-imidazo-[4,5-f][1,10]-phenanthroline) when hybrided to nuclear localisation transcription factor NF- κB (NLS) could be delivered to the nucleus when LL was bpy but was found in the nucleolus when LL was varied to DIP.[198]

However, like PIP-ruthenium complexes, Phen- and DPPZ-type *di*-nuclear complexes were synthesised.[208] For example, *di*-nuclear ruthenium complexes were prepared using bpy as ancillary ligands and connecting two phenanthrolines with a pyridinic[222] or 1,8-naphthyridinic ligands (**Figure 1.21 E** and **F**).[223] These molecules were designed to work as luminescent chemosensors of Hg^{2+} ions or Cu^{2+} / Fe^{3+} probes, respectively.[222, 223] Among the several *di*-nuclear ruthenium complexes with DPPZ derivatives using different ancillary ligands, the compound that provided more interesting results was $[(phen)_2Ru(tatpp)Ru(phen)_2](Cl)_4$ (tatpp = 9,11,20,22-tetraazatetrapyrido[3,2-*a*:2′,3′-*c*:3″,2″-1:2‴,3‴-*n*]pentacene) (**Figure 1.21 G**) given it displayed cytotoxic activity in aerobic and anaerobic conditions.[224]

However, ruthenium complexes commonly exhibit oxidation states of Ru(II) or Ru(III), which are easily switchable and are subject to ligand exchange.[197] Those properties play a key role in the functional principle of three promising anticancer drug candidates NAMI-A, TLD1433 and KP1339 (**Figure 1.22**).[225] Ru(III) complexes can also act as prodrugs until reduced to a more active Ru(II) form in a hypoxic environment, which is a distinctive characteristic of tumours.[226–228] The strategic activation of prodrugs is quite appealing due to spatial and temporal control for generating cytotoxic

molecules.[197] Owing to the versatility of the photophysical properties of ruthenium complexes, polypyridyl ruthenium complexes are excellent candidates for approaches *via* light irradiation[229] photodynamic therapy (PDT) and photoactivated chemotherapy (PACT).

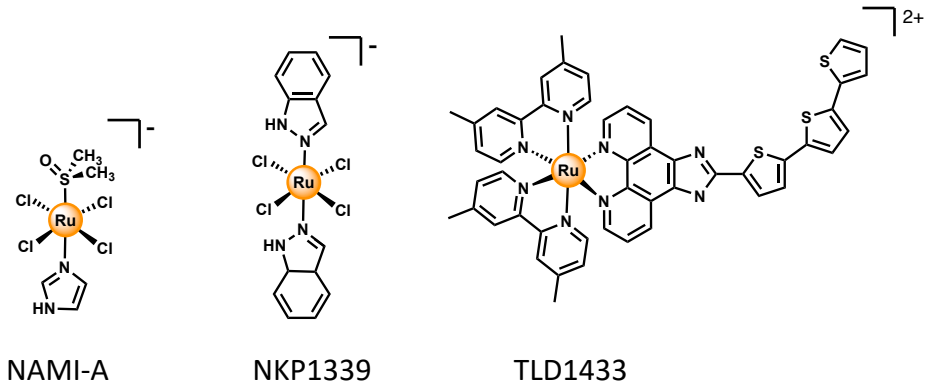

Figure 1.22 Molecular structures of NAMI-A, NK1339, and TDL1433**.**

PDT works through the cooperative actions of a photosensitiser (PS), molecular oxygen and light irradiation (**Figure 1.23**). Consequent to the light irradiation, PS is promoted to the singlet excited state $^{1}PS^{*}$ and undergoes to intersystem crossing (ISC) reaching the triplet excited state $^{3}PS^{*}$. The deactivation of the excited state with triplet character can occur through two different mechanisms: Type I and Type II. The first mechanism involves electron transfer with the surrounding biological substrates generating radical ions, which promptly react with molecular oxygen. In the type II mechanism, the interaction $^{3}PS^{*}$-substrates can undergo to proton exchange resulting in the generation of free radicals. In both cases, the reaction of the radical species with molecular oxygen leads to the development of cytotoxic reactive oxygen species (ROS). Another product of the energy transfer of $^{3}PS^{*}$ to molecular oxygen is the formation of its ground triplet state ($^{3}O_2$). At this point, $^{3}O_2$ can deactivate the excited triplet state of the photosynthesiser forming highly reactive singlet oxygen ($^{1}O_2$).

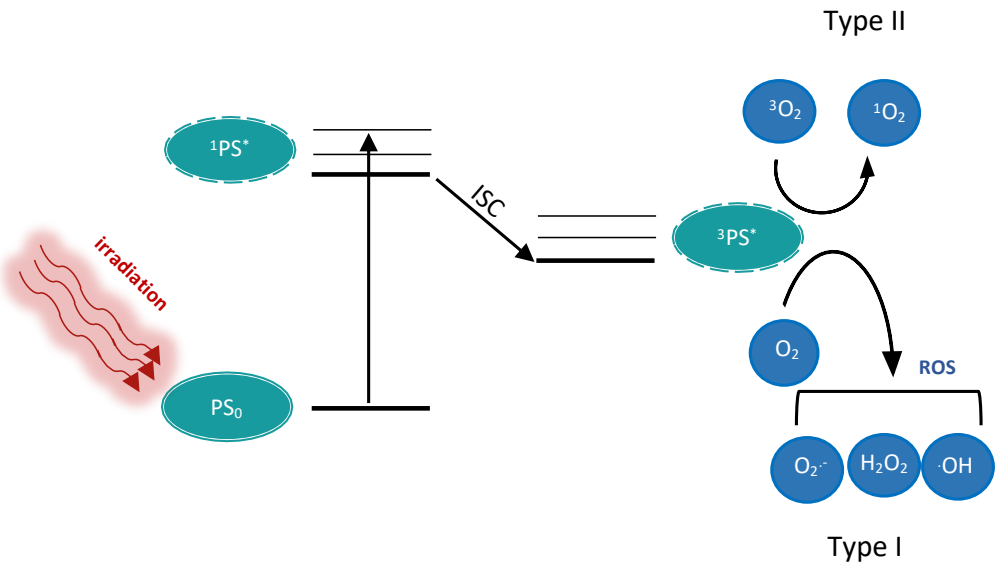

Figure 1.23 Schematic illustration of photodynamic therapy (PDT): excitation by light irradiation of the photosensitiser (PS) to the singlet excited state (^{1}PS*), converted by intersystem crossing (ISC) into the triplet excited state (^{3}PS*) which interacting with molecular oxygen can bring to the development ROS species (Type I) or with ground triplet state oxygen ($^3O_2$) can generate the highly reactive singlet oxygen species, $^1O_2$.

Whereas PACT does not rely on an oxygen-dependent mechanism, it can be consequently employed for treatment of diseases under hypoxic environment. PACT prompts cell death by ligand ejection, caging approaches or DNA crosslinking. In both therapies guanosines is the nucleoside target as the PDT mechanism involves DNA intercalation followed by the photocleavage *via* oxidative damage of guanosines[230] and in PACT ruthenium complexes can form cross-links with guanosines.[229] In particular, photo-binding has attracted significant attention leading to the selection of potential candidates for cancer cells which have acquired resistance to cisplatin.[231] Ruthenium complexes of 1,4,5,8-tetraazaphenanthrene (TAP) display an ability to form photo-adducts by cross-linking.[232,233] A covalent bond is formed between the exocyclic amine-group of guanine and one of the TAP ligands, which was promoted by the radical recombination of the ruthenium complex and the aromaticity restoration of the guanine.[233,234,235]

1.6.2 Ruthenium-DNA interaction

The interaction of a molecule with DNA can be covalent or non-covalent. Non-covalent binding has attracted significant attention, specifically in the study of metallo-intercalators. Three main categories can be identified here: external electrostatic binding,

groove binding and intercalation (along with semi-intercalation). External electrostatic binding is usually non-specific and the distribution of the small molecules is regulated by the negative charges of the phosphate groups of the DNA backbone. An example of external electrostatic DNA binding is reported in **Figure 1.24 A** with K^+. Groove binding can occur in either the major or minor groove. Generally, proteins interact with DNA in the major groove and small molecules binding in the minor groove.[236] In some cases, small molecules such as DAPI (**Figure 1.24 B**)[237,238] can be sequence-selective as a combined result of hydrogen bonding, hydrophobic contacts and specifically positioned electrostatic interactions. Intercalation involves the insertion of molecules between adjacent bases of DNA, causing elongation of DNA around one base with local helix winding. The mechanism of binding *via* intercalation is often complex due to diffusion of the intercalator to DNA as it moves to detect possible binding sites (an example of DNA intercalation with 1R-trans-anti-Benzo[c]phenanthrene is shown in **Figure 1.24 C**).

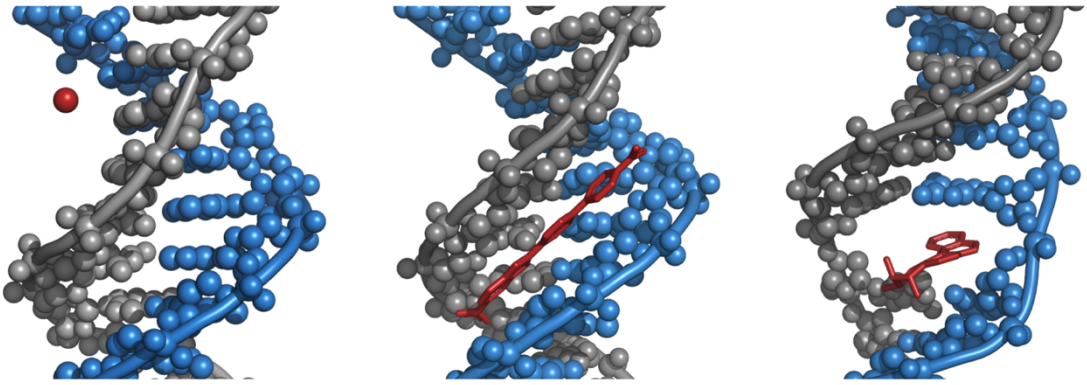

Figure 1.24 Non-covalent binding. **A)** external electrostatic binding with K^+ (PDB code: 1FQ2). **B)** Minor groove binding with DAPI (PDB code: 2B0K). **C)** Intercalation with 1R-trans-anti-Benzo[c]phenanthrene (PDB code: 2ROU).

Octahedral ruthenium complexes can bind DNA in different modes, with the predominant one being intercalation. The positive charge and the extended aromatic and hydrophobic ligands are driving forces of the good intercalative properties of ruthenium complexes. An early experiment with $[Ru(phen)_3]^{2+}$ demonstrated that there is enantio- and orientational preference in the "handness" with DNA.[239] Both enantiomers probably bind through "quasi-intercalation" without separation of base pairs, partly intercalating one phenanthroline edge into DNA.[240] Increasing the aromatic extension of phenanthroline and phenanzine ligands, such as $[Ru(phen)_2(DPPZ)]^{2+}$ (**Figure 1.25 A**

and **B**) and $[Ru(bpy)_2(DPPZ)]^{2+}$ (bpy=2,2-bipyridine), found a deeper intercalation between base pairs with DNA unwinding and drastic changes of the luminescence properties of the ruthenium complexes.[236] Computational studies on $[Ru(bpy)_2(DPPZ)]^{2+}$ showed that the emission was a balance between bright ^{3}MLCT states located on bpy and dark ^{3}MLCT and ^{3}IL states on DPPZ.[241,242] A different trend was observed in $[Ru(phen)_2(DPPZ)]^{2+}$, where the Δ enantiomer was found to be around 6-10 times more luminescent than the Λ.[243] Another interesting behaviour due to this interaction with DNA is provided by the complex $[Ru(TAP)_3]^{2+}$. The complex undergoes to enhanced luminescence when only interacting with poly[(A-T)].[244] Several investigations with $[Ru(LL)_2DPPZ]^{2+}$ (LL= bpy, phen, TAP) were performed for the identification of different binding modes of single enantiomers or racemic mixtures.[245] The Λ enantiomer always contacts the 3′ side of the sugar of the intercalation cavity[246] and can adopt two different intercalative modes: angled and symmetrical.[245] The angled mode was observed at different DNA steps, such as CC/GG, TC/GC and TT/AA and can occur by two different orientations aimed to maximise the purine-DPPZ stacking interaction. The symmetrical intercalation is specific for the TA/TA step provoking a twist angle of 40 Å and packing of the ancillary ligand (phen and TAP) against the sugar (**Figure 1.25 C**).[247] Δ enantiomers of $[Ru(bpy)_2(DPPZ)]^{2+}$ and $[Ru(phen)_2(DPPZ)]^{2+}$ were studied, where semi-intercalative binding mode was also observed.[248,249] In particular, $[Ru(bpy)_2(DPPZ)]^{2+}$ was found to bind A/A mismatches in the minor groove flipping out the adenine bases and stacking them onto the ancillary ligands with increased fluorescence intensity.[248] $[Ru(phen)_2(DPPZ)]^{2+}$ was found to have an affinity for well-matched DNA sequences displacing the T/A base pairs (**Figure 1.25 E**).[249]

DNA binding with racemic compounds was investigated due to difficult and expensive technique of chiral separation.[245] The racemic mixture of $[Ru(phen)_2(DPPZ)]^{2+}$ was investigated in the interaction with DNA (**Figure 1.25 D**).[250] Both enantiomers bind in the minor groove of DNA, but with different geometries and each complex has different DPPZ solvent accessibility.[250] In the Δ enantiomer one nitrogen of DPPZ is shielded by the water molecules, but in the Λ enantiomer both nitrogen atoms are accessible and consequently, the Λ enantiomer is less luminescent than the Δ enantiomer. It was identified that the variation of luminescent intensity follows the trend: Δ < *rac* < Λ.[250]

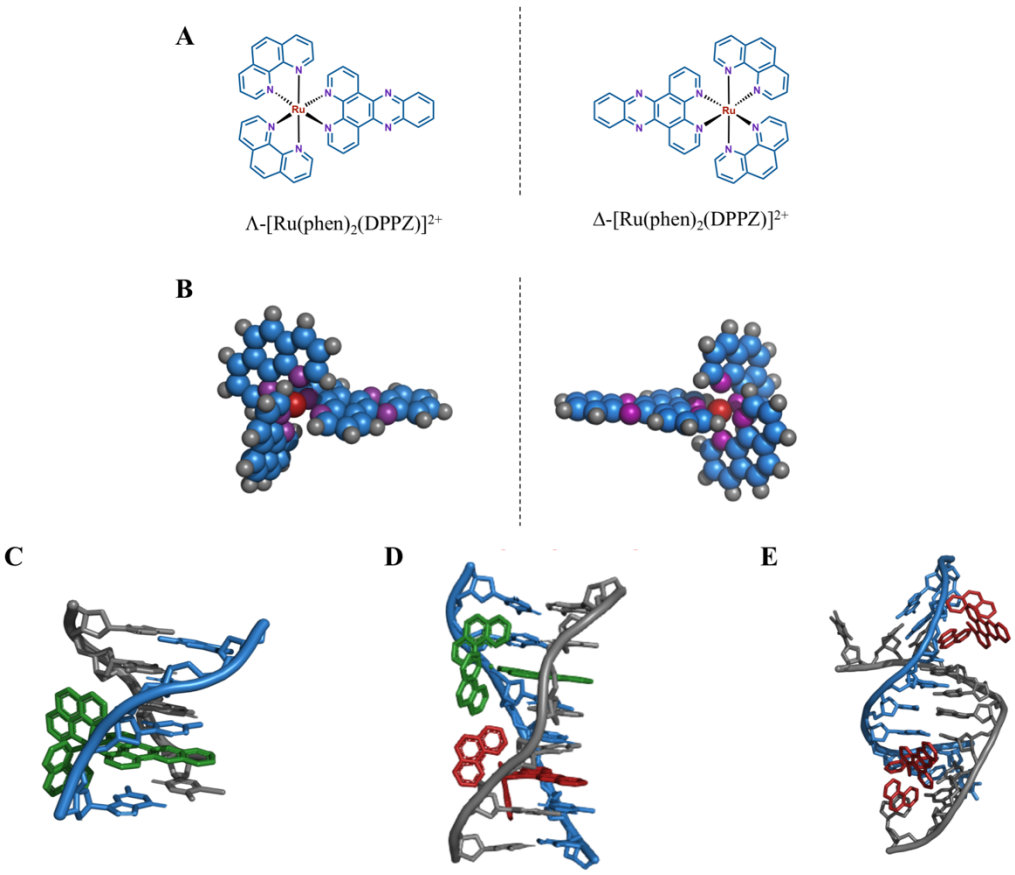

Figure 1.25 A) Molecular structure of Λ- and Δ-$[Ru(phen)_2(DPPZ)]^{2+}$. **B)** Crystal structures of the two enantiomers (Λ-$[Ru(phen)_2(DPPZ)]^{2+}$ PDB code: 4E7Y and Δ-$[Ru(phen)_2(DPPZ)]^{2+}$ PBD code: 5JEU). **C)** Λ-$[Ru(phen)_2(DPPZ)]^{2+}$ bounds to a short substitute DNA sequence (PDB code: 5LFW). **D)** DNA binding with a racemic mixture of $[Ru(phen)_2(DPPZ)]^{2+}$ (PDB code: 4JD8). **E)** Intercalation of Δ-$[Ru(phen)_2(DPPZ)]^{2+}$ at T/A site (PDB code: 5JEU).

1.6.3 Ruthenium modified oligonucleotides

In recent decades, ruthenium complexes have attracted attention as luminescent DNA probes and photo-cleaving and photo-oxidative agents. To induce specific binding capabilities to ruthenium complexes, an appealing strategy is their functionalisation with oligonucleotides. Oligonucleotides with terminal and internal ruthenium complex incorporation were developed as potential antigene and antisense drugs. In this context, the Barton group developed sequence-specific molecular light switches conjugating a 15-mer single-stranded DNA oligo to $[Ru(phen)_2DPPZ]^{2+}$ *via* an amide bond.[251] This Ru-oligonucleotide (Ru-ON) showed intense luminescence in the presence of a complementary strand due to intercalation with ssDNA (schematic representation in **Figure 1.26**).[252] In contrast to this, adding a non-complementary strand resulting in no luminescence enhancement. In 2002, Hélène and Norden generated the first example of luminescent triplex-forming oligonucleotides (*cf.* **Figure 1.26**).[253] The photophysical properties of the two hybrids were investigated in a binding study with the relative target showing thermal stabilisation of 12 °C for both the enantiomers but luminescence was observed only for the Δ-Ru(II) modified TFO.

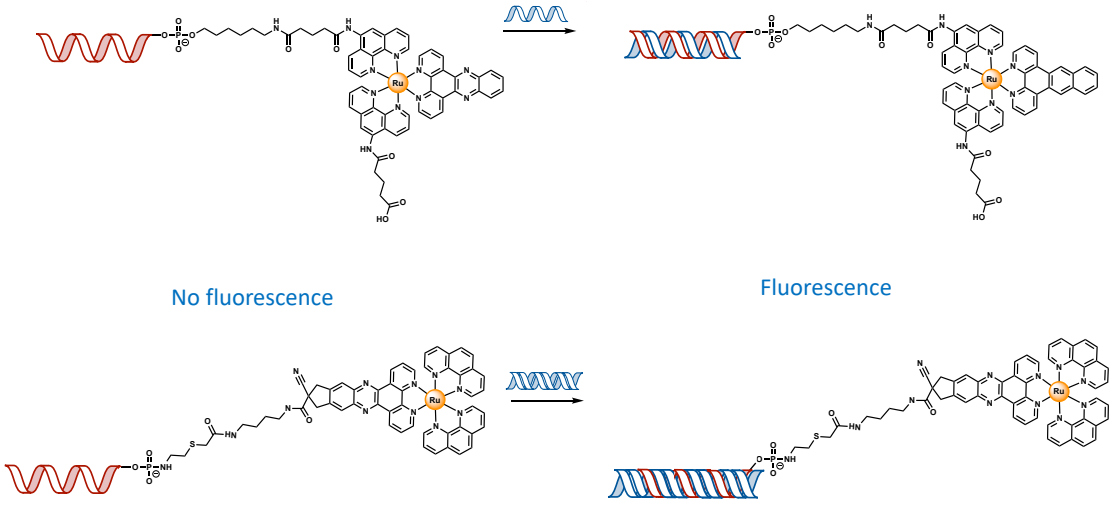

Figure 1.26 Schematic illustration of Ru-modified ON targeting the complementary strand and/or the relative duplex.

ONs tethered to ruthenium TAP complexes have been developed for antisense applications. $[Ru(TAP)_2(dppz)]^{2+}$-ON hybrids were already aforementioned for the ability of DPPZ ligand to adjust the metal central into the ideal orientation for crosslinking formation. In addition also the phen analogue, a $[Ru(TAP)_2(phen)]^{2+}$-ON

(**Figure 1.27**), was investigated and is the hybrid that provided most promising results.[254] This hybrid class showed extremely high selectivity as it formed an intramolecular photo-adduct, called seppuku, in the absence of the complementary strand with no adducts detected in the presence of a non-complementary strand preventing any possible off-targeting effect.[255] In view of these results, $[Ru(TAP)_2\ phen]^{2+}$ was tested in 2013 as an antisense agent against cervical cancer.[256]

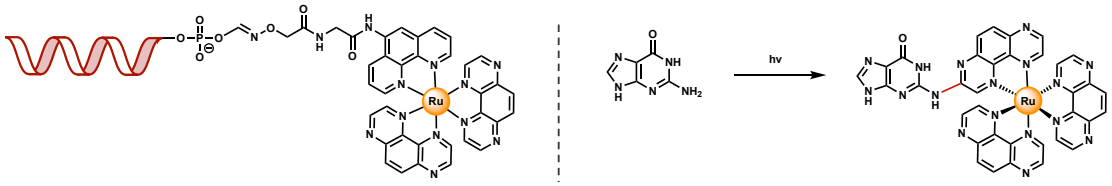

Figure 1.27 Molecular structures of ON functionalised with $[Ru(TAP)_2(phen)]^{2+}$ (left) and schematic representation of cross-linking reaction (right).

Ruthenium-modified oligonucleotides were also generated to identify the mechanism of long-range electron transfer between ruthenium complexes and DNA. In 1993 the Barton group prepared a DNA duplex, 15-mer in length, with a single strand bearing $[Ru(phen)_2DPPZ]^{2+}$ and complementary strand functionalised with the electron-acceptor $[Rh(phi)_2DPPZ]^{2+}$ (phi = phenanthrenequinone diamine, **Figure 1.28 A**).[257] The luminescence of the ruthenium complexes was quenched in the presence of the Rh-modified complementary strand over a distance of 40 Å due to the electron transfer occurring through π-π stacking of the nucleobases.[258] Analogous experiments involving an oligo bearing $[Ru(phen)_3]^{2+}$ showed no-quenching effects in the presence of complementary Rh-modified ODN.[257] This demonstrated the crucial role of a DNA intercalator for electron transfer as $[Ru(phen)_3]^{2+}$ is known only to semi-intercalate DNA.

Further investigations were performed by Meade and Kayem using $[Ru(NH_3)_4(py)]^{2+}$ as a donor and $[Ru(im)(py)_2]^{3+}$ as an acceptor (**Figure 1.28 B**).[259] The donor/acceptor interaction was also analysed by incorporating $[Os(bpy)_2$(3-ethynyl-1,10-phenathroline)$]^{2+}$ into a 19-mer ON as an acceptor and $[Ru(bpy)_2$(3-ethynyl-1,10-phenathroline)$]^{2+}$ as a donor, separated from 3 to 18 base pairs (**Figure 1.28 C**).[260] This study confirmed that energy transfer is mainly regulated by Förster dipole-dipole interactions. Electron-transfer reactions through DNA were also investigated using flash quenching by Barton *et al.* In sequences containing 5′-GG-3′ and 5′-GC-3′, photo-

oxidation of guanines was promoted by a [Ru(phen)(bpy)(Me_2DPPZ)]$^{2+}$-ON hybrid.[261] This hybrid was affected by the presence of mismatches[262] as lower levels of 5′-GG-3′ oxidation were found in the presence of G·T mismatches while higher levels were found for G·A mismatches.[262] The behaviour was rationalised as due to the local helix disruption caused at the mismatch sites and the structural similarity of G·A and G·C pairs.[263] This work therefore demonstrated that ruthenium complexes were useful tools for the detection of DNA mismatches.

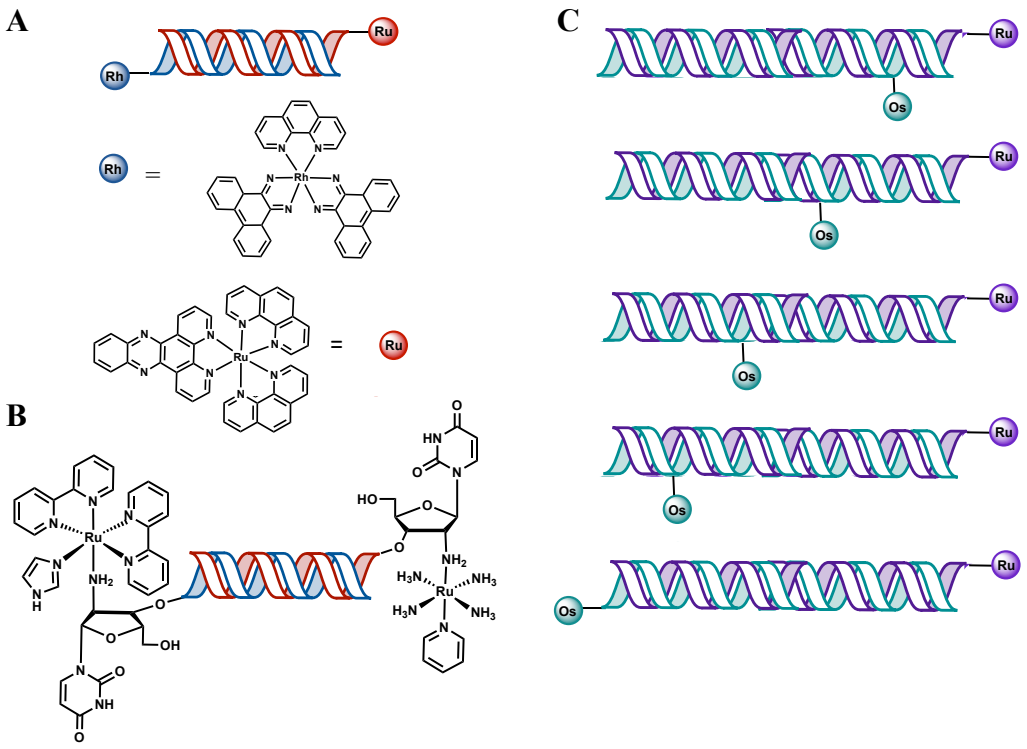

Figure 1.28 A) Schematic representing experiments conducted for long-range ET with a Ru- and Rh-complex modified 15 mer duplex , **B**) with two different ruthenium complexes acting as donor and acceptor (8-14 mer duplex, and **C**) Os and Ru- modified 19 mer duplexes.

Ruthenium-modified oligonucleotides also found application in the field of DNA nanotechnology for the generation of high-order dimensional structures with luminescent properties. The first attempt was performed by the Sleiman group, who developed a hybrid consisting of a *cis*-[Ru(bpy)$_2$(imidazo)]$^{2+}$ connected to two dT_{10} sequences *via* two hexyl spacers (**Figure 1.29 A**).[264] This compound could interact selectively with DNA and RNA sequences, but unfortunately no nanostructures with two metal complexes were obtained.[264] Afterwards, analogues hybrid was developed with shorter

spacers because the lack of higher order nanostructure was attributed to the excess flexibility (**Figure 1.29 B**).[265] This hybrid was tethered to different ONs and was able to form successfully dimeric structures.[265] It is also noteworthy to mention the hybrids with bis(terpyridine) complex functionalised to complementary strands, with which it was possible to generate dimeric or trimer structures modulating the ratio of the two components (**Figure 1.29 C**).[266]

Nucleic acids functionalised with ruthenium complexes also were employed for the detection of biologic activities. For example, the $Ru[(bpy)_2(mbpy\text{-}COOH)]Cl_2$ complex-ON (mbpy-COOH = 4′-methyl-2,2′-bipyridine-4-carboxylic acid) was designed to interact selectively with an oligonucleotides functionalised with gold nanoparticles with the aim of detecting the sensitivity of DNase I.[267] When the two systems were hybridised, the luminescence of the ruthenium complex was quenched, but was restored when the luminescent core was cleaved by DNase I.[267] Another interesting application was the use of hybrid systems ruthenium-PNA to study template-mediate ligations.[268] Overall, the photophysical properties of ruthenium complexes and their ease of incorporation into ON structures has allowed for the development of luminescent probes and potential gene silencing agents.

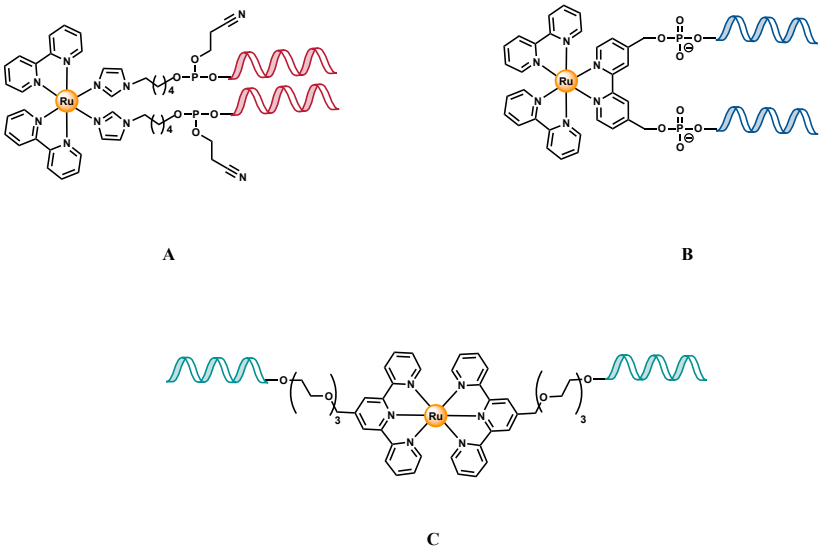

Figure 1.29 Schematic representation of **A**) cis-$[Ru(bpy)_2(imidazo)]^{2+}$ connected to two dT_{10} sequences via two hexyl spacers, **B**) cis-$[Ru(bpy)_3]^{2+}$ attached to DNA squences with short linkers **C**) ruthenium bis(terpyridine) complexes linked to two identical 20-mer DNA sequences through triethylene glycol linkers.

References

(1) Aiba, Y.; Sumaoka, J.; Komiyama, M. Artificial DNA Cutters for DNA Manipulation and Genome Engineering. *Chem. Soc. Rev.* **2011**, *40*, 5657–5668.

(2) Aiba, Y.; Lönnberg, T.; Komiyama, M. Manipulation of Single-Stranded DNA by Using an Artificial Site-Selective DNA Cutter Composed of Cerium(IV)/EDTA and Phosphonate-Oligonucleotide Conjugates. *Chem. - An Asian J.* **2011**, *6*, 2407–2411.

(3) Alonso-de Castro, S.; Terenzi, A.; Gurruchaga-Pereda, J.; Salassa, L. Catalysis Concepts in Medicinal Inorganic Chemistry. *Chem. - A Eur. J.* **2019**, *25*, 6651–6660.

(4) Pratviel, G.; Bernadou, J.; Meunier, B. Carbon—Hydrogen Bonds of DNA Sugar Units as Targets for Chemical Nucleases and Drugs. *Angew Chem Int Ed Engl* **1995**, *34*, 746–769.

(5) Fantoni, N.; Lauria, T.; Kellett, A. Genome Engineering with Synthetic Copper Nucleases. *Synlett* **2015**, *26*, 2623–2626.

(6) Mancin, F.; Scrimin, P.; Tecilla, P. Progress in Artificial Metallonucleases. *Chem. Commun.* **2012**, *48*, 5545–5559.

(7) David S. Sigman, Daniel R. Graham, Vito D'Aurora, and A.; Stern, M. Oxygen-Dependent Cleavage DNA by the 1,10-Phenanthroline.Cuprous Complex. *J. Biol. Chem.* **1979**, *254* (24), 12269–12272.

(8) Aurora, D.; Stern, M.; Sigman, S. INHIBITION OF E. Coli DNA POLYMERASE I BY 1,10-PHENANTHROLINE. **1977**, *78* (1), 170–176.

(9) Meijler, M. M.; Zelenko, O.; Sigman, D. S. Chemical Mechanism of DNA Scission by (1,10-Phenanthroline)Copper. Carbonyl Oxygen of 5-Methylenefuranone Is Derived from Water. *J. Am. Chem. Soc.* **1997**, *119*, 1135–1136.

(10) Spassky, A.; Sigman, D. S. Nuclease Activity of 1,10-Phenanthroline-Copper Ion. Conformational Analysis and Footprinting of the Lac Operon. *Biochemistry* **1985**, *24*, 8050–8056.

(11) Molphy, Z.; Prisecaru, A.; Slator, C.; Barron, N.; McCann, M.; Colleran, J.;

Chandran, D.; Gathergood, N.; Kellett, A. Copper Phenanthrene Oxidative Chemical Nucleases. *Inorg. Chem.* **2014**, *53*, 5392–5404.

(12) Bales, B. C.; Pitié, M.; Meunier, B.; Greenberg, M. M. A Minor Groove Binding Copper-Phenanthroline Conjugate Produces Direct Strand Breaks via β-Elimination of 2-Deoxyribonolactone. *J. Am. Chem. Soc.* **2002**, *124*, 9062–9063.

(13) Chen, T.; Greenberg, M. M. Model Studies Indicate That Copper Phenanthroline Induces Direct Strand Breaks via Beta-Elimination of the 2′-Deoxyribonolactone Intermediate Observed in Enediyne Mediated DNA Damage. *J. Am. Chem. Soc.* **1998**, *120* (15), 3815–3816.

(14) Chen, C. B.; Milne, L.; Landgraf, R.; Perrin, D. M.; Sigman, D. S. Artificial Nucleases. *Chembiochem* **2001**, *2* (10), 735–740.

(15) Slator, C.; Barron, N.; Howe, O.; Kellett, A. Exhibits Unique Superoxide-Mediated NCI-60 Chemotherapeutic Action through Genomic DNA Damage and Mitochondrial Dysfunction. *ACS Chem. Biol.* **2016**, *11* (1), 159–171.

(16) Humphreys, K. J.; Karlin, K. D.; Rokita, S. E. Efficient and Specific Strand Scission of DNA by a Dinuclear Copper Complex : Comparative Reactivity of Complexes with Linked Tris(2-Pyridylmethyl)amine Moieties. *JACS* **2002**, *12*, 6009–6019.

(17) Li, L.; Karlin, K. D.; Rokita, S. E. Changing Selectivity of DNA Oxidation from Deoxyribose to Guanine by Ligand Design and a New Binuclear Copper Complex. **2005**, *127*, 520–521.

(18) Rokita, S. E.; Sunita T.; Murthy, N. N.; Sarjeant, A. A. N.; Kenneth D. K. Selective DNA Strand Scission with Binuclear Copper Complexes: Implications for an Active Cu_2-O_2 Species. *J Am Chem Soc.* **2006**, *128* (21), 7003–7008.

(19) Slator, C.; Molphy, Z.; Mckee, V.; Long, C.; Brown, T.; Kellett, A. Di-Copper Metallodrugs Promote NCI-60 Chemotherapy via Singlet Oxygen and Superoxide Production with Tandem TA / TA and AT / AT Oligonucleotide Discrimination. *Nucleic Acids Res.* **2018**, *14*, 1–18.

(20) Molphy, Z.; Montagner, D.; Bhat, S. S.; Slator, C.; Long, C.; Erxleben, A.; Kellett, A. A Phosphate-Targeted Dinuclear Cu (II) Complex Combining Major Groove Binding and Oxidative DNA Cleavage. *Nucleic Acids Res.* **2018**, *46* (19),

9918-9931.

(21) Stulz, E.; Clever, G.; Shionoya, M. Artificial DNA Cutters for DNA Manipulation and Genome Engineering. *Chem. Soc. Rev.* **2011**, *40*, 5657–5668.

(22) Yamamoto, Y.; Mori, M.; Aiba, Y.; Tomita, T.; Chen, W.; Zhou, J. M.; Uehara, A.; Ren, Y.; Kitamura, Y.; Komiyama, M. Chemical Modification of Ce(IV)/EDTA-Based Artificial Restriction DNA Cutter for Versatile Manipulation of Double-Stranded DNA. *Nucleic Acids Res.* **2007**, *35* (7), 2–9.

(23) Miyajima, Y.; Ishizuka, T.; Yamamoto, Y.; Sumaoka, J.; Komiyama, M. Origin of High Fidelity in Target-Sequence Recognition by PNA Ce(IV)/EDTA Combinations as Site-Selective DNA Cutters. *J. Am. Chem. Soc.* **2009**, *131* (7), 2657–2662.

(24) Zelder, F. H.; Mokhir, A. a.; Krämer, R. Sequence Selective Hydrolysis of Linear DNA Using Conjugates of Zr(IV) Complexes and Peptide Nucleic Acids. *Inorg. Chem.* **2003**, *42* (26), 8618–8620.

(25) Chu, B. C.; Orgel, L. E. Nonenzymatic Sequence-Specific Cleavage of Single-Stranded DNA. *Proc. Natl. Acad. Sci. U. S. A.* **1985**, *82*, 963–967.

(26) Dreyer, G. B.; Dervan, P. B. Sequence-Specific Cleavage of Single-Stranded DNA: Oligodeoxynucleotide-EDTA X Fe(II). *Proc. Natl. Acad. Sci. U. S. A.* **1985**, *82*, 968–972.

(27) Zelder, F. H.; Mokhir, A. A.; Kra, R.; Institut, A.; Uni, V.; Feld, I. N. Sequence Selective Hydrolysis of Linear DNA Using Conjugates of Zr (IV) Complexes and Peptide Nucleic Acids. *Inorg. Chem.* **2003**, *42* (26), 8618–8620.

(28) Komiyama, M.; Takeda, N.; Takahashi, Y.; Uchida, H.; Shiiba, T.; Kodama, T.; Yashiro, M. Efficient and Oxygen-Independent Hydrolysis of Single-Stranded DNA by Cerium(IV) Ion. *J. Chem. Soc. Perkin Trans.* **1995**, *2*, 269–274.

(29) Shiiba, T.; Takahashi, Y.; Takeda, N.; Matsumura, K.; Kodama, T. Cerium(IV)-OligoDNA Hybrid as Highly Selective Artificial Nuclease. *Supramol. Chem.* **1994**, *4* (1), 31–34.

(30) Chen, W.; Kitamura, Y.; Zhou, J. M.; Sumaoka, J.; Komiyama, M. Site-Selective DNA Hydrolysis by Combining Ce(IV)/EDTA with Monophosphate-Bearing Oligonucleotides and Enzymatic Ligation of the Scission Fragments. *J. Am.*

Chem. Soc. **2004**, *126* (33), 10285–10291.

(31) Luige, O.; Murtola, M.; Ghidini, A.; Strömberg, R. Further Probing of Cu2+-Dependent PNAzymes Acting as Artificial RNA Restriction Enzymes. *Molecules* **2019**, *24* (4), 672.

(32) Murtola, M.; Wenska, M.; Strömberg, R. PNAzymes That Are Artificial RNA Restriction Enzymes. *J. Am. Chem. Soc.* **2010**, *132* (26), 8984–8990.

(33) Shigi, N.; Sumaoka, J.; Komiyama, M. Applications of PNA-Based Artificial Restriction DNA Cutters. *Molecules* **2017**, *22*, 1–14.

(34) Komiyama, M.; Aiba, Y.; Yamamoto, Y.; Sumaoka, J. Artificial Restriction DNA Cutter for Site-Selective Scission of Double-Stranded DNA with Tunable Scission Site and Specificity. *Nat. Protoc.* **2008**, *3* (4), 655–662.

(35) Demidov, V.; Frank-kamenetskii, M. D.; Egholm, M.; Buchardt, O.; Nielsen, P. E. Sequence Selective Double Strand DNA Cleavage by Peptide Nucleic Acid (PNA) Targeting Using Nuclease S1. *Nucleic Acids Res.* **1993**, *21* (9), 2103–2107.

(36) Rajendran, A.; Shigi, N.; Sumaoka, J.; Komiyama, M. Artificial Restriction DNA Cutter Using Nuclease S1 for Site-Selective Scission of Genomic DNA. *Curr. Protoc. Nucleic Acid Chem.* **2019**, *76* (1), 1–19.

(37) Sigman, D. S.; Bruice, T. W.; Mazumder, A.; Sutton, C. L. Targeted Chemical Nucleases. *Acc. Chem. Res.* **1993**, *26* (3), 98–104.

(38) François, J. C.; Saison-Behmoaras, T.; Barbier, C.; Chassignol, M.; Thuong, N. T.; Hélène, C. Sequence-Specific Recognition and Cleavage of Duplex DNA via Triple-Helix Formation by Oligonucleotides Covalently Linked to a Phenanthroline-Copper Chelate. *Proc. Natl. Acad. Sci. U. S. A.* **1989**, *86*, 9702–9706.

(39) Footer, M.; Egholm, M.; Kron, S.; Coull, J. M.; Matsudaira, P. Biochemical Evidence That a D-Loop Is Part of a Four-Stranded PNA-DNA Bundle. Nickel-Mediated Cleavage of Duplex DNA by a Gly-Gly-His Bis-PNA. *Biochemistry* **1996**, *35* (33), 10673–10679.

(40) Bigey, P.; Pratviel, G.; Meunier, B. Cleavage of Double-Stranded DNA by "metalloporphyrin-Linker Oligonucleotide" Molecules: Influence of the Linker.

Nucleic Acids Res. **1995**, *23* (19), 3894–3900.

(41) Joshi, R. R.; Ganesh, K. N. Duplex and Triplex Directed DNA Cleavage by Oligonucleotide-Cu(II)/Co(III) Metallodesferal Conjugates. *Biochim. Biophys. Acta* **1994**, *1201*, 454–460.

(42) Malvy, C.; Harel-Bellan, A.; Pritchard, L. L. *Triple Helix Forming*, 1st ed.; C. A. Stein, S. E., Ed.; **1999**, pp. 98-99.

(43) Escudé, C.; Nguyen, C. H.; Kukreti, S.; Janin, Y.; Sun, J. S.; Bisagni, E.; Garestier, T.; Hélène, C. Rational Design of a Triple Helix-Specific Intercalating Ligand. *Proc. Natl. Acad. Sci. U. S. A.* **1998**, *95* (7), 3591–3596.

(44) Zain, R.; Marchand, C.; Sun, J. S.; Nguyen, C. H.; Bisagni, E.; Garestier, T.; Hélène, C. Design of a Triple-Helix-Specific Cleaving Reagent. *Chem. Biol.* **1999**, *6* (11), 771-777.

(45) Zaid, A.; Sun, J. S.; Nguyen, C. H.; Bisagni, E.; Garestier, T.; Grierson, D. S.; Zain, R. Triple-Helix Directed Cleavage of Double-Stranded DNA by Benzoquinoquinoxaline-1,10-Phenanthroline Conjugates. *ChemBioChem* **2004**, *5* (11), 1550–1557.

(46) Amiri, H.; Nekhotiaeva, N.; Sun, J.-S.; Nguyen, C.-H.; Grierson, D. S.; Good, L.; Zain, R. Benzoquinoquinoxaline Derivatives Stabilize and Cleave H-DNA and Repress Transcription Downstream of a Triplex-Forming Sequence. *J. Mol. Biol.* **2005**, *351* (4), 776–783.

(47) Umek, T.; Sollander, K.; Bergquist, H.; Wengel, J.; Lundin, K. E.; Edvard Smith, C. I.; Zain, R. Oligonucleotide Binding to Non-B-DNA in MYC. *Molecules* **2019**, *24*, 1–11.

(48) Mashimo, T.; Takizawa, A.; Voigt, B.; Yoshimi, K.; Hiai, H.; Kuramoto, T.; Serikawa, T. Generation of Knockout Rats with X-Linked Severe Combined Immunodeficiency (X-SCID) Using Zinc-Finger Nucleases. *PLoS One* **2010**, *5* (1), 1–8.

(49) Bogdanove, A. J.; Schornack, S.; Lahaye, T. TAL Effectors: Finding Plant Genes for Disease and Defense. *Curr. Opin. Plant Biol.* **2010**, *13*, 394–401.

(50) Kim, Y. G.; Cha, J.; Chandrasegaran, S. Hybrid Restriction Enzymes: Zinc Finger Fusions to Fok I Cleavage Domain. *Proc. Natl. Acad. Sci. U. S. A.* **1996**,

93 (3), 1156–1160.

(51) Urnov, F. D.; Rebar, E. J.; Holmes, M. C.; Zhang, H. S.; Gregory, P. D. Genome Editing with Engineered Zinc Finger Nucleases. *Nat. Rev. Genet.* **2010**, *11*, 636–646.

(52) Maier, D. A.; Brennan, A. L.; Jiang, S.; Binder-Scholl, G. K.; Lee, G.; Plesa, G.; Zheng, Z.; Cotte, J.; Carpenito, C.; Wood, T.; et al. Efficient Clinical Scale Gene Modification via Zinc Finger Nuclease-Targeted Disruption of the HIV Co-Receptor CCR5. *Hum. Gene Ther.* **2013**, *24* (3), 245–258.

(53) Tebas, P.; Stein, D.; Tang, W. W.; Frank, I.; Wang, S. Q.; Lee, G.; Spratt, S. K.; Surosky, R. T.; Giedlin, M. A.; Nichol, G.; et al. Gene Editing of CCR5 in Autologous CD4 T Cells of Persons Infected with HIV. *N. Engl. J. Med.* **2014**, *370* (10), 901–910.

(54) Laoharawee, K.; DeKelver, R. C.; Podetz-Pedersen, K. M.; Rohde, M.; Sproul, S.; Nguyen, H. O.; Nguyen, T.; St. Martin, S. J.; Ou, L.; Tom, S.; et al. Dose-Dependent Prevention of Metabolic and Neurologic Disease in Murine MPS II by ZFN-Mediated In Vivo Genome Editing. *Mol. Ther.* **2018**, *26* (4), 1127–1136.

(55) Li, H.; Haurigot, V.; Li, Y. D. T.; Wong, S. Y.; Bhagwat, A. S.; Malani, N.; Sharma, X. M. A. R.; Ivanciu, L.; Murphy, S. L.; Finn, J. D.; et al. In Vivo Genome Editing Restores Hemostasis in a Mouse Model of Hemophilia. *Nature* **2012**, *475* (7355), 217–221.

(56) Brown, K.; Green, G. The Haemophilia Drug Market. *Nat. Rev. Drug Discov.* **2018**, *17* (8), 541–542.

(57) Christian, M.; Cermak, T.; Doyle, E. L.; Schmidt, C.; Zhang, F.; Hummel, A.; Bogdanove, A. J.; Voytas, D. F. Targeting DNA Double-Strand Breaks with TAL Effector Nucleases. *Genetics* **2010**, *186*, 756–761.

(58) Mussolino, C.; Morbitzer, R.; Lütge, F.; Dannemann, N.; Lahaye, T.; Cathomen, T. A Novel TALE Nuclease Scaffold Enables High Genome Editing Activity in Combination with Low Toxicity. *Nucleic Acids Res.* **2011**, *39* (21), 9283–9293.

(59) Gardner, R.; Wu, D.; Cherian, S.; Fang, M.; Hanafi, L. A.; Finney, O.; Smithers, H.; Jensen, M. C.; Riddell, S. R.; Maloney, D. G.; et al. Acquisition of a CD19-Negative Myeloid Phenotype Allows Immune Escape of MLL-Rearranged B-

ALL from CD19 CAR-T-Cell Therapy. *Blood* **2016**, *127* (20), 2406–2410.

(60) Vanoli, F.; Tomishima, M.; Feng, W.; Lamribet, K.; Babin, L.; Brunet, E.; Jasin, M. CRISPR-Cas9–Guided Oncogenic Chromosomal Translocations with Conditional Fusion Protein Expression in Human Mesenchymal Cells. *Proc. Natl. Acad. Sci.* **2017**, *114* (14), 3696–3701.

(61) Ran, F. A.; Hsu, P. D.; Wright, J.; Agarwala, V.; Scott, D. A.; Zhang, F. Genome Engineering Using the CRISPR-Cas9 System. *Nat. Protoc.* **2013**, *8* (11), 2281–2308.

(62) Barrangou, R.; Doudna, J. A. Applications of CRISPR Technologies in Research and Beyond. *Nat. Biotechnol.* **2016**, *34* (9), 933–941.

(63) Szczelkun, M. D.; Tikhomirova, M. S.; Sinkunas, T.; Gasiunas, G.; Karvelis, T.; Pschera, P.; Siksnys, V.; Seidel, R. Direct Observation of R-Loop Formation by Single RNA-Guided Cas9 and Cascade Effector Complexes. *Proc. Natl. Acad. Sci. U. S. A.* **2014**, *111* (27), 9798–9803.

(64) Barrangou, R.; Horvath, P. A Decade of Discovery: CRISPR Functions and Applications. *Nat. Microbiol.* **2017**, *2*, 1–9.

(65) Mojica, F. J. M.; Díez-Villaseñor, C.; García-Martínez, J.; Almendros, C. Short Motif Sequences Determine the Targets of the Prokaryotic CRISPR Defence System. *Microbiology* **2009**, *155* (3), 733–740.

(66) Adli, M. The CRISPR Tool Kit for Genome Editing and Beyond. *Nat. Commun.* **2018**, *9* (1911), 1–13.

(67) Loureiro, A.; Da Silva, G. J. Crispr-Cas: Converting a Bacterial Defence Mechanism into a State-of-the-Art Genetic Manipulation Tool. *Antibiotics* **2015**, *65*, 1314–1326.

(68) Kim, D.; Kim, J.; Hur, J. K.; Been, K. W.; Yoon, S. H.; Kim, J. S. Genome-Wide Analysis Reveals Specificities of Cpf1 Endonucleases in Human Cells. *Nat. Biotechnol.* **2016**, *34* (8), 863–868.

(69) Taemaitree, L.; Shivalingam, A.; El-Sagheer, A. H.; Brown, T. An Artificial Triazole Backbone Linkage Provides a Split-and-Click Strategy to Bioactive Chemically Modified CRISPR SgRNA. *Nat. Commun.* **2019**, *10* (1), 1–8.

(70) Zeisel, M. B.; Lucifora, J.; Mason, W. S.; Sureau, C.; Beck, J.; Levrero, M.;

Kann, M.; Knolle, P. A.; Benkirane, M.; Durantel, D.; et al. Towards an HBV Cure: State-of-the-Art and Unresolved Questions-Report of the ANRS Workshop on HBV Cure. **2015**, *64* (8), 1314–1326.

(71) Kaminski, R.; Chen, Y.; Fischer, T.; Tedaldi, E.; Napoli, A.; Zhang, Y.; Karn, J.; Hu, W.; Khalili, K. Elimination of HIV-1 Genomes from Human T-Lymphoid Cells by CRISPR/Cas9 Gene Editing. *Sci. Rep.* **2016**, *6*, 1–14.

(72) Citorik, R. J.; Mimee1, M.; Lu, T. K. Sequence-Specific Antimicrobials Using Efficiently Delivered RNA-Guided NucleasesIH Public Access. *Nat Biotechnol. 2014* **2014**, *32* (11), 1141–1145.

(73) Bikard, D.; Euler, C. W.; Jiang, W.; Nussenzweig, P. M.; Goldberg, G. W.; Duportet, X.; Fischetti, V. A.; Marraffini, L. A. Exploiting CRISPR-Cas Nucleases to Produce Sequence-Specific Antimicrobials. *Nat. Biotechnol.* **2014**, *32* (11), 1146–1150.

(74) Kolb, H. C.; Finn, M. G.; Sharpless, K. B. Click Chemistry : Diverse Chemical Function from a Few Good Reactions. *Angew Chem Int Ed* **2001**, *40*, 2004–2021.

(75) Moses, J. E.; Moorhouse, A. D. The Growing Applications of Click Chemistry. *Chem. Soc. Rev.* **2007**, *36*, 1249–1262.

(76) Kolb, H. C.; Finn, M. G.; Sharpless, K. B. Click Chemistry: Diverse Chemical Function from a Few Good Reactions. *Angew. Chem. Int. Ed. Engl.* **2001**, *40* (11), 2004–2021.

(77) Rolf Huisgen. 1,3-Dipolar Cycloadditions. *Proc. Chem. Soc.* **1961**, 357 – 69.

(78) Huisgen, R. 1,3-Dipolar Cycloadditions. Past and Future. *Angew. Chemie* **1963**, *2* (10), 565–632.

(79) Bräse, S.; Gil, C.; Knepper, K.; Zimmermann, V. Organic Azides: An Exploding Diversity of a Unique Class of Compounds. *Angew. Chemie - Int. Ed.* **2005**, *44* (33), 5188–5240.

(80) Rostovtsev, V. V.; Green, L. G.; Fokin, V. V.; Sharpless, K. B. A Stepwise Huisgen Cycloaddition Process: Copper(I)-Catalyzed Regioselective "Ligation" of Azides and Terminal Alkynes. *Angew. Chemie - Int. Ed.* **2002**, *41* (14), 2596–2599.

(81) Tornøe, C. W.; Christensen, C.; Meldal, M. Peptidotriazoles on Solid Phase:

[1,2,3]-Triazoles by Regiospecific Copper(I)-Catalyzed 1,3-Dipolar Cycloadditions of Terminal Alkynes to Azides. *J. Org. Chem.* **2002**, *67*, 3057–3064.

(82) Bock, V. D.; Hiemstra, H.; van Maarseveen, J. H. CuI-Catalyzed Alkyne-Azide "Click" Cycloadditions from a Mechanistic and Synthetic Perspective. *European J. Org. Chem.* **2006**, *2006* (1), 51–68.

(83) Chan, T. R.; Hilgraf, R.; Sharpless, K. B.; Fokin, V. V. Polytriazoles as Copper(I)-Stabilizing Ligands in Catalysis. *Org. Lett.* **2004**, *6* (17), 2853–2855.

(84) Hong, V.; Steinmetz, N. F.; Manchester, M.; Finn, M. G. Labeling Live Cells by Copper-Catalyzed Alkyne-Azide Click Chemistry. *Bioconjug. Chem.* **2010**, *21* (10), 1912–1916.

(85) Kappe, C. O.; Van der Eycken, E. Click Chemistry under Non-Classical Reaction Conditions. *Chem. Soc. Rev.* **2010**, *39* (4), 1280–1290.

(86) Liang, L.; Astruc, D. The Copper(I)-Catalyzed Alkyne-Azide Cycloaddition (CuAAC) "Click" Reaction and Its Applications. An Overview. *Coord. Chem. Rev.* **2011**, *255* (23–24), 2933–2945.

(87) Jewett, J. C.; Bertozzi, C. R. Cu-Free Click Cycloaddition Reactions in Chemical Biology. *Chem. Soc. Rev.* **2010**, *39*, 1272–1279.

(88) Anderton, G. I.; Bangerter, A. S.; Davis, T. C.; Feng, Z.; Furtak, A. J.; Larsen, J. O.; Scroggin, T. L.; Heemstra, J. M. Accelerating Strain-Promoted Azide-Alkyne Cycloaddition Using Micellar Catalysis. *Bioconjug. Chem.* **2015**, *26* (8), 1687–1691.

(89) Remzi Becer, C.; Hoogenboom, R.; Schubert, U. S. Click Chemistry beyond Metal-Catalyzed Cycloaddition. *Angew. Chemie - Int. Ed.* **2009**, *48* (27), 4900–4908.

(90) Baskin, J. M.; Prescher, J. A.; Laughlin, S. T.; Agard, N. J.; Chang, P. V.; Miller, I. A.; Lo, A.; Codelli, J. A.; Bertozzi, C. R. Copper-Free Click Chemistry for Dynamic in Vivo Imaging. *PNAS* **2007**, *104* (43), 16793–16797.

(91) Codelli, J. a.; Baskin, J. M.; Agard, N. J.; Bertozzi, C. R. Second-Generation Difluorinated Cyclooctynes for Copper-Free Click Chemistry. *J. Am. Chem. Soc.* **2008**, *130* (34), 11486–11493.

(92) Ning, X.; Guo, J.; Wolfert, M. A.; Boons, G.-J. Visualizing Metabolically-Labeled Glycoconjugates of Living Cells by Copper-Free and Fast Huisgen Cycloadditions. *Angew Chem Int Ed Engl.* **2008**, *47* (12), 2253–2255.

(93) Jewett, J. C.; Sletten, E. M.; Bertozzi, C. R. Rapid Cu-Free Click Chemistry with Readily Synthesized Biarylazacyclooctynones. *J. Am. Chem. Soc.* **2010**, *132*, 3688–3690.

(94) Bertozzi, C. R.; Sletten, E. M. A Hydrophilic Azacyclooctyne for Cu-Free Click Chemistry. *Org. Lett.* **2008**, *10* (14), 3097–3099.

(95) Ostrovskis, P.; Volla, C. M. R.; Turks, M.; Markovic, D. Application of Metal Free Click Chemistry in Biological Studies. **2013**, *17* (6), 610–640.

(96) Sletten, E. M.; Bertozzi, C. R. From Mechanism to Mouse: A Tale of Two Bioorthogonal Reactions. *Acc. Chem. Res.* **2011**, *44* (9), 666–676.

(97) Beatty, K. E.; Fisk, J. D.; Smart, B. P.; Lu, Y. Y.; Szychowski, J.; Hangauer, M. J.; Baskin, J. M.; Bertozzi, C. R.; Tirrell, D. A. Live-Cell Imaging of Cellular Proteins by a Strain-Promoted Azide-Alkyne Cycloaddition. *ChemBioChem* **2010**, *11*, 2092–2095.

(98) Dieterich, D. C.; Hodas, J. J. L.; Gouzer, G.; Shadrin, I. Y.; Ngo, J. T.; Triller, A.; Tirrell, D. A.; Schuman, E. M. In Situ Visualization and Dynamics of Newly Synthesized Proteins in Rat Hippocampal Neurons. *Nat. Neurosci.* **2010**, *13* (7), 897–905.

(99) Laughlin, S. T.; Baskin, J. M.; Amacher, S. L.; Bertozzi, C. R. In Vivo Imaging of Glycans in Membrane-Associated Developing Zebrafish. *Science* **2008**, *320* (8), 664–667.

(100) Neef, A. B.; Schultz, C. Selective Fluorescence Labeling of Lipids in Living Cells. *Angew. Chem. Int. Ed.* **2009**, *48*, 1498–1500.

(101) Dommerholt, J.; Schmidt, S.; Temming, R.; Hendriks, L. J. A.; Rutjes, F. P. J. T.; Van Hest, J. C. M.; Lefeber, D. J.; Friedl, P.; Van Delft, F. L. Readily Accessible Bicyclononynes for Bioorthogonal Labeling and Three-Dimensional Imaging of Living Cells. *Angew. Chemie - Int. Ed.* **2010**, *49*, 9422–9425.

(102) Lutz, J. F. Copper-Free Azide-Alkyne Cycloadditions: New Insights and Perspectives. *Angew. Chemie Int. Ed.* **2008**, *47*, 2182–2184.

(103) El-Sagheer, A. H.; Brown, T. Click Chemistry with DNA. *Chem. Soc. Rev.* **2010**, *39* (4), 1388–1405.

(104) Gramlich, P. M. E.; Wirges, C. T.; Manetto, A.; Carell, T. Postsynthetic DNA Modification through the Copper-Catalyzed Azide-Alkyne Cycloaddition Reaction. *Angew. Chemie - Int. Ed.* **2008**, *47* (44), 8350–8358.

(105) Jawalekar, A. M.; Meeuwenoord, N.; Cremers, J. G. O.; Overkleeft, H. S.; Van Der Marel, G. A.; Rutjes, F. P. J. T.; Van Delft, F. L. Conjugation of Nucleosides and Oligonucleotides by [3+2] Cycloaddition. *J. Org. Chem.* **2008**, *73* (1), 287–290.

(106) Seo, T. S.; Li, Z.; Ruparel, H. Click Chemistry to Construct Fluorescent Oligonucleotides for DNA Sequencing. *J. Org. Chem.* **2003**, No. 16, 609–612.

(107) Seo, T. S.; Bai, X.; Ruparel, H.; Li, Z.; Turro, N. J.; Ju, J. Characterization of Individual Polynucleotide Molecules Using a Membrane Channel. *PNAS* **2004**, *101* (15), 5488–5493.

(108) Seo, T. S.; Bai, X.; Kim, D. H.; Meng, Q.; Shi, S.; Ruparel, H.; Li, Z.; Turro, N. J.; Ju, I. Four-Color DNA Sequencing by Synthesis on a Chip Using Photocleavable Fluorescent Nucleotides. *Proc. Natl. Acad. Sci.* **2005**, *102* (17), 5926–5931.

(109) Devaraj, N. K.; Miller, G. P.; Ebina, W.; Kakaradov, B.; Collman, J. P.; Kool, E. T.; Chidsey, C. E. D. Chemoselective Covalent Coupling of Oligonucleotide Probes to Self-Assembled Monolayers. *J. Am. Chem. Soc.* **2005**, *127*, 8600–8601.

(110) Rozkiewicz, D. I.; Gierlich, J.; Burley, G. a.; Gutsmiedl, K.; Carell, T.; Ravoo, B. J.; Reinhoudt, D. N. Transfer Printing of DNA by “Click” Chemistry. *ChemBioChem* **2007**, *8* (16), 1997–2002.

(111) Duckworth, B. P.; Chen, Y.; Wollack, J. W.; Sham, Y.; Mueller, J. D.; Taton, T. A.; Distefano, M. D. A Universal Method for the Preparation of Covalent Protein – DNA Conjugates for Use in Creating Protein Nanostructures. *Angew. Chem. Int. Ed.* **2007**, *46*, 8819–8822.

(112) Kumar, R.; El-Sagheer, A.; Tumpane, J.; Lincoln, P.; Wilhelmsson, L. M.; Brown, T. Template-Directed Oligonucleotide Strand Ligation, Covalent

Intramolecular DNA Circularization and Catenation Using Click Chemistry. *J. Am. Chem. Soc.* **2007**, *129* (21), 6859–6864.

(113) Shelbourne, M.; Chen, X.; Brown, T.; El-Sagheer, A. H. Fast Copper-Free Click DNA Ligation by the Ring-Strain Promoted Alkyne-Azide Cycloaddition Reaction. *Chem. Commun.* **2011**, *47* (22), 6257–6259.

(114) Gierlich, J.; Burley, G. a.; Gramlich, P. M. E.; Hammond, D. M.; Carell, T. Click Chemistry as a Reliable Method for the High-Density Postsynthetic Functionalization of Alkyne-Modified DNA. *Org. Lett.* **2006**, *8* (17), 3639–3642.

(115) Seela, F.; Sirivolu, V. R. DNA Containing Side Chains with Terminal Triple Bonds: Base-Pair Stability and Functionalization of Alkynylated Pyrimidines and 7-Deazapurines. *Chem. Biodivers.* **2006**, *3* (5), 509–514.

(116) Sirivolu, V. R.; Chittepu, P.; Seela, F. DNA with Branched Internal Side Chains: Synthesis of 5-Tripropargylamine-DU and Conjugation by an Azide-Alkyne Double Click Reaction. *ChemBioChem* **2008**, *9* (14), 2305–2316.

(117) Gramlich, P. M. E.; Warncke, S.; Gierlich, J.; Carell, T. Click-Click-Click: Single to Triple Modification of DNA. *Angew. Chemie - Int. Ed.* **2008**, *47* (18), 3442–3444.

(118) Bouillon, C.; Meyer, A.; Jochum, A.; Chevolot, Y.; Cloarec, J.; Praly, J.; Vasseur, J.; Ii, M.; Place, E.; Cedex, M.; et al. Microwave Assisted " Click " Chemistry for the Synthesis of Multiple Labeled-Carbohydrate Oligonucleotides on Solid Support † A Versatile Approach Has Been Developed for the Multiple Labeling of Oligonucleotides . First , Three Linkers as a H - Phosphonat. *J. Org. Chem. 2006,* **2006**, *71*, 4700–4702.

(119) Chittepu, P.; Sirivolu, V. R.; Seela, F. Nucleosides and Oligonucleotides Containing 1,2,3-Triazole Residues with Nucleobase Tethers: Synthesis via the Azide-Alkyne "click" Reaction. *Bioorganic Med. Chem.* **2008**, *16* (18), 8427–8439.

(120) Fujino, T.; Yamazaki, N.; Isobe, H. Convergent Synthesis of Oligomers of Triazole-Linked DNA Analogue (TLDNA) in Solution Phase. *Tetrahedron Lett.* **2009**, *50*, 4101–4103.

(121) El-Sagheer, A. H.; Kumar, R.; Findlow, S.; Werner, J. M.; Lane, A. N.; Brown,

T. A Very Stable Cyclic DNA Miniduplex with Just Two Base Pairs. *ChemBioChem* **2008**, *9* (1), 50–52.

(122) Pujari, S. S.; Ingale, S. A.; Seela, F. High-Density Functionalization and Cross-Linking of DNA: " Click " and " Bis-Click " Cycloadditions Performed on Alkynylated Oligonucleotides with Fluorogenic Anthracene Azides. *Bioconjugate Chem.* **2014**, *25*, 1855−1870.

(123) Xiong, H.; Seela, F. Cross-Linked DNA: Site-Selective "Click" Ligation in Duplexes with Bis-Azides and Stability Changes Caused by Internal Cross-Links. *Bioconjug. Chem.* **2012**, *23* (6), 1230–1243.

(124) Kočalka, P.; Andersen, N. K.; Jensen, F.; Nielsen, P. Synthesis of 5-(1,2,3-Triazol-4-Yl)-2′-Deoxyuridines by a Click Chemistry Approach: Stacking of Triazoles in the Major Groove Gives Increased Nucleic Acid Duplex Stability. *ChemBioChem* **2007**, *8* (17), 2106–2116.

(125) Sau, S. P.; Hrdlicka, P. J. C2 ′ -Pyrene-Functionalized Triazole-Linked DNA: Universal DNA/RNA Hybridization Probes. *J. Org. Chem.* **2012**, *77*, 5–16.

(126) Nielsen, P. E.; Egholm, M.; Berg, R. H.; Buchardt, O. Sequence-Selective Recognition of DNA by Strand Displacement with a Thymine-Substituted Polyamide. *Science* **1991**, *254*, 1497–1500.

(127) Braasch, D. a; Corey, D. R. Locked Nucleic Acid (LNA): Fine-Tuning the Recognition of DNA and RNA. *Chem. Biol.* **2001**, *8* (1), 1–7.

(128) Singh, S. K.; Nielsen, P.; Koshkin, A. a.; Wengel, J. A (Locked Nucleic Acids): Synthesis and High-Affinity Nucleic Acid Recognition. *Chem. Commun.* **1998**, 455–456.

(129) Fox, K. R.; Brown, T.; Rusling, D. A. *DNA-Targeting Molecules as Therapeutic Agents*; **2018**, pp. 6-7.

(130) Karkare, S.; Bhatnagar, D. Promising Nucleic Acid Analogs and Mimics: Characteristic Features and Applications of PNA, LNA, and Morpholino. *Appl. Microbiol. Biotechnol.* **2006**, *71*, 575–586.

(131) P.Stirchak, E.; E.Summerton, J.; D.Weller, D. Uncharged Stereoregular Nucleic Acid Analogs: 2. Morpholino Nucleoside Oligomers with Carbamate Internucleoside Linkages. *Nucleic Acids Res.* **1981**, *17* (5), 6129–6141.

(132) Gramlich, P. M. E.; Wirges, C. T.; Gierlich, J.; Carell, T. Synthesis of Modified DNA by PCR with Alkyne-Bearing Purines Followed by a Click Reaction. *Org. Lett.* **2008**, *10* (2), 249–251.

(133) Lane, A. N.; Chaires, J. B.; Gray, R. D.; Trent, J. O. Stability and Kinetics of G-Quadruplex Structures. *Nucleic Acids Res.* **2008**, *36* (17), 5482–5515.

(134) Nadrian C. Seeman. An Overview of Structural DNA Nanotechnology Nadrian. *Mol Biotechnol.* **2007**, *37* (3), 246–257.

(135) Yatsunyk, L. a.; Piétrement, O.; Albrecht, D.; Tran, P. L. T.; Renčiuk, D.; Sugiyama, H.; Arbona, J. M.; Aimé, J. P.; Mergny, J. L. Guided Assembly of Tetramolecular G-Quadruplexes. *ACS Nano* **2013**, *7* (7), 5701–5710.

(136) Guédin, A.; De Cian, A.; Gros, J.; Lacroix, L.; Mergny, J. L. Sequence Effects in Single-Base Loops for Quadruplexes. *Biochimie* **2008**, *90* (5), 686–696.

(137) Tsu-Ju, F.; Seeman, N. C. DNA Double-Crossover Molecules. *Biochemistry* **1993**, *32*, 3211–3220.

(138) Helleday, T.; Lo, J.; van Gent, D. C.; Engelward, B. P. DNA Double-Strand Break Repair: From Mechanistic Understanding to Cancer Treatment. *DNA Repair* **2007**, *6*, 923–935.

(139) Carrascosa, L. G.; Gómez-Montes, S.; Aviñó, A.; Nadal, A.; Pla, M.; Eritja, R.; Lechuga, L. M. Sensitive and Label-Free Biosensing of RNA with Predicted Secondary Structures by a Triplex Affinity Capture Method. *Nucleic Acids Res.* **2012**, *40* (8), 1–11.

(140) Wu, Q.; Gaddis, S. S.; MacLeod, M. C.; Walborg, E. F.; Thames, H. D.; DiGiovanni, J.; Vasquez, K. M. High-Affinity Triplex-Forming Oligonucleotide Target Sequences in Mammalian Genomes. *Mol. Carcinog.* **2007**, *46*, 15–23.

(141) Wilson, W. D.; Hopkins, H. P.; Mizan, S.; Hamilton, D. D.; Zon, G. Thermodynamics of DNA Triplex Formation in Oligomers with and without Cytosine Bases: Influence of Buffer Species, PH, and Sequence. *J. Am. Chem. Soc.* **1994**, *116* (8), 3607–3608.

(142) Kohwi, Y.; Kohwi-Shigematsu, T. Magnesium Ion-Dependent Triple-Helix Structure Formed by Homopurine-Homopyrimidine Sequences in Supercoiled Plasmid DNA. *Proc. Natl. Acad. Sci.* **1988**, *85*, 3781–3785.

(143) James, P. L.; Brown, T.; Fox, K. R. Thermodynamic and Kinetic Stability of Intermolecular Triple Helices Containing Different Proportions of C+.GC and T.AT Triplets. *Nucleic Acids Res.* **2003**, *31* (19), 5598–5606.

(144) Chandrasekaran, A. R.; Rusling, D. A. Triplex-Forming Oligonucleotides : A Third Strand for DNA Nanotechnology. **2018**, *46* (3), 1021-1037.

(145) Rougée, M.; Faucon, B.; Mergny, J. L.; Giovannangeli, C.; Garestier, T.; Hélène, C.; Barcelo, F. Kinetics and Thermodynamics of Triple-Helix Formation: Effects of Ionic Strength and Mismatches. *Biochemistry* **1992**, *31*, 9269–9278.

(146) Mergny, J. L.; Sun, J. S.; Rougée, M.; Montenay-Garestier, T.; Chomilier, J.; Hélène, C.; Barcelo, F. Sequence Specificity in Triple-Helix Formation: Experimental and Theoretical Studies of the Effect of Mismatches on Triplex Stability. *Biochemistry* **1991**, *30*, 9791–9798.

(147) Walsh, S.; El-Sagheer, A. H.; Brown, T. Fluorogenic Thiazole Orange TOTFO Probes Stabilise Parallel DNA Triplexes at PH 7 and Above. *Chem. Sci.* **2018**, *9* (39), 7681–7687.

(148) Akinori, S.; Shindo, H. Thermodynamic and Kinetic Analyses of Dna Triplex Formation: Application of Filter-Binding Assay. *J. Biomol. Struct. Dyn.* **1993**, *11* (2), 245–252.

(149) Lee, J. S.; Woodsworth, M. L.; Latimer, L. J. P.; Morgan, A. R. Poly(Pyrimidine) Poly(Purine) Synthetic DNAs Containing 5-Methylcytosine Form Stable Triplexes at Neutral PH. *Nucleic Acids Res.* **1984**, *12* (16), 6603–6614.

(150) Berressem, R.; Engels, J. W. 6-Oxocytidine a Novel Protonated C-Base Analogue for Stable Triple Helix Formation. *Nucleic Acids Res.* **1995**, *23* (17), 3465–3472.

(151) Gamper, H. B.; Kutyavin, I. V.; Rhinehart, R. L.; Lokhov, S. G.; Reed, M. W.; Meyer, R. B. Modulation of C m /T, G/A, and G/T Triplex Stability by Conjugate Groups in the Presence and Absence of KCl. *Biochemistry* **1997**, *36* (48), 14816–14826.

(152) Nara, H.; Matsuda, A.; Ono, A. Nucleosides and Nucleotides. 135. DNA Duplex and Triplex Formation and Resistance to Nucleolytic Degradation of

Oligodeoxynucleotides Containing Syn-Norspermidine at the 5-Position of 2'-Deoxyuridine. *Bioconjug. Chem.* **1995**, *6*, 54–61.

(153) Rajeev, K. G.; Jadhav, V. R.; Ganesh, K. N. Triplex Formation at Physiological PH: Comparative Studies on DNA Triplexes Containing 5-Me-DC Tethered at N4 with Spermine and Tetraethyleneoxyamine. *Nucleic Acids Res.* **1997**, *25* (21), 4187–4193.

(154) Bijapur, J.; Keppler, M. D.; Bergqvist, S.; Brown, T.; Fox, K. R. 5-(1-Propargylamino)-2′-Deoxyuridine (U(P)): A Novel Thymidine Analogue for Generating DNA Triplexes with Increased Stability. *Nucleic Acids Res.* **1999**, *27* (8), 1802–1809.

(155) Kibler-Herzog, L.; Kell, B.; Zon, G.; Shinozuka, K.; Mizan, S.; Wilson, W. D. Sequence Dependent Effects in Methylphosphonate Deoxyribonucleotide Double and Triple Helical Complexes. *Nucleic Acids Res.* **1990**, *18* (12), 3545–3555.

(156) Gryaznov, S. M.; Lloyd, D. H.; Chen, J. K.; Schultz, R. G.; DeDionisio, L. A.; Ratmeyer, L.; Wilson, W. D. Oligonucleotide N3'->P5' Phosphoramidates. *Proc. Natl. Acad. Sci. U. S. A.* **1995**, *92*, 5798–5802.

(157) Asensio, J. L.; Carr, R.; Brown, T.; Lane, A. N. Conformational and Thermodynamic Properties of Parallel Intramolecular Triple Helices Containing a DNA, RNA, or 2′-OMeDNA Third Strand. *J. Am. Chem. Soc.* **1999**, *121* (48), 11063–11070.

(158) Pabon-Martinez, Y. V.; Xu, Y.; Villa, A.; Lundin, K. E.; Geny, S.; Nguyen, C. H.; Pedersen, E. B.; Jørgensen, P. T.; Wengel, J.; Nilsson, L.; et al. LNA Effects on DNA Binding and Conformation: From Single Strand to Duplex and Triplex Structures. *Sci. Rep.* **2017**, *7* (11043), 1–16.

(159) Torigoe, H.; Hari, Y.; Sekiguchi, M.; Obika, S.; Imanishi, T. 2′-O,4′-C-Methylene Bridged Nucleic Acid Modification Promotes Pyrimidine Motif Triplex DNA Formation at Physiological PH. Thermodynamic and Kinetic Studies. *J. Biol. Chem.* **2001**, *276* (4), 2354–2360.

(160) Sun, B. W.; Babu, B. R.; Sørensen, M. D.; Zakrzewska, K.; Wengel, J.; Sun, J. S. Sequence and PH Effects of LNA-Containing Triple Helix-Forming Oligonucleotides: Physical Chemistry, Biochemistry, and Modeling Studies. *Biochemistry* **2004**, *43*, 4160–4169.

(161) Morita, K.; Hasegawa, C.; Kaneko, M.; Tsutsumi, S.; Sone, J.; Ishikawa, T.; Imanishi, T.; Koizumi, M. 2′-O,4′-C-Ethylene-Bridged Nucleic Acids (ENA): Highly Nuclease-Resistant and Thermodynamically Stable Oligonucleotides for Antisense Drug. *Bioorganic Med. Chem. Lett.* **2002**, *12*, 73–76.

(162) Rahman, S. M. A.; Seki, S.; Utsuki, K.; Obika, S.; Miyashita, K.; Imanishi, T. 2′,4′-BNANC: A Novel Bridged Nucleic Acid Analogue with Excellent Hybridizing and Nuclease Resistance Profiles. *Nucleosides, Nucleotides and Nucleic Acids* **2007**, *26* (10–12), 1625–1628.

(163) Torigoe, H.; Nakagawa, O.; Imanishi, T.; Obika, S.; Sasaki, K. Chemical Modification of Triplex-Forming Oligonucleotide to Promote Pyrimidine Motif Triplex Formation at Physiological PH. *Biochimie* **2012**, *94* (4), 1032–1040.

(164) Obika, S.; Onoda, M.; Morita, K.; Andoh, J. I.; Koizumi, M.; Imanishi, T. 3′-Amino-2′,4′-BNA: Novel Bridged Nucleic Acids Having an N3′→ P5′ Phosphoramidate Linkage. *Chem. Commun.* **2001**, *1* (19), 1992–1993.

(165) Tarköy, M.; Leumann, C. Synthesis and Pairing Properties of Decanucleotides from (3′S,5′R)-2′-Deoxy-3′, 5′-ethanoβ-D-ribofuranosyladenine and -thymine. *Angew. Chemie Int. Ed. English* **1993**, *32* (10), 1432–1434.

(166) Filichev, V. V.; Nielsen, M. C.; Bomholt, N.; Jessen, C. H.; Pedersen, E. B. High Thermal Stability of 5′-5′-Linked Alternate Hoogsteen Triplexes at Physiological PH. *Angew. Chemie - Int. Ed.* **2006**, *45* (32), 5311–5315.

(167) Jessen, C. H.; Pedersen, E. B. Design of an Intercalating Linker Leading to the First Efficiently 5′,5′-Linked Alternate-Strand Hoogsteen Triplex with High Stability and Specificity. *Helv. Chim. Acta* **2004**, *87*, 2465–2471.

(168) Blaskó, A.; Dempcy, R. O.; Minyat, E. E.; Bruice, T. C. Association of Short-Strand DNA Oligomers with Guanidinium-Linked Nucleosides. A Kinetic and Thermodynamic Study. *J. Am. Chem. Soc.* **1996**, *118*, 7892–7889.

(169) Chaturvedi, S.; Horn, T.; Letsinger, R. L. Stabilization of Triple-Stranded Oligonucleotide Complexes: Use of Probes Containing Alternating Phosphodiester and Stereo-Uniform Cationic Phosphoramidate Linkages. *Nucleic Acids Res.* **1996**, *24* (12), 2318–2323.

(170) Michel, T.; Debart, F.; Heitz, F.; Vasseur, J. J. Highly Stable DNA Triplexes

Formed with Cationic Phosphoramidate Pyrimidine α-Oligonucleotides. *ChemBioChem* **2005**, *6*, 1254–1262.

(171) Cuenoud, B.; Casset, F.; Hüsken, D.; Natt, F.; Wolf, R. M.; Altmann, K. H.; Martin, P.; Moser, H. E. Dual Recognition of Double-Stranded DNA by 2′-Aminoethoxy-Modified Oligonucleotides. *Angew. Chemie - Int. Ed.* **1998**, *37*, 1288–1291.

(172) Mayer, A.; Häberli, A.; Leumann, C. J. Synthesis and Triplex Forming Properties of Pyrrolidino Pseudoisocytidine Containing Oligodeoxynucleotides. *Org. Biomol. Chem.* **2005**, *3*, 1653–1658.

(173) Häberli, A.; Leumann, C. J. DNA Binding Properties of Oligodeoxynucleotides Containing Pyrrolidino C-Nucleosides. *Org. Lett.* **2002**, *4*, 3275–3278.

(174) Sollogoub, M.; Darby, R. A. J.; Cuenoud, B.; Brown, T.; Fox, K. R. Stable DNA Triple Helix Formation Using Oligonucleotides Containing 2′-Aminoethoxy,5-Propargylamino-U. *Biochemistry* **2002**, *41*, 7224–7231.

(175) Osborne, S. D.; Powers, V. E. C.; Rusling, D. A.; Lack, O.; Fox, K. R.; Brown, T. Selectivity and Affinity of Triplex-Forming Oligonucleotides Containing 2′-Aminoethoxy-5-(3-Aminoprop-1-Ynyl)Uridine for Recognizing AT Base Pairs in Duplex DNA. *Nucleic Acids Res.* **2004**, *32* (15), 4439–4447.

(176) Rusling, D. A.; Broughton-Head, V. J.; Tuck, A.; Khairallah, H.; Osborne, S. D.; Brown, T.; Fox, K. R. Kinetic Studies on the Formation of DNA Triplexes Containing the Nucleoside Analogue 2′-O-(2-Aminoethyl)-5-(3-Amino-1-Propynyl)Uridine. *Org. Biomol. Chem.* **2008**, *6*, 122–129.

(177) Brennan, L.; Peng, G.; Srinivasan, N.; Fox, K. R.; Brown, T. 2′-O-Dimethylaminoethoxyuridine and 5-Dimethylaminopropargyl Deoxyuridine for at Base Pair Recognition in Triple Helices. *Nucleosides, Nucleotides and Nucleic Acids* **2007**, *26*, 1283–1286.

(178) Christensen, U. B.; Pedersen, E. B. Intercalating Nucleic Acids Containing Insertions of 1-O-(1-Pyrenylmethyl)Glycerol: Stabilisation of DsDNA and Discrimination of DNA over RNA. *Nucleic Acids Res.* **2002**, *30* (22), 4918–4925.

(179) Christensen, U. B.; Pedersen, E. B. Intercalating Nucleic Acids with Pyrene

Nucleotide Analogues as Next-Nearest Neighbors for Excimer Fluorescence Detection of Single-Point Mutations under Nonstringent Hybridization Conditions. *Helv. Chim. Acta* **2003**, *86* (6), 2090–2097.

(180) Nielsen, C. B.; Petersen, M.; Pedersen, E. B.; Hansen, P. E.; Christensen, U. B. NMR Structure Determination of a Modified DNA Oligonucleotide Containing a New Intercalating Nucleic Acid. *Bioconjug. Chem.* **2004**, *15*, 260–269.

(181) Schneider, U. V.; Mikkelsen, N. D.; Jøhnk, N.; Okkels, L. M.; Westh, H.; Lisby, G. Optimal Design of Parallel Triplex Forming Oligonucleotides Containing Twisted Intercalating Nucleic Acids-TINA. *Nucleic Acids Res.* **2010**, *38* (13), 4394–4403.

(182) Osman, A. M. A.; Jørgensen, P. T.; Bomholt, N.; Pedersen, E. B. Using an Aryl Phenanthroimidazole Moiety as a Conjugated Flexible Intercalator to Improve the Hybridization Efficiency of a Triplex-Forming Oligonucleotide. *Bioorganic Med. Chem.* **2008**, *16*, 9937–9947.

(183) Schneider, U. V; Géci, I.; Jøhnk, N.; Mikkelsen, N. D.; Pedersen, E. B.; Lisby, G. Increasing the Analytical Sensitivity by Oligonucleotides Modified with Para- and Ortho-Twisted Intercalating Nucleic Acids-TINA. *PLoS One* **2011**, *6* (6), 1–10.

(184) Filichev, V. V.; Astakhova, I. V.; Malakhov, A. D.; Korshun, V. A.; Pedersen, E. B. 1-, 2-, and 4-Ethynylpyrenes in the Structure of Twisted Intercalating Nucleic Acids: Structure, Thermal Stability, and Fluorescence Relationship. *Chem. - A Eur. J.* **2008**, *14*, 9968–9980.

(185) Bomholt, N.; Osman, A. M. a; Pedersen, E. B. High Physiological Thermal Triplex Stability Optimization of Twisted Intercalating Nucleic Acids (TINA). *Org. Biomol. Chem.* **2008**, *6*, 3714–3722.

(186) Paramasivam, M.; Cogoi, S.; Filichev, V. V.; Bomholt, N.; Pedersen, E. B.; Xodo, L. E. Purine Twisted-Intercalating Nucleic Acids: A New Class of Anti-Gene Molecules Resistant to Potassium-Induced Aggregation. *Nucleic Acids Res.* **2008**, *36* (10), 3494–3507.

(187) Sun, J. S.; François, J. C.; Montenay-Garestier, T.; Saison-Behmoaras, T.; Roig, V.; Thuong, N. T.; Hélène, C. Sequence-Specific Intercalating Agents: Intercalation at Specific Sequences on Duplex DNA via Major Groove

Recognition by Oligonucleotide-Intercalator Conjugates. *Proc. Natl. Acad. Sci. U. S. A.* **1989**, *86*, 9198–9202.

(188) Takasugi, M.; Guendouz, A.; Chassignol, M.; Decout, J. L.; Lhomme, J.; Thuong, N. T.; Hélène, C. Sequence-Specific Photo-Induced Cross-Linking of the Two Strands of Double-Helical DNA by a Psoralen Covalently Linked to a Triple Helix- Forming Oligonucleotide. *Proc. Natl. Acad. Sci. U. S. A.* **1991**, *88*, 5602–5606.

(189) Sandor, Z.; Bredberg, A. Repair of Triple Helix Directed Psoralen Adducts in Human Cells. *Nucleic Acids Res.* **1994**, *22*, 2051–2056.

(190) Gasparro, F. P.; Havre, P. A.; Olack, G. A.; Gunther, E. J.; Glazer, P. M. Site-Specific Targeting of Psoralen Photoadducts with a Triple Helix-Forming Oligonucleotide: Characterization of Psoralen Monoadduct and Crosslink Formation. *Nucleic Acids Res.* **1994**, *22* (14), 2845–2852.

(191) Giovannangéli, C.; Thuong, N. T.; Héléne, C. Oligodeoxynucleotide-Directed Photo-Induced Cross-Linking of HIV Proviral DNA via Triple-Helix Formation. *Nucleic Acids Res.* **1992**, *20* (16), 4275–4281.

(192) Sandor, Z.; Bredberg, A. Triple Helix Directed Psoralen Adducts Induce a Low Frequency of Recombination in an SV40 Shuttle Vector. *BBA - Gene Struct. Expr.* **1995**, *1263*, 235–240.

(193) Raha, M.; Wang, G.; Seidman, M. M.; Glazer, P. M. Mutagenesis by Third-Strand-Directed Psoralen Adducts in Repair-Deficient Human Cells: High Frequency and Altered Spectrum in a Xeroderma Pigmentosum Variant. *Proc. Natl. Acad. Sci.* **1996**, *93*, 2941–2946.

(194) Wang, G.; Levy, D. D.; Seidman, M. M.; Glazer, P. M. Targeted Mutagenesis in Mammalian Cells Mediated by Intracellular Triple Helix Formation. *Mol. Cell. Biol.* **1995**, *15* (3), 1759–1768.

(195) Tyson, D. S.; Bialecki, J.; Castellano, F. N. Ruthenium(II) Complex with a Notably Longexcited State Lifetime. *Chem. Commun.* **2000**, 2355–2356.

(196) Garcìa-Fresnadillo, D.; Orellana, G. Interaction of Sulfonated Ruthenium(Ii) Polypyridine Complexes with Surfactants Probed by Luminescence Spectroscopy. *Helv. Chim. Acta* **2001**, *84*, 2708–2730.

(197) Mari, C.; Pierroz, V.; Ferrari, S.; Gasser, G. Combination of Ru(II) Complexes and Light: New Frontiers in Cancer Therapy. *Chem. Sci.* **2015**, *6*, 2660–2686.

(198) Blackmore, L.; Moriarty, R.; Dolan, C.; Adamson, K.; Forster, R. J.; Devocelle, M.; Keyes, T. E. Peptide Directed Transmembrane Transport and Nuclear Localization of Ru(II) Polypyridyl Complexes in Mammalian Cells. *Chem. Commun.* **2013**, *49*, 2658–2660.

(199) Byrne, A.; Burke, C. S.; Keyes, T. E. Precision Targeted Ruthenium(II) Luminophores; Highly Effective Probes for Cell Imaging by Stimulated Emission Depletion (STED) Microscopy. *Chem. Sci.* **2016**, *7*, 6551–6562.

(200) Paul Rillema, D.; Allen, G.; Meyer, T. J.; Conrad, D. Redox Properties of Ruthenium(II) Tris Chelate Complexes Containing the Ligands 2,2′-Bipyrazine, 2,2′-Bipyridine, and 2,2/-Bipyrimidine. *Inorg. Chem.* **1983**, *22*, 1617–1622.

(201) Barton, J. K.; Boynton, A. N.; Boyle, K. M. DNA-Targeting Molecules as Therapeutic Agents, The Royal Society of Chemistry. *R. Soc. Chem.* **2018**, 367–390.

(202) Clark, C. D.; Hoffman, M. Z.; Rillema, D. P.; Mulazzani, Q. G. Photophysics of Ruthenium(II) Complexes with 2-(2′-Pyridyl)Pyrimidine and 2,2′-Bipyridine Ligands in Fluid Solution. *J. Photochem. Photobiol. A Chem.* **1997**, *110*, 285–290.

(203) Barton, J. K.; Danishefsky, A. T.; Goldberg, J. M. Tris(Phenanthroline)Ruthenium(II): Stereoselectivity in Binding to DNA. *J. Am. Chem. Soc.* **1984**, *106*, 2172–2176.

(204) Eriksson, M.; Leijon, M.; Gräslund, A.; Hiort, C.; Nordén, B. Binding of Δ and Λ-$[Ru(Phen)_3]^{2+}$ to $[d(CGCGATCGCG)]_2$ Studied by NMR. *Biochemistry* **1994**, *33* (17), 5031–5040.

(205) Liu, Z.; Zhang, W.; Hu, L.; Li, H.; Zhu, S.; Xu, G. Label-Free and Signal-On Electrochemiluminescence Aptasensor for ATP Based on Target-Induced Linkage of Split Aptamer Fragments by Using $[Ru(Phen)_3]^{2+}$ Intercalated into Double-Strand DNA as a Probe. *Chem. - A Eur. J.* **2010**, *16*, 13356–13359.

(206) Bu, N. N.; Gao, A.; He, X. W.; Yin, X. B. Electrochemiluminescent Biosensor of ATP Using Tetrahedron Structured DNA and a Functional Oligonucleotide for

$Ru(Phen)_3^{2+}$ Intercalation and Target Identification. *Biosens. Bioelectron.* **2013**, *43*, 200–204.

(207) Tang, C. X.; Zhao, Y.; He, X. W.; Yin, X. B. A "Turn-on" Electrochemiluminescent Biosensor for Detecting Hg2+ at Femtomole Level Based on the Intercalation of $Ru(Phen)_3^{2+}$ into Ds-DNA. *Chem. Commun.* **2010**, *46*, 9022–9024.

(208) Notaro, A.; Gasser, G. Monomeric and Dimeric Coordinatively Saturated and Substitutionally Inert Ru(II) Polypyridyl Complexes as Anticancer Drug Candidates. *Chem. Soc. Rev.* **2017**, *46*, 7317–7337.

(209) Hotze, A. C. G.; Van Der Geer, E. P. L.; Kooijman, H.; Spek, A. L.; Haasnoot, J. G.; Reedijk, J. Characterization by NMR Spectroscopy, X-Ray Analysis and Cytotoxic Activity of the Ruthenium(II) Compounds [RuL3](PF6)2 (L = 2-Phenylazopyridine or o-Tolylazopyridine) and [RuL′ 2L″](PF6)2 (L′, L″ = 2-Phenylazopyridine, 2,2′-Bipyridine). *Eur. J. Inorg. Chem.* **2005**, 2648–2657.

(210) Friedman, A. E.; Barton, J. K.; Chambron, J. C.; Sauvage, J. P.; Turro, N. J.; Barton, J. K. Molecular "Light Switch" for DNA: $Ru(Bpy)_2(Dppz)^{2+}$. *J. Am. Chem. Soc.* **1990**, *112*, 4960–4962.

(211) Troian-Gautier, L.; Moucheron, C. RutheniumII Complexes Bearing Fused Polycyclic Ligands: From Fundamental Aspects to Potential Applications. *Molecules* **2014**, *19*, 5028–5087.

(212) Poynton, F. E.; Hall, J. P.; Keane, P. M.; Schwarz, C.; Sazanovich, I. V.; Towrie, M.; Gunnlaugsson, T.; Cardin, C. J.; Cardin, D. J.; Quinn, S. J.; et al. Direct Observation by Time-Resolved Infrared Spectroscopy of the Bright and the Dark Excited States of the $[Ru(Phen)_2(Dppz)]^{2+}$ Light-Switch Compound in Solution and When Bound to DNA. *Chem. Sci.* **2016**, *7*, 3075–3084.

(213) Mcconnell, A. J.; Lim, M. H.; Olmon, E. D.; Song, H.; Dervan, E. E.; Barton, J. K. Luminescent Properties of Ruthenium(II) Complexes with Sterically Expansive Ligands Bound to DNA Defects. **2012**, *51* (2), 12511-12520.

(214) Byrne, A.; Burke, S.; Keyes, T. E. Chemical Science Highly e Ff Ective Probes for Cell Imaging by Stimulated Emission Depletion (STED) Microscopy. *Chem. Sci.* **2016**, *7*, 6551–6563.

(215) Mari, C.; Pierroz, V.; Ferrari, S.; Gasser, G. Combination of Ru(II) Complexes and Light: New Frontiers in Cancer Therapy. *Chem. Sci.* **2015**, *6*, 2660–2686.

(216) Fan, S. H.; Zhang, A. G.; Ju, C. C.; Gao, L. H.; Wang, K. Z. A Triphenylamine-Grafted Imidazo[4,5-f][1,10]Phenanthroline Ruthenium(II) Complex: Acid-Base and Photoelectric Properties. *Inorg. Chem.* **2010**, *49*, 3752–3763.

(217) Liu, J.; Chen, Y.; Li, G.; Zhang, P.; Jin, C.; Zeng, L.; Ji, L.; Chao, H. Ruthenium(II) Polypyridyl Complexes as Mitochondria-Targeted Two-Photon Photodynamic Anticancer Agents. *Biomaterials* **2015**, *56*, 140–153.

(218) Zeng, L.; Chen, Y.; Liu, J.; Huang, H.; Guan, R.; Ji, L.; Chao, H. Ruthenium(II) Complexes with 2-Phenylimidazo[4,5-f][1,10]Phenanthroline Derivatives That Strongly Combat Cisplatin-Resistant Tumor Cells. *Sci. Rep.* **2016**, *6*, 1–13.

(219) Yu, B.; Rees, T. W.; Liang, J.; Jin, C.; Chen, Y.; Ji, L.; Chao, H. DNA Interaction of Ruthenium(II) Complexes with Imidazo[4,5-f] [1,10]Phenanthroline Derivatives. *Dalt. Trans.* **2019**, *48*, 3914–3921.

(220) Zheng, C.; Liu, Y.; Liu, Y.; Qin, X.; Zhou, Y.; Liu, J. Dinuclear Ruthenium Complexes Display Loop Isomer Selectivity to C-MYC DNA G-Quadruplex and Exhibit Anti-Tumour Activity. *J. Inorg. Biochem.* **2016**, *156*, 122–132.

(221) Neugebauer, U.; Pellegrin, Y.; Devocelle, M.; Forster, R. J.; Signac, W.; Moran, N.; Keyes, T. E. Ruthenium Polypyridyl Peptide Conjugates: Membrane Permeable Probes for Cellular Imaging. *Chem. Commun.* **2008**, 5307–5309.

(222) Cheng, F.; Ren, M.; He, C.; Yin, H. Luminescent Chemosensor for Hg^{2+} Ion Based on a Dinuclear Ru(II) Complex Containing Open Chain Azacrown Ether. *Inorganica Chim. Acta* **2016**, *450*, 170–175.

(223) He, C.; Yu, S.; Ma, S.; Liu, Z.; Yao, L.; Cheng, F.; Liu, P. A Novel Ruthenium (II) Polypyridyl Complex Bearing 1,8-Naphthyridine as a High Selectivity and Sensitivity Fluorescent Chemosensor for Cu^{2+} and Fe^{3+} Ions. *Molecules* **2019**, *24* (22), 4032–4045.

(224) Janaratne, T. K.; Yadav, A.; Ongeri, F.; MacDonnell, F. M. Preferential DNA Cleavage under Anaerobic Conditions by a DNA-Binding Ruthenium Dimer. *Inorg. Chem.* **2007**, *46* (9), 3420–3422.

(225) Coverdale, J.; Laroiya-McCarron, T.; Romero-Canelón, I. Designing Ruthenium

Anticancer Drugs: What Have We Learnt from the Key Drug Candidates *Inorganics* **2019**, *7* (31), 1–15.

(226) Hartinger, C. G.; Zorbas-Seifried, S.; Jakupec, M. A.; Kynast, B.; Zorbas, H.; Keppler, B. K. From Bench to Bedside - Preclinical and Early Clinical Development of the Anticancer Agent Indazolium Trans-[Tetrachlorobis(1H-Indazole)Ruthenate(III)] (KP1019 or FFC14A). *J. Inorg. Biochem.* **2006**, *100* (5–6), 891–904.

(227) Clarke, M. J. Ruthenium Metallopharmaceuticals. *Coord. Chem. Rev.* **2003**, *236* (1–2), 209–233.

(228) Clarke, M. J.; Zhu, F.; Frasca, D. R. Non-Platinum Chemotherapeutic Metallopharmaceuticals. *Chem. Rev.* **1999**, *99*, 2511–2533.

(229) Schatzschneider, U. Photoactivated Biological Activity of Transition-Metal Complexes. *Eur. J. Inorg. Chem.* **2010**, 1451–1467.

(230) Monro, S.; Colón, K. L.; Yin, H.; Roque, J.; Konda, P.; Gujar, S.; Thummel, R. P.; Lilge, L.; Cameron, C. G.; McFarland, S. A. Transition Metal Complexes and Photodynamic Therapy from a Tumor-Centered Approach: Challenges, Opportunities, and Highlights from the Development of TLD1433. *Chem. Rev.* **2019**, *119*, 797–828.

(231) Ostrowski, A. D.; Ford, P. C. Photoactivated Chemotherapy (PACT): The Potential of Excited-State d-Block Metals in Medicine. *Dalt. Trans.* **2009**, 10660–10669.

(232) Jacquet, L.; Kelly, J. M.; Kirsch-De Mesmaeker, A. Photoadduct between Tris(1,4,5,8-Tetraazaphenanthrene)Ruthenium(II) and Guanosine Monophosphate - A Model for a New Mode of Covalent Binding of Metal Complexes to DNA. *J. Chem. Soc. Chem. Commun.* **1995**, No. 9, 913–914.

(233) Jacquet, L.; Jeremy, R.; Davies, H.; Mesmaeker, A. K. De; Kelly, J. M. Photoaddition of Ru(Tap)2(Bpy)2+ to DNA: A New Mode of Covalent Attachment of Metal Complexes to Duplex DNA. *J. Am. Chem. Soc.* **1997**, *119* (49), 11763–11768.

(234) Troian-Gautier, L.; Mugeniwabagara, E.; Fusaro, L.; Moucheron, C.; Kirsch-De Mesmaeker, A.; Luhmer, M. PH Dependence of Photoinduced Electron Transfer

with [Ru(TAP)3]2+. *Inorg. Chem.* **2017**, *56*, 1794–1803.

(235) Troian-Gautier, L.; Mugeniwabagara, E.; Fusaro, L.; Cauët, E.; Kirsch-De Mesmaeker, A.; Luhmer, M. Photo-CIDNP Reveals Different Protonation Sites Depending on the Primary Step of the Photoinduced Electron-/Proton-Transfer Process with Ru(II) Polyazaaromatic Complexes. *J. Am. Chem. Soc.* **2017**, *139* (42), 14909–14912.

(236) Linciln, P.; Wilhelmsson, M.; Norden, B. DNA-Targeting Molecules as Therapeuthic Agents. *R. Soc. Chem.* **2018**, 45–69.

(237) Tanious, F. A.; Veal, J. M.; Buczak, H.; Ratmeyer, L. S.; Wilson, W. D. DAPI (4', 6-Diamidino-2-Phenylindóle) Binds Differently to DNA and RNA: Minor-Groove Binding at AT Sites and Intercalation at AU Sites. *Biochemistry* **1992**, *31*, 3103–3112.

(238) Eriksson, S.; Kim, S. K.; Kubista, M.; Nordén, B. Binding of 4′,6-Diamidino-2-Phenylindole (DAPI) to AT Regions of DNA: Evidence for an Allosteric Conformational Change. *Biochemistry* **1993**, *32*, 2987–2998.

(239) Norden, B.; Tjerneld, F. Binding of Inert Metal Complexes To Deoxyribonucleic Acid DETECTED BY LINEAR DICHROISM. *FEBS Lett.* **1976**, *67* (3), 368–370.

(240) Lincoln, P.; Nordén, B. DNA Binding Geometries of Ruthenium(II) Complexes with 1,10-Phenanthroline and 2,2′-Bipyridine Ligands Studied with Linear Dichroism Spectroscopy. Borderline Cases of Intercalation. *J. Phys. Chem. B* **1998**, *102*, 9583–9594.

(241) Chantzis, A.; Very, T.; Daniel, C.; Monari, A.; Assfeld, X. Theoretical Evidence of Photo-Induced Charge Transfer from DNA to Intercalated Ruthenium (II) Organometallic Complexes. *Chem. Phys. Lett.* **2013**, *578*, 133–137.

(242) Véry, T.; Ambrosek, D.; Otsuka, M.; Gourlaouen, C.; Assfeld, X.; Monari, A.; Daniel, C. Photophysical Properties of Ruthenium(II) Polypyridyl Dna Intercalators: Effects of the Molecular Surroundings Investigated by Theory. *Chem. Eur. J.* **2014**, *20*, 12901–12909.

(243) Hiort, C.; Lincoln, P.; Nordén, B. DNA Binding of Δ- and Λ-$[Ru(Phen)_2DPPZ]^{2+}$. *J. Am. Chem. Soc.* **1993**, *115*, 3448–3454.

(244) Kelly, J. M.; McConnell, D. J.; OhUigin, C.; Tossi, A. B.; Mesmaeker, A. K. De; Masschelein, A.; Nasielski, J. Ruthenium Polypyridyl Complexes; Their Interaction with DNA and Their Role as Sensitisers for Its Photocleavage. *J. Chem. Soc. Chem. Commun.* **1987**, No. 24, 1821–1823.

(245) Cardin, C. J.; Hall, J. P. DNA-Targeting Molecules as Therapeuthic Agents. In *Royal Society of Chemistry*; 2018; pp 198–224.

(246) Keane, P. M.; Hall, J. P.; Poynton, F. E.; Poulsen, B. C.; Gurung, S. P.; Clark, I. P.; Sazanovich, I. V.; Towrie, M.; Gunnlaugsson, T.; Quinn, S. J.; et al. Inosine Can Increase DNA′s Susceptibility to Photo-Oxidation by a Ru(II) Complex Due to Structural Change in the Minor Groove. *Chem. Eur. J.* **2017**, *23*, 10344–10351.

(247) Niyazi, H.; Hall, J. P.; O'Sullivan, K.; Winter, G.; Sorensen, T.; Kelly, J. M.; Cardin, C. J. Crystal Structures of λ-[Ru(Phen)2dppz]2+ with Oligonucleotides Containing TA/TA and AT/AT Steps Show Two Intercalation Modes. *Nat. Chem.* **2012**, *4*, 621–628.

(248) Song, H.; Kaiser, J. T.; Barton, J. K. Crystal Structure of Δ-Ru(Bpy)2 Dppz2+ Bound to Mismatched DNA Reveals Side-by-Side Metalloinsertion and Intercalation. *Nat. Chem.* **2012**, *4* (8), 615–620.

(249) Hall, J. P.; Keane, P. M.; Beer, H.; Buchner, K.; Winter, G.; Sorensen, T. L.; Cardin, D. J.; Brazier, J. A.; Cardin, C. J. Delta Chirality Ruthenium 'Light-Switch' Complexes Can Bind in the Minor Groove of DNA with Five Different Binding Modes. *Nucleic Acids Res.* **2016**, *44* (19), 9472–9482.

(250) Hall, J. P.; Cook, D.; Morte, S. R.; McIntyre, P.; Buchner, K.; Beer, H.; Cardin, D. J.; Brazier, J. A.; Winter, G.; Kelly, J. M.; et al. X-Ray Crystal Structure of Rac-$[Ru(Phen)_2dppz]^{2+}$ with $d(ATGCAT)_2$ Shows Enantiomer Orientations and Water Ordering. *J. Am. Chem. Soc.* **2013**, *135*, 12652–12659.

(251) Jenkins, Y.; Barton, J. K. A Sequence-Specific Molecular Light Switch : Complex of Ruthenium (II). *J. Am. Chem. Soc. 1992,* **1992**, *114*, 8736–8738.

(252) Olson, E. J. C.; Hu, D.; Hörmann, A.; Jonkman, A. M.; Arkin, M. R.; Stemp, E. D. A.; Barton, J. K.; Barbara, P. F. First Observation of the Key Intermediate in the "Light-Switch" Mechanism of $[Ru(Phen)_2dppz]^{2+}$. *J. Am. Chem. Soc.* **1997**, *119*, 377–384.

(253) Grimm, G. N.; Boutorine, A. S.; Lincoln, P.; Norde, B.; Helene, C. Formation of DNA Triple Helices by an Oligonucleotide Conjugated to a Fluorescent Ruthenium Complex. *ChemBioChem* **2002**, *3*, 324–331.

(254) Marcélis, L.; Van Overstraeten-Schlögel, N.; Lambermont, J.; Bontems, S.; Spinelli, N.; Defrancq, E.; Moucheron, C.; Mesmaeker, A. K. De; Raes, M. Light-Triggered Green Fluorescent Protein Silencing in Human Keratinocytes in Culture Using Antisense Oligonucleotides Coupled to a Photoreactive Ruthenium(II) Complex. *Chempluschem* **2014**, *79*, 1597–1604.

(255) Marcélis, L.; Ghesquière, J.; Garnir, K.; Kirsch-De Mesmaeker, A.; Moucheron, C. Photo-Oxidizing RuII Complexes and Light: Targeting Biomolecules via Photoadditions. *Coord. Chem. Rev.* **2012**, *256*, 1569–1582.

(256) Reschner, A.; Bontems, S.; Le Gac, S.; Lambermont, J.; Marcélis, L.; Defrancq, E.; Hubert, P.; Moucheron, C.; Kirsch-De Mesmaeker, A.; Raes, M.; et al. Ruthenium Oligonucleotides, Targeting HPV16 E6 Oncogene, Inhibit the Growth of Cervical Cancer Cells under Illumination by a Mechanism Involving P53. *Gene Ther.* **2013**, *20*, 435–443.

(257) Barton, J. K.; Murphy, C. J.; Arkin, M. R.; Jenkins, Y.; Ghatlia, N. D.; Bossmann, S. H.; Turro, N. J. Long-Range Photoinduced Electron Transfer Through a DNA Helix. *Science (80-.).* **1993**, *262*, 1025–1029.

(258) Park, M. J.; Fujitsuka, M.; Kawai, K.; Majima, T. Direct Measurement of the Dynamics of Excess Electron Transfer through Consecutive Thymine Sequence in DNA. *J. Am. Chem. Soc.* **2011**, *133*, 15320–15323.

(259) Meade, T. J.; Kayyem, J. F. Electron Transfer through DNA: Site-Specific Modification of Duplex DNA with Ruthenium Donors and Acceptors. *Angew. Chemie Int. Ed. English* **1995**, *34* (3), 352–354.

(260) Hurley, D. J.; Tor, Y. Donor/Acceptor Interactions in Systematically Modified RuII-OsII Oligonucleotides. *J. Am. Chem. Soc.* **2002**, *124*, 13231–13241.

(261) Stemp, E. D. A.; Barton, J. K. The Flash-Quench Technique in Protein-DNA Electron Transfer: Reduction of the Guanine Radical by Ferrocytochrome C. *Inorg. Chem.* **2000**, *39*, 3868–3874.

(262) Bhattacharya, P. K.; Barton, J. K. Influence of Intervening Mismatches on Long-

Range Guanine Oxidation in DNA Duplexes. *J. Am. Chem. Soc.* **2001**, *123* (36), 8649–8656.

(263) Arkin, M. R.; Stemp, E. D. A.; Pulver, S. C.; Barton, J. K. Long-Range Oxidation of Guanine by Ru(III) in Duplex DNA. *Chem. Biol.* **1997**, *4*, 389–400.

(264) Vargas-baca, I.; Mitra, D.; Zulyniak, H. J.; Banerjee, J.; Sleiman, H. F. Solid-Phase Synthesis of Transition Metal Linked, Branched Oligonucleotides. *Angew. Chem. Int. Ed.* **2001**, *40* (24), 4629–4632.

(265) Mitra, D.; Di Cesare, N.; Sleiman, H. F. Self-Assembly of Cyclic Metal-DNA Nanostructures Using Ruthenium Tris(Bipyridine)-Branched Oligonucleotides. *Angew. Chemie - Int. Ed.* **2004**, *43*, 5804–5808.

(266) Stewart, K. M.; McLaughlin, L. W. Design and Synthesis of DNA-Tethered Ruthenium Complexes That Self-Assemble into Linear Arrays. *Chem. Commun.* **2003**, *3*, 2934–2935.

(267) Cao, X. H.; Wang, Q.; Li, J.; Yi, C.; Li, M. J. Gold Nanoparticles Functionalized with Ru(II)Bipyridyl Labeled DNA as a Luminescent Probe for the Sensitive Determination of DNase I. *Microchim. Acta* **2017**, *184* (9), 3273–3279.

(268) Anzola, M.; Winssinger, N. Turn On of a Ruthenium(II) Photocatalyst by DNA-Templated Ligation. *Chem. - A Eur. J.* **2019**, *25* (1), 334–342.

CHAPTER 2

Synthesis and characterisation of new copper(II)- and ruthenium(II)-coordinating azide ligands and their hybridisation to oligonucleotides

2.1 Introduction

In this chapter synthetic procedures and the biophysical methods developed for the characterisation of hybrid materials are reported. The synthetic methods can be categorised into three sections: *i*.) the generation of azide-functionalised *mono*-nuclear phenanthroline/phenanzine derivates (ligands **A**, **B**, **C**, **D**, **E** and **F**) and the copper complex [Cu(**A**)]$(NO_3)_2$, exploited for crystallographic analysis; *ii*.) the synthesis of *di*-nuclear derivative (**G**) with the relative reference compound ($\mathbf{G_R}$) and the novel *di*-nuclear complexes [Cu_2(N,N'-phenanthrene)$_2$($\mathbf{G_R}$)]$(NO_3)_4$ and ; *iii*.) the procedures to prepare ruthenium(II) complexes containing azide-modified ligands. The organic azides reported in sections *i*. and *ii*. were designed for the generation of copper artificial nucleases while the ruthenium complexes in section *iii*. for the development of luminescent probes. The final step of each synthetic pathway was characterised using NMR, ATR, and mass analysis with the exception of compounds already reported in literature. The mass analysis is in agreement with the sensitivity of the instrument used for the characterisation. Preliminary elemental analysis was performed on several of the compounds, however the accuracy of the constituent ratios was poor. These results were difficult to reconcile with other successful analysis performed, however a previous publication has shown plausible inaccuracies in elemental analysis of nitrogen-rich compounds including azides, which are widely recognised as labile.[1] The second half of this chapter reports methods for the preparation of alkyne-modified oligonucleotides, corresponding hybrids that were generated through click chemistry, and the procedures developed for the characterisation of triplex formation, DNA cleavage, and the selectivity of nuclease activity by copper artificial nucleases. The luminescent properties of ruthenium(II) labelled oligonucleotides are also detailed in this section.

2.2 Materials and methods

All chemical reagents and solvents were obtained from Sigma-Aldrich (Ireland) Ltd. and unless otherwise stated were used without further purification. C8-Alkyne-dU-CEP was purchased from BaseClick GmbH. NMR spectra were recorded on Bruker AC 400 MHz or 600 MHz spectrometers (Appendix A-C). FT-IR spectra were collected on Perkin Elmer Spectrum Two spectrometer (Appendix A-E). Crystallographic data was collected at 100(1)K on a Synergy Dualflex, AtlasS2 diffractometer. The structure was solved by dual space methods and refined on F^2 using all the reflections (SHELXL-2018, Appendix

F). ESI-MS analysis was performed on a Bruker HCT Mass Spectrometer. pH was monitored using a Mettler Toledo InLab Expert Pro-ISM pH probe. Mass analysis of oligonucleotides was characterised at Matrix Assisted Laser Desorption Ionization Time of Flight (MALDI-TOF) on a Bruker Daltonics Autoflex II instrument (Appendix G). Thermal melting experiments were conducted on Agilent Cary 100 UV-Vis dual beam spectrophotometer equipped with a 6 × 6 Peltier multicell system with temperature controller. Fluorescence spectra were recorded on a Perkin Elmer LC55. UV–Vis spectra were recorded on a Jasco UV–vis spectrophotometer. Polyacrylamide gels were imaged on Syngene G:Box mini 9 gel documentation system.

2.3 Synthetic routes of azide-functionalised ligands

2.3.1 Preparation of 5-azido-1,10-phenanthroline (A, Route I)

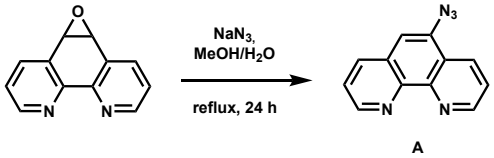

Scheme 2.1 Synthetic route for the generation of the ligand **A (Route I)**.

A three-step method for the synthesis and isolation of **A** has been reported,[2] however, a more efficient route was developed as follows. To a solution of 5,6-epoxy-5,6-dihydro-1,10-phenanthroline (100 mg, 0.51 mmol) in a 4:1 MeOH/H_2O mixture (8 mL of MeOH and 2 mL of H_2O), NaN_3 (99 mg, 1.53 mmol) was added and refluxed at 80 °C for 24 h. The resulting precipitate was removed by vacuum filtration and the filtrate was reduced to precipitate the product. Yield = 113 mg, quantitative yield. ^{1}H NMR and ^{13}C NMR data are consistent with those reported in literature.[2]

2.3.2 Preparation of 2-(4-azidophenyl)-1H-imidazo[4,5-f]-1,10-phenanthroline (B, Route II)

Ligand **B** was prepared in a similar manner to previously stated methods[3,4] with some modifications.

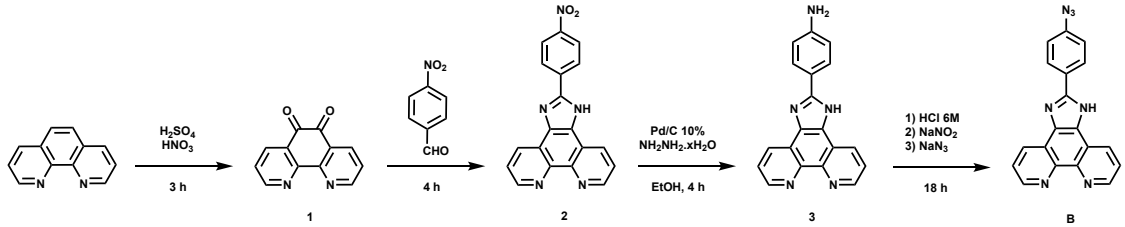

Scheme 2.2 Synthetic route for the generation of the ligand **B** (**Route II**).

1,10-phenanthroline-5,6-dione (**1**)

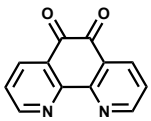

Coumpound **1** was prepared according to the literature method reported in literature.[5] 1,10-Phenanthroline (4.0 g, 22.19 mmol) and KBr (4.0 g, 33.6 mmol) were mixed and slowly added to an ice-cold mixture of H_2SO_4 and HNO_3 (2:1, 40 mL of H_2SO_4 and 20 mL of HNO_3).[4] The solution was refluxed for 3 h at 160 °C and, after cooling to room temperature, it was poured over crushed ice and adjusted with an aqueous NaOH solution to pH 4, yielding a yellow solution. The solution was extracted with $CHCl_3$ (in 8 × 100 mL portions) and the organic layers combined, dried over anhydrous magnesium sulfate and filtered before reducing to dryness to isolate a yellow powder. Yield: 4.19 g, 90%. ^{1}H NMR and ^{13}C NMR data are consistent with those reported in literature.[5]

2-(4-nitrophenyl)-1H-imidazo-[4,5-f]-1,10-phenanthroline (**2**)

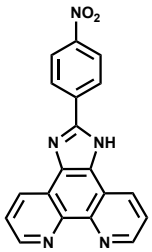

Coumpund **2** was prepared according to the literature method reported in literature.[6] Compound **1** (500 mg, 2.38 mmol), 4-nitrobenzaldehyde (540 mg, 3.57 mmol) and ammonium acetate were stirred in acetic acid (16 mL) under reflux for 2 h. The resulting solution was neutralised with ammonia and the product was recrystallised in the same mixture. Yield: 570 mg, 70%. ^{1}H NMR and ^{13}C NMR data are consistent with those reported in literature.[6]

4-(1H-imidazo-[4,5-f]-1,10-phenanthrolin-2-yl)aniline (**3**)

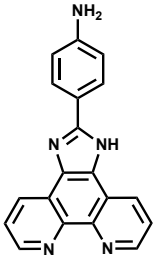

Coumpund **3** was prepared according to the literature method reported in literature with slight modifications.[7] Compound **2** (500 mg, 1.47 mmol) was treated with Pd/C 10% (0.1% m/m) in 110 mL of MeOH. An excess of hydrazine hydrate (5 mL) was added dropwise and refluxed for 2 h. The mixture was cooled to room temperature and stirred for 2 h. The solution was filtered on celite® and reduced until a yellow precipitate formed. Yield: 412 mg, 90%. ^{1}H NMR and ^{13}C NMR data are consistent with those reported in literature.[7]

2-(4-azidophenyl)-1H-imidazo[4,5-f]-1,10-phenanthroline (**B**)

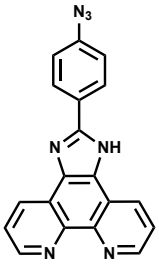

Ligand **B** was prepared according to the literature method reported in literature with slight modifications.[7] Compound **3** (200 mg, 0.64 mmol) was stirred in a 6 M HCl aqueous solution (10 mL) for 20 min at 0°C. $NaNO_2$ (66 mg, 0.96 mmol) in H_2O (1 mL) was added dropwise and stirred for 30 min, after which an aqueous solution of NaN_3 (125 mg, 1.92 mmol, 1 mL of H_2O) was added dropwise and stirred for a further 2 h. The mixture was neutralised with ammonia and the yellow product was isolated by vacuum filtration. Yield: 201 mg, 93%. ^{1}H NMR and ^{13}C NMR data are consistent with those reported in literature.[7]

2.3.3 Preparation of 11-azidodipyrido[3,2-a:2',3'-c]phenazine (C, Route II)

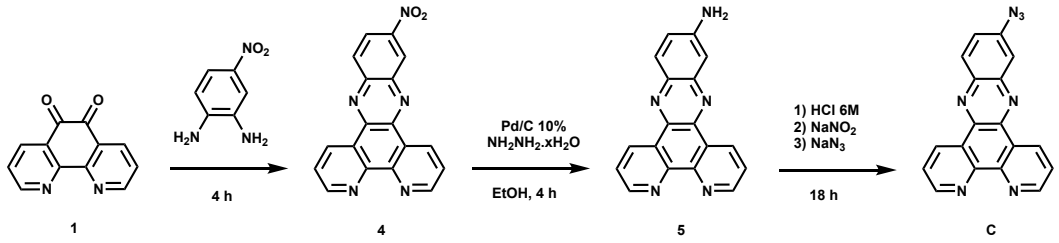

Scheme 2.3 Synthetic route for the generation of the ligand **C** (**Route II**).

11-nitrodipyrido[3,2-a:2',3'-c]phenazine (**4**)

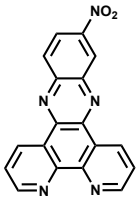

Coumpound **1** (500 mg, 2.38 mmol) and 4-nitrobenzene-1,2-diamine (547 mg, 3.57 mmol) were stirred in a mixture ethyl acetate/MeOH (7:1, 35 mL of ethyl acetate and 5 mL of MeOH) under reflux for 4 h. The resulting solid was recrystallised in the same mixture. Yield: 662 mg, 85%. ^{1}H NMR (600 MHz, $CDCl_3$) δ [ppm]: 9.63 (ddd, *J* = 8.0, 7.3, 1.8 Hz, 2H), 9.32 (td, *J* = 4.4, 1.8 Hz, 2H), 9.28 (d, *J* = 2.4 Hz, 1H), 8.67 (dd, *J* = 9.2, 2.5 Hz, 1H), 8.50 (d, *J* = 9.2 Hz, 1H), 7.84 (dt, *J* = 8.2, 4.2 Hz, 2H).^{13}C NMR (151 MHz, $CDCl_3$) δ [ppm]: 153.72, 153.54, 149.16, 148.81, 148.22, 144.29, 143.64, 143.22, 140.95, 134.40, 134.15, 131.28, 126.92, 126.87, 126.08, 124.60, 124.51, 123.74.

Dipyrido[3,2-a:2',3'-c]phenazin-11-amine (**5**)

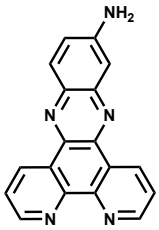

Compound **5** was prepared according to previously reported methods[8,9] with some modifications as follows: compound **4** (500 mg, 1.53 mmol) was treated with Pd/C 10% (0.1% m/m) in EtOH (60 mL). An excess of hydrazine hydrate (10 mL) was added dropwise and the mixture of reaction refluxed for 1 h. The hot solution was filtered on celite and filtrate was reduced to isolate a red precipitate. Yield: 409 mg, 90%. ^{1}H NMR and ^{13}C NMR data are consistent with those reported in literature.[8,9]

11-azidodipyrido[3,2-a:2',3'-c]phenazine (**C**)

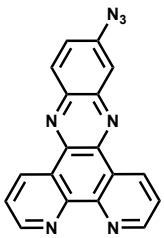

C oumpound **5 (**250 mg, 0.84 mmol) was treated with 10 mL of 6N HCl solution for 20 min at 70 °C. The solution was cooled to 0 °C and aqueous $NaNO_2$ (174 mg, 2.52 mmol, 1 mL of H_2O) was added dropwise and stirred for 30 min. The resulting solution was added dropwise to NaN_3 dissolved in H_2O (164 mg, 2.52 mmol, 1 mL of H_2O) and stirred for a further 2 h. The mixture was neutralised with ammonia and the red-brownish

precipitate was isolated by filtration. Yield: 250 mg, 92%. ^{1}H-NMR (600 MHz, $CDCl_3$) δ [ppm]: 9.57 (td, *J* = 8.2, 1.8 Hz, 2H), 9.27 (ddd, *J* = 8.7, 4.4, 1.8 Hz, 2H), 8.29 (d, *J* = 9.0 Hz, 1H), 7.93 (d, *J* = 2.5 Hz, 1H), 7.79 (ddd, *J* = 7.8, 4.4, 3.3 Hz, 2H), 7.54 (dd, *J* = 9.0, 2.5 Hz, 1H). ^{13}C NMR (151 MHz, $CDCl_3$) δ [ppm]: 152.94, 152.67, 148.70, 148.35, 143.12, 142.98, 141.90, 140.60, 140.58, 133.96, 133.69, 131.46, 127.62, 127.45, 124.56, 124.34, 124.32, 116.44. FT-IR (ATR, cm^{-1}): 2111, 1613, 1578, 1490, 1408, 1358, 1265, 1215, 1110, 1071, 809, 739. ESI-MS: *m*/*z* calcd., 324.1 $[M+H]^+$; found, 324.0.

2.3.4 Preparation of 5-amino-1,10-phenanthroline (7, Route III)

5-nitro-1,10-phenanthroline (**6**)

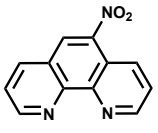

Compound **6** was synthesised using a method previously reported in literature.[10] 1,10-Phenanthroline (4.00 g, 22.19 mmol) was dissolved in ice-cold mixture of 2:1 H_2SO_4:HNO_3 (24 mL of H_2SO_4 and 12 mL of HNO_3) was slowly added. The solution was refluxed for 3 h at 160 °C, cooled down to room temperature and poured over crushed ice. The pH was adjusted (pH = 3) with aqueous NaOH to obtain a pale-yellow precipitate, which was then vacuum filtered and washed with H_2O. Yield: 5.00 g, quantitative yield. ^{1}H NMR and ^{13}C NMR data are consistent with those reported in literature.[10]

5-amino-1,10-phenanthroline (**7**)

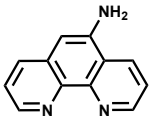

Compound **7** was synthesised using a method previously reported in literature with slight modifications.[11] Compound **7** (2 g, 8.88 mmol) was treated with Pd/C 10% (0.1% m/m) in the minimum amount of EtOH (40 mL). An excess of hydrazine hydrate (10 mL) was added dropwise and refluxed for 4 h. The hot solution was filtered on celite and the filtrate was reduced yielding a yellow precipitate. Yield: 1.70 g, 98%. ^{1}H NMR and ^{13}C NMR data are consistent with those reported in literature.[11]

2.3.5 Preparation of 5-azido-*N*-(1,10-phenanthrolin-5-yl)-pentanamide (D, Route IV)

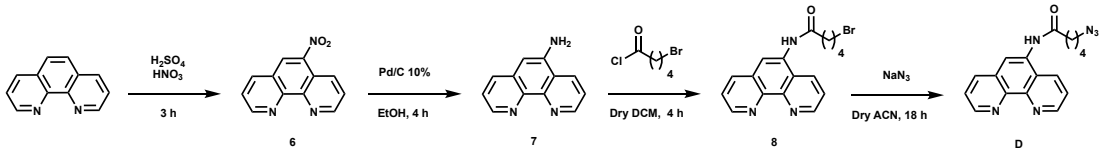

Scheme 2.4 Synthetic route for the generation of the ligand **D** (**Route IV**).

5-bromo-*N*-(1,10-phenanthrolin-5-yl)-pentanamide (**8**)

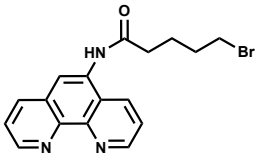

Compound **8** was prepared with minor modifications to an existing procedure.[12] Compound **7** (100 mg, 0.51 mmol) was treated with TEA (2 eq, 1.02 mmol) in dry DCM (10 mL) and stirred for 10 min at room temperature. The mixture was cooled and 5-bromovateryl acid chloride (1 eq, 0.51 mmol) was added dropwise at 0 °C and stirred for 4 h. The precipitate was collected by vacuum filtration, washed with DCM and the filtrate was collected and precipitated again in CH_2Cl_2. Yield: 178 mg, 97%. ^{1}H NMR and ^{13}C NMR data are consistent with those reported in literature.[12]

5-azido-*N*-(1,10-phenanthrolin-5-yl)-pentanamide (**D)**

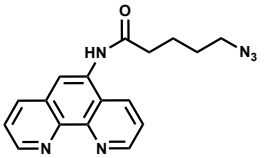

Compound **8 (**100 mg, 0.28 mmol) was treated with NaN_3 (18 mg, 0.28 mmol) in dry ACN (10 mL) and refluxed at 70 °C overnight. The precipitate was isolated by vacuum filtration and recrystallised in ACN. Yield: 88 mg, 98%. ^{1}H NMR (600 MHz, DMSO-d_6) δ [ppm]: 10.34 (s, 1H), 9.13 (dd, J = 4.2, 1.6 Hz, 1H), 9.02 (dd, J = 4.3, 1.7 Hz, 1H), 8.69 (d, J= 1H), 8.48 (d, J = 8.2 Hz, 1H), 8.19 (s, 1H), 7.85 (dd, J = 8.3, 4.3 Hz, 1H), 7.77 (dd, J = 8.0, 4.3 Hz, 1H), 3.72 (t, J = 6.3 Hz, 1H), 3.42 (t, J = 6.3 Hz, 1H), 2.61 (quintuplet, J = 6.7 Hz, 2H), 1.90−178 (quintuplet, 2H), 1.78–1.71 (quintuplet, 2H). ^{13}C NMR (151 MHz, DMSO-d_6) δ [ppm]: 172.13, 149.95, 149.37, 145.61, 143.46, 136.04, 132.08, 131.87, 128.12, 124.51, 123.72, 122.95, 119.79, 50.45, 45.17, 35.46, 31.64, 27.94, 22.60, 22.45. FT-IR (ATR, cm^{-1}): 3187, 3032, 2088, 1683, 1533, 1420, 1315, 1218, 1195, 878. ESI-MS: m/z calcd, 343.1 $[M+Na]^+$; found, 342.8.

2.3.6 Preparation of *N*-(4-azidobenzyl)-1,10-phenanthrolin-5-amine (E, Route V)

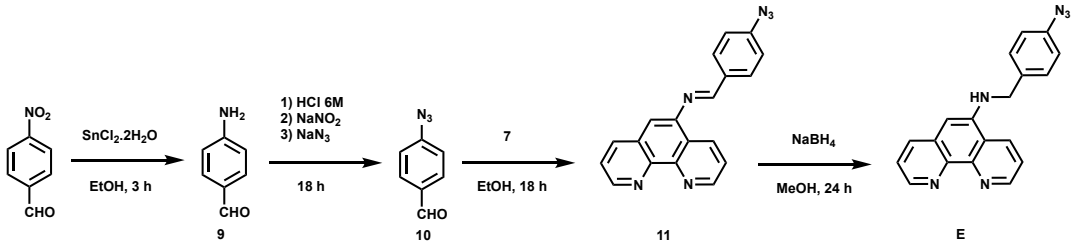

Scheme 2.5 Synthetic route for the generation of the ligand **E** (**Route V**).

4-aminobenzaldehyde (**9**)

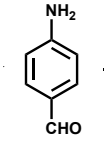

Compound **9** was synthesised as reported in literature.[13] 4-nitrobenzaldehyde (0.50 g, 3.31 mmol) and $SnCl_2 \cdot 2H_2O$ (5.04 g, 22.33 mmol) were refluxed in 10 mL EtOH at 70 °C for 1 h. The reaction mixture was then poured over ice and quenched with a saturated solution of sodium bicarbonate, extracted with ethyl acetate (200 mL), before adjusting to pH 5 with acetic acid. The product was extracted again with ethyl acetate where the combined organic layers were concentrated and dried under vacuum yielding an orange powder. Yield: 397 mg, 98%. ^{1}H NMR data are consistent with those reported in literature.[13]

4-azidobenzaldehyde (**10)**

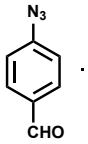

Compound **10** was synthesised as reported with some modifications.[14] 200 mg (1.65 mmol) of **9** was treated with 6 N HCl solution (5 mL) for 1 h on ice. Sodium nitrite (0.34 g, 4.97 mmol) dissolved in 1 mL of cold H_2O was added dropwise resulting in a brown-yellow solution which was stirred for 1 h. NaN_3 (0.32 g, 4.99 mmol, 1 mL of cold H_2O) was added dropwise and the solution was stirred overnight on ice. The reaction mixture was allowed to equilibrate to room temperature before adjustment to pH 7 with ammonia. The solution was extracted with ethyl acetate (400 mL), concentrated under vacuum to yield a dark yellow-brownish oil. Yield: 213 mg, 88%. ^{1}H NMR data are consistent with those reported in literature.[15]

(*E*)-1-(4-azidophenyl)-*N*-(1,10-phenanthrolin-5-yl)methanimine (**11**)

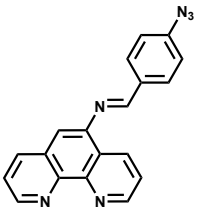

The compound **11** was synthesised using a similar procedure reported in literature with some modifications.[16] Coumpound **10** (213 mg, 1.45 mmol) and **7** (283 mg, 1.45 mmol) were refluxed overnight in dry MeOH (10 mL) with a catalytic amount of glacial acetic acid. A hot filtration was performed to collect the precipitate. The product was dried under vacuum and recrystallised with MeOH. Yield: 470 mg, ≥ 98%. ^{1}H NMR (600 MHz, DMSO-d_6) δ [ppm]: 9.16 (dd, J = 4.3, 2.0 Hz, 1H), 9.04 (dd, J = 4.4, 2.1 Hz, 1H), 8.89 (s, 1H), 8.80 (dd, J = 8.3, 2.2 Hz, 1H), 8.48 (dd, J = 8.1, 2.0 Hz, 1H), 8.21–811 (m, 2H), 7.83 (dd, J = 8.2, 4.2 Hz, 1H), 7.77 (dd, J = 8.1, 4.3 Hz, 1H), 7.70 (s, 1H), 7.38–7.31 (d, 2H). ^{13}C NMR (151 MHz, DMSO-d_6) δ [ppm]: 161.36, 150.24, 148.94, 147.00, 143.05, 136.49, 132.72, 132.13, 130.92, 129.41, 125.91, 123.60, 123.20, 119.71, 111.31. FT-IR (ATR, cm^{-1}): 2974, 2120, 1624, 1597, 1505, 1424, 1281, 1170, 1052, 805. ESI-MS: *m*/*z* calcd., 325.1 $[M+H]^+$; found, 324.7.

N-(4-azidobenzyl)-1,10-phenanthrolin-5-amine (**E**)

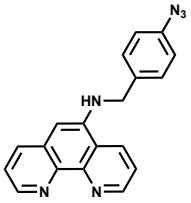

100 mg of compound **11 (**0.31 mmol) was treated with $NaBH_4$ (1 eq, 12 mg, 0.31 mmol) in dry MeOH at room temperature overnight. The mixture was dried under vacuum and purified with silica gel column chromatography in gradient of DCM:MeOH with 1% ammonia (9:1-8:2). Yield: 75 mg, 75%. ^{1}H NMR (600 MHz, DMSO-d_6) δ [ppm]: 9.07 (dd, J = 4.2, 1.5 Hz, 1H), 8.84 (dd, J = 8.5, 1.6 Hz, 1H), 8.67 (dd, J = 4.2, 1.7 Hz, 1H), 7.99 (dd, J = 8.2, 1.6 Hz, 1H), 7.78 (dd, J = 8.4, 4.2 Hz, 1H), 7.56 – 7.45 (m, 3H), 7.34 (t, 1H, -NH), 7.13 – 7.05 (d, J = 8.5 Hz, 2H), 6.60 (s, 1H), 4.58 (d, J = 5.6 Hz, 2H). ^{13}C NMR (151 MHz, DMSO-d_6) δ [ppm]: 149.43, 146.10, 145.04, 141.33, 140.51, 137.77, 136.45, 133.23, 130.37, 130.22, 128.75, 123.28, 122.00, 122.00, 119.10, 98.90, 45.82. FT-IR (ATR, cm^{-1}): 3258, 2105, 1594, 1537, 1506, 1413, 1280, 1107, 821, 740. ESI-MS: *m*/*z* calcd. for $C_{19}H_{14}N_6$ $[M+H]^+$ 327.1, found 327.0.

2.3.7 Preparation of 4-azido-*N*-(dipyrido[3,2-a:2',3'-c]phenazin-11-yl)butanamide (F, Route VI)

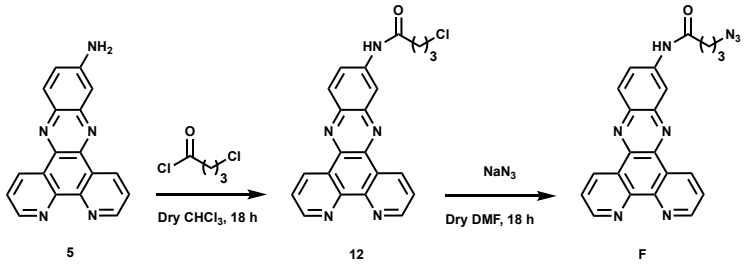

Scheme 2.6 Synthetic route for the generation of the ligand **F (Route VI)**.

4-chloro-*N*-(dipyrido[3,2-a:2',3'-c]phenazin-11-yl)butanamide (**12**)

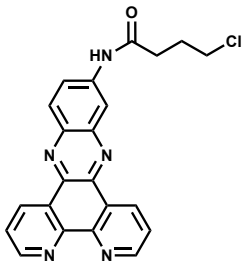

Compound **12** was synthesised using a method previously reported in literature with slight modification.[8] Compound **5** (100 mg, 0.34 mmol) was treated with TEA (2 eq, 0.68 mmol) in dry $CHCl_3$ (10 mL) and stirred for 10 min at room temperature. The mixture was cooled and 4-chlorobuteryl acid chloride (1 eq, 0.34 mmol) was added dropwise at 0 °C and stirred at room temperature overnight. The precipitate was collected by vacuum filtration, washed with chloroform and used immediately to prepare ligand **F**. Yield: 131 mg, 97%. ^{1}H NMR (600 MHz, DMSO-d_6) δ [ppm]: 10.81 (s, 1H), 9.79-9.59 (dd, J = 20.7, 7.0 Hz, 1H), 9.28 (ddd, J = 7.6, 2H), 8.91 (d, J = 2.2, 1H), 8.37 (d, J = 9.2 Hz, 1H), 8.12 (ddd, J = 11.6, 8.6, 3.4 Hz, 3H), 3.79 (t, J = 6.5 Hz, 2H), 2.66 (t, J=2.68, 2H), 2.14 (quint, J = 13.0, 6.7 Hz, 2H).

4-azido-*N*-(dipyrido[3,2-a:2',3'-c]phenazin-11-yl)butanamide (**F**)

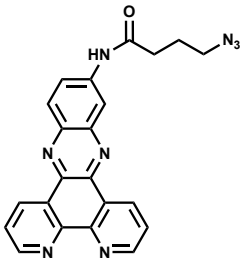

Compound **12** (100 mg, 0.249 mmol) was treated NaN_3 (16 mg, 0.249 mmol) in dry DMF (10 mL) and refluxed at 85 °C overnight. The mixture was poured over ice and vacuum filtered. Yield: 100 mg, quantitative yield. ^{1}H NMR (600 MHz, DMSO-d_6) δ [ppm]: 10.64 (s, 1H), 9.49 (dd, J = 8.1, 1.7 Hz, 1H), 9.45 (dd, J = 8.1, 1.7 Hz, 1H), 9.18 (ddd, J = 11.0, 4.3, 1.7 Hz, 2H), 8.81 (d, J = 2.2 Hz, 1H), 8.26 (d, J = 9.1 Hz, 1H), 8.00 (d, J = 2.3 Hz, 1H), 7.91 (ddd, J = 8.0, 4.3, 1.9 Hz, 2H), 3.48 (t, J = 6.8 Hz, 2H), 2.58 (t, J = 7.3 Hz, 2H), 1.94 (p, J = 7.0 Hz, 2H). ^{13}C NMR (151 MHz, DMSO-d_6) δ [ppm]: 171.97, 152.69, 152.35, 148.26, 147.87, 143.26, 141.63, 141.35, 139.34, 133.57, 133.11, 130.14, 127.54, 127.36, 125.95, 124.90,

114.84, 50.78, 34.02, 24.61. FT-IR (ATR, cm^{-1}): 2100, 1674, 1624, 1558, 1495, 1446, 1360, 1215, 1072, 1031. ESI-MS: *m*/*z* calcd., 407.1 $[M-H]^-$; found, 407.0.

2.3.8 Preparation of $[Cu(A)(NO_3)_2]$

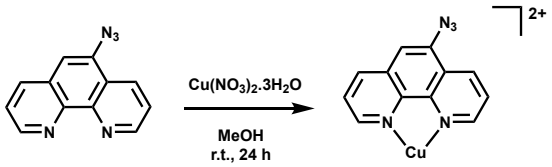

Scheme 2.7 Synthesis of $[Cu(\mathbf{A})_2](NO_3)_2$.

A solution of **A (**0.08 g, 0.36 mmol) in 5 mL of MeOH was added dropwise to a solution of copper(II) nitrate trihydrate (0.10 g, 0.41 mmol,) in 10 mL MeOH. The solution was left stirring overnight whereupon the colour changed from light blue to green. The product was filtered off, washed with diethyl ether and dried by desiccation. Yield: 0.10 g, 93%. FT-IR [neat, cm^{-1}]: 2131, 2062, 1431, 1471, 1396, 1277, 1015, 879, 807, 728. ESI-MS: *m*/*z* calcd. 345.99 $[M - (NO_3)]^+$; found, 345.99. The sample was obtained as dark green crystals from EtOH/H_2O (1:1) solution, which was allowed to stand at room temperature and after slow evaporation the crystals formed within 15 days.

2.3.9 Preparation of *N*,*N*'-((5-azido-1,3-phenylene)bis(methylene))bis(1,10-phenanthrolin-5-amine) (G)

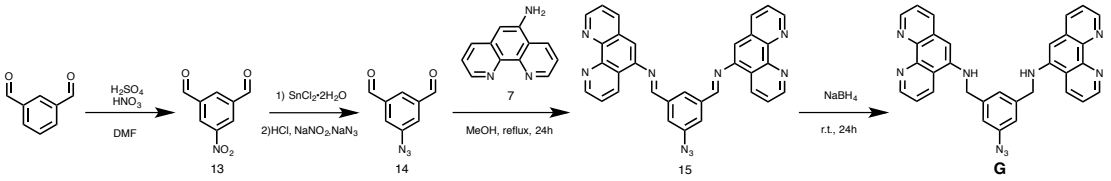

Scheme 2.8 Synthetic route for the generation of the ligand **G**.

5-nitroisophthalaldehyde (**13**)

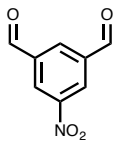

5-nitroisophthalaldehyde was prepared according to a method reported in literature with some modifications.[17] To a mixture of 2 g (15.13 mmol) of ammonium sulphate in 3.30 mL of sulphuric acid and 0.70 mL of nitric acid, 500 mg (3.73 mmol) of isophthalaldehyde solubilised in 3.30 mL of concentrated sulphuric acid were added. After 2 days the mixture was poured into ice to afford the precipitation of the white product which was filtered off and washed with copious H_2O. Yield: 334 mg, 50%. ^1H NMR (600 MHz, DMSO-d_6) δ [ppm]: 10.21 (s, 2H, -CHO), 8.96 (d, 2H), 8.72 (t, 1H).

5-azidoisophthalaldehyde (**14**)

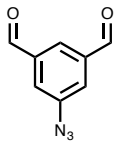

Compound **13** (0.20 g, 1.12 mmol), $SnCl_2.2H_2O$ (1.26 g, 5.6 mmol) and EtOH(10 mL) were refluxed at 70 °C for 3 h. The reaction mixture was then poured over ice and quenched with a saturated solution of sodium bicarbonate. The product was then extracted several times with ethyl acetate, before adjusting to pH 5 with acetic acid. The product was then extracted again with ethyl acetate. The combined organic layers were concentrated using the rotary evaporator and dried under vacuum overnight yielding a dark yellow powder. 100 mg (0.67 mmol) of the product was treated with 6 N HCl (5 mL) solution for 1 h on an ice bath. Afterwards, 3 equivalents of sodium nitrite (0.14 g, 2.011 mmol) in a 1 mL of cold H_2O was added dropwise with stirring, giving a brownish solution. After 1 hour, a solution of NaN_3 (0.13 g, 2.011 mmol, 1 mL of H_2O) was added dropwise and stirred overnight on ice. The mixture of reaction was allowed to equilibrate to room temperature before adjustment to pH 7 with ammonia. The solution was extracted 10 times with ethyl acetate. It was then concentrated (in darkness) to yield a dark orange-yellowish oil. Yield: 0.17 g, 87%. ^{1}H NMR (600 MHz, DMSO-d_6) δ [ppm]: 10.08 (s, 2H), 8.14 (t, 1H), 7.78 (d, 2H). FTIR-ATR (neat, cm^{-1}): 3066, 2924, 2853, 2131, 1689, 1595, 1463, 1392, 1379, 1316.

(1*E*,1'*E*)-1,1'-(5-azido-1,3-phenylene)bis(*N*-(1,10-phenanthrolin-5-yl)methanimine*)* (**15**)

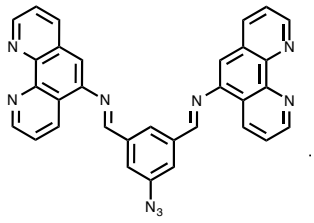

Compound **15** was synthesised using the same procedure adopted for **E**. Compound **14** (0.10 g, 0.57 mmol) and **7** (0.33g, 1.71 mmol, 3 eq) were stirred in dry MeOH (20 mL) under reflux and overnight with catalytic amount of glacial acetic acid. Afterwards, a hot filtration was performed. The solid was collected, dried under vacuum and recrystallised with MeOH. Yield: 0.303 g, ≥ 98%. ^{1}H NMR (600 MHz, $CDCl_3$): δ 9.26 (dd, J = 4.3, 1.8 Hz, 2H), 9.16 (dd, J = 4.3, 1.7 Hz, 2H), 8.84 – 8.76 (m, 4H), 8.41 (t, J = 1.4 Hz, 1H), 8.27 – 8.23 (m, 2H), 7.94 (d, J = 1.4 Hz, 2H), 7.70 (dd, J = 8.2, 4.3 Hz, 2H), 7.64 (dd, J = 8.0, 4.3 Hz, 2H), 7.38 (s, 2H). ^{13}C NMR (151 MHz, $CDCl_3$): δ 159.67, 151.07, 149.89, 149.84, 147.23, 146.53, 145.65, 142.38, 138.40, 135.98, 132.77, 128.88, 127.12, 126.83, 126.04, 123.56, 123.15, 122.05, 111.04, 77.37, 77.16, 76.95, 1.16. FT-IR (ATR, cm^{-1}): 3332, 3030, 2109, 1631, 1581, 1420, 1312, 1136, 1060, 890.

N,*N*'-((5-azido-1,3-phenylene)bis(methylene))bis(1,10-phenanthrolin-5-amine) (**G**)

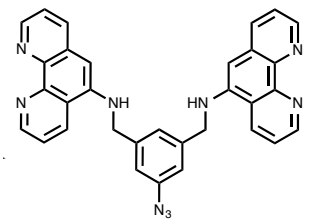

Compound **15** (100 mg, 0.19 mmol) was treated with $NaBH_4$ (21 mg, 0.56 mmol, 3 eq) in dry MeOH (10 mL) at room temperature overnight. The mixture was dried under vacuum and purified with silica gel column chromatography in DCM:MeOH with gradient 9:1 – 8:2 and 1% ammonia. Yield: 60 mg, 60%. ^{1}H NMR (600 MHz, MeOD-d4 + $CDCl_3$): δ 8.95 (d, J = 4.3 Hz, 2H), 8.58 (d, J = 4.4 Hz, 2H), 8.47 (d, J = 8.4 Hz, 2H), 7.66 – 7.49 (m, 4H), 7.40 – 7.24 (m, 3H), 7.05 (s, 2H), 6.34 (s, 2H), 4.61 (s, 4H). FT-IR (ATR, cm^{-1}): 3280, 2104, 1611, 1593, 1536, 1410, 1299, 1219, 1165, 1106. ESI-MS: *m*/*z* calcd. 534.2 $[M+H]^+$; found 534.2.

2.4 Preparation of *N*,*N*'-(1,3-phenylenebis(methylene))bis(1,10-phenanthrolin-5-amine) (G_R)

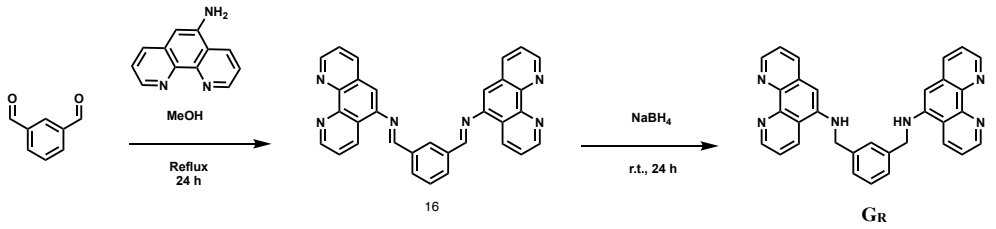

Scheme 2.9 Synthetic route for the generation of the ligand G_R.

(1*E*,1'*E*)-1,1'-(5-azido-1,3-phenylene)bis(N-(1,10-phenanthrolin-5-yl)methanimine*)* (**16**).

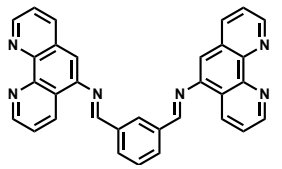

The compound **16** was synthesised using a similar procedure reported in literature with some modifications.[16] Isophthalaldehyde (82 mg, 0.61 mmol, 1 eq) and compound **7** (2 eq) were stirred in 10 mL of dry MeOH under reflux overnight with a catalytic amount of glacial acetic acid. The solid was collected by hot filtration, dried under vacuum and recrystallised with MeOH. Yield: 300 mg, ≥ 98%. ^{1}H NMR (600 MHz, $CDCl_3$): δ 9.26 (dd, J = 4.3, 1.8 Hz, 2H), 9.16 (dd, J = 4.3, 1.7 Hz, 2H), 8.88 – 8.78 (m, 4H), 8.75 – 8.69 (m, 1H), 8.30 – 8.22 (m, 4H), 7.77 (t, J = 7.6 Hz, 1H), 7.70 (dd, J = 8.2, 4.3 Hz, 2H), 7.65 (dd, J = 8.0, 4.3 Hz, 2H), 7.39 (s, 2H). ^{13}C NMR (151 MHz, $CDCl_3$): δ 160.77, 151.00, 149.70, 147.68, 146.56, 145.58, 136.88, 135.92, 132.85, 132.52, 130.01, 129.88, 129.02, 126.18, 123.53, 123.10, 110.93, 77.37, 77.16, 76.95.

N,*N*'-(1,3-phenylenebis(methylene))bis(1,10-phenanthrolin-5-amine (**G_R**).

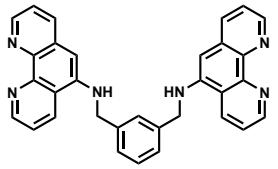

The compound **16** was synthesised using a similar procedure reported in literature with some modifications.[16] 300 mg of compound **16** (0.61 mmol) was treated with $NaBH_4$ (10 eq, 232 mg, 6.1 mmol) in dry MeOH at room temperature and overnight. The mixture was diluted with H_2O and extracted with chloroform. Yield: 300 mg, ≥ 98%. ^{1}H NMR (600 MHz, $CDCl_3$): δ 9.19 (dd, J = 4.3, 1.6 Hz, 2H), 8.91 (dd, J = 4.3, 1.7 Hz, 2H), 8.21 (dd, J = 8.4, 1.6 Hz, 2H), 7.91 (dd, J = 8.1, 1.7 Hz, 2H), 7.64 – 7.53 (m, 3H), 7.50 – 7.40 (m, 5H), 6.71 (s, 2H), 4.77 (t, J = 5.2 Hz, 2H), 4.62 (d, J = 5.2 Hz, 4H). ^{13}C NMR (151 MHz, $CDCl_3$): δ 150.20, 146.95, 146.89, 142.08, 140.71, 139.22, 133.89, 130.30, 129.64, 128.49, 127.25, 126.95, 123.52, 122.38, 122.13, 101.23, 48.57. FT-IR (ATR, cm^{-1}): 3307, 1615, 1594, 1563, 1538, 1412, 1323, 1301, 1223, 1166.

2.4.1 Preparation of $[Cu_2(N,N'\text{-phenanthrene})_2(G_R)](NO_3)_4$ (where N,N'-phenanthrene= Phen, DPQ and DPPZ)

For the generation of the novel *di*-nuclear copper complexes, procedures were followed to generate mono-nuclear N,N'-phenanthrene complexes $[Cu(Phen)(NO_3)_2]$, $[Cu(DPQ)(NO_3)_2]$ and $[Cu(DPPZ)(NO_3)_2]$,[5,18] followed thereafter by the addition of ligand **G_R**.

General procedure for the preparation of $[Cu(N,N'\text{-phenanthrene})(NO_3)_2]$: A solution of 1,10-phenanthroline monohydrate (Phen, 0.081 g, 0.41 mmol) or pyrazino[2,3-*f*][1,10]phenanthroline (DPQ, 0.095 g, 0.41 mmol) or dipyrido[3,2-*a*:2',3'-*c*]phenazine (DPPZ, 0.12 g, 0.41 mmol) in 5 mL of EtOH was added dropwise to a solution of copper(II) nitrate trihydrate (0.10 g, 0.41 mmol) in 5 mL EtOH. The mixture of reaction was refluxed for 4 h and stirred overnight. The resulting precipitate was filtered off, washed with diethyl ether and dried by desiccation.

General procedure for the preparation of $[Cu_2(N,N'\text{-phenanthrene})_2(\mathbf{G_R})](NO_3)_4$:

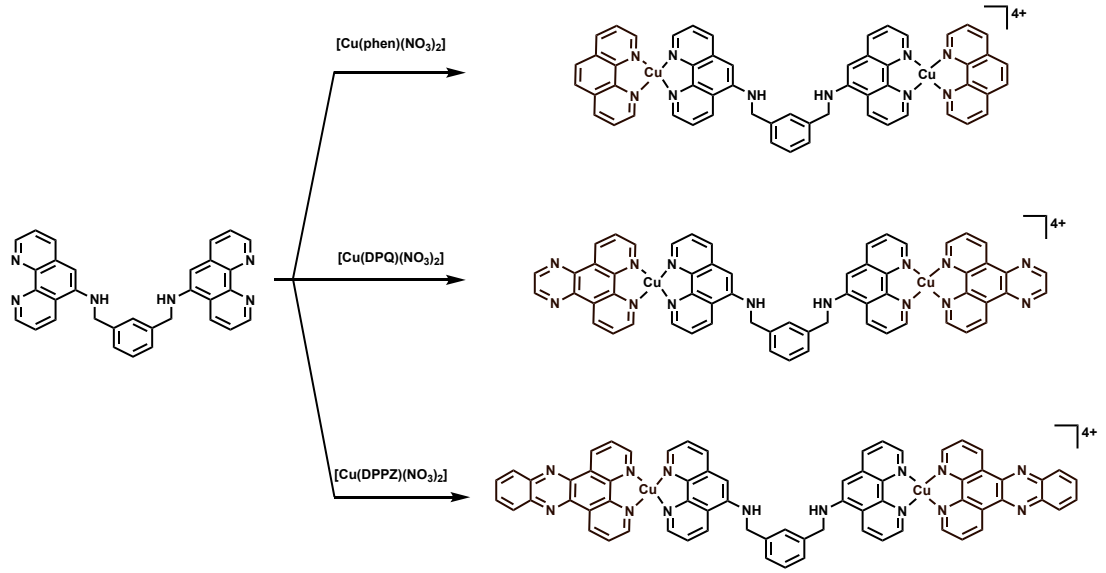

Scheme 2.10 Synthetic route for the generation of the complexes $[Cu_2(N,N'\text{-phenanthrene})_2(\mathbf{G_R})](NO_3)_4$.

A hot ethanolic solution of $\mathbf{G_R}$ (50 mg, 0.1 mmol) was added dropwise to a solution of 2 eq. of the mono-copper-phenanthroline species: $[Cu(Phen)](NO_3)_2$, 0.073 g, 0.2 mmol; $[Cu(DPQ)](NO_3)_2$, 0.084 g, 0.2 mmol; or $[Cu(DPPZ)](NO_3)_2$, 0.094 g, 0.2 mmol. The mixture was then refluxed overnight and the products were collected by filtration and washed several times with diethyl ether.

$[Cu_2(Phen)_2(\mathbf{G_R})](NO_3)_4.3H_2O$: Yield: 103 mg, 90%. Dark yellow-green solid. Anal. Calc. for $C_{56}H_{46}Cu_2N_{14}O_{15}$: C, 52.46; H, 3.62; N, 15.29. %Found C, 52.39; H, 3.84; N, 15.24. FT-IR (ATR, cm^{-1}): 3344, 3077, 1621, 1601, 1538, 1464, 1427, 1314, 1169, 1117, 1037, 992, 918.

$[Cu_2(DPQ)_2(\mathbf{G_R})](NO_3)_4.5H_2O$+EtOH: Yield: 119 mg, 85%. Dark yellow-green solid. Anal. Calc. for $C_{62}H_{56}Cu_2N_{18}O_{18}$: C, 50.72; H, 3.84; N, 17.17. %Found C, 51.16; H, 3.76; N, 16.85. FT-IR (ATR, cm^{-1}): 3345, 3077, 1621, 1601, 1586, 1533, 1464, 1436, 1373, 1289, 1171, 1083, 1021.

$[Cu_2(DPPZ)_2(\mathbf{G_R})](NO_3)_4.5H_2O$: Yield: 103 mg, 87%. Dark yellow-green solid. Anal. Calc. for $C_{68}H_{54}Cu_2N_{18}O_{17}$: C, 53.65; H, 3.58; N, 16.56. %Found C, 52.85; H, 3.26; N, 17.21. FT-IR (ATR, cm^{-1}): 3352, 3069, 1620, 1600, 1539, 1495, 1460, 1425, 1308, 1189, 1138, 1117.38, 1034.

2.5 Preparation of ruthenium(II) complexes

2.5.1 Preparation of [Ru(1,10-phenanthroline)$_2$(5-azido-1,10-phenanthroline)](PF$_6$)$_2$

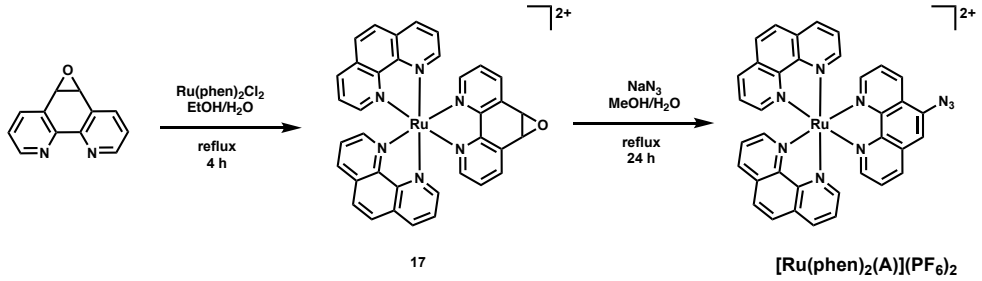

Scheme 2.11 Synthetic route for the generation of the complex [Ru(phen)$_2$(**A**)](PF$_6$)$_2$.

[Ru(1,10-phenanthroline)$_2$(5,6-epoxy-5,6-dihydro-1,10 phenanthroline)](PF$_6$)$_2$ (**17**).

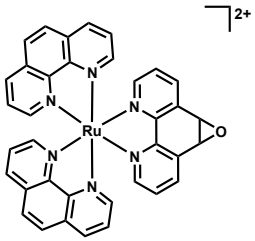

This compound was synthesised using a method reported in literature for [Ru(2,2'-bipyridine)$_2$(5,6-epoxy-5,6-dihydro-1,10-phenanthroline)] (PF$_6$)$_2$.[19] [Ru(1,10-phenanthroline)$_2$Cl$_2$][20] (0.10 g, 0.19 0.188 mmol) and 5,6-dihydro-1,10-phenanthroline (0.036 g, 0.18 mmol) were refluxed for 4 h under N_2 in a mixture of H_2O:EtOH (4:1, 8 mL H_2O and 2 mL EtOH). The reaction mixture was then allowed to equilibrate to room temperature and added dropwise to a saturated solution of ammonium hexafluorophosphate. The product was filtered and washed with EtOH and diethyl ether to give [Ru(1,10-phenanthroline)$_2$(5,6-epoxy-5,6-dihydro-1,10-phenanthroline)](PF$_6$)$_2$ as an orange powder. Yield: 0.155 g, 87%. ^{1}H NMR (600 MHz in DMSO-d_6): δ 8.85 (m, 2H); 8.75 (m, 2H); 8.5 (m, 2H); 8.35 (m, 4H); 8.25 (d, 1H); 8.15 (d, 1H); 7.95 (m, 3H); 7.85 (m, 1H); 7.8 (d, 1H); 7.7 (m, 2H); 7.65 (d, 1H); 7.55 (m, 1H); 7.45 (m, 1H); 5.15 (m, 2H).

[Ru(1,10-phenanthroline)$_2$(5-azido-1,10-phenanthroline)](PF$_6$)$_2$ ([Ru(phen)$_2$(**A**)](PF$_6$)$_2$).

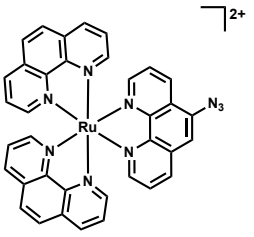

[Ru(phen)$_2$(**A**)](PF$_6$)$_2$ was synthesised as outlined above using ligand **A**. After the reaction mixture was allowed to cool excess solvent was reduced under a nitrogen flux and the resultant precipitate was filtered and washed with diethyl ether to give [Ru(1,10-phenanthroline)$_2$(5-azido-1,10-phenanthroline)](PF$_6$)$_2$ as a red powder. Yield: 0.122 g, 77%. ^{1}H NMR (600 MHz in DMSO-d_6): δ 8.75 (m, 4H); 8.65 (m, 2H); 8.35 (m, 5H); 8.15 (m, 1H); 8.07 (m, 2H); 8.05 (m, 2H); 7.98 (m, 1H); 7.75

(m, 6H). FT-IR (ATR, neat, cm^{-1}): 2119, 1600, 1420, 1317, 1275, 832, 740, 720, 556, 528. ESI-MS: *m/z* calcd. for $[C_{36}H_{23}N_9Ru]^{2+}$ $[M\text{-}N_2]^{2+}$ 327.5, found 327.6.

2.5.2 Preparation of of [Ru(1,10-phenanthroline)$_2$(2-(4-azidophenyl)-1-H-imidazo[4,5-f][1,10]-phenanthroline)](PF$_6$)$_2$

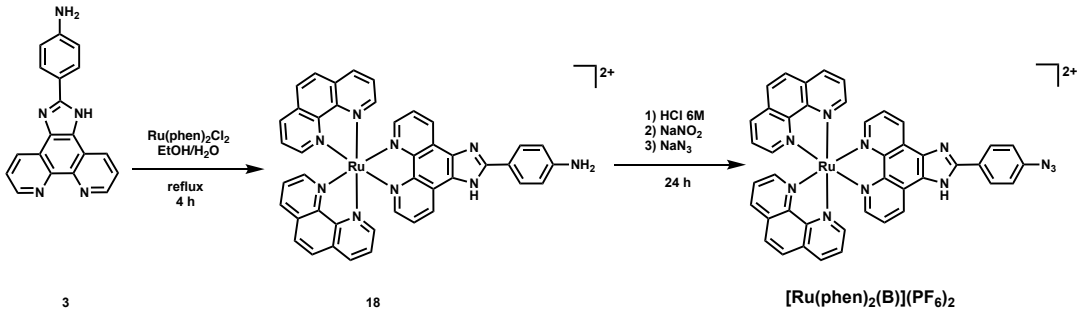

Scheme 2.12 Synthetic route for the generation of the complex [Ru (phen)$_2$(**B**)](PF$_6$)$_2$.

[Ru(1,10-phenanthroline)$_2$ (4(1-H-imidazo[4,5-f][1,10]-phenanthrolin-2-yl)aniline)](PF$_6$)$_2$ (**18**).

[Ru(1,10-phenanthroline)$_2$Cl$_2$] (0.086 g, 0.16 mmol), and compound **3** (0.058 g, 0.17 mmol) were refluxed in EtOH (2 mL) and deionised H_2O (8 mL) under inert conditions for 4 h. The reaction mixture was allowed to cool and was then added dropwise to a saturated solution of ammonium hexafluorophosphate. The resultant precipitate was then filtered and washed with diethyl ether to give a black solid. The filtrate was re-precipitated with ammonium hexafluorophosphate and re-filtered to give a pale brown solid. Yield: 0.104 g, 86%. ^{1}H NMR (600 MHz in DMSO-d_6): δ 13.85 (s, 1H), 9.02 (ddd, J = 8.4, 4.0, 1.3 Hz, 2H), 8.77 (dd, J = 8.2, 1.3 Hz, 4H), 8.39 (s, 4H), 8.16 – 8.05 (m, 4H), 8.02 – 7.91 (m, 4H), 7.78 (ddd, J = 19.9, 8.4, 5.3 Hz, 6H), 6.82 – 6.72 (m, 2H), 5.78 (s, 2H).

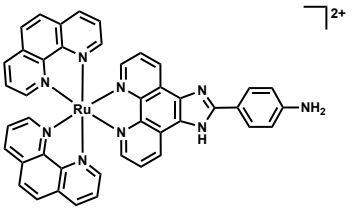

[Ru(1,10-phenanthroline)$_2$(2-(4-azidophenyl)-1-H-imidazo[4,5-f][1,10]-phenanthroline)](PF$_6$)$_2$ ([Ru(phen)$_2$(**B**)](PF$_6$)$_2$).

[Ru(1,10-phenanthroline)$_2$(4(1-H-imidazo[4,5-f][1,10]-phenanthrolin-2-yl)aniline)](PF$_6$)$_2$ (0.104 g, 0.093 mmol) was stirred with a solution of HCl 6 M for 1 h on ice. The solution was black in colour. Afterwards, sodium nitrite (1 eq) in the minimum amount of H_2O was added dropwise to give a brown solution and stirred on ice for 1 h. A solution of NaN_3 (1 eq) in the minimum amount of H_2O was

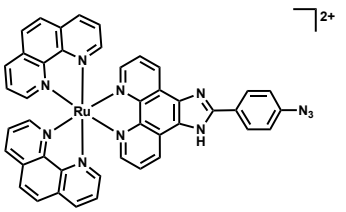

added dropwise and stirred overnight on ice. The precipitate was filtered and washed with ether. The final product [Ru(1,10-phenanthroline)$_2$(2-(4-azidophenyl)-1-*H*-imidazo[4,5-*f*][1,10]-phenanthroline)](PF$_6$)$_2$ was a brown-orange solid. Yield: 0.086 g, 81%. ^{1}H NMR (600 MHz in DMSO-d_6): δ 9.29 – 9.17 (m, 2H), 8.80 – 8.74 (m, 4H), 8.52 – 8.45 (m, 2H), 8.39 (s, 4H), 8.13 (d, J = 5.4 Hz, 2H), 8.10 – 8.06 (m, 2H), 8.03 – 7.98 (m, 2H), 7.78 (ddd, J = 20.1, 8.3, 5.3 Hz, 6H), 7.44 – 7.35 (m, 2H). FT-IR (neat, cm^{-1}): 3098, 2263, 1932, 1589, 1428, 1248, 1202, 1202, 1147, 1079, 832. ESI-MS: *m*/*z* calcd. for $[C_{43}H_{27}N_{11}Ru]^{2+}$ [M -N]$^{2+}$ 392.9, found 393.4 and [M-N$_3$]$^{2+}$ 378.6, found 378.5.

2.5.3 Preparation of [Ru)(1,10-phenanthroline)$_2$(11-azidodipyrido[3,2-a:2',3'-c]phenazine)](PF$_6$)$_2$

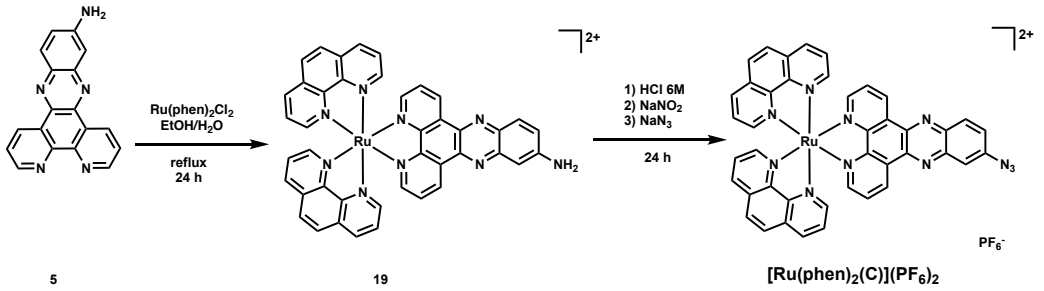

Scheme 2.13 Synthetic route for the generation of the complex [Ru(phen)$_2$(**C**)](PF$_6$)$_2$.

[Ru(1,10-phenanthroline)$_2$(dipyrido[3,2-a:2',3'-c]phenazin-11-amine)](PF$_6$)$_2$ (**19**).

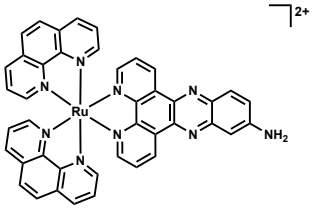

This intermediate was synthesised using a different method to that reported in the literature.[21] [Ru(1,10-phenanthroline)$_2$Cl$_2$] (0.052 g, 0.098 mmol) and compound **5** (0.0271 g, 0.087 mmol) were refluxed in EtOH (10 mL) overnight, under inert conditions. The reaction mixture was allowed to cool and the solvent in excess was dried under N_2. The reaction mixture was added dropwise to a solution of ammonium hexafluorophosphate in the minimum amount of H_2O. The resultant precipitate was filtered and washed with EtOH and diethyl ether to give [Ru(1,10-phenanthroline)$_2$(dipyrido[3,2-*a*:2',3'-*c*]phenazin-11-amine)](PF$_6$)$_2$ as a red powder. The product was recrystallised in ACN. Yield: 0.095 g, 87%. ^{1}H NMR (600 MHz in DMSO-d_6): δ 9.55 (d, 1H); 9.45 (d, 1H); 8.6 (t, 4H); 8.4 (t, 4H); 8.25 (m, 2H); 8.15 (dd, 2H); 8.05 (m, 3H); 7.8 (m, 6H); 7.6 (m, 1H); 7.15 (s, 1H); 6.85 (s, 2H).

[Ru(1,10-phenanthroline)$_2$(11-azidodipyrido[3,2-*a*:2',3'-*c*]phenazine)](PF$_6$)$_2$ ([Ru(phen)$_2$(**C**)](PF$_6$)$_2$).

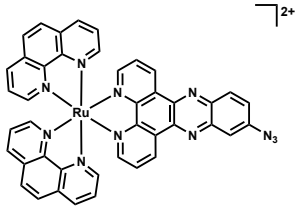

This complex was synthesised using the same method outlined for [Ru(phen)$_2$(**B**)](PF$_6$)$_2$. The final product Ru(1,10-phenanthroline)$_2$(11-azidodipyrido[3,2-*a*:2',3'-*c*]phenazine) (Ru(phen)$_2$(**C**)](PF$_6$)$_2$). was isolated as a red-orange powder. Yield: 52%. ^{1}H NMR (600 MHz in DMSO-d_6): δ 9.55 (q, 1H); 9.4 (q, 1H); 9.05 (m, 1H); 8.8 (m, 4H); 8.5 (m, 1H); 8.4 (m, 5H); 8.3 (m, 1H); 8.2 (dd, 1H); 8.05 (m, 3H); 7.9 (m, 3H); 7.8 (m, 2H); 7.75 (m, 2H). FTIR-ATR (neat, cm^{-1}): 3285, 2086, 1611, 1491, 1412, 1347, 1251, 1079, 829, 699.

2.5.4 Preparation of [Ru(5-azido-N-(1,10-phenanthrolin-5yl)pentanamide)(1,10-phenanthroline)$_2$]$(PF_6)_2$

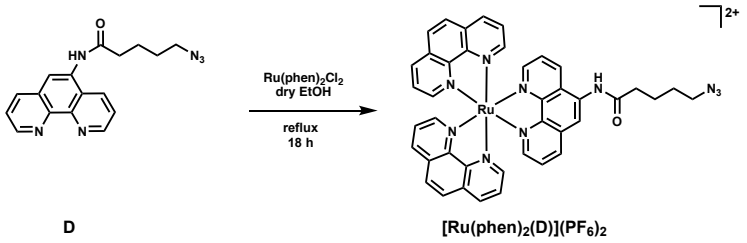

Scheme 2.14 Synthetic route for the generation of the complex [Ru(phen)$_2$(**D**)](PF$_6$)$_2$.

[Ru(1,10-phenanthroline)$_2$(5-azido-N-(1,10-phenanthrolin-5-yl)pentanamide)](PF$_6$)$_2$ ([Ru(phen)$_2$(**D**)](PF$_6$)$_2$).

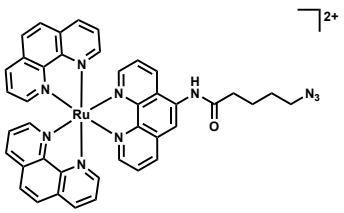

[Ru(1,10-phenanthroline)$_2$Cl$_2$] (0.050 g, 0.094 mmoles) and ligand **D** (0.030 g, 0.094 mmoles) were refluxed in dry EtOH (5 mL) under inert conditions for 18 h. The reaction mixture was allowed to cool and was then added dropwise to a solution of ammonium hexafluorophosphate in the minimum amount of deionised H_2O. The resultant precipitate was then filtered and washed with diethyl ether to give a black solid. The filtrate was re-precipitated with ammonium hexafluorophosphate and re-filtered to give a bright red solid. Yield: 0.083 g, 79%. ^{1}H NMR (600 MHz in DMSO-d_6): δ 10.44 (s, 1H), 8.87 (dd, J = 8.6, 1.0 Hz, 1H), 8.80 – 8.68 (m, 5H), 8.65 (d, J = 1.2 Hz, 1H), 8.38 (s, 4H), 8.07 (dd, J = 3.6, 2.6 Hz, 5H), 7.96 (dd, J = 5.2, 1.2 Hz, 1H), 7.79 – 7.73 (m, 4H), 7.68 (s, 2H), 3.72 (t, J = 6.2 Hz, 1H), 3.41 (t, 1H), 2.63 (t, J = 5.8 Hz, 2H), 1.83 (dd, J = 7.4, 4.5 Hz, 2H), 1.75 (dd, J = 15.1, 7.6 Hz, 1H), 1.65 (dd, J = 14.1, 7.2 Hz, 1H). FTIR-ATR (neat, cm^{-1}): 2096, 1699, 1631, 1599, 1516, 1462, 1426, 1235, 1184, 829. ESI-MS: *m/z* calcd. for [Ru($C_{41}H_{32}N_{10}O$)](PF$_6$)$_2$, [M-PF$_6^-$]$^+$ 927.1, found 927.1.

2.6 UV-vis analysis of G_R and $[Cu_2(N,N'\text{-phenanthrene})_2(G_R)](NO_3)_4$

A detailed UV-vis study of **G_R** and $[Cu_2(N,N'\text{-phenanthrene})_2(\mathbf{G_R})](NO_3)_4$ was undertaken. The stock solution of the ligand **G_R** was prepared in DMF and diluted to 25 μM with either ACN and H_2O. Spectra were recorded at the Shimadzu UV 600 spectrophotometer. Data was recorded every 0.5 nm in the 185-900 nm range. In ACN the ligand **G_R** exhibits $\pi \rightarrow \pi*$ or $n \rightarrow \pi*$ transitions at 197, 280 and 330 nm (**Figure 2.1 I**). The band at 197 and 280 nm were ascribed to the transition $\pi \rightarrow \pi*$ centred on the phenyl-ring and the band at 330 nm to the transition $\pi \rightarrow \pi*$ centred on the amino-phenanthroline moieties. Coordination with Cu^{2+}, Cu-Phen and Cu-DPQ induced a splitting of the band at 280 nm and bathochromic shift of the band at 330 nm (**Figure 2.1 I**). In presence of Cu-DPPZ, the UV-vis spectrum presents characteristics consistent with a hyperchromic effect. Analysis in H_2O showed hypochromic effect for **G_R** and the di-copper complexes with Cu^{2+} and Cu-DPPZ (**Figure 2.1 I**). Comparison between the *di*-nuclear complexes and the single Cu(II)(N,N'-phenanthrene) shows that their UV-vis spectra are dominated by the N,N'-phenanthrene ligand (**Figure 2.1 I**). At the working concentration of 25 μM, the *d-d* bands were not detectable and, consequently were analysed at a higher concentration of 5 mM in DMF showing an absorbance peak at a wavelength of 700 nm (**Figure 2.1 II**).

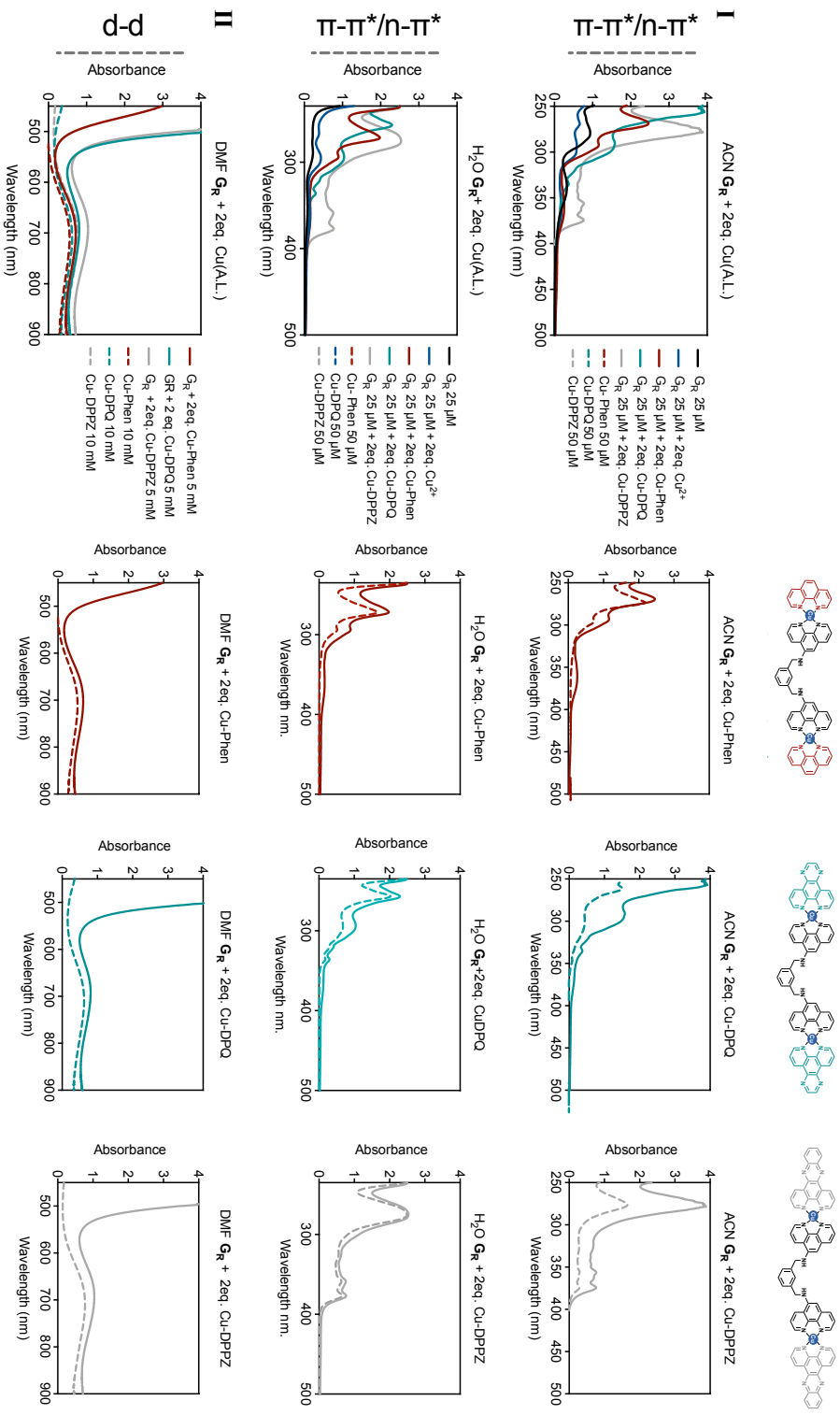

Figure 2.1 I UV study of $\mathbf{G_R}$ at 25 µM with and without complexation with 2 eq of Cu(II) and ancillary ligands in ACN and H_2O (solid line). Spectra are shown in comparison to the solutions of Cu-Phen, Cu-DPQ and Cu-DPPZ 50 µM in ACN and H_2O (dotted line). **II** *d-d* transition of $\mathbf{G_R}$(Cu-Phen)$_2$, $\mathbf{G_R}$(Cu-DPQ)$_2$ and $\mathbf{G_R}$(Cu-DPPZ)$_2$ 5 mM in DMF compared to the solutions of Cu-Phen, Cu-DPQ and Cu-DPPZ 10 mM in DMF.

2.7 Crystallography

Data for all the structures were collected at 100(1)K on a Synergy Dualflex, AtlasS2 diffractometer using Cu*K*α radiation (λ = 1.54184 Å) and the *CrysAlis PRO* suite. The structures were solved by dual space methods (SHELXT) and refined on F^2 using all the reflections (SHELXL-2018/3). Full occupancy non-hydrogen atoms were refined using anisotropic atomic displacement parameters and hydrogen atoms were inserted at calculated positions using a riding model. Further details for the individual structures are included in the Appendix F. Crystal data, data collection and structure refinement details are summarised in Table F1 (Appendix F).

2.8 Oligonucleotide synthesis

TFOs were prepared on an Applied Biosystems Incorporated 394 automated synthesizer. Phosphoramidites and solid supports columns were purchased from Glen Research, Link Technology, and ChemGene Corporation. The synthesis of alkyne-bearing oligonucleotides was performed in a 1 μmol scale with the standard DNA synthesis cycles DMT-off (trityl off mode). Post synthesis, sequences were deprotected using 1 mL of AMA (ammonium hydroxide:methylamine, 50:50), vortexed for 5 min, heated for 15 min at 65 °C, cooled on ice and centrifuged for 3 min, removed the supernatant and decanted with 0.5 mL of Milli-Q® H_2O, vortexed for 3 min and collected the supernatant. The addition of Milli-Q® H_2O and the collection of the supernatant were performed three times and the supernatant was evaporated using a SpeedVac concentrator. Sequences bearing the benzoyl group were treated with the protocol above however utilising ammonium hydroxide in place of AMA for two days. For desalting, the sequences were solubilised with 100 μL of sodium acetate, precipitated with 1 mL of cold EtOH (with 5% of diethyl ether) and centrifuged for 1 h and 30 min at 0 °C. Afterwards, the supernatant was removed and the oligos were then freeze-dried. Preliminary analysis was conducted on analytical RP-HPLC using a *Macherey-Nagel* Nucleodur, 100-3 C18ec column, on 2695 Separation Module, equipped with a Waters Alliance 2996 Photodiode Array Detector (flow 0.5 mL/min). Afterwards, the TFOs were purified with a semi-preparative RP-HPLC, performed using a *Macherey-Nagel* C18 column (5 mm, 9.4 × 250 mm) using a Waters Breeze 2487 Dual λ Array Detector, 1525 Binary HPLC Pump. Alkyne-modified TFOs and hybrids were isolated using a mobile phase gradient buffer

A to buffer B (0-40%) where buffer A is 0.1 M TEAA (triethylammonium acetate) in H_2O and buffer B is 0.1 M TEAA in 80% ACN.

The collected fractions were characterised by MALDI-ToF. The concentration of the oligonucleotide solutions was determined by UV absorbance at 260 nm using a Nanodrop ND-1000 spectrophotometer.

2.9 Generation of TFO-hybrid materials *via* click chemistry

Small scale preparation: A 5 µL solution of alkyne-modified TFO (5 nmol, 1 eq) and azide ligand (50 nmol, 10 eq) were prepared in a 1:1 DMSO/H_2O mixture (85.25 µL) and stirred. A freshly prepared solution of tris(3-hydroxypropyltriazolylmethyl)amine (THPTA, 50 nmol, 50 eq) and $CuSO_4$ (75 nmol, 15 eq) was then added, followed by the addition of 2.5 µL of a Na-*L*-ascorbate (Asc) solution (250 nmol, 50 eq). The solution was mixed for 2 h at room temperature after which time 9 µL of a 50 mM solution of EDTA was added. After diluting the reaction mixture with H_2O to reduce the amount of DMSO to 5% the product was freeze-dried and purified by RP-HPLC (TEAA buffer, pH = 8.0) or directly using Amicon Ultra 0.5 mL centrifugal filters (MWCO = 3000) according to the operating instructions. Briefly, the diluted fractions were spun down using the mini-columns to remove the excess of organic azide, Asc, THPTA, copper and EDTA. The pure product was then recovered in a collection tube by centrifuging the inverted column.

Large scale preparation: Alkyne-modified TFOs (25 nmol) and 25 µL of 10 mM DMSO solutions of azides **A**-**F** (1 eq) were prepared in 475.25 µL of a 1:1 DMSO/H_2O mixture. The reactions were catalysed with the addition of $CuSO_4$ (625 nmol, 25 eq) THPTA (1.25 µmol, 50 eq) and Asc (1.25 µmol). For ligand **G**, TFO (25 nmol) and 59.5 µL of a 4.2 mM DMSO solution of **G** was prepared in 440.7 µL of 1:1 DMSO/H_2O mixture. The reaction was catalysed with the addition of $CuSO_4$ (1.25 µmol, 50 eq) THPTA (2.5 µmol, 100 eq) and Asc (1.25 µmol). After 5 hours the mixture was quenched with 45 µL of an excess of EDTA disodium salt aqueous solution (50 mM) and freeze-dried overnight. For the ruthenium hybrids, the same post-functionalisation method for azides **A-F** was adopted, but with a reaction time of 2.5 h. The solid was re-dissolved in H_2O and purified using Amicon Ultra 0.5 mL centrifugal filters (MWCO = 3000). All hybrid materials were quantified *via* the Nanodrop spectrometer, characterised by MALDI-ToF (Appendix G) where the TFO showed no signs of self-degradation. Yield= [90-98]%

SPAAC: 25 nmol of BCN-modified sequence (TFO7) and 4.2 mM of ligand **G** (60 μL in DMSO) were prepared in 440.73 μL of 1:1 DMSO:H_2O. The reaction was stirred at room temperature overnight and diluted with deionised H_2O and purified with Amicon Ultra 0.5 mL centrifugal filters (MWCO = 3000).

2.10 Molecular biological and biophysical techniques

2.10.1 Thermal melting experiments

Duplex targets (D) where purchased from Integrated DNA Technologies (D1: 26-mer, TFO1 and TFO4; D2: 31-mer, TFO2 and TFO5; D3: 40-mer, TFO3 and TFO6). Oligonucleotides were quantified (1 μM) and samples were prepared of D:TFO 1:2.5 in 10 mM phosphate buffer with 150 mM NaCl and 2 mM $MgCl_2$ (pH = 6.0). For experiments investigating the stabilisation effects of TFOs modified with ligand G and copper-modified ancillary ligands, D:TFO:Cu^{2+} ratios were reduced to 1:1.25:2.5. Oligonucleotides were denatured using a heating ramp from 20−90 °C at 10 °C/min (held at 90 °C for 10 min). Sequences were annealed by cooling from 90−12 °C at 0.5 °C/min (held for 2 min at every 0.5 °C). UV melting curves were then recorded at 260 nm upon heating from 12–90 °C at 0.5 °C/min (held for 10 min at 90 °C). Melting curves were recorded for three consecutive heating cycles.

2.10.2 Triplex formation and nuclease activity

PAGE gels were prepared using an Invitrogen SureCast™ system and reagents. All PAGE reactions followed the general procedure unless otherwise stated. Cleavage reactions were performed with Cu^{2+} and Asc present, while triplex formation experiments were conducted in the absence of both. TFOs (12.5 pmol) were incubated with Cu^{2+} ($CuSO_4$) for 30 min at 37 °C and then added to a solution containing the target duplex (1.25 pmol) in the presence or absence of Asc (12.5 nmol). All samples were prepared in a final volume of 5.5 μL using 10 mM phosphate buffer with 150 mM NaCl and 2 mM $MgCl_2$ (pH 6.0). Unless otherwise stated, experiments with varying ratios of target duplex (D) and TFO, the relative amount of Cu^{2+} and Asc were kept to 1 and 100 eq of TFO, respectively (i.e. D:TFO:Cu^{2+}:Asc = 1:X:X:100X). Cleavage experiments involving on- (D_{ON}) and off-targets (D_{OFF}) were conducted in a similar manner to the cleavage reactions mentioned above. For TFO hybrids containing ligand **G**, samples were prepared at a ratio of 1:10:20:1000 D:TFO:Cu^{2+}:Asc and were incubated at 37°C for either 6, 12 or 24 h and then loaded onto a 22% PAGE gel (50 mM Tris acetate, 150 mM NaCl, 5 mM $MgCl_2$)

with 6× loading dye and subjected to native electrophoresis for 14 h at 50 V in 50 mM tris-acetate running buffer (pH 6.0). Gels were soaked in a SybrGold solution for 30 min and visualised using a Syngene G:Box Mini 9 system.

2.10.3 Site-selective cleavage with fluorescently labelled DNA

The target duplex D2 was appropriately fluorescently-functionalised to probe site-selective DNA damage. The template strands S1 and S2 of the fluorescently-tagged strands of target duplex were labelled at the 5'-position with FAM and with Cy3 respectively. Corresponding fragment probes of DNA damage were also rationally designed (F1 and F2) based on the proposed cleavage site giving FAM- and Cy3-labelled sequences as fragmentary products of S1 and S2, all of which were purchased from Sigma Aldrich Ltd:

S1:5′-[6FAM]AACGTGGCGGAAAGGAAGGGAAGAAAGCGA-3′;
S2:5′-[Cy3]TCGCTTTCTTCCCTTCCTTTCTCGCCACGTT-3′;
F1:5′-[6FAM]AACGTGGCG-3′;
F2:5′-[Cy3]TCGCTTTCTTCCCTTCCTTTCT-3′.

Target strands (S1 and S2, 10 pmol) were annealed and treated with varying amounts of TFO (D:TFO:Cu^{2+}:Asc = 1:X:2X:1500X, where X = 1-25 eq). All reactions were carried out as stated above with 40 h incubation. The samples were loaded onto 22.5% denaturing PAGE gel (1× TBE with 7.4 M urea, pH 8.3) and subjected to electrophoresis for 1.5 h at 15 mA in 1× TBE buffer.

2.10.4 Photophysical properties of Ru(II) complexes

Stock solutions of Ru-complexes with azide-modified ligands were prepared in DMF (40 mM) and diluted to 25 μM with either ACN, H_2O, PBS (10 mM Phosphate, 137 mM NaCl and 2.7 mM KCl, pH=7.4) or triplex buffer (10 mM Phosphate, 150 mM NaCl and 2mM $MgCl_2$, pH=6). UV-vis spectra were recorded using a Shimadzu UV 600 spectrophotometer. every 0.5 nm in the 185-900 nm range. Emission spectra were recorded across a range of concentrations (25 μM, 5 μM and 1 μM) with an excitation wavelength of 444 nm for [Ru(Phen)$_2$(**A**)](PF$_6$)$_2$, 457 nm for [Ru(Phen)$_2$(**B**)](PF$_6$)$_2$ and 447 nm for [Ru(Phen)$_2$(**D**)](PF$_6$)$_2$ in either ACN, H_2O, PBS and triplex buffer. Emission data was collected in the range 200 – 900 nm (excitation slit: 2.5 nm/emission slit: 5 nm).

The binding of $[Ru(Phen)_2(\mathbf{B})]^{2+}$ and the hybrid of this complex with TFO3 (TFO3-Ru**B**) using target duplex (D3) was investigated in triplex buffer. Experiments were conducted using a fixed concentration of hybrid or complex (5 μM) with duplex:TFO-hybrid (or Ru(II)-complex) ratios of 0.02:1, 0.04:1, 0.05:1, 0.067:1, 0.1.1, 0.2:1, 0.4:1 and 1:1 (final volume = 500 mL). Each addition was followed by one hour of incubation at 37 °C in darkness and analysed in the range of 460-800 nm at the excitation wavelength of 457 nm (excitation slit: 2.5 nm/emission slit: 5 nm). The same method was applied to $[Ru(Phen)_2(\mathbf{D})]^{2+}$ and the hybrid TFO3-Ru**D** at the concentration of 1 μM performing the analysis at the wavelength of 447 nm.

2.10.5 Data analysis

Melting curves were plotted in GraphPad Prism V6.0 and interpolated to sigmoidal curve models, with thermal melting values obtained from first derivatives (where $n = 3 \pm$ S.D.). The extent of triplex formation was quantified with cleaved DNA calculated by band densitometry using Syngene GeneTools analysis software and mean ± S.D. ($n = 3$) were plotted in GraphPad Prism V6.0. For statistical analysis, comparisons between datasets were analysed with two-way ANOVAs in GraphPad Prism. Differences between means were analysed post-hoc with Tukey's test at 95% confidence level. Differences between groups were considered to be statistically significant if $P \leq 0.05$ ($^{*}P \leq 0.05$; $^{**}P \leq 0.01$; $^{***}P \leq 0.001$).

References

(1) Fadeeva, V. P.; Tikhova, V. D.; Nikulicheva, O. N. Elemental Analysis of Organic Compounds with the Use of Automated CHNS Analyzers. *J. Anal. Chem.* **2008**, *63* (11), 1094–1106.

(2) Ohata, J.; Vohidov, F.; Aliyan, A.; Huang, K.; Martí, A. A.; Ball, Z. T. Luminogenic Iridium Azide Complexes. *Chem. Commun.* **2015**, *51*, 15192–15195.

(3) Sergeeva, N. N.; Donnier-Marechal, M.; Vaz, G. M.; Davies, A. M.; Senge, M. O. Simple but Powerful: Phenanthroline-Based Small Molecules for Cellular Imaging and Cancer Screening. *Bioorganic Med. Chem. Lett.* **2011**, *21*, 4385–4388.

(4) Wang, H.; Zhou, K.; Xie, Y.; Zeng, J.; Chai, N.; Li, J.; Zhang, H. Photoactive Graphene Sheets Prepared by " Click " Chemistry. *Chem. Commun.* **2011**, No. 47, 5747–5749.

(5) Molphy, Z.; Prisecaru, A.; Slator, C.; Barron, N.; McCann, M.; Colleran, J.; Chandran, D.; Gathergood, N.; Kellett, A. Copper Phenanthrene Oxidative Chemical Nucleases. *Inorg. Chem.* **2014**, *53*, 5392–5404.

(6) Gou, G.; Ren, R.; Li, S.; Guo, S.; Dong, Z.; Xie, M.; Ma, J. Eu(Iii)-Coupled Graphene Oxide as a Luminescent Material. *New J. Chem.* **2013**, *37*, 3861–3864.

(7) Wang, H.; Zhou, K.; Xie, Y.; Zeng, J.; Chai, N.; Li, J.; Zhang, H. Photoactive Graphene Sheets Prepared by " Click " Chemistry. *Chem. Commun.* **2011**, *47*, 5747–5749.

(8) Jones, J. E.; Jenkins, R. L.; Hicks, R. S.; Hallett, A. J.; Pope, S. J. A. Water-Soluble, Luminescent Iridium(III)–Ytterbium(III) Complexes Using Dipyrido[3,2-a:2′,3′-c]Phenazine Derivatives as Bridging Units. *Dalt. Trans.* **2012**, *41*, 10372–10381.

(9) Lin, G.-J.; Jiang, G.-B.; Xie, Y.-Y.; Huang, H.-L.; Liang, Z.-H.; Liu, Y.-J. Cytotoxicity, Apoptosis, Cell Cycle Arrest, Reactive Oxygen Species, Mitochondrial Membrane Potential, and Western Blotting Analysis of Ruthenium(II) Complexes Gan-Jian. *J Biol Inorg Chem* **2013**, *18*, 873–882.

(10) Ji, S.; Guo, H.; Yuan, X.; Li, X.; Ding, H.; Gao, P.; Zhao, C.; Wu, W.; Wu, W.; Zhao, J. A Highly Selective OFF-ON Red-Emitting Phosphorescent Thiol Probe with Large Stokes Shift and Long Luminescent Lifetime. *Org. Lett.* **2010**, *12* (12), 2876–2879.

(11) Duskova, K.; Gude, L.; Arias-Pérez, M.-S. N-Phenanthroline Glycosylamines: Synthesis and Copper(II) Complexes. *Tetrahedron* **2014**, *70*, 1071–1076.

(12) Shiu, H.-Y.; Wong, M.-K.; Che, C.-M. "Turn-on" FRET-Based Luminescent Iridium(III) Probes for the Detection of Cysteine and Homocysteine. *Chem. Commun. (Camb).* **2011**, *47*, 4367–4369.

(13) Lill, A. P.; Rödl, C. B.; Steinhilber, D.; Stark, H.; Hofmann, B. Development and Evaluation of ST-1829 Based on 5-Benzylidene-2-Phenylthiazolones as Promising Agent for Anti-Leukotriene Therapy. *Eur. J. Med. Chem.* **2015**, *89*, 503–523.

(14) Yin, Y.; Xu, S.; Chang, D.; Zheng, H.; Li, J.; Liu, X.; Xu, P.; Xiong, F. One-Pot Synthesis of Biopolymeric Hollow Nanospheres by Photocrosslinking. *Chem. Commun.* **2010**, *46*, 8222–8224.

(15) Su, C.; Liu, X. Synthesis of Novel 4(3H)-Quinazolinones with 1,2,3-Triazoles Moiety Conjugated by Schiff Base 2. *Asian J. Chem.* **2014**, *26* (16), 5301–5304.

(16) Cheng, F.; Ren, M.; He, C.; Yin, H. Luminescent Chemosensor for Hg^{2+} Ion Based on a Dinuclear Ru(II) Complex Containing Open Chain Azacrown Ether. *Inorganica Chim. Acta* **2016**, *450*, 170–175.

(17) Jennings, K. F. An Attempted Synthesis of Perhydro-2 : 8-Methylenepyridocoline. *J. Chem. Soc.* **1967**, 1172–1175.

(18) McGivern, T. J. P.; Slator, C.; Kellett, A.; Marmion, C. J. Innovative DNA-Targeted Metallo-Prodrug Strategy Combining Histone Deacetylase Inhibition with Oxidative Stress. *Mol. Pharm.* **2018**, *15*, 5058–5071.

(19) Wei, H.; Yin, J.; Wang, E. Bis(2,2′-Bipyridine)(5,6-Epoxy-5,6-Dihydro-[1,10] Phenanthroline)Ruthenium: Synthesis and Electrochemical and Electrochemiluminescence Characterization. *Anal. Chem.* **2008**, *80*, 5635–5639.

(20) Al-Rawashdeh, N. a F.; Chatterjee, S.; Krause, J. a.; Connick, W. B. Ruthenium Bis-Diimine Complexes with a Chelating Thioether Ligand: Delineating 1,10-Phenanthrolinyl and 2,2′-Bipyridyl Ligand Substituent Effects. *Inorg. Chem.* **2014**, *53*, 294–307.

(21) Jiang, G. Bin; Xie, Y. Y.; Lin, G. J.; Huang, H. L.; Liang, Z. H.; Liu, Y. J. Synthesis, Characterization, DNA Interaction, Antioxidant and Anticancer Activity Studies of Ruthenium(II) Polypyridyl Complexes. *J. Photochem. Photobiol. B Biol.* **2013**, *129*, 48–56.

CHAPTER 3

Phenanthrene-modified TFOs stabilise parallel DNA triplexes and promote targeted oxidative cleavage

3.1 Introduction

Gene editing systems are characterised by the fusion of two functional domains: a sequence-specific DNA-binding component and a non-specific DNA cleavage module. The most widely applied editors include zinc-finger nucleases (ZFNs),[1,2] TALENs (transcription activator-like effector nucleases),[3–5] and CRISPR-Cas (clustered regulatory interspaced short palindromic repeats/CRISPR-associated protein) RNA-guided nucleases.[6–8] Their versatility combined with the programmability of their DNA-binding domains has paved the way for numerous applications including precision genome editing and functional inactivation of genes in human cells. Inactivation usually relies on hydrolytic double-strand breaks stimulating non-homologous end joining (NHEJ) cellular DNA repair,[9] while gene editing requires homology-directed repair. ZFNs were the first gene editing tools introduced but presented some limitations relating to gene targeting.[10] These limitations were largely addressed with TALENs and CRISPR-Cas, which is now recognised as the state-of-art. However, CRISPR off-target effects can be problematic leading to mosaic genetic changes that arise from imperfect single guide RNA hybridisation and prolonged activity of Cas9 after the desired editing event.[11] Furthermore, since Cas9-induced double strand DNA breaks favour NHEJ, nucleotide deletions or insertions can arise resulting in undesired therapeutic outcomes.

Another class of considerable research interest comprises the artificial metallo-nucleases (AMNs). These systems mimic type II restriction enzymes and can cleave single-strand and double-strand DNA through oxidative mechanisms with higher selectivity than natural enzymes.[12,13] Copper phenanthrene-based AMNs, in particular, present a promising class that induces direct strand scission by oxidative damage of DNA.[14–16] The phenanthrene ligand coordinates copper—or other transition metals ions[17,18]—and intercalates or semi-intercalates duplex DNA. Copper phenanthrene AMNs preferentially bind TAT rich regions in the minor groove of DNA, with the subsequent abstraction of C1′-hydrogen *via* β–elimination resulting in strand scission.[19] In recent years we have refined and extended this class of AMN, investigating the effects of nuclearity,[20–22] geometry[23] and planar ligand extension[16,24] on DNA binding affinity[25–27] and nuclease activity. When coupled to a suitable DNA-targeting vector, copper AMNs have previously demonstrated sequence-specific DNA oxidation.[28–30] A minor groove binding copper-phenanthroline conjugate produces direct strand breaks via β-elimination of 2-deoxyribonolactone Sigman and Hélène, in particular, identified that 1,10-

phenanthroline (phen) conjugates of short (7-11-mer) homopyrimidine oligomers were effective targeting triplexes.[28,31,32] However, the presence of a cationic adjuvant (spermine) was required to stabilise the negatively charged triple-helical structure.[28] Recent work to improve triplex stability have focused on inserting stabilising groups in the phosphate backbone and at internal or terminal nucleobase positions of triplex forming oligonucleotides (TFOs).[32] Examples of TFOs containing stabilising intercalating modifications include: thiazole orange-coupled TFOs,[33] intercalating nucleic acids (INAs)[34] and twisting intercalating nucleic acids (TINAs).[35–37] These chemically modified oligomers are, however, devoid of DNA cleavage capability.

In this work, we report a new class of phenanthrene-modified TFO that stabilises parallel DNA triplexes and promotes targeted oxidative cleavage. Their design relies on nucleic acid 'click' chemistry[38–41] whereby copper catalysed azide-alkyne cycloaddition (CuAAC) reactions couple azide-modified phenanthrene ligands to alkyne base-modified parallel TFOs. We selected TFOs as they are amenable to engineering[42] and can target extended sequences with low propensity to bind to non-target sites. Using this approach, fast generation of AMN-TFO libraries targeted to a portion of the green fluorescent protein (GFP) recombinant gene were possible. Crucially, the presence of clicked *N,N*-phenanthrene ligands enabled both *in situ* copper chelation—required for targeted oxidative cleavage—and promoted triplex stabilisation. In an effort to find suitable modifications, a range of aromatic and aliphatic ligands, some with flexible linkers, were developed and incorporated in the hybrid TFOs. *In vitro* experiments to identify potential targeted gene knockout and cleavage specificity were undertaken with several hybrids demonstrating desirable properties. By combining a sequence-specific DNA-binding component (TFO) with a non-specific DNA cleavage module (copper-phenanthrene) *via* nucleic acid click chemistry, a new type of copper chelating intercalating nucleic acid (CINA) was developed. This work represents the first step towards future applications of this class.

3.2 Results and discussion

3.2.1 Design of hybrid AMN-TFO systems

Two principal components were required to produce potential gene-targeting hybrids: a parallel TFO bearing an alkyne-base modification and an intercalating phenanthrene group containing an azide-modification (**Figure 3.1 I**). In particular, after the coupling of phenantrene with TFO by click chemistry triplex formation was investigated by UV and PAGE electrophoresis. Successively, the influence of nuclease activity by the phenantrene ligand was evaluated by densitometry analysis and the sequence- and site-selectivity was determined respectively through off-targeting and fluorophore-tagged experiments. With this in mind, a series of six copper-binding *N*,*N*-phenanthrene ligands containing either aromatic or aliphatic azide linkers were developed (**Figure 3.1 II**). Using solid-phase synthesis, alkyne-base modified phosphoramidites (**Figure 3.1 III**; C8-dU) were incorporated into pyrimidine-rich parallel TFOs targeted to the GFP recombinant cloning vector. Both internal- and 5'-base-modified sequences (**Figure 3.1 IV**; TFO1-6) were designed such that a library of 36 AMN-TFO hybrids could be generated.

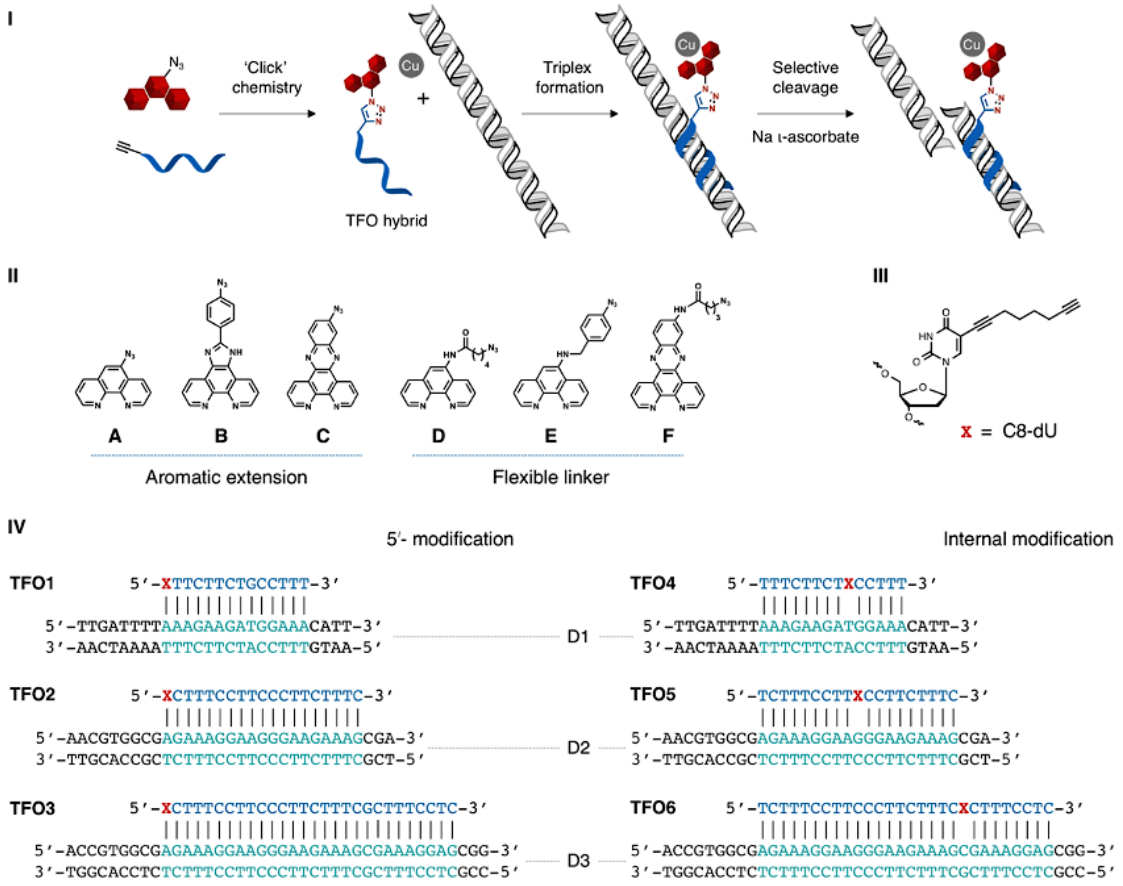

Figure 3.1 I Generation of phenanthrene-functionalised TFOs using 'click' chemistry. Coordination of copper to TFO hybrids induces targeted DNA cleavage. **II** Library of azide-functionalised phenanthroline and phenazine derivatives: **A**-**F**. **III** Alkyne-modified nucleobase inserted at 5′-terminal or internal position of the TFO. **IV** Library of alkyne-modified TFOs of various lengths showing modification position (X) with corresponding duplex targets designed from the GFP cloning vector.

3.2.2 Preparation of N,N-intercalators

A family of six phenanthrene analogues (**Figure 3.1 II**) was prepared according to the synthetic routes described in **Figure 3.2** (Route I-VI) with detailed procedures in Chapter 2. The main difference between mono-chelating ligands **A**, **B** and **C** are the extent of the conjugated system: **B** and **C** are extended versions of **A** and are designed for enhancing DNA binding affinity by incorporating a more rigid aromatic structures. *Ligands* **D**, **E** and **F** incorporate aliphatic and aromatic spacers that were designed to identify *if* duplex-triplex hybridization and cleavage activity were enhanced as a result of this greater flexibility. The synthesis of 5-azido-1,10-phenanthroline (**A**) was reported previously using a three-step method involving the nucleophilic ring-opening of 5,6-epoxy-5,6-1,10-phenathroline, the acetylation of the resulting hydroxyl group followed by the elimination

of the resulting acetate group to restore the aromaticity in the presence of a non-nucleophile base.[43] Here, we report a simplified one-step route with excellent yield (**Figure 3.2**, Route I). Treatment of 5,6-epoxy-5,6-1,10-phenathroline with NaN_3 at room temperature (RT) yields primarily 6-azido-1,10-phenanthrolin-5-ol with product **A** as minor product. However, increasing the temperature from RT to 80 °C, with an excess of sodium azide, leads the kinetic reaction in fully conversion of 5,6-epoxy-5,6-1,10-phenathroline into 5-azido-1,10-phenathroline.

The extended aromatic ligands **B** and **C** were also obtained with high yield (**Figure 3.2**, Route II) by synthesising amino derivatives, conversion to diazonium salts and generating the final azides in situ. The synthesis of **B** is also reported in literature,[44] but each step was optimised to result in higher yield; in particular in the azidation step the amino-derivate of **B** was treated with more concentrated acid solution (6 N HCl) leading to a significant increment of the final organic azide. The synthesises of the nitro- (**Figure 3.2**, **4**) and amino- intermediates (**Figure 3.2**, **5**) of **C** are already known and were modified replacing EtOH, the solvent normally used, with the mixture of ACN/MeOH obtaining the precipitate of **4** avoiding the purification via column chromatography. The reaction time for the generation **5** was decreased to 1 h preventing the development of minor products which would affect the yield and the purity. **C** was generated using the same method optimised for **B**, but in the acid treatment the mixture of reaction was heated at 70 °C due to the low solubility of **5**. This intermediate was also used as for the synthesis of 2-azido-N-(dipyrido[3,2-a:2',3'-c]phenazin-11-yl)acetamide (ligand **F**) by exploiting the high reactivity of acyl chloride for the introduction of the aliphatic spacer, followed by the substitution of the chloride with an azide group (Figure 3.2, Route VI). A similar an approach was adopted for the synthesis of 2-azido-N-(1,10-phenanthrolin-5-yl)acetamide (ligand **D**) using 5-bromovaleryl chloride (**Figure 3.2**, Route III and IV). For the synthesises of **D** and **F**, highly reactive reagents were employed because of the low reactivity of **5** and **7** due the extended aromaticity. In the preparation of ligand **E**, the introduction of the aromatic spacer was achieved by synthesising 4-azidobenzaldehyde (compound **10**) using existing methods.[45,46] Subsequently, it was condensed with 5-amino-1,10-phenanthroline to obtain a Schiff base (**11**). Since the imine bond is susceptible to hydrolysis during the click chemistry reaction it was reduced to an amine using sodium borohydride to give the product N-(4-azidobenzyl)-1,10-phenanthrolin-5-amine (ligand **E**, Route V). The complete series of azide-functionalised,

copper chelating moieties are aromatic intercalators **A** – **C** and aliphatic ligands **D** – **F** (5-azido-1,10-phenanthroline, **A**; 2-(4-azidophenyl)-1H-imidazo[4,5-f]-1,10-phenanthroline, **B**; 11-azidodipyrido[3,2-a:2',3'-c]phenazine, **C**; 5-azido-N-(1,10-phenanthrolin-5-yl)pentanamide, **D**; N-(4-azidobenzyl)-1,10-phenanthrolin-5-amine, **E**; 4-azido-N-(dipyrido[3,2-a:2',3'-c]phenazin-11-yl)butanamide, **F**).

Single crystal structure analyses were carried out for ligands **B**, **C**, **D** and Cu(**A**)$(NO_3)_2$, a Cu(II) complex of ligand **A** (**Table 3.1**). In each case, the ligand has the expected, essentially planar structure and the azido group is unambiguously located. In the complex Cu(**A**)$(NO_3)_2$ the nitrate anions also coordinate to the axial sites of neighbouring copper ions, so that the structure comprises a 1-D polymer of Cu(Ligand **A**)$(NO_3)_2$ units linked by Cu–O–Cu and Cu–O-N-O–Cu bridges. Further structural descriptions and additional figures are included in Appendix F.

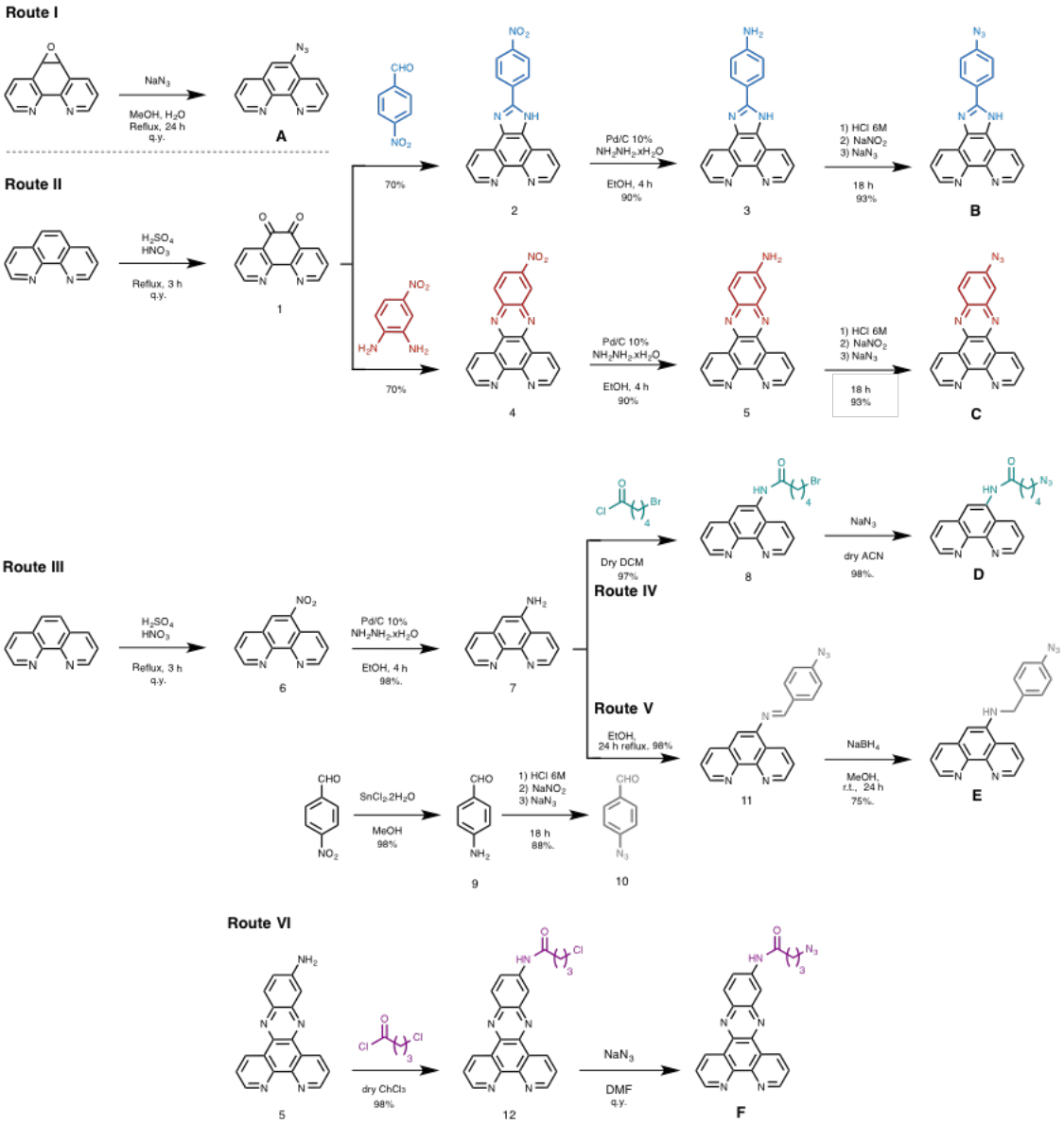

Figure 3.2 Synthetic routes to phenanthrene derivatives bearing an azide group (ligands **A**-**F**). **Route I**: azidation of epoxy-1,10-phenanthroline to generate ligand **A** (q.y.=quantitative yield). **Route II**: Diazotization for the generation of ligands **B** and **C**. **Route III**: Synthesis of the 5-amino-1,10-phenanthroline (**7**) allowed subsequent formation of ligands **D** and **E** *via* **Routes IV and V**, respectively. **Route VI**: Treatment of amino-DPPZ (**5**) with an acyl chloride followed by azidation provided ligand **F**.

Table 3.1. Crystal data and structure refinement data (100 K, CuKα radiation). Figures show 50% displacement ellipsoids for non-hydrogen atoms.

	Cu(A)$(NO_3)_2$	B	C	D
	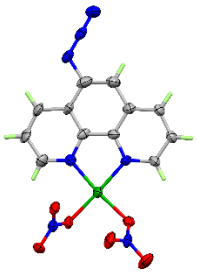	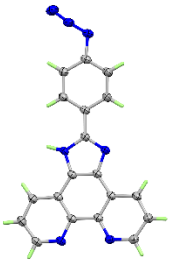	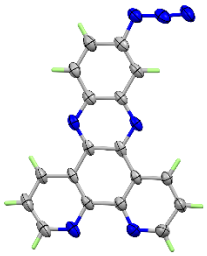	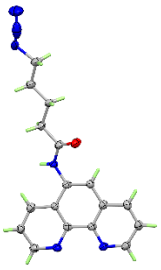
Empirical formula	$C_{12}H_7CuN_7O_6$	$C_{39.6}H_{29.2}N_{14.8}O_{2.4}$	$C_{18}H_9N_7 \cdot 0.7(C_2H_3N)$	$C_{17}H_{20}N_6O_3$
Formula weight	408.79	750.78	349.92	356.39
Crystal system	monoclinic	triclinic	monoclinic	triclinic
Space group	$P2_1/c$	$P\bar{1}$	$P2_1/c$	$P\bar{1}$
a /Å	10.1423(9)	11.0232(7)	12.3819(7)	4.7966(6)
b /Å	20.8669(18)	12.1290(7)	6.8151(3)	13.132(2)
c /Å	6.7999(7)	15.0612(10)	18.3837(8)	14.3075(12)
α /°	90	69.677(5)	90	109.511(12)
β /°	90.538(8)	72.981(6)	97.123(4)	93.670(9)
γ /°	90	77.617(5)	90	90.203(11)
Volume /Å^3	1439.1(2)	1791.3(2)	1539.32(13)	847.44(19)
Z	4	2	4	2
F (000)	820.0	779.0	721.0	376.0
R_{int}, R_{sigma}	0.0805, 0.0493	0.039, 0.0324	0.0699, 0.0360	0.0649, 0.0649
Data/restraints/param.	2535/7/244	9149/22/541	2229/9/255	3169/21/251
Goodness-of-fit on F^2	1.091	1.036	1.147	0.997
R_1, wR_2 [I>=2σ (I)]	0.1090, 0.2728	0.0544, 0.1568	0.1141, 0.3628	0.0734, 0.1897
R_1, wR_2 [all data]	0.1129, 0.2758	0.0688, 0.1666	0.1288, 0.3710	0.0998, 0.2028
Residual density /e Å^{-3}	1.55/-0.71	1.11/-0.29	0.43/-0.43	0.41/-0.44
CCDC number	1952708	1952707	1952710	1952709

3.2.3 Preparation of AMN-TFO hybrids

Pyrimidine-rich oligomers were used to design parallel TFOs targeted to purine rich regions of the GFP recombinant gene (pGFP-C1). Six sequences ranging between 14-28 nucleotides (nt) in length were prepared with alkyne-nucleobase modifications at either terminal 5′ (TFO1-TFO3) or internal sites (TFO4-TFO6) (**Figure 3.1 IV**). TFO1 and TFO3 each contain 1 triplet inversion site (G; there is no Hoogsteen binding of the TFO to the major groove of the target purine-rich sequence at this position) while TFO2 contains none. These inversion sites were replaced with alkyne-nucleobases (**Figure 3.1 IV**) in the corresponding internally modified TFOs (TFO4 and TFO6), while a single inversion site containing alkyne-dU was introduced in TFO5. The probe strands were synthesised using a solid-phase oligo synthesiser and purified by HPLC. Alkyne-TFOs were then clicked to the organic azides **A-F** to yield the final library of hybrid materials *via* copper-catalysed click chemistry. The click reaction was optimised to provide complete conversion from the alkyne-TFO to the final hybrid with no self-digestion of the TFO. The method developed involved the use of Cu(II), which was reduced into Cu(I) *in situ* by the addition of Na-L-ascorbate (Asc) and the THPTA ligand. EDTA was added to stop the reaction and to remove bound copper from the phenanthrene ligand before hybrid purification. The hybrids were then isolated in high purity using molecular weight cut-off centrifugal filters and characterised by MALDI-ToF analysis (Appendix G). In total, 36 AMN-TFO hybrids were generated from alkyne modified TFOs 1-6 and azide-functionalised *N,N*-phenanthrene ligands **A-F** and are referred to as **TFO1A** etc.

3.2.4 Triplex formation

Using a method reported in Chapter 2, triplexes were allowed to form in the presence of the target by heating to 90 °C followed by slow annealing to 12 °C. Triplex formation was investigated using UV thermal melting experiments where the absorbance at 260 nm was recorded at pH 6.0 to ensure stable C^+-GC triplet formation (**Figure 3**). Experiments were designed to target duplex gene fragments containing flanking base pairs on each side of the TFO binding site (*cf.* **Figure 3.1 IV**). Overall, all of the modifications introduced by click chemistry—with the exception of few hybrids (**TFO5A**: -0.8 ± 0.1; **TFO5D**: -0.8 ± 0.3; **TFO6D**: -0.4 ± 0.2)—conferred significant stabilising effects toward triplexes. The increase in denaturation temperature of triplexes was determined by different factors: the length of TFO-sequence; the location of the modification; the

extension of the aromaticity; protonatable functional groups; and the flexibility of the 'clicked' linkers.

The majority of TFO-hybrids containing 14 nt (TFO1 and TFO4) had melting temperatures (ΔT_M) that were either not detectable or too low to be considered significant (20-25 °C). However, **TFO1B**, **TFO1C** and **TFO1F** had slightly higher ΔT_M values in the range 30-32 °C (Appendix H, **Table H1**). In TFOs containing >14 nt, triplex formation with alkyne-modified oligonucleotides showed T_M values in the range 30-46 °C, which were used as comparison for the appropriate clicked phenanthrene ligand TFOs (**Figure 3.3 I**).

The position of the alkyne-modified nucleobase also affected the thermal stability since TFOs with internal modification were generally less stable than terminally modified TFOs. T_M of **TFO5** (T_M = 30.3 °C ± 0.2) is noticeable lower than **TFO2** (T_M = 43.3 °C ± 0.3), but the difference of thermal stability of T**FO3** (T_M = 46.1 °C ± 0.0) and **TFO6** (T_M = 44.2 °C ± 0.2) is less significant probably compensated by the sequence length.

Increasing the aromaticity of the phenanthrene ligands enhanced triplex stability, in particular for TFO-hybrids modified with ligand **B**. TFOs modified with a Phen ligand (**A**) had lower overall stability, perhaps due to limited flexibility imparted by the neighbouring triazole ring, and this limitation was addressed by using extended ligands **B** and **C**. There is a remarkable stabilization with **B**, perhaps due to the single bond between the imidazole-ring and benzene ring which probably permits additional rotational freedom in the structure.

Another factor that would affect the stabilising property of **B** is the pH dependence of the imidazole ring. Derivatives of 2-phenyl-1*H*-imidazo[4,5-*f*][1,10]phenanthroline have a pK_a value in the range of [4-5],[47] consequently it is possible that the nitrogen group of the imidazole ring is still partially protonated at pH 6 contributing positively to the triplex stability. Probably, at lower pH the protonation of the imidazole ring would have a higher impact on the thermal stability of triple helices.

Consequently, it was expected that adding flexible aliphatic spacers would furnish more stable triplexes. However, hybrids with ligand **D** containing a flexible aliphatic linker did not further stabilise TFO3 (ΔT_M = 3.9 °C ± 0.8) , TFO5 (ΔT_M = -0.8 °C ± 0.3), or TFO6 (ΔT_M = -0.4 °C ± 0.2). The unexpected results of the hybrids with **D** can be explained as the excess of the flexibility provided by the aliphatic spacer and the chain of eight

carbons of the alkyne group attached to the oligonucleotides is not compensated by an extended rigid structure, consequently the high flexibility and freedom degree does not provide suitable intercalation of the target. In contrast, hybrids incorporating ligands **E** and **F** provided notable improvements to triplex stabilisation due to the combination of additional aromaticity and flexibility contribution. Ligand **E**, in particular, furnishes the highest overall stabilisation when combined with TFO3 (ΔT_M = 11.6 °C ± 0.3) compared to **TFO3A** (ΔT_M = 4.4 °C ± 0.3) and ligand **F** when attached to TFO2 (ΔT_M = 22.0 °C ± 0.5) provided 13.5 °C of stabilisation more than **TFO2B** (ΔT_M = 8.4 °C ± 0.1).

For direct comparison of the ΔT_M values (**Figure 3.3 II**), a general trend in ligand stabilisation is: **B** > **F** > **C** > **E** > **A** > **D**. It is noteworthy that TFOs containing ligands **B** and **F** can provide stabilising effects of *ca*. +20 °C. Overall, it appears ligands of extended aromatic structure (**B**, **C**, **E**, **F**) are more effective than phenanthroline ligands (**A**, **D**). TFOs containing internally modified ligands were, overall, less stable than corresponding 5′-modified sequences and this trend is likely due to the reorganisation energy required to facilitate intercalation in the central, rather than flanking, regions of the duplex GFP target. A selection of the most stabilising TFOs where examined at neutral pH 7.4 (Appendix H, **Table H2**) where T_M values above 20 °C were observed. The influence of copper(II) on triplex formation was also investigated, no significant changes were identified—indicating that the triplex stabilisation is mainly provided by the phenanthrene ligand.

I

T_M at pH 6.0

		5′- modification		Internal modification	
	Ligand	**TFO2**	**TFO3**	**TFO5**	**TFO6**
T_M (°C)	TFO–≡	41.4 ± 0.3	45.1 ± 0.0	30.3 ± 0.2	44.2 ± 0.2
ΔT_M (°C)	A	15.9 ± 0.2	5.5 ± 0.3	-0.8 ± 0.1	2.3 ± 0.5
	B	10.7 ± 0.1	21.5 ± 0.5	12.1 ± 0.3	18.9 ± 0.4
	C	16.6 ± 0.2	13.1 ± 0.2	7.8 ± 0.2	5.3 ± 0.2
	D	11.7 ± 0.3	5.0 ± 0.8	-0.8 ± 0.3	-0.4 ± 0.2
	E	9.4 ± 0.5	12.8 ± 0.3	3.5 ± 0.5	8.4 ± 0.3
	F	23.9 ± 0.5	11.0 ± 0.7	12.1 ± 0.3	18.9 ± 0.4

II

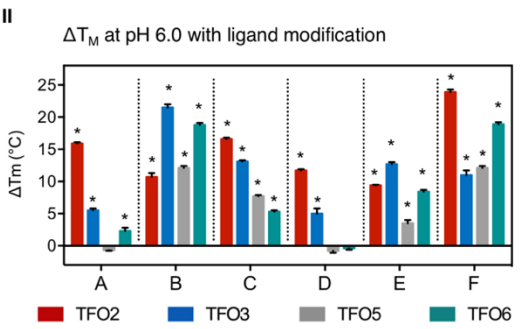

Figure 3.3 I Thermal melting (T_M) values of TFO-hybrids containing ligands **A-F** in TFO2, 3, 5 and 6 along with non-clicked alkyne-modified TFO (TFO 1 and 4 omitted as T_M < 20 °C). Tm values for duplex D2 (TFO 2 and 5) = 73.2 ± 0.2 °C and duplex D3 (TFO 3 and 6) = 79.0 ± 0.7 °C. Samples were prepared in 10 mM phosphate buffer with 150 mM NaCl and 2 mM $MgCl_2$ (pH = 6.0). **II** Direct comparison of ΔT_M with ligand modification of TFO-hybrids.

3.2.5 PAGE analysis

To confirm the triplex formation, PAGE was performed using identical duplex GFP targets employed in the thermal melting study (Appendix H, **Figure H1**). In particular, triplex formation was identified by a band migrating slower than the target. In this regard, the impact of the stoichiometric ratio duplex:TFO (D:TFO), the ligand modification, and the incubation time were examined for direct interaction duplex-TFO without annealing, but simulating biological systems. Experiments to monitor the ratio of TFO hybrid and incubation time were examined first. The concentration of AMN-TFO was determined by monitoring triplex formation of **TFO3C** and its alkyne-modified precursor (TFO–≡) with duplex target D3 (41 bp) using 2.5, 10 and 25 equivalents of TFO incubated at 37 °C for 6 hours (**Figure 3.4 I**). At 10 and 25 equivalents, suitable triplex formation was identified and the ratio duplex:TFO = 1:10 was selected for further studies. The presence of specific AMN ligands was found to affect triplex formation (**Figure 3.4 III**). TFO3 modified with ligands **A**, **C**, **E** and **F** all displayed appropriate triplex formation, however, ligands **B** and **D** did not perform well at this ratio (Duplex:TFO = 1:10). The behaviour displayed by **D** can be attributed to the excess of flexibility, but the trend observed with **B** was unexpected and needed further investigation. Consequently, the effect of incubation time was next studied using **TFO3B** using 1, 10 and 25 equivalents of the hybrid over 6, 12 and 24 h. Triplex formation essentially reached equilibrium by 6 h at 25 equivalents (Appendix H, **Figure 3.4 II**), but using the ratio duplex:TFO = 1:10 24 h were required. Finally, PAGE experiments with copper(II) (**Figure H1. IV**) and Asc (Appendix H, **Figure H1. V**) were examined under identical conditions. While ascorbate had negligible effects on triplex formation of all hybrid, with the exception of **TFO3B**, the equilibrium of triplex:duplex formation by **TFO3E** was perturbed by titrated copper(II).

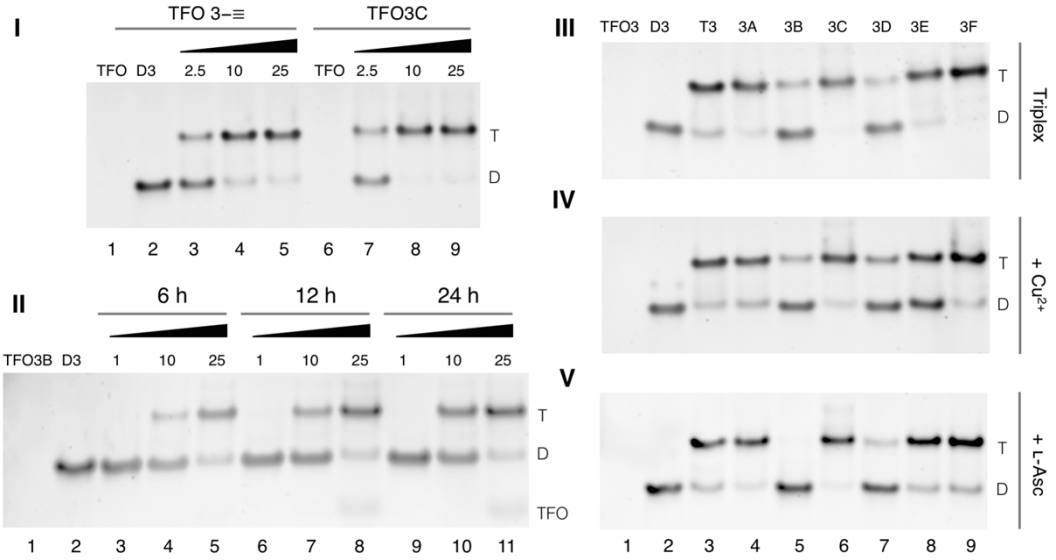

Figure 3.4 I Triplex formation with varying amounts of non-clicked TFO–≡ and hybrid **TFO3C**. The duplex GFP target D3 (1.25 pmol, lane 2) was treated with increasing equivalents of TFO for 6 h. **II** Triplex formation of **TFO3B** examined across various incubation times. **TFO3C** showed full triplex formation in the incubation of 6 hours at 37 °C already at the ratio D:TFO=1:10. **III** Triplex formation of TFO3 (T3) and TFO3 hybrids **IV**, in the presence of titrated Cu^{2+} (12.5 pmol) and **V**, with Na-L-ascorbate (12.5 nmol). The results of triplex formation of TFO3 hybrids are in agreement with the thermal melting data with the exception of the TFO3B, which showed slower kinetic at this D:TFO ratio. Negligible effect of Cu^{2+} and Na-L-ascorbate on triplex formation apart for **TFO3B** and **TFO3E**, which are slightly perturbed. All samples were prepared in 10 mM phosphate buffer, 150 mM NaCl, 2 mM $MgCl_2$ (pH 6.0) in a total volume of 5.5 μL. Reactions were incubated at 37 °C for 6 h (**I-III-IV-V**), loaded onto 22% PAGE gel and subjected to electrophoresis for 14 h at 50 V in 50 mM tris-acetate running buffer (pH 6.0).

3.2.6 Chemical nuclease activity

Firstly, targeted nuclease activity was studied with hybrids of TFO3 in the presence of copper(II) nitrate and Asc—a reductant natively found in biological systems. For the determination of the amount of reductant agent to employ for cleaving studies, a ratio of 1:10:10 was selected for the duplex:TFO:Cu^{2+} mixture and cleavage reactions were initiated upon the addition of Asc (TFO:Cu:Asc = 1:1:X; **Figure 3.5 I**). Results show controlled depletion of the triplex ratio TFO:Cu:Asc = 1:1:100, but with higher Asc concentrations unselective ablation of the triplex and the duplex target and interference of triplex formation were observed. To compare the cleavage activity of TFO3 hybrids **A**-**F**, triplicate experiments with 100 equivalents of Asc to TFO were examined (**Figure 3.5 II**). Band densitometry analysis was applied to provide information on triplex depletion (**Figure 3.5 III**).

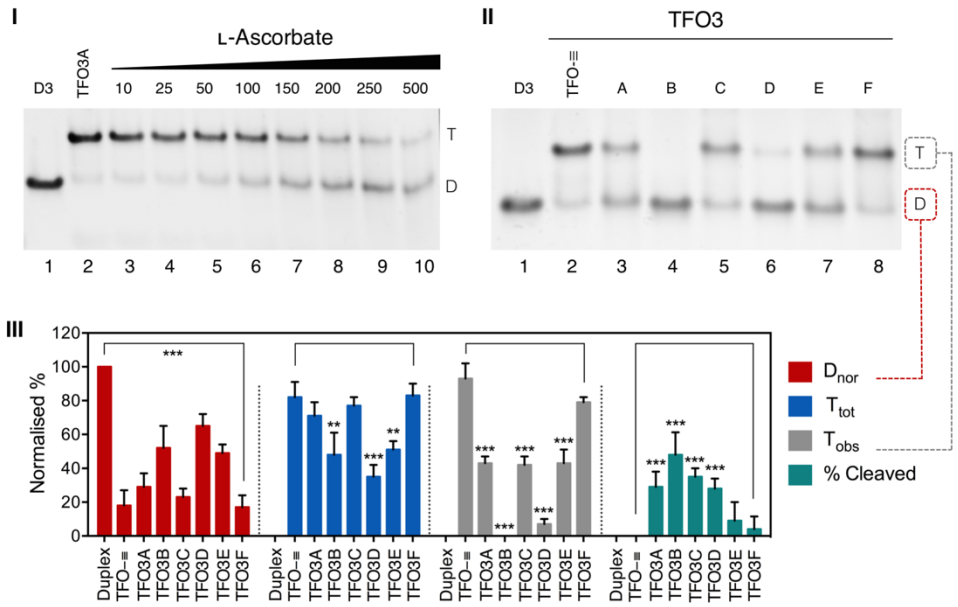

Figure 3.5 I Optimisation of cleavage conditions with varying amounts of ascorbate reductant. Target duplex (1.25 pmol, lane 1) was treated with TFO3A (12.5 pmol, lane 2), Cu^{2+} (12.5 pmol) and increasing amounts of ascorbate with TFO:Cu:Asc = 1:1:X where X = 10-500 equivalents (0.125 nmol, lane 3; 0.312 nmol, lane 4; 0.625 nmol, lane 5; 1.25 nmol, lane 6; 1.87 nmol, lane 7; 2.5 nmol, lane 8; 3.12 nmol, lane 9; 5 nmol, lane 10). **II** Cleavage reactions of TFO 3 hybrids. Target duplex (1.25 pmol, lane 1) was treated with unclicked TFO (TFO–≡, 12.5 pmol, lane 2) or TFO hybrids (A - F, lane 3 - 8) with Na-ι-ascorbate (1.25 nmol) and Cu^{2+} (12.5 pmol). All samples were prepared in 10 mM phosphate buffer, 150 mM NaCl, 2 mM $MgCl_2$ (pH 6.0) in a total volume of 5.5 µL. Reactions were incubated at 37 °C for 6 h, loaded onto 22% PAGE gel and subjected to electrophoresis for 14 h at 50 V in 50 mM tris-acetate running buffer (pH 6.0). **III** Band densitometry of cleavage reactions of TFO3 hybrids. The target duplex band (D) was normalised to lane 1 (D_{nor}) and used to calculate the corresponding theoretical values of triplex formed (100% - D_{nor} = T_{tot}, lanes 2-8 in **II**). T_{tot} was then compared with triplex observed (T_{obs}) to provide the extent of DNA cleavage ($T_{tot} - T_{obs}$ = % cleaved). The hybrids functionalised with the organic azides **B** and **C** showed higher cleaving activity in the incubation of 6 hours.

The most efficient hybrids were those containing ligand modifications **B** and **C**, which also provide high thermal stabilisation. Cleavage experiments for AMN hybrids of TFO2, TFO5 and TFO6 were conducted under identical conditions (Appendix H, **Figure H2**). Overall, hybrids of TFO5 had attenuated activity with TFO3 being the most active series in 6 h. The triplex formation of TFO2- and TFO6-hybrids was particularly affected by the presence of Asc, consequently they have a slower kinetic of the cleavage activity and there is noticeable DNA damage after an incubation time at 37°C of 24 h.

3.2.7 Cleavage specificity

To identify cleavage specificity, experiments comparing cleavage activity towards a GFP target duplex (D_{ON}) and an off-target duplex (D_{OFF}) were designed (**Figure 3.5 I**). Studies were initially conducted using a fixed concentration of Cu(II)-bound hybrids of TFO2, TFO3 and TFO6 in the presence of excess reductant. In all cases either low or no D_{OFF} damage was observed (Appendix H, **Figure H3**). **TFO3A** and **TFO6B** were further investigated across a higher concentration range (**Figure 3.5 III**)—on the basis of triplex formation, modification site and extent of phenanthrene aromaticity—where cleavage of D_{ON} was clearly visible, particularly at higher hybrid loading (25 and 50 equivalents). Significantly, in these experiments D_{OFF} remained largely intact but some shearing is present demonstrating that using higher quantity of TFO-hybrids leads to the diminution of selectivity.

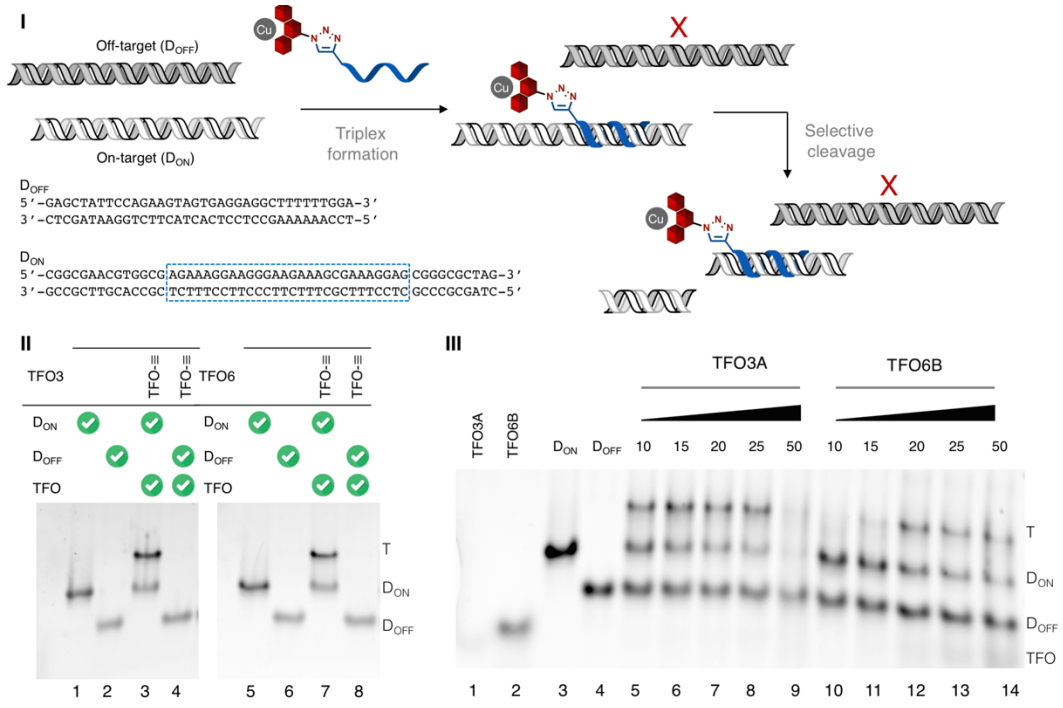

Figure 3.6 I Targeting experiment design: Cu(II) coordinated TFO-hybrids were co-treated with a target duplex (on-target, D_{ON}) and a non-target duplex (off-target, D_{OFF}). In the presence of excess Asc, cleavage specificity can be measured. **II** Triplex formation with non-clicked TFO3 and TFO6 was monitored in the presence of D_{ON} and D_{OFF}. **III** Cleavage activity towards D_{ON} and D_{OFF} by **TFO3A** and **TFO6B** was identified in the presence of $Cu(NO3)_2$ (TFO:Cu^{2+} = 1:1) and Asc (1.25 nmol).

Finally, site selective scission was examined using denaturing experiments with a fluorophore-labelled target. The experimental design is outlined in **Figure 3.7 I** where complementary FAM (6-carboxyfluorescein) and Cy3 (cyanine 3) labelled strands containing the recognition sequence for **TFO2C** were used (S1 and S2, lanes 1-2). Single

stranded oligos—matching the potential fragmentation pattern of the S1:S2 duplex—were also designed and labelled with FAM and Cy3 fluorophores (F1 and F2, lanes 3-4). Cleavage experiments were then performed with 1-25 equivalents of **TFO2C** in the presence of Cu(II) and Asc (**Figure 3.7 II**, lanes 5-11). At low reductant loading (lanes 5-7), the S1:S2 duplex was extensively sheared and by using the FAM filter, it was possible to visualise a faint band in the degradation products that align with fluorophore fragment F1 (lane 3). The intensity of this band increased using the Cy3 filter and a second fragmentation band close to the expected F2 standard (lane 4) was identified. It is likely, therefore, that double stand breaks of the fluorophore-tagged target, along with widespread non-specific shearing, occur with **TFO2C**.

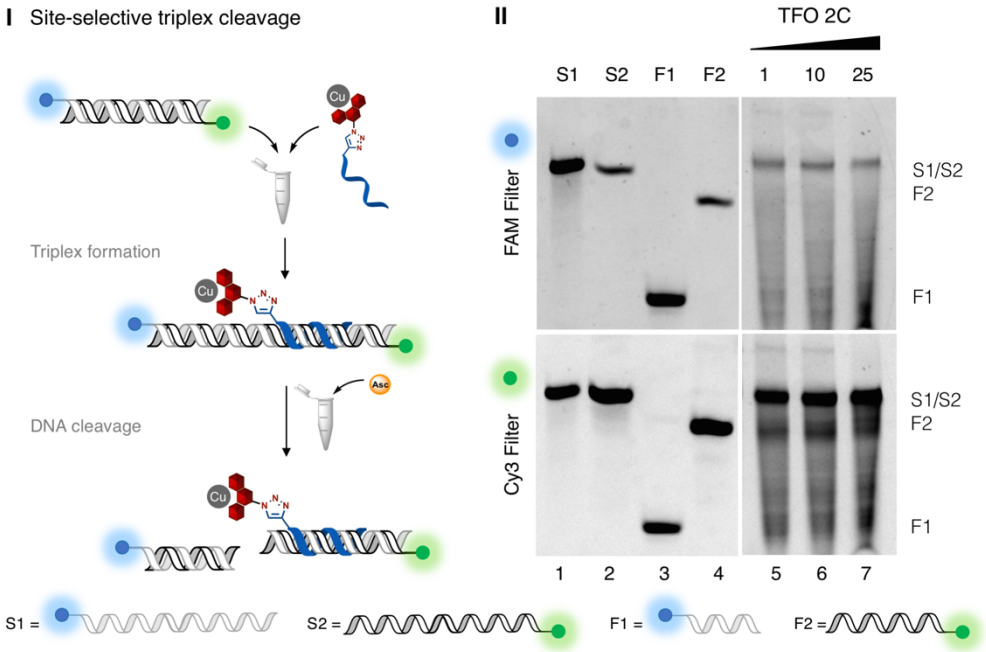

Figure 3.7 Site-selective cleavage of **TFO2C**. **I** Cleavage experiments were designed using fluorescently-tagged complementary single strands of the target duplex (S1 labelled with FAM and S2 labelled with Cy3) and rationally designed fragment probes (F1 and F2) based on proposed cleavage site. **II** Denaturing PAGE experiments with the S1:S2 target treated with varying amounts of TFO in lanes 5-7 (D:TFO:Cu:Asc = 1:X:2X:1500X, where X = 1, 10 or 25 equivalents). S1 and S2 are shown in lane 1 and 2 while F1 and F2 are shown in lane 3 and 4. All reactions were carried out in 10 mM phosphate buffer, 150 mM NaCl, 2 mM $MgCl_2$ (pH 6.0) in a total volume of 10 μL and incubated for 40 h at 37 °C. Samples were loaded onto 22.5% denaturing gel (1× TBE with 7.4 M urea, pH 8.3) PAGE and subjected to electrophoresis for 1.5 h at 15 mA in 1× TBE buffer. The alignment of the degradation products with the fragments references allowed to identify the double stand breaks (DSBs) of the fluorophore-tagged target, along with non-specific shearing at higher loading of hybrid and Asc.

3.2.8 *Di*-copper AMN-TFO systems

Although there is evidence of selective targeting by TFO-hybrids A-F, non-specific cleavage activity toward off-targets was detected. This is likely due to the high oxidizing capacity of vacant sites on the metal centre since copper is bound only to a single *N*,*N*-phenanthrene ligand. To develop more efficient AMNs, recent efforts by our group have focused on *i*.) *di*-nuclear copper system that afford higher nuclease efficiency and enhanced sequence discrimination,[19,21,22] and *ii*.) the introduction of designer intercalating phenazine ligands for superior duplex DNA binding affinity.[19 48] With this in mind, we designed a chemical nuclease comprising a *bis*-phenanthroline *di*-copper binding ligand analogue for the synthesis of the ligand **E** (**G**; **Figure 3.8 I**). Likewise, as control the ligand $\mathbf{G_R}$ was synthesised using similar synthetic route with quantitative yield for each step of synthesis. Moreover, the relative di-copper complexes were developed generating the ancillary ligands $[Cu(Phen)](NO_3)_2$, $[Cu(DPQ)](NO_3)_2$ and $[Cu(DPPZ)](NO_3)_2$ with the methods established in the group,[25,26] followed by the coordination of the ligand $\mathbf{G_R}$.

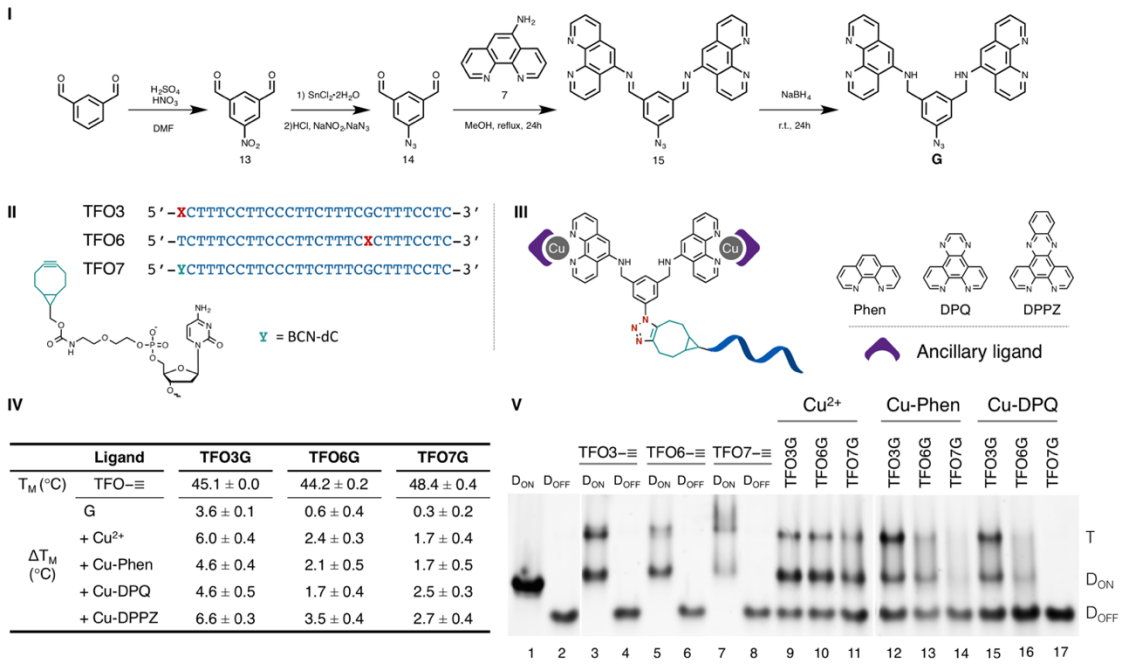

	Ligand	TFO3G	TFO6G	TFO7G
T_M (°C)	TFO–≡	45.1 ± 0.0	44.2 ± 0.2	48.4 ± 0.4
ΔT_M (°C)	G	3.6 ± 0.1	0.6 ± 0.4	0.3 ± 0.2
	+ Cu^{2+}	6.0 ± 0.4	2.4 ± 0.3	1.7 ± 0.4
	+ Cu-Phen	4.6 ± 0.4	2.1 ± 0.5	1.7 ± 0.5
	+ Cu-DPQ	4.6 ± 0.5	1.7 ± 0.4	2.5 ± 0.3
	+ Cu-DPPZ	6.6 ± 0.3	3.5 ± 0.4	2.7 ± 0.4

Figure 3.8 I Synthetic route of ligand **G**, N,N'-((5-azido-1,3-phenylene)bis(methylene))bis(1,10-phenanthrolin-5-amine). **II** Alkyne-modified TFO3 and TFO6 for CuAAC (X = C8-dU) or TFO7 for SPAAC (**Y** = BCN-dC). **III** TFO7G-hybrid with copper chelating and phenazine ancillary ligands Phen, DPQ and DPPZ. **IV** Thermal melting values of TFO-hybrids containing ligand **G** in TFO3, TFO6 and TFO7 along with non-clicked alkyne-modified TFO in the presence of Cu^{2+}, Cu-Phen, Cu-DPQ and Cu-DPPZ (D:TFO:Cu^{2+} = 1:1.25:2.5). Samples were prepared in 10 mM phosphate buffer with 150 mM NaCl and 2 mM $MgCl_2$ (pH = 6.0). The marginal stabilisation induced by the presence of the dinuclear system was observed, but Increased triplex stability was detected upon the introduction of copper(II) ions or coordinated ancillary ligands. **V** Targeting experiment design: Cu(II) coordinated **G**-TFO hybrids were co-treated with a target duplex (on-target, D_{ON}) and a non-target duplex (off-target, D_{OFF}). Selective on-target cleavage was identified at D:TFO:Cu^{2+}:Asc = 1:10:20:1000. All samples were prepared in 10 mM phosphate buffer, 150 mM NaCl, 2 mM $MgCl_2$ (pH 6.0) in a total volume of 5.5 µL. Reactions were incubated at 37 °C for 6 h, loaded onto 22% PAGE gel and subjected to electrophoresis for 14 h at 50 V in 50 mM tris-acetate running buffer (pH 6.0). The damage of the on-target was remarkably enhanced by the addition of the ancillary ligands with the target selectivity fully preserved.

This ligand was then clicked to TFO3 and 6 by CuAAC and also *via* copper-free strain-promoted click chemistry to TFO7—a probe containing a 5′-BCN (bicyclo[6.1.0]non-4-yne) modification (**Figure 3.8 II**). The copper-catalysed method was properly modified for the *di*-nuclear ligand, duplicating the amount of Cu(II), reducing agent and THPTA and prolonging the reaction time. Three new hybrids TFO3G, 6G and 7G were then functionalised with designer ancillary ligands of Phen, DPQ and DPPZ (**Figure 3.8 III**). In contrast to ligands **A-F**, negligible triplex stabilisation was observed for TFOs modified with ligand **G** (**Figure 3.8 IV**). Increased triplex stability was however observed

upon the introduction of copper(II) ions or coordinated ancillary ligands. These stabilisation effects are specific to TFO-hybrids ligated with copper phenanthrenes and differ from randomised binding events observed by discrete Cu-Phen, Cu-DPQ or Cu-DPPZ complexes with unclicked TFOs (Appendix H, **Table H3**). In addition, the triplex formation of TFO3−≡ was examined in presence of the ligand $\mathbf{G_R}$, detecting an increasing of the denaturation temperature of the duplex *ca* 2.40 °C, but not for the triplex. Consequently, the effects of the discrete complexes of non-azide functionalised ligand $\mathbf{G_R}$(*N*,*N*'-(1,3-phenylenebis(methylene))bis(1,10-phenanthrolin-5-amine) in the presence of the target presented uniform stabilisation of the duplex (Appendix H, **Table H4**), demonstrating preferential duplex affinity in its free form and preferential triplex stabilisation in the hybridised form.

PAGE analysis revealed the presence of a double triplex band for TFO3G and TFO7G, when investigating triplex formation conditions using 2.5, 10 and 25 equivalents of TFO incubated at 37 °C for 6 hours (**Figure 3.9 I** to **II**, lane 1-8), which were not observed in the interaction of unclicked triplexes with *di*-copper complexes of $\mathbf{G_R}$ previously coordinated *in situ*. This leads to the conclusion that the *di*-nuclear ligand is not the source of generation of the double band. The stabilising effects attributed to coordinated copper and ancillary ligands was investigated all the TFO-hybrids, detecting the double triplex band only for the terminal modified hybrids (D:TFO = 1:10, **Figure 3.9 III)**.To probe this, **TFO3G** was compared to its mono-chelating counterpart **TFO3E** (**Figure 3.9 IV**). The intensity of the two bands are proportional to the relative amounts of TFO3G:TFO3E when increased from 0:100 to 100:0. This demonstrates two distinct, yet simultaneous binding events for **TFO3G** by one or both phenanthroline moieties within a DNA molecule. The single band of **TFO6G** can be explain as the result of synergistical cooperation of the *di*-nuclear system and TFO moiety due to less freedom degree at internal position.

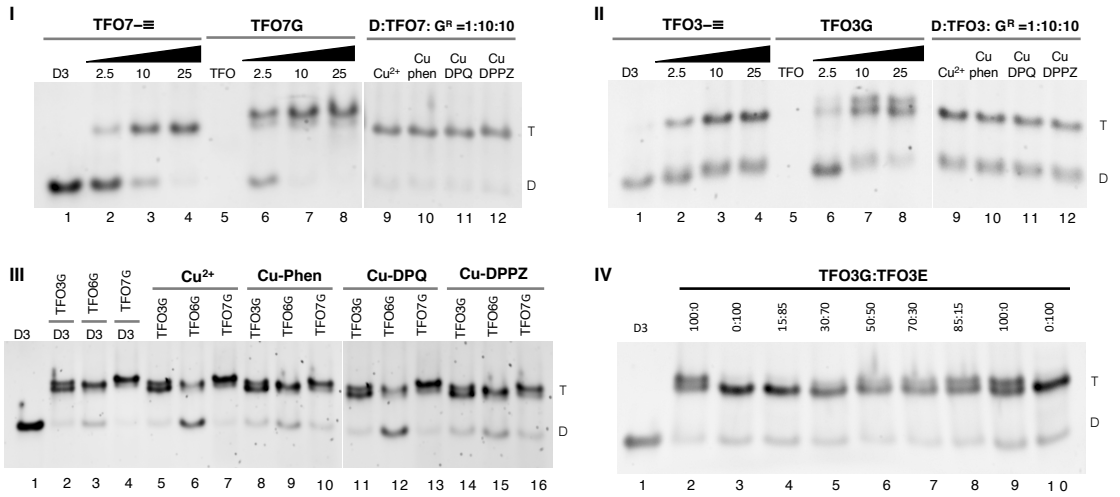

Figure 3.9 Optimisation of triplex formation and cleavage conditions. **I-II** Triplex formation with varying amounts of unclicked TFO–≡, TFO7G (**I**) and TFO3G (**II**), compared to the unclicked triplex interacting with the Cu_2(N,N'-phenanthrene)$_2$(G)]$^{2+}$. Duplex D3 (1.25 pmol, lane 1) was treated with increasing amount of D:TFO = 1:X, where X = 2.5-25 equivalents (3.12 pmol, lane 2,6; 12.5 pmol, lane 3,7; 31.2 pmol, lane 4,8) for 6 h; compared to the unclicked triplex interacting with $\mathbf{G^R}$ previously coordinated in situ with Cu^{2+} and ancillary ligands (A.L., line 9-12). **III** Triplex formation of all the hybrids in presence and in absence of the ancillary ligands and Cu^{2+} (D:TFO:Cu(A.L.) = 1:10:20, incubation time of 6 hours at 37°C). **IV** Competitive study of triplex formation using TFO3E and TFO3G at different ratios: TFO3E:TFO3G = 100:0, 85:15; 70:30; 50:50; 30:70; 15:85; 0:100 (D:TFO=TFO3E+TFO3G) = 1:10). All reactions were carried out in 10 mM phosphate buffer, 150 mM NaCl, 2 mM $MgCl_2$ (pH 6.0) in a total volume of 5.5 µL and incubated at 37 °C. Samples were loaded onto 22% PAGE and subjected to electrophoresis for 14 h at 50 V in 50 mM tris-acetate running buffer (pH 6.0).

Nuclease activity experiments were conducted using 25 equivalences of TFO-hybrids varying the amount of Asc reductant, at different incubation times and in the presences of ancillary ligands (Appendix H, **Figure H4 I** and **II**). The cleaving activity was clearly enhanced with complexation of Cu-Phen and Cu-DPQ but sequence-selectivity was lost under excessive cleavage conditions (Appendix H, **Figure H4 III**). In contrast, in the presence of Cu-DPPZ was found to have greatly attenuated cleavage activity (Appendix H, **Figure H6**). By altering the severity of reaction conditions (D:TFO:Cu = 1:10:20), Appendix H, **Figure H5**), cleavage experiments with on- (D_{ON}) and off-target (D_{OFF}) duplexes identified **TFO7G**, when coordinated to either Cu-Phen or Cu-DPQ, as highly selective knockout agents where D_{ON} was ablated with no apparent D_{OFF} cleavage (**Figure 3.8 V**). These results indicate that although there is a trade-off in triplex stability by using the bulker ligand **G**, selective knockout with no apparent off-target effects appear to be accessible when ancillary Cu-Phen or Cu-DPQ complexes are coordinated to a 5′-BCN modified hybrid by strain-promoted click chemistry.

3.3 Conclusions

We employed nucleic acid click chemistry to develop a new family of chelating intercalating nucleic acid (CINA) hybrids. Their preparation involved conjugating azide-modified phenanthrene ligands to alkyne-modified triplex forming oligonucleotides (TFOs). The *N,N*-phenanthrene unit was introduced in an attempt to furnish TFO hybrids with artificial metallo-nuclease (AMN) activity for targeted gene knockout. Since TFOs are programmable, we exploited their unique base-base recognition properties to target extended sequences of the green fluorescent protein (GFP) recombinant gene. TFO stability, however, remains a barrier since binding of the third strand at the Hoogsteen face produces high electrostatic repulsion. To help overcome this limitation, a library of intercalating *N,N*′-phenanthrenes was developed to contain extended aromatic structures or flexible aliphatic spacers. These ligands were then clicked to alkyne-modified TFOs of between 14-28 nt in length to generate a library of 36 AMN-TFO hybrids targeted to the GFP gene. Both 5′- and internally modified AMN-TFOs were examined and the most promising hybrids contained at least 18 nt. Several of the hybrids provided outstanding triplex stability with melting temperatures exceeding +20 °C when compared to non-clicked TFOs. Almost all 5′-modifications provided higher stabilisation than the internally modified TFOs. Two ligands imparting most stabilisation to internal and 5′-modified TFOs (ligands **B** and **E**) both contain an azido-phenyl substituent linked to the 1,10-phenanthroline core and this design may provide important clues for the future development of triplex stabilising modifications. While the presence of copper(II) had negligible effects on triplex stability, copper-bound hybrids were effective chemical nucleases where targeted cleavage of GFP gene duplexes was triggered in the presence of exogenous ascorbate. Significantly, the addition of stabilising ligands (*e.g.* spermine) or the employment of excessively high loading of the active nuclease (TFO / copper(II)) were not required to initiate targeted oxidation. Degradation of GFP genetic sequences are instead controlled by the concentration of ascorbate with experiments involving on- and off-target duplexes identifying reasonably specific cleavage effects. Finally, the use of fluorescently tagged oligomers provided support for some sequence-specific cleavage by this hybrid AMN-TFO class although high resolution cleavage at the single nucleotide level was not achieved. The final aspect of this study involved the development of a *di*-copper binding TFO hybrid and when this probe was ligated with specific ancillary

ligands (*e.g*. Phen or DPQ) high targeting effects were achieved. Overall, this study has combined nucleic acid click chemistry with the sequence-targeting properties of TFOs to produce a new class of gene-directed artificial nucleases. A future avenue for this technology may be the preparation of therapeutically relevant AMN and TFO combinations for *in cellulo* analysis. These efforts will, however, require backbone or ribose modified TFOs that protect against cellular deactivation and oxidation barriers intrinsic to the AMN hybrid.

References

(1) Kim, Y. G.; Cha, J.; Chandrasegaran, S. Hybrid Restriction Enzymes: Zinc Finger Fusions to Fok I Cleavage Domain. *Proc. Natl. Acad. Sci. U. S. A.* **1996**, *93* (3), 1156–1160.

(2) Urnov, F. D.; Rebar, E. J.; Holmes, M. C.; Zhang, H. S.; Gregory, P. D. Genome Editing with Engineered Zinc Finger Nucleases. *Nat. Rev. Genet.* **2010**, *11*, 636–646.

(3) Christian, M.; Cermak, T.; Doyle, E. L.; Schmidt, C.; Zhang, F.; Hummel, A.; Bogdanove, A. J.; Voytas, D. F. Targeting DNA Double-Strand Breaks with TAL Effector Nucleases. *Genetics* **2010**, *186*, 756–761.

(4) Mussolino, C.; Morbitzer, R.; Lütge, F.; Dannemann, N.; Lahaye, T.; Cathomen, T. A Novel TALE Nuclease Scaffold Enables High Genome Editing Activity in Combination with Low Toxicity. *Nucleic Acids Res.* **2011**, *39* (21), 9283–9293.

(5) Joung, J. K.; Sander, J. D. TALENs: A Widely Applicable Technology for Targeted Genome Editing. *Nat. Rev. Mol. Cell Biol.* **2013**, *14*, 49–55.

(6) Pickar-Oliver, A.; Gersbach, C. A. The next Generation of CRISPR–Cas Technologies and Applications. *Nat. Rev. Mol. Cell Biol.* **2019**, *20*, 490–507.

(7) Cong, L.; Ran, F. A.; Cox, D.; Lin, S.; Barretto, R.; Habib, N.; Hsu, P. D.; Wenyan, J.; Wu, X.; Marraffini, L. A.; et al. Multiplex Genome Engineering Using CRISPR/Cas Systems. *Science* **2013**, *339* (6121), 819–823.

(8) Jinek, M.; Chylinski, K.; Fonfara, I.; Hauer, M.; Doudna, J. A.; Charpentier, E. A Programmable Dual-RNA–Guided DNA Endonuclease in Adaptive Bacterial Immunity. *Science* **2012**, *337*, 816–822.

(9) Katada, H.; Harumoto, T.; Shigi, N.; Komiyama, M. Chemical and Biological Approaches to Improve the Efficiency of Homologous Recombination in Human Cells Mediated by Artificial Restriction DNA Cutter. *Nucleic Acids Res.* **2012**, *40* (11), 1–8.

(10) Vanoli, F.; Tomishima, M.; Feng, W.; Lamribet, K.; Babin, L.; Brunet, E.; Jasin, M. CRISPR-Cas9–Guided Oncogenic Chromosomal Translocations with Conditional Fusion Protein Expression in Human Mesenchymal Cells. *Proc. Natl. Acad. Sci.* **2017**, *114* (14), 3696–3701.

(11) Adli, M. The CRISPR Tool Kit for Genome Editing and Beyond. *Nat. Commun.* **2018**, *9* (1911), 1–13.

(12) Stulz, E.; Clever, G.; Shionoya, M.; Mao, C. DNA in a Modern World. *Chem.*

Soc. Rev. **2011**, *40*, 5633–5635.

(13) Stulz, E.; Clever, G.; Shionoya, M. Artificial DNA Cutters for DNA Manipulation and Genome Engineering. *Chem. Soc. Rev.* **2011**, *40*, 5657–5668.

(14) David S. Sigman, Daniel R. Graham, Vito D'Aurora, and A.; Stern, M. Oxygen-Dependent Cleavage DNA by the 1,10-Phenanthroline.Cuprous Complex. *J. Biol. Chem.* **1979**, *254* (24), 12269–12272.

(15) Chen, T.; Greenberg, M. M. Model Studies Indicate That Copper Phenanthroline Induces Direct Strand Breaks via Beta-Elimination of the 2'-Deoxyribonolactone Intermediate Observed in Enediyne Mediated DNA Damage. *J. Am. Chem. Soc.* **1998**, *120* (15), 3815–3816.

(16) Molphy, Z.; Prisecaru, A.; Slator, C.; Barron, N.; McCann, M.; Colleran, J.; Chandran, D.; Gathergood, N.; Kellett, A. Copper Phenanthrene Oxidative Chemical Nucleases. *Inorg. Chem.* **2014**, *53*, 5392–5404.

(17) Niyazi, H.; Hall, J. P.; O'Sullivan, K.; Winter, G.; Sorensen, T.; Kelly, J. M.; Cardin, C. J. Crystal Structures of λ-$[Ru(Phen)_2Dppz]^{2+}$ with Oligonucleotides Containing TA/TA and AT/AT Steps Show Two Intercalation Modes. *Nat. Chem.* **2012**, *4*, 621–628.

(18) Barton, J. K.; Boynton, A. N.; Boyle, K. M. *DNA-Targeting Molecules as Therapeutic Agents,* The Royal Society of Chemistry; 2018, pp. 367–390.

(19) Molphy, Z.; Slator, C.; Chatgilialoglu, C.; Kellett, A. DNA Oxidation Profiles of Copper Phenanthrene Chemical Nucleases. *Front. Chem.* **2015**, *3*, 1–9.

(20) Prisecaru, A.; Devereux, M.; Barron, N.; McCann, M.; Colleran, J.; Casey, A.; McKee, V.; Kellett, A. Potent Oxidative DNA Cleavage by the Di-Copper Cytotoxin: $[Cu_2(\mu\text{-Terephthalate})(1,10\text{-Phen})_4]^{2+}$. *Chem. Commun.* **2012**, *48*, 6906–6908.

(21) Molphy, Z.; Montagner, D.; Bhat, S. S.; Slator, C.; Long, C.; Erxleben, A.; Kellett, A. A Phosphate-Targeted Dinuclear Cu(II) Complex Combining Major Groove Binding and Oxidative DNA Cleavage. *Nucleic Acids Res.* **2018**, *46* (19), 9918–9931.

(22) Slator, C.; Molphy, Z.; Mckee, V.; Long, C.; Brown, T.; Kellett, A. Di-Copper Metallodrugs Promote NCI-60 Chemotherapy via Singlet Oxygen and Superoxide Production with Tandem TA / TA and AT / AT Oligonucleotide Discrimination. **2018**, 14, 1–18.

(23) McCann, M.; McGinley, J.; Ni, K.; O'Connor, M.; Kavanagh, K.; McKee, V.;

Colleran, J.; Devereux, M.; Gathergood, N.; Barron, N.; et al. A New Phenanthroline-Oxazine Ligand: Synthesis, Coordination Chemistry and Atypical DNA Binding Interaction. *Chem. Commun.* **2013**, *49* (23), 2341–2343.

(24) Zuin Fantoni, N.; Molphy, Z.; Slator, C.; Menounou, G.; Toniolo, G.; Mitrikas, G.; McKee, V.; Chatgilialoglu, C.; Kellett, A. Polypyridyl-Based Copper Phenanthrene Complexes: A New Type of Stabilized Artificial Chemical Nuclease. *Chem. - A Eur. J.* **2019**, *25*, 221–237.

(25) Kellett, A.; Molphy, Z.; Slator, C.; McKee, V.; Farrell, N. P. Molecular Methods for Assessment of Non-Covalent Metallodrug-DNA Interactions. *Chem. Soc. Rev.* **2019**, *48*, 971–988.

(26) Kellett, A.; Molphy, Z.; McKee, V.; Slator, C. *Metal-Based Anticancer Agents; Chapter 4: Recent Advances in Anticancer Copper compounds,* The Royal Society of Chemistry*,* **2019**, pp. 91–119.

(27) Chen, C. B.; Sigmant, D. S. Nuclease Activity of 1,10-Phenanthroline-Copper: Sequence-Specific Targeting. *Proc. Nati. Acad. Sci. USA* **1986**, *83*, 7147–7151.

(28) François, J. C.; Saison-Behmoaras, T.; Barbier, C.; Chassignol, M.; Thuong, N. T.; Hélène, C. Sequence-Specific Recognition and Cleavage of Duplex DNA via Triple-Helix Formation by Oligonucleotides Covalently Linked to a Phenanthroline-Copper Chelate. *Proc. Natl. Acad. Sci. U. S. A.* **1989**, *86*, 9702–9706.

(29) Sun, J. S.; François, J. C.; Montenay-Garestier, T.; Saison-Behmoaras, T.; Roig, V.; Thuong, N. T.; Hélène, C. Sequence-Specific Intercalating Agents: Intercalation at Specific Sequences on Duplex DNA via Major Groove Recognition by Oligonucleotide-Intercalator Conjugates. *Proc. Natl. Acad. Sci. U. S. A.* **1989**, *86*, 9198–9202.

(30) Bales, B. C.; Pitié, M.; Meunier, B.; Greenberg, M. M. A Minor Groove Binding Copper-Phenanthroline Conjugate Produces Direct Strand Breaks via β-Elimination of 2-Deoxyribonolactone. *J. Am. Chem. Soc.* **2002**, *124*, 9062–9063.

(31) Bruice, T. W.; Mazumder, A.; Sutton, C. L. Targeted Chemical Nucleases. **1993**, 23, 180–186.

(32) Fox, K. R.; Brown, T.; Rusling, D. A. *DNA-Targeting Molecules as Therapeutic Agents*; *Chapter 1: DNA recognition by Parallel triplex formation,* The Royal Society of Chemistry, **2018**, pp. 1–32.

(33) Walsh, S.; El-Sagheer, A. H.; Brown, T. Fluorogenic Thiazole Orange TOTFO

Probes Stabilise Parallel DNA Triplexes at PH 7 and Above. *Chem. Sci.* **2018**, *9* (39), 7681–7687.

(34) Christensen, U. B.; Pedersen, E. B. Intercalating Nucleic Acids Containing Insertions of 1-O-(1-Pyrenylmethyl)Glycerol: Stabilisation of DsDNA and Discrimination of DNA over RNA. **2002**, *30* (22), 4918–4925.

(35) Géci, I.; Filichev, V. V.; Pedersen, E. B. Stabilization of Parallel Triplexes by Twisted Intercalating Nucleic Acids (TINAs) Incorporating 1,2,3-Triazole Units and Prepared by Microwave-Accelerated Click Chemistry. *Chem. - A Eur. J.* **2007**, *13*, 6379–6386.

(36) Pedersen, E. B.; Osman, A. M.; Globisch, D.; Paramasivam, M.; Cogoi, S.; Bomholt, N.; Jørgensen, P. T.; Xodo, L. E.; Filichev, V. V. Triplex Glue by Synthesizing Conjugated Flexible Intercalators. *Nucleic Acids Symp. Ser.* **2008**, 52, 37–38.

(37) Paramasivam, M.; Cogoi, S.; Filichev, V. V.; Bomholt, N.; Pedersen, E. B.; Xodo, L. E. Purine Twisted-Intercalating Nucleic Acids: A New Class of Anti-Gene Molecules Resistant to Potassium-Induced Aggregation. *Nucleic Acids Res.* **2008**, *36* (10), 3494–3507.

(38) Gierlich, J.; Burley, G. a.; Gramlich, P. M. E.; Hammond, D. M.; Carell, T. Click Chemistry as a Reliable Method for the High-Density Postsynthetic Functionalization of Alkyne-Modified DNA. *Org. Lett.* **2006**, *8* (17), 3639–3642.

(39) Gramlich, P. M. E.; Warncke, S.; Gierlich, J.; Carell, T. Click-Click-Click: Single to Triple Modification of DNA. *Angew. Chemie - Int. Ed.* **2008**, *47* (18), 3442–3444.

(40) Kukwikila, M.; Gale, N.; El-Sagheer, A. H.; Brown, T.; Tavassoli, A. Assembly of a Biocompatible Triazole-Linked Gene by One-Pot Click-DNA Ligation. *Nat. Chem.* **2017**, *9*, 1089–1098.

(41) El-Sagheer, A. H.; Brown, T. Click Chemistry with DNA. *Chem. Soc. Rev.* **2010**, *39* (4), 1388–1405.

(42) Rusling, D. a.; Powers, V. E. C.; Ranasinghe, R. T.; Wang, Y.; Osborne, S. D.; Brown, T.; Fox, K. R. Four Base Recognition by Triplex-Forming Oligonucleotides at Physiological PH. *Nucleic Acids Res.* **2005**, *33* (9), 3025–3032.

(43) Ohata, J.; Vohidov, F.; Aliyan, A.; Huang, K.; Martí, A. A.; Ball, Z. T. Luminogenic Iridium Azide Complexes. *Chem. Commun.* **2015**, *51*, 15192–

15195.

(44) Lill, A. P.; Rödl, C. B.; Steinhilber, D.; Stark, H.; Hofmann, B. Development and Evaluation of ST-1829 Based on 5-Benzylidene-2-Phenylthiazolones as Promising Agent for Anti-Leukotriene Therapy. *Eur. J. Med. Chem.* **2015**, *89*, 503–523.

(45) Yin, Y.; Xu, S.; Chang, D.; Zheng, H.; Li, J.; Liu, X.; Xu, P.; Xiong, F. One-Pot Synthesis of Biopolymeric Hollow Nanospheres by Photocrosslinking. *Chem. Commun.* **2010**, *46*, 8222–8224.

(46) Molphy, Z.; Slator, C.; Chatgilialoglu, C.; Kellett, A. DNA Oxidation Profiles of Copper Phenanthrene Chemical Nucleases. *Front. Chem.* **2015**, *3* (April), 1–9.

CHAPTER 4

Generation of ruthenium-labelled triplex forming oligonucleotides *via* click chemistry

4.1 Introduction

Ruthenium complexes are of particular interest owing to the photophysical properties of their metal-to-ligand charge-transfer (MLCT) excited state.[1] (Polypyridine)ruthenium(II) complexes are known to display strong absorption bands in the UV-vis region, orange-red emission at room temperature with a large Stokes shift, good emission quantum yields and long luminescence lifetimes (e.g. 0.1 ± 10 ms).[2] Owing to their thermal and photochemical stability and tuneable design of ligands, ruthenium complexes can be employed in a wide range of applications. In the diagnostic area, ruthenium(II) polypyridine complexes have found application as luminescent DNA probes due to 'light switch' properties[3,4] and higher photostability compared to organic fluorophores.[5] Ru(II) polypyridyl complexes are also capable of selectively targeting specific organelles in living cells when conjugated to cell penetrating peptides (CPPs), which act as permeabilising agents and allow the penetration across the plasma membrane.[6,5,7] In this context, the Keyes group developed a variety of ruthenium complexes conjugated to specific peptides for selective cell targeting. For example, Ru(II)DPPZ complexes were linked to a nuclear localisation transcription factor NF-κB (NLS) for targeting the nucleus of HeLa cells.[6] When hybridised to a mitochondrial penetrating peptide (MPP), Ru(II) complexes could also be directed to the mitochondria.[8] The targeting properties were found to be tuneable also by the selection of the ancillary ligands present in the metal complex. An example of this strategy was provided by the $[Ru(LL)_2PIC]ClO_4$ system (where PIC = 2-(4-carboxyphenyl)-imidazo-[4,5-f][1,10]-phenanthroline) when conjugated to NLS; when LL is 2,2-bipyridine, the hybrid could reach the nucleus but when LL was varied to 4,7-diphenyl-1,10-phenanthroline, the ruthenium hybrid became concentrated in the nucleolus.[9]

In presence of water molecules the fluorescent properties of ruthenium complexes (notably dppz compounds) are attenuated or quenched but in a hydrophobic environment their emissive capabilities are restored.[10] However, by interacting with DNA, these complexes are protected from the collisional quenching effects of water[11] and, in some cases, DNA itself catalyses the electronic transfer (ET) leading to enhanced photophysical properties.[12] Barton *et al.* investigated mechanism of long-range electron transfer between ruthenium complexes and DNA.[13] In sequences containing 5′ -GG- 3′ and 5′ -GC- 3′ quenching of photophysical properties occurs because of the photo-

oxidation of guanines.[14] Similar studies were conducted also by the Kelly group using $[Ru(phen)_3]^{2+}$ modified ONs[15,16] and enantiomerically resolved $[Ru(TAP)_2(DPPZ)]^{2+}$ (TAP = 1,4,5,8-tetraaza-phenanthrene).[17] Long-range guanine oxidation is affected by the presence of mismatches,[18] which provokes localised disruption in the double helix leading to different levels of oxidative damage in presence of G·T and G·A mismatches. In view of their desirable fluorescent and DNA intercalating properties, covalently linked Ru(II)-oligonucleotides conjugates (Ru-ON) were developed. The first of these Ru-ON involved the conjugation of a 15 mer to $[Ru(Phen)_2DPPZ]^{2+}$ tethered *via* an amide bond[19] and showed luminescent properties only after hybridization with the complementary strand. Afterwards, DNA duplexes modified with ruthenium donor and acceptor complexes and duplexes functionalised with ruthenium and rhodium were used to provide a deeper comprehension of electron transfer (ET).[10] Triplex-formation oligonucleotides (TFOs) covalently modified with Ru(II) complexes are known and have been developed for photo-oxidation- and luminescent-guided anti-gene applications.[20] Although nucleic acid click chemistry was not applied to prepare these hybrids, their design strategies focused on developing TFOs with terminal and internal Ru(II) complex incorporation.[19,20,3]

In this chapter, TFOs modified with Ru(II) polypyridyl complexes were generated using nucleic acid click chemistry methods developed in chapter 3. The goal, therefore, was to establish a new scalable method for rapidly preparing Ru(II)-TFO hybrids and to conduct preliminary experiments to understand their diagnostic applications as possible luminescent probes for DNA. To achieve this, azide-modified phenanthrene ligands **A**, **B**, **C** and **D**, were selected from chapter 3 and coordinated to ruthenium polypyridyl complexes such that conjugation to alkyne-modified TFOs could be attempted. Hybrids that were successfully developed were then studied for their ability to form stable triplexes with luminescent probe functionality.

4.2 Results and discussion

4.2.1 Design of ruthenium complexes bearing azide-functionality

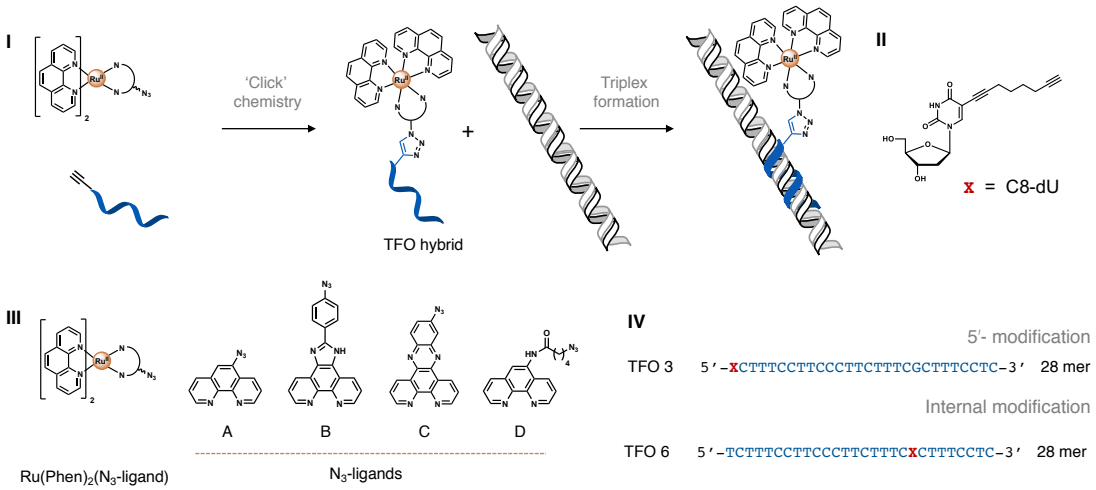

Figure 4.1 I Azide-modifed Ru(II) complexes [Ru(Phen)$_2$(N$_3$-Phenanthrene)](PF$_6$)$_2$ were conjugated to alkyne-modified triplex forming oligonucleotide (TFOs) through copper-catalysed azide-alkyne cycloaddition (CuAAC) reactions. **II** The alkyne-modified nucleobase C8-Alkyne-dU was positioned at either 5′-termini or at internal position within the TFO probe. **III** Ru(II) complexes were designed with either 5-azido-1,10-phenanthroline (**A**), 2-(4-azidophenyl)-1H-imidazo[4,5-f][1,10]-phenanthroline (**B**), 11-azidodipyrido[3,2-a:2′,3′-c]phenazine (**C**), or 5-azido-N-(1,10-phenanthrolin-5-yl)pentanamide (**D**) ligands. **iv)** Alkyne-modified TFOs with GFP sequence recognition contain modification sites highlighted in red (X).

For the development of Ru(II) complexes, a set of four compounds bearing an azide-ligand of general formula [Ru(Phen)$_2$(N$_3$-Phenanthrene)](PF$_6$)$_2$ were prepared (Figure 4.1). Four phenanthrene ligands (**A-D**) were selected from chapter 3 as these ligands have different degrees of conjugation and the placement of the azide group also varied somewhat. The initial approach was to directly coordinate the N$_3$-Phenanthrene ligand to [Ru(1,10-phenanthroline)$_2$Cl$_2$] and this proved successful with ligand **D** (**Figure 4.2**, *Route iii)*). However, for the other ligands (**A-C**), this method gave rise to either impurities or low yields or a combination thereof. Consequently, a synthetic strategy for preparing [Ru(Phen)$_2$(**A**)](PF$_6$)$_2$, **[**Ru(Phen)$_2$(**B**)](PF$_6$)$_2$, and [Ru(Phen)$_2$(**D**)](PF$_6$)$_2$ was changed whereby *in situ* azidation of the ruthenium complexes was achieved. For the preparation of [Ru(Phen)$_2$(**A**)](PF$_6$)$_2$, two approaches were made:

Method A: Coordination of the 5-amino-1,10-phenanthroline ligand to [Ru(Phen)$_2$Cl$_2$] followed by functional group interconversion of the amine to an azide *via* the diazonium salt.[21]

Method B: Coordination of 5,6-epoxy-5,6-dihydro-1,10-phenanthroline to a Ru(II) bipyridine complex was previously identified as a suitable intermediate ligand for azidation.[22] This approach was adopted here with a different starting material of $[Ru(Phen)_2Cl_2]$.

A similar approach to *method A* was previously applied to generate an iridium complex of ligand **A** with quite high yield.[23] However, on this occasion the reaction furnished a final Ru(II) product mixture that was highly impure and with very low yield. In contrast, *method B* successfully provided the complex $[Ru(Phen)_2(\mathbf{A})](PF_6)_2$ (**Figure 4.2**, *Route i)*). For complexes of ligands **B** and **C**, *method A* was successful for the generation of $[Ru(Phen)_2(\mathbf{B})](PF_6)_2$ and $[Ru(Phen)_2(\mathbf{C})](PF_6)_2$ (**Figure 4.2**, *Route ii)*). The intermediates $[Ru(Phen)_2(\mathbf{3})]^{2+}$ and $[Ru(Phen)_2(\mathbf{5})]^{2+}$ were generated in high yield for direct coordination of **3** and **5** to $[Ru(Phen)_2Cl_2]$ in a mixture of EtOH and H_2O under inert conditions, followed by diazotization. After the azidation step, $[Ru(Phen)_2(\mathbf{B})](PF_6)_2$ was obtained with high purity and yield but $[Ru(Phen)_2(\mathbf{C})](PF_6)_2$ contained a number of impurities and not significant yield. Consequently, complexes $[Ru(Phen)_2(\mathbf{A})](PF_6)_2$, $[Ru(Phen)_2(\mathbf{B})](PF_6)_2$ and $[Ru(Phen)_2(\mathbf{D})](PF_6)_2$ were selected for conjugation to alkyne-bearing TFOs.

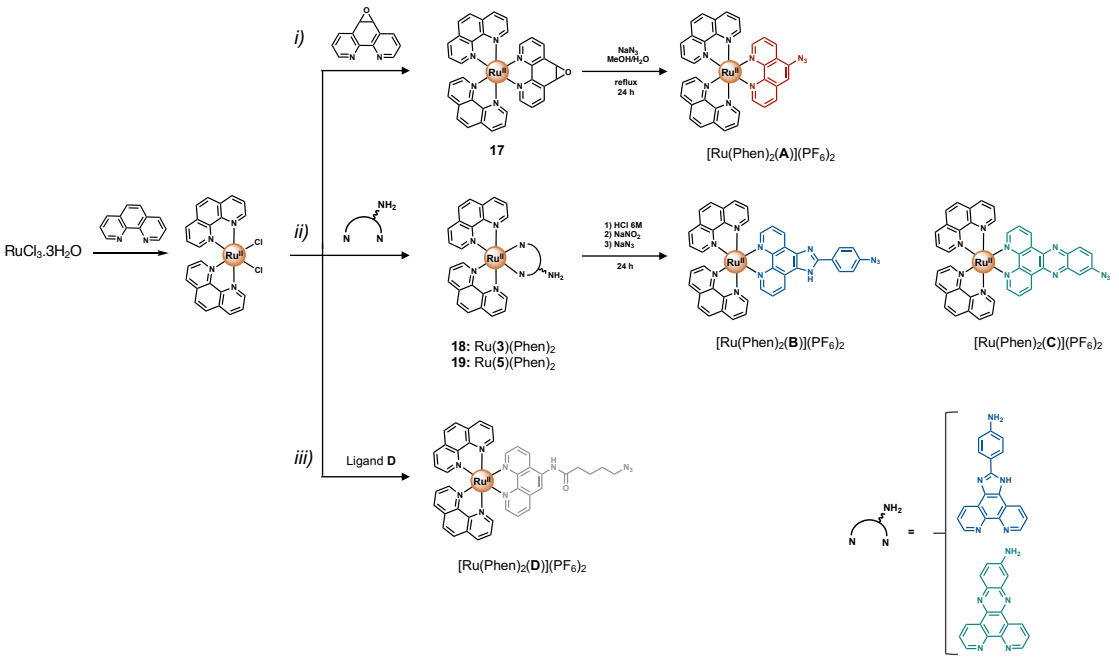

Figure 4.2 Synthetic routes for azide-modified Ru(II) complexes. Route i) Epoxy-1,10-phenanthroline was complexed and followed thereafter by the azidation to release the desired product $[Ru(Phen)_2(\mathbf{A})](PF_6)_2$. Route ii) Complexation of the amino-derivates of dipyrido[3,2-a:2',3'-c]phenazine and 2-phenyl-1H-imidazo[4,5-f]-1,10-phenanthroline provided intermediates for products $[Ru(Phen)_2(\mathbf{B})](PF_6)_2$ and $[Ru(Phen)_2(\mathbf{C})](PF_6)_2$. Route iii) $[Ru(Phen)_2(\mathbf{D})](PF_6)_2$ was prepared by directly coordinating 5-azido-N-(1,10-phenanthrolin-5-yl)pentanamide to $[Ru(Phen)_2Cl_2]$.

4.2.2 TFO design and triplex formation

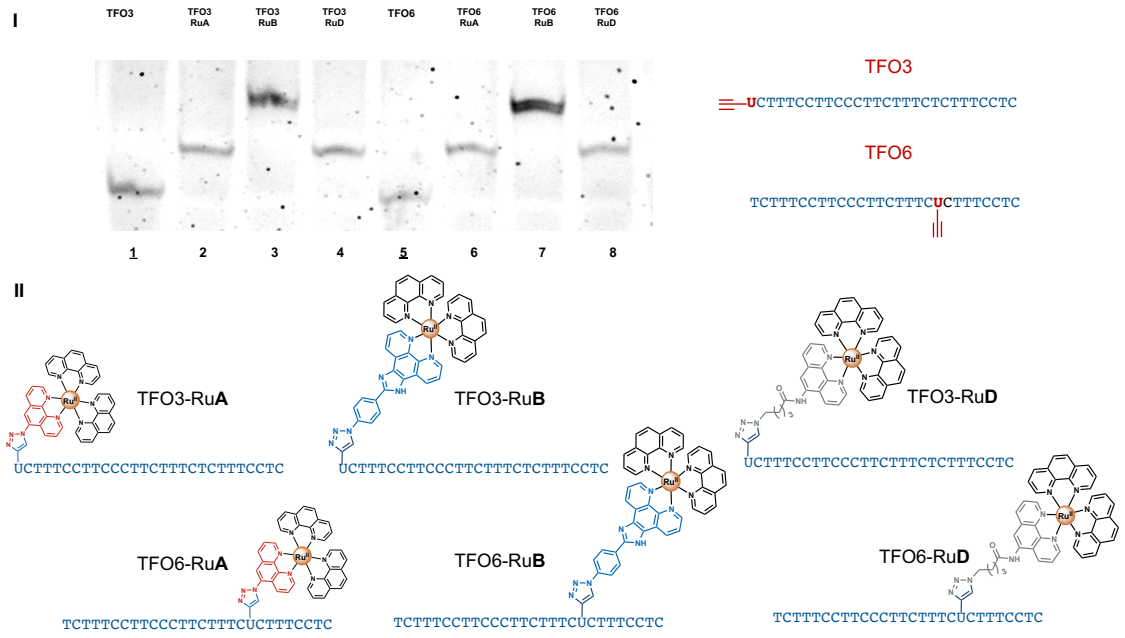

Figure 4.3 Synthesis of Ru(II)-hybrids using the in-house method of 'click chemistry' **I** Control (TBE) PAGE gel for the CuAAC chemistry for the Ru(II) complexes with TFO3 and TFO6. Samples were loaded onto 22% PAGE and subjected to electrophoresis for 2 h at 80 V TBE (1X) running buffer. **II** Schematic representation of Ru(II)-TFO hybrids.

TFO3 and TFO6 (**Figure 4.3 I-II**) were selected owing to their high thermal stability reported in chapter 3. Initially, click chemistry was utilised to combine $[Ru(Phen)_2(\mathbf{A})](PF_6)_2$ with an alkyne-functionalised TFOs using the protocol previously reported in chapter 2 and the reaction progress was monitored using native TBE-PAGE gel electrophoresis (data not reported). Formation of the Ru(II)-TFO hybrid was observed, however there was also significant degradation of the TFO starting material. The unwanted degradation was most likely due to the presence of high amounts of Cu(II) and Na-L-ascorbate alongside the long incubation period which were initially deemed necessary to ensure the progression of the click reaction. Previously—when performing the click chemistry experiments reported in chapter 3—large quantities of Cu(II) and Na-L-ascorbate were required to ensure the progression of the click reaction. This was caused by the sequestration of Cu(II) by the phenanzine/phenanthrene ligands which inhibited the click reaction. Subsequently, as the Ru(II) complexes did not present any open chelation site, the reaction conditions were optimised to decrease the reaction time and consequently avoided degradation of the TFO starting material to obtain complete

formation of the Ru(II)-hybrids. This was confirmed by the TBE-PAGE gel experiments (**Figure 4.3 III**) and by MALDI-TOF analysis (Appendix G).

I

		TFO3		TFO6	
	Ru(Ligand)	**Triplex**	**Duplex**	**Triplex**	**Duplex**
T_m (°C)	TFO–≡	45.1 ± 0.0	79.0 ± 0.6	44.2 ± 0.2	79.0 ± 0.6
ΔT_m (°C)	Ru**A**	1.1 ± 0.4	2.2 ± 0.04	1.3 ± 0.7	2.3 ± 0.3
	Ru**B**	9.4 ± 0.4	2.5 ± 0.3	6.7 ± 0.1	2.2 ± 0.3
	Ru**D**	1.94 ± 0.3	1.90 ± 0.1	-1.2 ± 0.2	2.4 ± 0.3

II

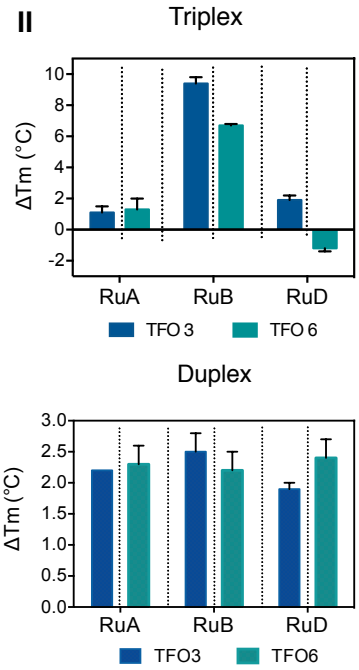

III

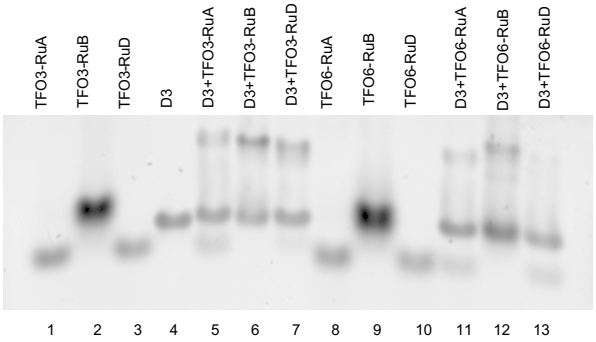

Figure 4.4 I Stabilisation of triplex and duplex thermal melting induced by the Ru(II) complexes in TFO3 and TFO6 compared to control TFOs. **II** Direct comparison of ΔT_m of the triple and double helixes of TFO3 (blue) and TFO6 (green) prompted by the presence of the Ru(II) complexes. **III** Triplex formation of Ru(II)-hybrids (Duplex:TFO = 1:10) incubated for 6 hours at 37 °C in 10 mM phosphate buffer, 150 mM NaCl, 2 mM $MgCl_2$ (pH 6.0) in a total volume of 5 µL. The samples were loaded onto 22% PAGE and subjected to electrophoresis for 14 h at 50 V in 50 mM tris-acetate running buffer (pH 6.0).

Triplex formation and thermal stabilisation (ΔT_m) of the Ru(II)-TFO hybrids were investigated using UV thermal melting experiments recorded at 260 nm in 10 mM phosphate buffer 150 mM NaCl and 2 mM $MgCl_2$ (pH 6). The presence of TFO3-Ru**A** and TFO3-Ru**D** were observed to provide marginal increases in triplex stabilisation. In contrast, a relatively significant increase in stabilisation was observed for TFO3-Ru**B** (**Figure 4.4 I**). Ru(II)-TFO hybrids bearing a 5'-terminal modification were more stable and it was possible to identify a trend for the TFO3 hybrids: $[Ru(phen)_2(\mathbf{B})](PF_6)_2$ > $[Ru(phen)_2(\mathbf{D})](PF_6)_2$ > $[Ru(phen)_2(\mathbf{A})](PF_6)_2$. Conversely, TFO6-Ru**D** was found to destabilise the triplex by *ca* 1.2 °C. Overall, the hybrids bearing ligand **B** were the most stabilising, confirming the findings reported in chapter 3. With regard to duplex stabilisation, direct comparison of ΔT_m for TFO3 and TFO6 with Ru(II) complex modification displayed no significant difference in duplex stabilisation when accounting for terminal and internal functionalisation, with an overall stabilisation of *ca* 2.2 °C

(**Figure 4.4 II**). For further investigation, the triplex formation was analysed by PAGE (**Figure 4.4 III**) using the method reported previously in chapter 2. As expected, the TFO3 hybrids provided a higher amount of triplex formation in comparison to the TFO6 hybrids. No triplex formation was observed for TFO6-Ru**D** and is in consistent with the destabilising contribution observed in the thermal melting analysis.

4.2.3 Preliminary photophysical analysis

I

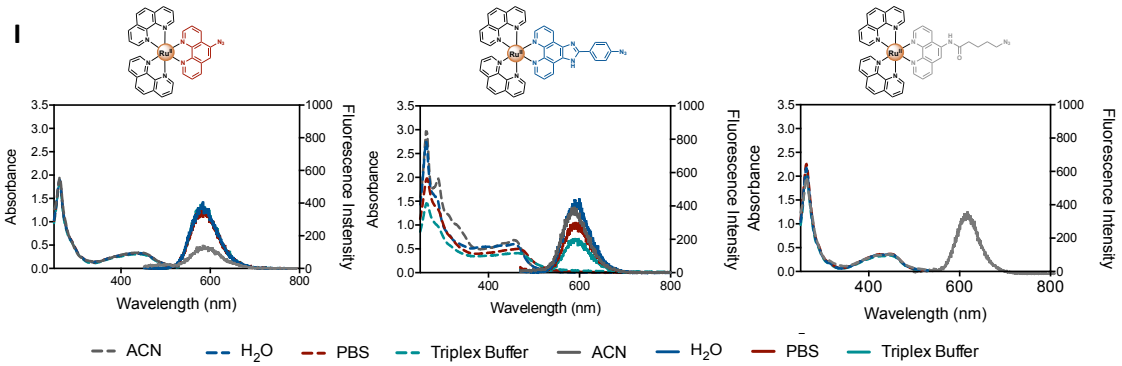

II

		λ_{max}	ε	λ_{em}
[Ru(phen)$_2$(**A**)](PF$_6$)$_2$	Solvent*	444	13480	590
[Ru(phen)$_2$(**B**)](PF$_6$)$_2$	ACN	457	28320	585
	H_2O	457	25120	592
	PBS	464	20600	589
	Triplex Buffer	464	15960	593
[Ru (phen)$_2$(**D**)](PF$_6$)$_2$	Solvent*	447	13760	595

*Solvent = identical results observed with ACN, H_2O, PBS or Triplex Buffer (10 mM Phosphate 150mM NaCl 2mM $MgCl_2$).

Figure 4.5 I UV (dotted line) and fluorescent (solid line) analysis of [Ru(phen)$_2$(**A**)](PF$_6$)$_2$, [Ru(phen)$_2$(**B**)](PF$_6$)$_2$ and [Ru(phen)$_2$(**D**)](PF$_6$)$_2$ 25 μM in ACN, H_2O, PBS (pH=7.4) and 10 mM phosphate 150 mM NaCl and 2 mM $MgCl_2$ buffer (pH=6). Fluorescence analysis of the complex [Ru(phen)$_2$(**D**)](PF$_6$)$_2$ was performed at 1 μM because of the high luminescence properties of the complex. Emission slit: 2.5 nm/excitation slit: 5 nm. **II** Table of λ_{max}, ε and λ_{em} of [Ru(phen)$_2$(**A**)](PF$_6$)$_2$, [Ru(phen)$_2$(**B**)](PF$_6$)$_2$ and [Ru(phen)$_2$(**D**)](PF$_6$)$_2$.

A preliminary photophysical study of [Ru(Phen)$_2$(**A**)](PF$_6$)$_2$, [Ru(Phen)$_2$(**B**)](PF$_6$)$_2$ and [Ru(Phen)$_2$(**D**)](PF$_6$)$_2$ was undertaken in ACN, H_2O, PBS and triplex buffer (10 mM phosphate buffer, 150 mM NaCl, 2 mM $MgCl_2$, pH 6.0). The absorbance spectra were measured at a concentration of 25 μM and are shown in **Figure 4.5 I**. In all solvents used, the complexes exhibit strong absorption bands in the UV-visible region at ~263 nm and this band was unambiguously assigned to a spin-allowed $\pi \rightarrow \pi^*$ ligand-centred (LC) transitions. [Ru(Phen)$_2$(**A**)](PF$_6$)$_2$, and [Ru(Phen)$_2$(**D**)](PF$_6$)$_2$ exhibit broad bands of low intensity in the visible region at 444 and 447 nm respectively, which were assigned to a spin-allowed MLCT transition. The MLCT band of [Ru(**B**)(Phen)$_2$](PF$_6$)$_2$ in ACN was

identified at 457 nm and this is likely due to the extended aromatic system present in ligand **B**.

Subsequently, further experimentation was conducted to investigate the photophysical properties of the Ru(II) complexes, performed using the same concentration as before (25 μM), on a PerkinElmer LS-55 Fluorometer. Within this experiment, $[Ru(phen)_2(\mathbf{A})](PF_6)_2$, $[Ru(phen)_2(\mathbf{B})](PF_6)_2$ and $[Ru(phen)_2(\mathbf{D})](PF_6)_2$ in ACN, H_2O, PBS and triplex buffer were analysed at excitation wavelengths of 444, 457 and 446 nm respectively (**Figure 4.5 I**). At this concentration, the Ru(II) complexes exhibited an emission peak at *ca.* 595 nm and, $[Ru(phen)_2(\mathbf{D})](PF_6)_2$ showed the signal of highest intensity providing an out of scale emissive peak in H_2O, PBS and triplex buffer. For this reason, the concentration of the complexes was progressively decreased identifying as optimal concentration of 5 μM for $[Ru(phen)_2(\mathbf{A})](PF_6)_2$, and $[Ru(phen)_2(\mathbf{B})](PF_6)_2$ and 1 μM for $[Ru(phen)_2(\mathbf{D})](PF_6)_2$ (Appendix I, **Figure I1**). The emissive properties of $[Ru(phen)_2(\mathbf{A})](PF_6)_2$ and $[Ru(phen)_2(\mathbf{D})](PF_6)_2$ in aqueous solutions were unaffected by the change in salt concentration and pH. A different trend was detected for $[Ru(phen)_2(\mathbf{B})](PF_6)_2$, which displayed similarities with tuneable luminescent complexes[24–27] by displaying reduced band intensity at lower pH.

Subsequently, $[Ru(phen)_2(\mathbf{B})](PF_6)_2$ and $[Ru(phen)_2(\mathbf{D})](PF_6)_2$ were selected for comparative luminescence analysis with the related TFO-hybrids,TFO3-Ru**B** and TFO3-Ru**D**, at a concentration of 5 μM and 1 μM, respectively (**Figure 4.6**). $[Ru(phen)_2(\mathbf{A})](PF_6)_2$ displayed a lower luminescent intensity in comparison and therefore was not chosen for this analysis (Appendix I).

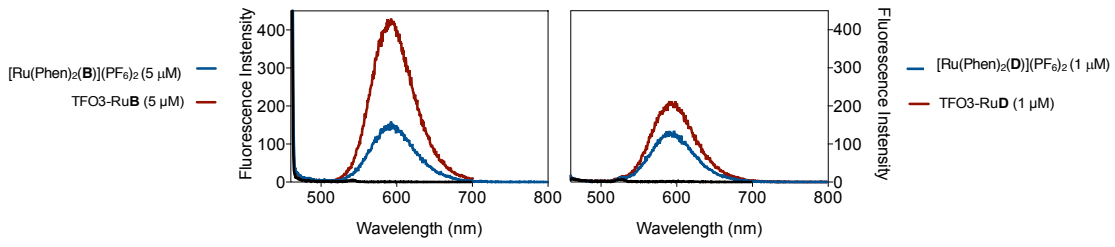

Figure 4.6 Comparison of the emission spectra of $[Ru(Phen)_2(\mathbf{B})](PF_6)_2$ (5 μM) and $[Ru(Phen)_2(\mathbf{D})](PF_6)_2$ complexes (1 μM) and equivalent TFO-hybrids clicked to TFO3 in 10 mM phosphate buffer 150 mM NaCl 2 mM $MgCl_2$ (pH=6). λ_{ex} of $[Ru(Phen)_2(\mathbf{B})](PF_6)_2$: 457 nm and λ_{ex} of $[Ru(Phen)_2(\mathbf{D})](PF_6)_2$: 447 nm. Emission slit: 2.5 nm/excitation slit: 5 nm.

After click conjugation to TFOs, a significant enhancement in the emission intensity was identified for TFO3-Ru**B** along with a marginal increase in TFO3-Ru**D**. The luminescence intensity increase for TFO3-Ru**B** is likely due to direct conjugation of the triazole ring to the aromatic moiety.

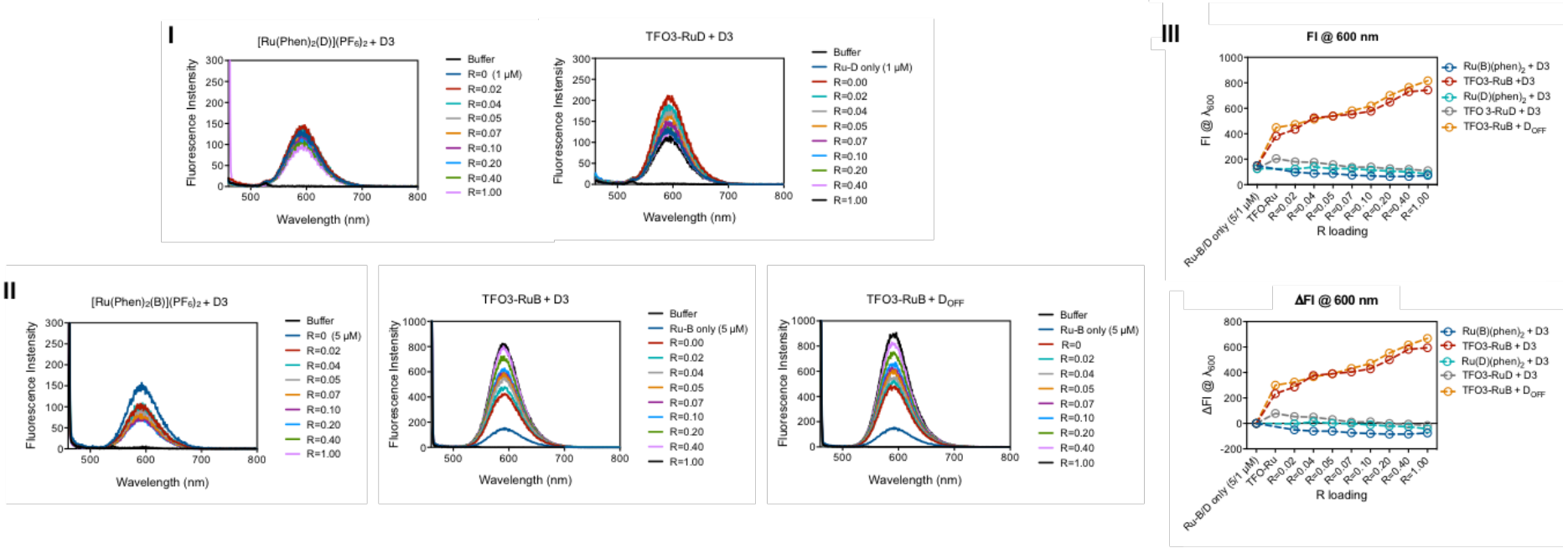

Figure 4.7 I Titration of [Ru(phen)$_2$(**D**)](PF$_6$)$_2$ and TFO3-Ru**D** at the concentration of 1 μM with the target D3. **II** [Ru(phen)$_2$(**B**)](PF$_6$)$_2$ and TFO3-Ru**B** at the concentration of 5 μM with the target D3. **III** Direct comparison of variation of luminescence intensity (FI) and normalised luminescence intensity (ΔFI) of the titration of [Ru(phen)$_2$(**B**)](PF$_6$)$_2$, TFO3-Ru**B**, [Ru(phen)$_2$(**D**)](PF$_6$)$_2$and TFO3-Ru**D** with D3 and TFO3-Ru**B** with D$_{OFF}$ detected at 600 nm. The titration was conducted with the loading ratio R=0.00 - 1.00 in 10 mM phosphate buffer 150 mM NaCl and 2 mM MgCl$_2$ (pH=6). λ_{ex} of [Ru(Phen)$_2$(**B**)](PF$_6$)$_2$: 457 nm and λ_{ex} of [Ru(Phen)$_2$(**D**)](PF$_6$)$_2$: 447 nm. Emission slit: 2.5 nm/excitation slit: 5 nm.

The interaction of Ru(II)-functionalised TFOs with DNA was examined by titrating a target duplex (D3, 40 bp) against TFO3-Ru**B** and, as an experimental control, the titration was also performed with $[Ru(phen)_2(\mathbf{B})](PF_6)_2$ (**Figure 4.7 II)**. After each aliquot of duplex was added, there was an enhancement in the emission of TFO3-Ru**B**. Conversely, for $[Ru(phen)_2(\mathbf{B})](PF_6)_2$ reduced intensity was noted upon the addition of duplex DNA. The same experiment was then conducted for TFO3-Ru**D** and $[Ru(phen)_2(\mathbf{D})](PF_6)_2$ in which a consistent decrease in intensity of the emission signal was detected for both systems (**Figure 4.7 I**). As a negative control, an off-target experiment was conducted, titrating TFO3-Ru**B** with an off-target duplex of comparable size (**Figure 4.7 II**). A similar trend to the on-target experiment was identified, which led to the conclusion that the variation in luminescence was likely due to the interaction of the Ru(II)-complex with DNA and not due to a contribution from the triplex.

4.3 Conclusion

Triplex forming oligonucleotides (TFOs) were functionalised with novel ruthenium(II) complexes utilising the copper-catalysed azide-alkyne cycloaddition (CuAAC) reaction. Ruthenium complexes were designed to contain a single azide-modified N,N-phenanthrene ligand and contained the general formula $[Ru(Phen)_2(N_3\text{-}Phenanthrene)](PF_6)_2$. Four ligands (**A-D**), identified from earlier experiments in chapter 3 to possess desirable stabilisation properties, were selected for complexation. Furthermore, the length of alkyne-modified TFOs employed (28 nt) was also informed by earlier work with copper(II) TFO hybrids. Two TFO modification positions were selected at the 5′-base and at an internally base-modified position and click chemistry was applied to generate a small library of Ru(II)-TFO hybrids. Almost all hybrids provided enhanced triplex stability but TFOs modified with ligand **B** (2-(4-azidophenyl)-1*H*-imidazo[4,5-*f*][1,10]phenanthroline) provided the highest stabilisation of the group with + 9.4 °C (5′-modified) and + 6.7 °C (internally modified) values recorded. Overall, terminal modifications provided higher stabilisation than the internally modified TFOs. A comparative study of the luminescence properties and thermal stability of Ru(II)-TFO hybrids led to the selection of two hybrids for further investigation—the 5′-base modified TFO clicked to $[Ru(Phen)_2(\mathbf{B})](PF_6)_2$ and $[Ru(Phen)_2(\mathbf{D})](PF_6)_2$. In DNA binding studies both Ru(II)-TFO hybrids showed two different trends: enhanced luminescence for TFO3-Ru**B** and decreased luminescence for TFO3-Ru**D**. However, both Ru(II) control

complexes, $[Ru(Phen)_2(\mathbf{B})](PF_6)_2$ and $[Ru(Phen)_2(\mathbf{D})](PF_6)_2$, displayed a consistent decrease in their luminescent signals, likely due to the interaction with specific sections of DNA target. Another possible explanation can be related to the presence of the azide group, which is known to deactivate fluorophores[28,29] and iridium complexes.[23] The results of the on/off-target experiment were comparable indicating that the ruthenium-DNA interaction was the predominant binding mode. Overall, this chapter has demonstrated a new method for preparing base-modified Ru(II) complex-TFO hybrids and provided preliminary data for their application as potentially useful diagnostic probes. The future development of these hybrids could be guided by Ru(II) polypyridyl complexes containing ligand **B** since this modification provides TFO hybrids with enhanced stabilisation and luminescence properties.

References

(1) Tyson, D. S.; Bialecki, J.; Castellano, F. N. Ruthenium(II) Complex with a Notably Longexcited State Lifetime. *Chem. Commun.* **2000**, 2355–2356.

(2) Garcìa-Fresnadillo, D.; Orellana, G. Interaction of Sulfonated Ruthenium(Ii) Polypyridine Complexes with Surfactants Probed by Luminescence Spectroscopy. *Helv. Chim. Acta* **2001**, *84*, 2708–2730.

(3) Flamme, M.; Clarke, E.; Gasser, G.; Hollenstein, M. Applications of Ruthenium Complexes Covalently Linked to Nucleic Acid Derivatives. *Molecules* **2018**, *23*, 28–31.

(4) Erkkila, K. E.; Odom, D. T.; Barton, J. K. Recognition and Reaction of Metallointercalators with DNA. *Chem. Rev.* **1999**, *9*, 2777–2795.

(5) Neugebauer, U.; Pellegrin, Y.; Devocelle, M.; Forster, R. J.; Signac, W.; Moran, N.; Keyes, T. E. Ruthenium Polypyridyl Peptide Conjugates: Membrane Permeable Probes for Cellular Imaging. *Chem. Commun.* **2008**, 5307–5309.

(6) Article, E.; Byrne, A.; Burke, S.; Keyes, T. E. Chemical Science Highly e Ff Ective Probes for Cell Imaging by Stimulated Emission Depletion (STED) Microscopy. *Chem. Sci.* **2016**, *7*, 6551-6563.

(7) Wang, T.; Zabarska, N.; Wu, Y.; Lamla, M.; Fischer, S.; Monczak, K.; Ng, D. Y. W.; Rau, S.; Weil, T. Receptor Selective Ruthenium-Somatostatin Photosensitizer for Cancer Targeted Photodynamic Applications. *Chem. Commun.* **2015**, *51*, 12552–12555.

(8) Burke, C. S.; Byrne, A.; Keyes, T. E. Highly Selective Mitochondrial Targeting by a Ruthenium (II) Peptide Conjugate : Imaging and Photoinduced Damage of Mitochondrial DNA. *Angew.Chem. Int. Ed.* **2018**, *57*, 12420–12424.

(9) Blackmore, L.; Moriarty, R.; Dolan, C.; Adamson, K.; Forster, R. J.; Devocelle, M.; Keyes, T. E. Peptide Directed Transmembrane Transport and Nuclear Localization of Ru(II) Polypyridyl Complexes in Mammalian Cells. *Chem. Commun.* **2013**, *49*, 2658–2660.

(10) Murphy, C. J.; Barton, J. K. Ruthenium Complexes as Luminescent Reporters of DNA. *Methods Enzymol.* **1993**, *226*, 576–594.

(11) Poynton, F. E.; Hall, J. P.; Keane, P. M.; Schwarz, C.; Sazanovich, I. V.; Towrie, M.; Gunnlaugsson, T.; Cardin, C. J.; Cardin, D. J.; Quinn, S. J.; et al. Direct Observation by Time-Resolved Infrared Spectroscopy of the Bright and the Dark

Excited States of the $[Ru(Phen)^2(Dppz)]^{2+}$ Light-Switch Compound in Solution and When Bound to DNA. *Chem. Sci.* **2016**, *7*, 3075–3084.

(12) Purugganan, M. D.; Kumar, C. V; Turro, N. J.; Jacqueline, K. Accelerated Electron Transfer between Metal Complexes Mediated by DNA. *Science* **1988**, *24*, 1645–1649.

(13) Arkin, M. R.; Stemp, E. D. A.; Pulver, S. C.; Barton, J. K. Long-Range Oxidation of Guanine by Ru(III) in Duplex DNA. *Chem. Biol.* **1997**, *4*, 389–400.

(14) Stemp, E. D. A.; Barton, J. K. The Flash-Quench Technique in Protein-DNA Electron Transfer: Reduction of the Guanine Radical by Ferrocytochrome C. *Inorg. Chem.* **2000**, *39*, 3868–3874.

(15) Kelly, J. M.; McConnell, D. J.; OhUigin, C.; Tossi, A. B.; Mesmaeker, A. K. De; Masschelein, A.; Nasielski, J. Ruthenium Polypyridyl Complexes; Their Interaction with DNA and Their Role as Sensitisers for Its Photocleavage. *J. Chem. Soc. Chem. Commun.* **1987**, *24*, 1821–1823.

(16) Crean, C. W.; Kavanagh, Y. T.; O'Keeffe, C. M.; Lawler, M. P.; Stevenson, C.; Davies, R. J. H.; Boyle, P. H.; Kelly, J. M. Targeting of Photooxidative Damage on Single-Stranded DNA Representing the Bcr-Abl Chimeric Gene Using Oligonucleotide-Conjugates Containing $[Ru(Phen)_3]^{2+}$-like Photosensitiser Groups. *Photochem. Photobiol. Sci.* **2002**, *1* (12), 1024–1033.

(17) Keane, P. M.; Poynton, F. E.; Hall, J. P.; Clark, I. P.; Sazanovich, I. V.; Towrie, M.; Gunnlaugsson, T.; Quinn, S. J.; Cardin, C. J.; Kelly, J. M. Monitoring Guanine Photo-Oxidation by Enantiomerically Resolved Ru(II) Dipyridophenazine Complexes Using Inosine-Substituted Oligonucleotides. *Faraday Discuss.* **2015**, *185*, 455–469.

(18) Bhattacharya, P. K.; Barton, J. K. Influence of Intervening Mismatches on Long-Range Guanine Oxidation in DNA Duplexes. *J. Am. Chem. Soc.* **2001**, *123* (36), 8649–8656.

(19) Jekins, Y.; Barton, J. K. A Sequence-Specific Molecular Light Switch : Tethering of an Oligonucleotide to a Dyridophenazine Complex of Ruthenium (II). *J. Am. Chem. Soc.* **1992**, *114* (22), 8736–8738.

(20) Grimm, G. N.; Boutorine, A. S.; Lincoln, P.; Norde, B.; Helene, C. Formation of DNA Triple Helices by an Oligonucleotide Conjugated to a Fluorescent Ruthenium Complex. *ChemBioChem* **2002**, *3*, 324–331.

(21) Banert, K.; Brase, S. Organic Azides. *Wiley* **2010**, pp. 80.

(22) Wei, H.; Yin, J.; Wang, E. Bis(2,2′-Bipyridine)(5,6-Epoxy-5,6-Dihydro-[1,10] Phenanthroline)Ruthenium: Synthesis and Electrochemical and Electrochemiluminescence Characterization. *Anal. Chem.* **2008**, *80*, 5635–5639.

(23) Ohata, J.; Vohidov, F.; Aliyan, A.; Huang, K.; Martí, A. A.; Ball, Z. T. Luminogenic Iridium Azide Complexes. *Chem. Commun.* **2015**, *51*, 15192–15195.

(24) Meng, T. T.; Wang, H.; Zheng, Z. B.; Wang, K. Z. PH-Switchable "Off-On-Off" Near-Infrared Luminescence Based on a Dinuclear Ruthenium(II) Complex. *Inorg. Chem.* **2017**, *56* (9), 4775–4779.

(25) Gao, F.; Chao, H.; Zhou, F.; Peng, B.; Ji, L. N. PH Responsive 'off-on-off' Luminescent Switch of a Novel Ruthenium(II) Complex $[Ru(Bpy)_2(PipipH_2)]^{2+}$. *Inorg. Chem. Commun.* **2007**, *10*, 170–173.

(26) Giordano, P. J.; Bock, O.; Wrighton, M. S. Excited State Proton Transfer of Ruthenium(II) Complexes of 4,7-Dihydroxy- 1,10-Phenanthroline. Increased Acidity in the Excited State. *J. Am. Chem. Soc.* **1978**, *100* (22), 6960–6965.

(27) Han, M. J.; Chen, Y. M.; Wang, K. Z. Ruthenium(II) Complexes of 6-Hydroxydipyrido[3,2-a:2′,3′-c] Phenazine: Self-Association, and Concentration-Dependent Acid-Base and DNA-Binding Properties. *New J. Chem.* **2008**, *32*, 970–980.

(28) Seela, F.; Pujari, S. S. Azide - Alkyne 'Click' Conjugation of 8-Aza-7-Deazaadenine-DNA: Synthesis, Duplex Stability, and Fluorogenic Dye Labeling. *Bioconjug. Chem.* **2010**, *21*, 1629–1641.

(29) Seela, F.; Sirivolu, V. R.; Chittepu, P. Modification of DNA with Octadiynyl Side Chains: Synthesis, Base Pairing, and Formation of Fluorescent Coumarin Dye Conjugates of Four Nucleobases by the Alkyne-Azide 'Click' Reaction. *Bioconjug. Chem.* **2008**, *19*, 211–224.

CHAPTER 5

Future work

5.0 Future work

This chapter is organised into four sections relative to general cell validation experiments and additional investigations which could be conducted specifically for each family of TFO-hybrid developed.

5.1 Cell validation Experiments

TFO hybrids with the highest triplex stabilisations will be further investigated for their on-targeting cleavage capabilities within diseased cells. *In vitro* studies have been designed based on the genetic sequence of green fluorescent protein (GFP). Cells expressing GFP could be transfected with lead metal complex hybrids to identify gene knockout. Metabolic degradation could be inhibited by introducing modified DNA backbones in the form of locked nucleic acids (LNA), peptide nucleic acids (PNA), morpholine oligomers, while also enhancing cellular delivery by negating the negative backbone charge. Cellular and nuclear accumulation can be directed by incorporating cellular targeting vectors such as nuclear localisation factors and cell-penetrating peptides.

5.2 Mono-nuclear AMN-hybrids:

Triplex formation studies on *mono*-nuclear chelating intercalating nucleic acids (CINAs) identified 18 nt (TFO2 and TFO5) as the minimum length necessary for biological studies. A triplex formation studies of phenanthrene hybrids of TFO1- and TFO4- showed noticeable stabilisation compared to the control TFOs, but still the temperatures of triplex denaturation were lower than 37 °C (Appendix H). For this reason, they were investigated as hybridisation probes for potential use as antisense oligonucleotides (ASOs). Preliminary data of the change in melting temperature of the hybrid probes is presented in **Figure 5.1**.

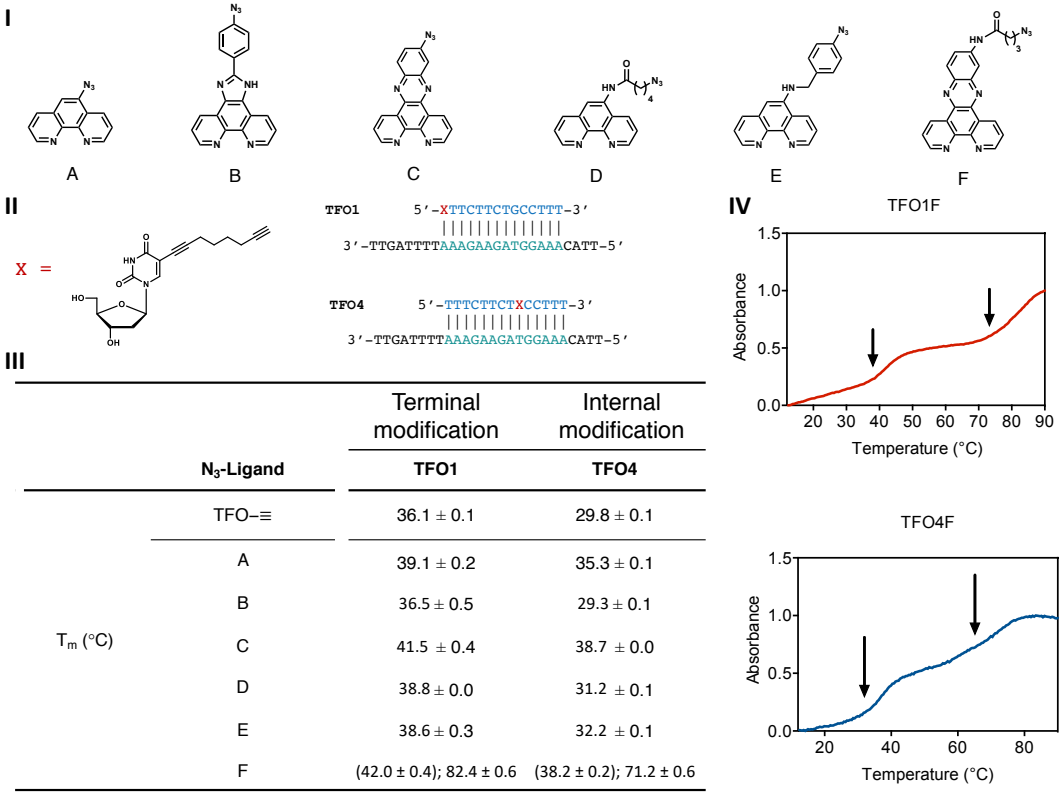

		Terminal modification	Internal modification
	N_3-Ligand	TFO1	TFO4
T_m (°C)	TFO–≡	36.1 ± 0.1	29.8 ± 0.1
	A	39.1 ± 0.2	35.3 ± 0.1
	B	36.5 ± 0.5	29.3 ± 0.1
	C	41.5 ± 0.4	38.7 ± 0.0
	D	38.8 ± 0.0	31.2 ± 0.1
	E	38.6 ± 0.3	32.2 ± 0.1
	F	(42.0 ± 0.4); 82.4 ± 0.6	(38.2 ± 0.2); 71.2 ± 0.6

Figure 5.1 I Library of azide-functionalised phenanthroline and phenazine derivatives: **A-F**. **II** Structures of alkyne-modified TFO1 and TFO4 and single-strand target. **III** Thermal stability of hybrid duplexes TFO1(A-F) and TFO4(A-F) compared to unclicked hybridisation probes. Samples were prepared at the concentration of 4 μM in PBS. **IV** Double-sigmoidal profile of TFO1F and TFO4F.

Hybrid probes containing internally modified phenanthrene ligands are, overall, less stable than corresponding 5′-modified sequences, but the most significant stabilising effects were observed in TFO4. It is also possible to recognise a general trend: **C** > **F** > **A** > **E** ≥ **D** > **B** and it is noteworthy that ligands **C** and **F** are the most stabilising and **B** is the least effective. **C** and **F** provided stabilising effects of *ca*. + 5.5 °C with TFO1 and *ca* + 8.6 °C with TFO4. TFO1F and TFO4F present double-sigmoid melting profiles, which is indicative a 2-step event and this is potentially worthy of future study (**Figure 5.1 IV**). It would also be of interest to study the chemical nuclease activity of these hybrids and this could be achieved by the addition of Na-L-ascorbate at 3 and 6 hours of incubation at 37 °C. It is probable that a shorter incubation period will be required because of the vicinity of the nuclease moiety to the cleaving site and faster rate of the duplex formation as compared with triplex formation.

5.3 Di-nuclear AMN-hybrids:

Based on the photophysical properties of the *di*-nuclear system *N*,*N*'-(1,3-phenylenebis(methylene))bis(1,10-phenanthrolin-5-amine) (**G_R**), preliminary fluorescent analysis was conducted at a concentration of 1 μM in both ACN and H_2O. The emission scan of **G_R** at the excitation of 280 nm showed 3 peaks: 351, 485 and 610 nm (Appendix L, **Figure L1**). **G_R** was also analysed over the range time of two hours revealing a decreased fluorescent intensity for the signal at 485 nm.

Table 5.1 λ_{max}, ε and λ_{em} of **G_R** and $[Cu(\mathbf{G_R})(N,N\text{-phenanthrene})_2]^{2+}$ in ACN

	λ_{ex}	ε	λ_{em}
G_R	280	37440	321 485 610*
$[Cu_2(\mathbf{G_R})]^{4+}$	280	21440	321 610*
$[Cu_2(\mathbf{G_R})(Phen)_2]^{4+}$	280	55720	321 610*
$[Cu_2(\mathbf{G_R})(DPQ)_2]^{4+}$	280	61800	321 610*
$[Cu_2(\mathbf{G_R})(DPPZ)_2]^{4+}$	280	147280	321 610*

*2nd harmonic light

The fluorescent properties of *di*-copper complexes were also investigated and emission signals were detected at excitation 280 nm. Interestingly, the photophysical characterisation in H_2O did not lead to the detection of any emissive signal (Appendix L, **Figure L2**).

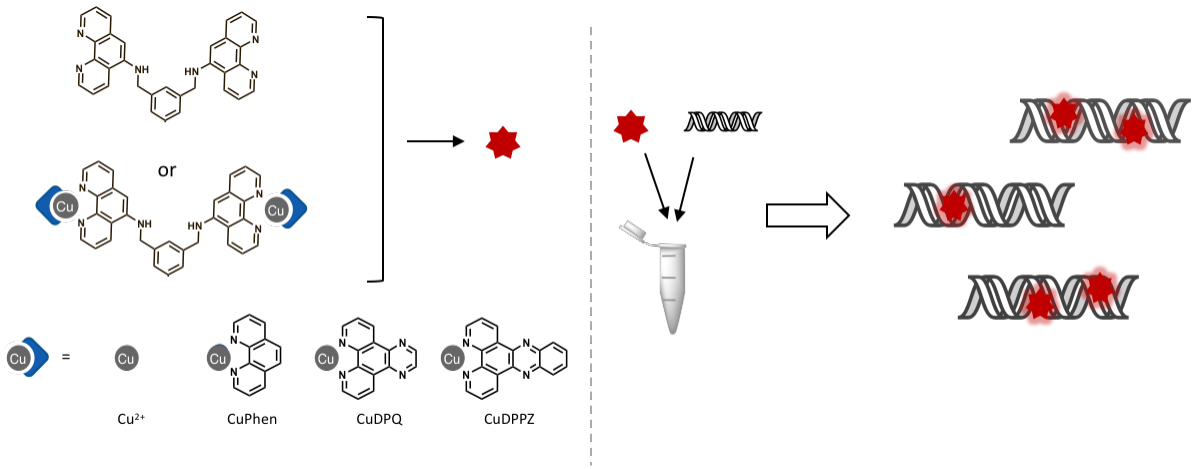

Figure 5.2 Schematic representation of the experiment to investigate the "light switch" properties of G and its complexes.

A future avenue of research would be to investigate the photophysical properties of *di*-nuclear hybrids TFO3G, TFO6G and TFO7G generated in Chapter 3, and in the presence of Cu(II) and the ancillary ligands. In addition, it would be interesting to adapt the study from chapter 4 to examine the emission properties of the *di*-nuclear hybrids and $\mathbf{G_R}$ in the presence of DNA at different duplex:TFO ratios with / without Cu(II) bound ancillary ligands.

5.4 Ruthenium hybrids:

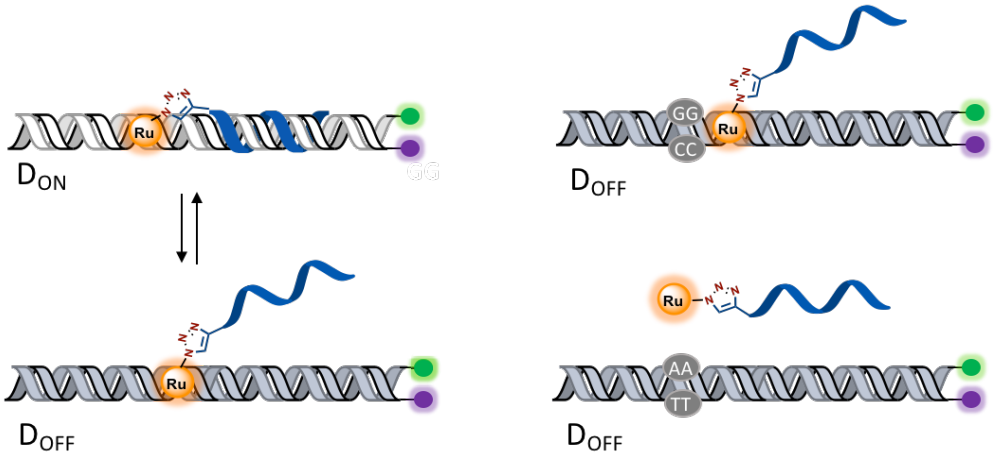

Figure 5.3 Left: hypothesis for the same trend of luminescence activity observed performing D_{ON} and D_{OFF} titration. Right: Possible strategy for further elucidating the fluorescent properties of Ru-TFOs.

Ruthenium-based probes were generated using click chemistry and the most luminescent hybrids were selected for binding study in the presence of D_{ON} or D_{OFF} targets (**Figure 4.8**). Since the results of these titrations were similar, it would be worth developing modified hybrids that can discriminate, in terms of luminescence properties, on and off targets. Furthermore, to determine whether the ruthenium complex or TFO binding is the predominant interaction for triplex stabilisation, a luminescence study could be investigated in conjugation with rationally designed duplex fluorescent probes in DNA melting experiments (**Figure 5.3**). The same experiment could also be conducted using off-targets with carefully selected bases near the intercalation site to investigate sequence binding preferences. Another interesting study would be to investigate the DNA cleavage properties of ruthenium TFO hybrids by photo-oxidation.

CONCLUSION

The major objective of this work was aimed to the design and development of a novel class of hybridised biomaterials with sequence-specific targeting abilities and enhanced nuclease activity for application as potential antigene agents. A family of azide-functionalised phenanthrene derivatives was generated and conjugated to triplex formation oligonucleotides (TFOs) through copper-catalysed azide-alkyne cycloaddition 'click chemistry'. To this end, a new class of chelating intercalating nucleic acid (CINA) was discovered. Triplex formation was analysed by UV-vis spectroscopy revealing exceptional stabilising properties of TFOs modified with specific intercalating phenanthrene ligands. More specifically, hybrids functionalised to ligands with extended aromaticity were characterised by very high triplex stability. Upon coordination to copper(II), targeted cleavage was triggered in the presence of ascorbate and observed using polyacrylamide gel electrophoresis. The ability of these hybrids to discriminate target and non-target sequences and their site-selectivity was identified with fluorophore-labelled DNA.

Targeted chemical nuclease activity was, as expected, shown to depend on the phenanthrene ligand-modification. It was possible to identify a trend in nuclease affinity by densiometric analysis, which revealed that ligands **B** and **C**, both of which contain extended aromatic structures, were the most active. In order to develop hybrids with higher sequence selectivity and cleavage affinity, a second generation of hybrids bearing *di*-nuclear phenanthroline functionality were developed using both CuAAC and strain-promoted azide-alkyne cycloaddition (SPAAC) methods. In contrast to the mononuclear TFO hybrids, the *di*-nuclear systems provided lower triplex stabilisation due to the bulkiness of the *di*-nuclear ligand, however, they displayed remarkable nuclease activity and enhanced sequence discrimination when bound to Cu-Phen and Cu-DPQ complexes. In particular, a BCN-modified hybrid provided complete depletion of its target while leaving an off-target completely intact. Considering the versatility of click chemistry and the ease at which copper(II) complex-modified TFOs could be generated, the application of this technology was extended to generate ruthenium(II)-based luminescent probes. Ruthenium(II) complexes bearing azide-phenanthrene ligands were prepared and conjugated to TFO sequences and a preliminary investigation was conducted to identify their potential diagnostic applications. More work will be needed to identify if target duplex sequences can be discriminated from non-target sites but if this could be achieved, a new area of ruthenium(II) probe development could be envisioned.

APPENDICES

List of Content

APPENDIX A. NMR spectra, mass analysis and FTIR-ATR spectra of azide-functionalised ligands and intermediates.

APPENDIX B. Spectral characterisation of $[Cu(A)(NO_3)_2]$.

APPENDIX C. NMR spectra, ESI-MS and FTIR-ATR analysis of ligands **G** and $\mathbf{G_R}$ and intermediates.

APPENDIX D. FTIR-ATR of $[Cu_2(\mathbf{G_R})(N,N\text{-phenanthrene})_2](NO_3)_4$.

APPENDIX E. NMR spectra, ESI-MS and FTIR-ATR of azide-functionalised Ru(II) complexes and intermediates.

APPENDIX F. X-Ray Crystallography.

APPENDIX G. MALDI analysis of TFO hybrids

APPENDIX H. Thermal melting analysis and electrophoretic gels.

APPENDIX I. Emission spectra of azide-modified Ru(II) complexes.

APPENDIX L. Emission spectra of $\mathbf{G_R}$, $[Cu_2(\mathbf{G_R})(N,N\text{-phenanthrene})_2](NO_3)_4$ and *di*-nuclear TFO hybrids.

APPENDIX A

NMR spectra, mass analysis and FTIR-ATR spectra of azide-functionalised ligands and intermediates

Ligand A:

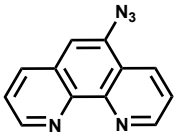

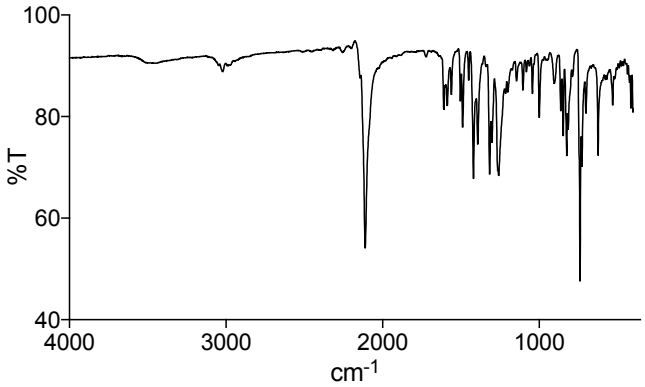

Figure A1. FTIR-ATR for ligand **A**.

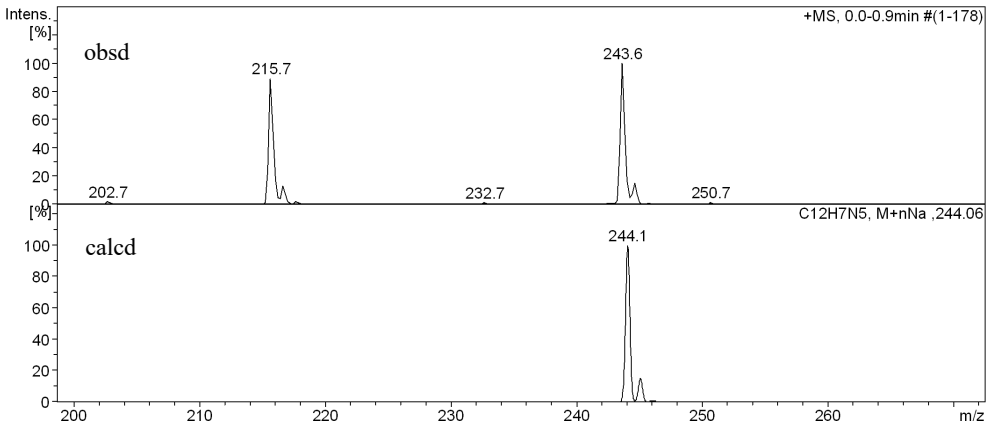

Figure A2. ESI-MS for ligand **A.**

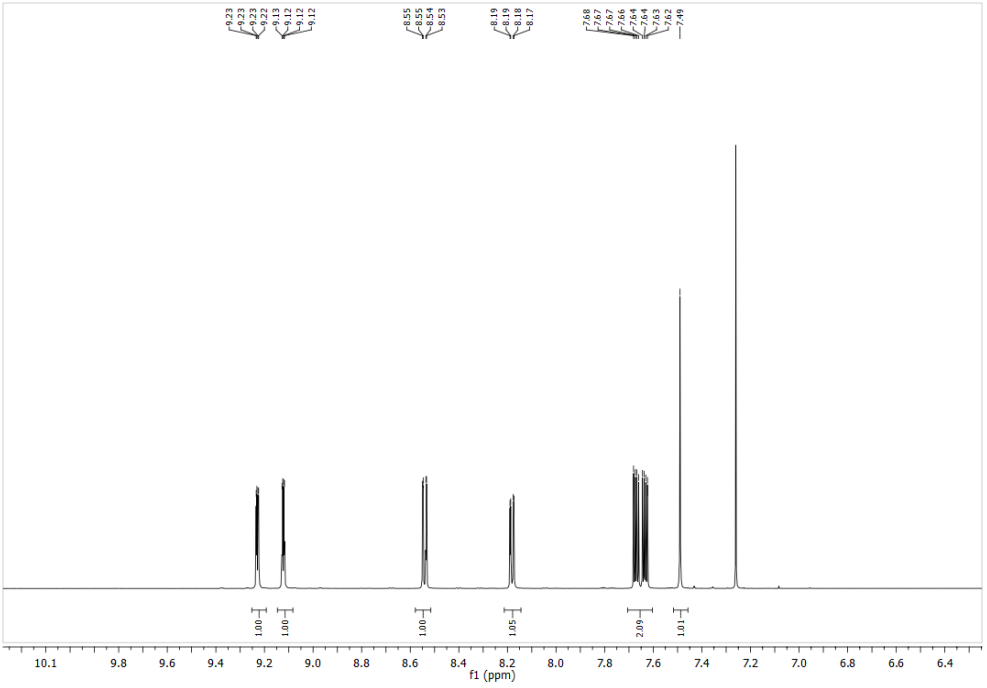

Figure A3. ^{1}H NMR spectrum (600 MHz) for ligand **A** in $CDCl_3$.

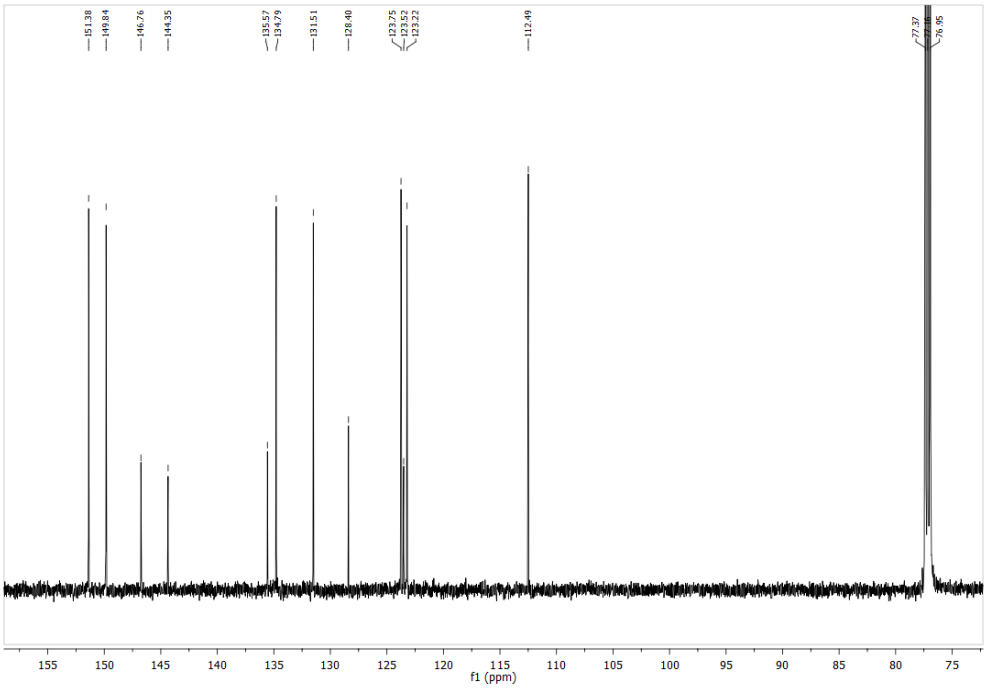

Figure A4. ^{13}C NMR (151 MHz) spectrum for ligand **A** in $CDCl_3$.

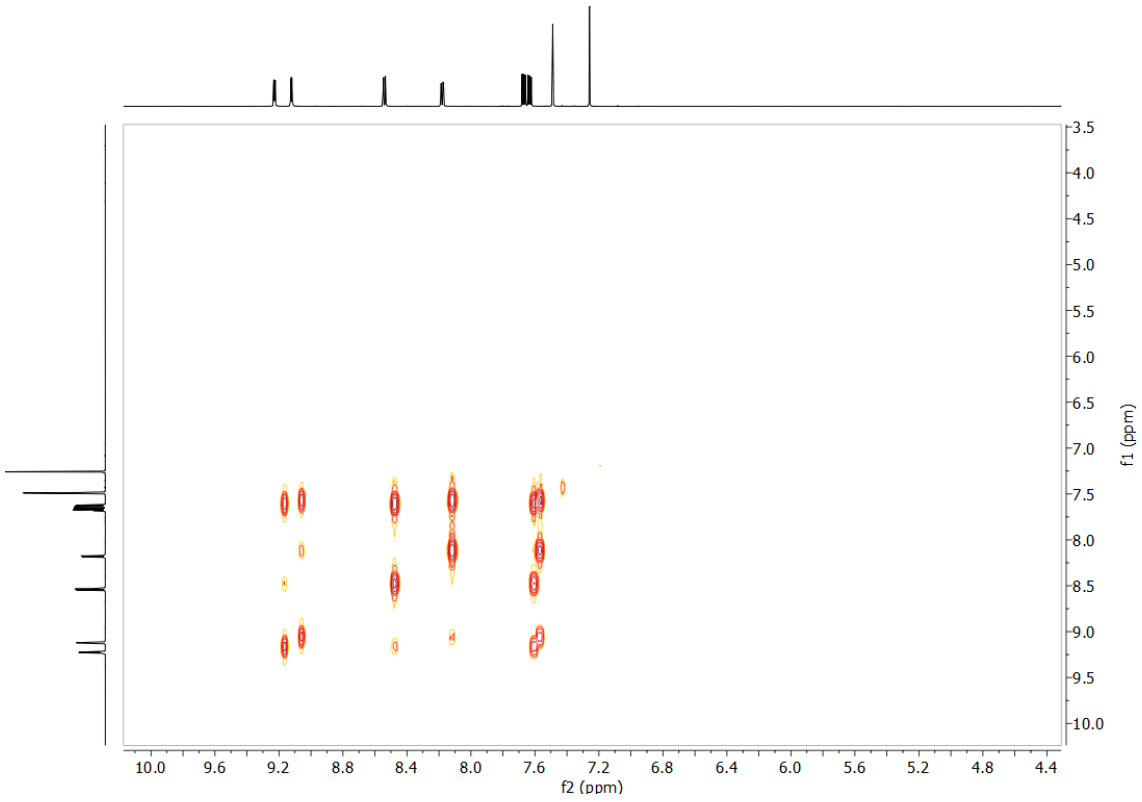

Figure A5. COSY spectrum for ligand **A** in $CDCl_3$.

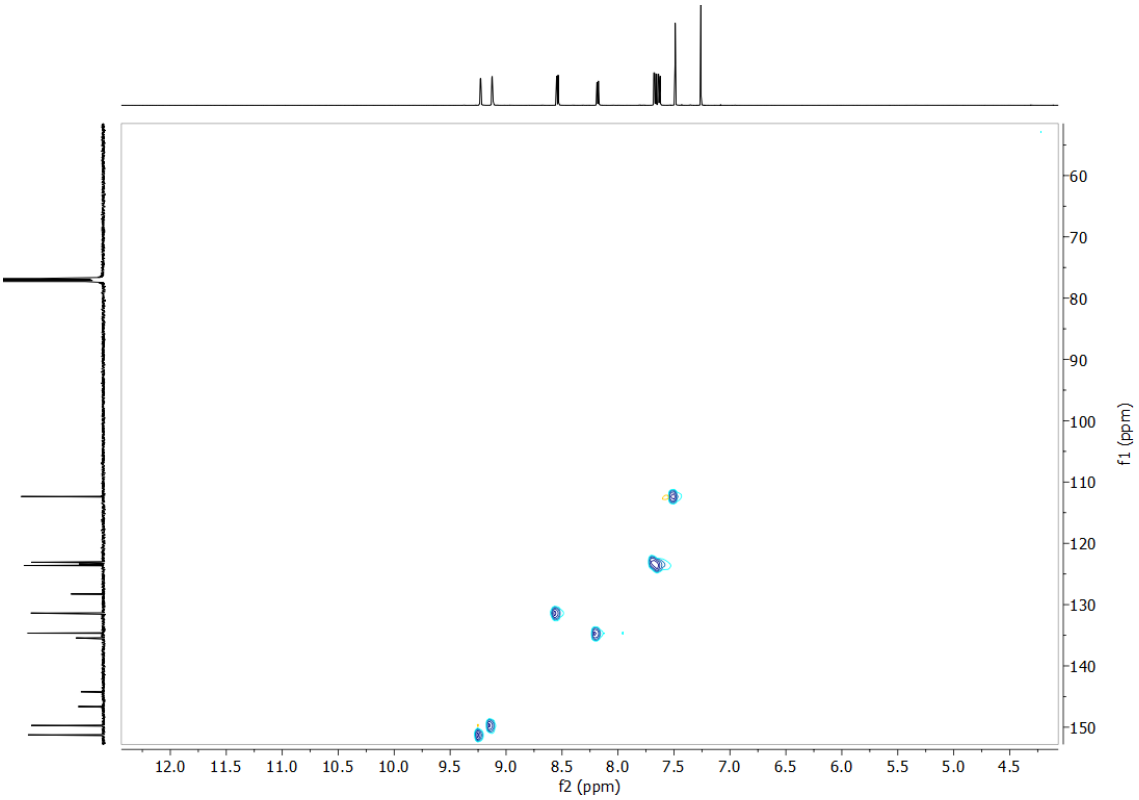

Figure A6. HSQC spectrum for ligand **A** in $CDCl_3$.

Compound 1:

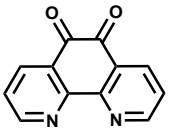

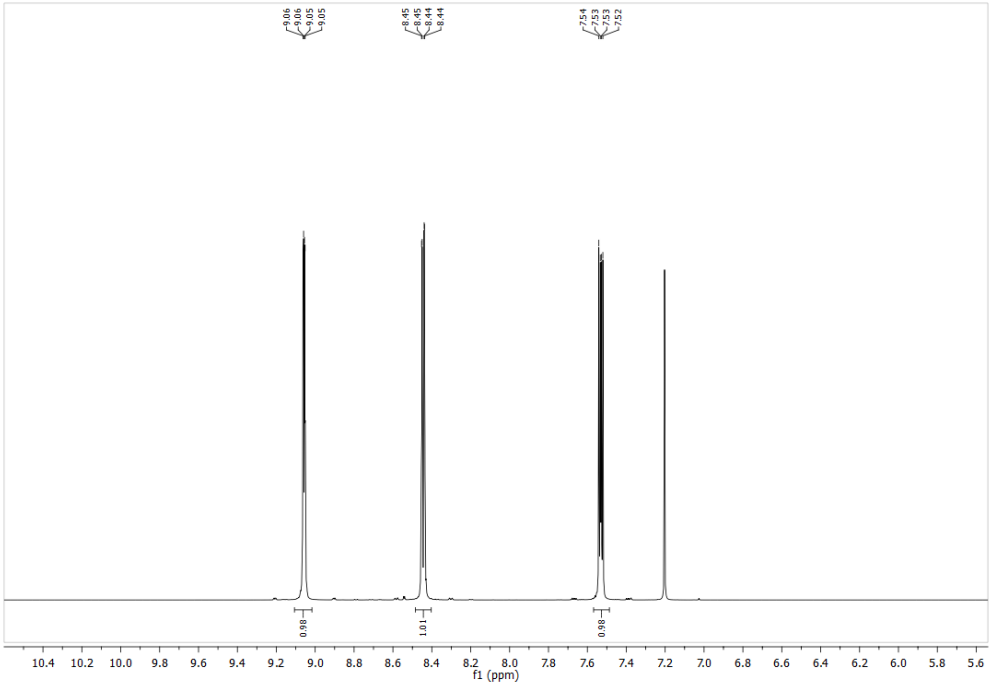

Figure A7. ^{1}H NMR spectrum (600 MHz) for compound **1** in $CDCl_3$.

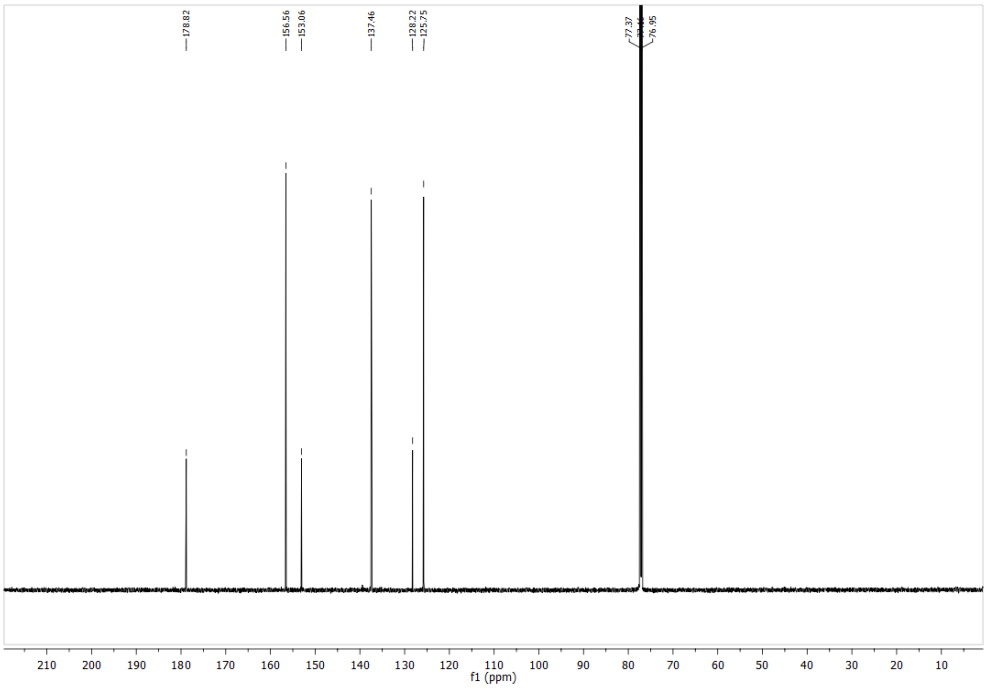

Figure A8. ^{13}C NMR spectrum (151 MHz) for compound **1** in $CDCl_3$.

Compound 2:

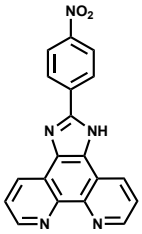

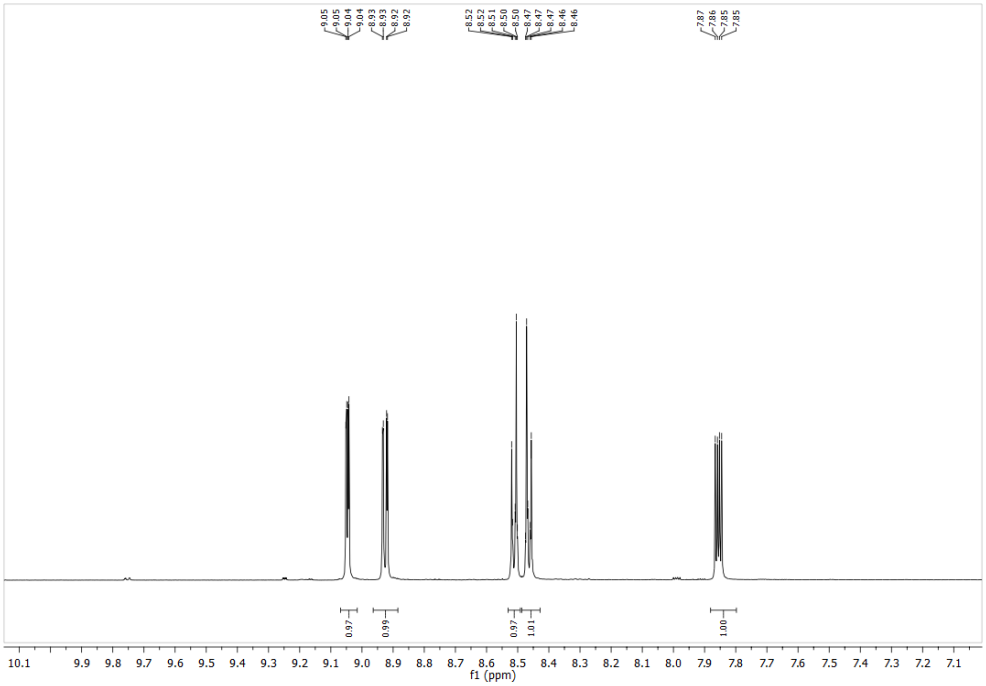

Figure A9. ^{1}H NMR spectrum (600 MHz) for compound **2** in $CDCl_3$.

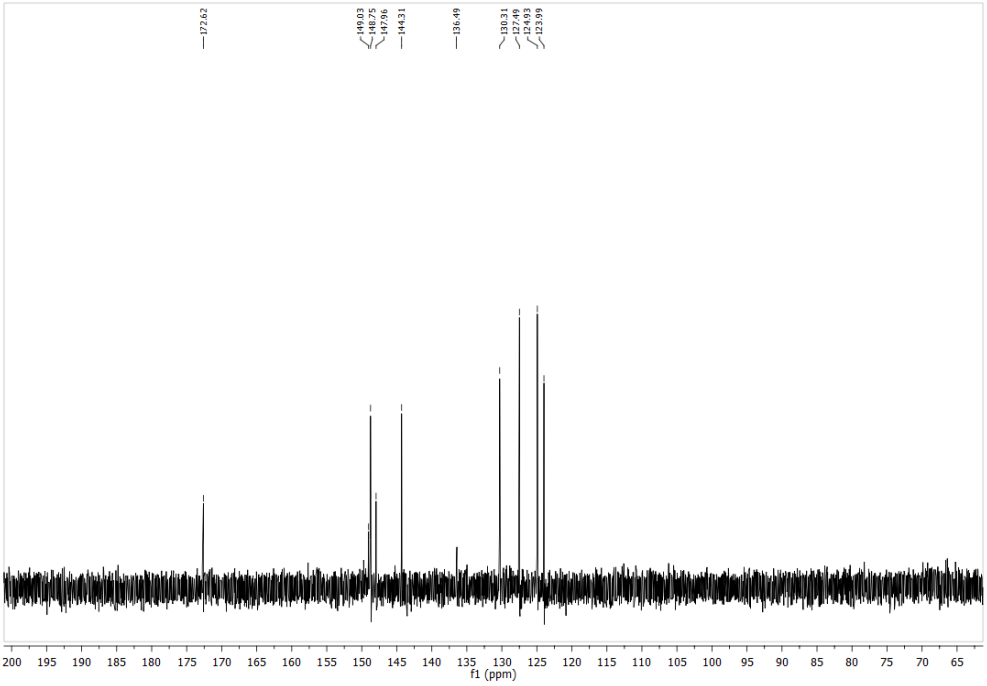

Figure A10. ^{13}C NMR spectrum (151 MHz) for compound **2** in $CDCl_3$.

Compound 3:

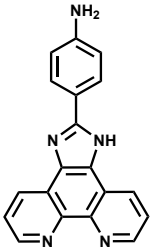

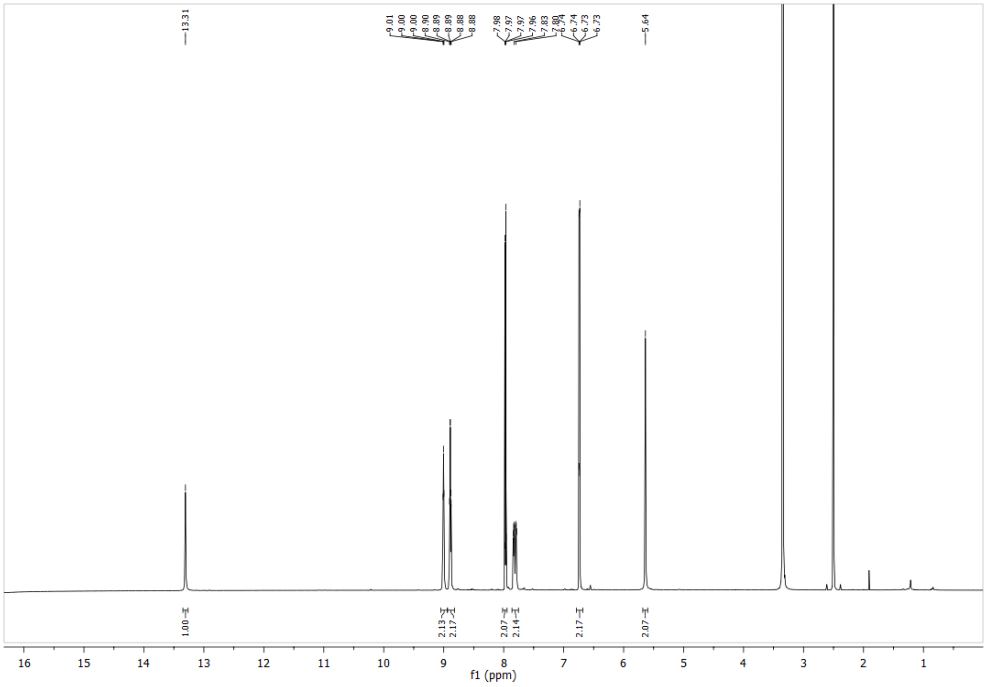

Figure A11. ^{1}H NMR spectrum (600 MHz) for compound **3** in DMSO-d_6.

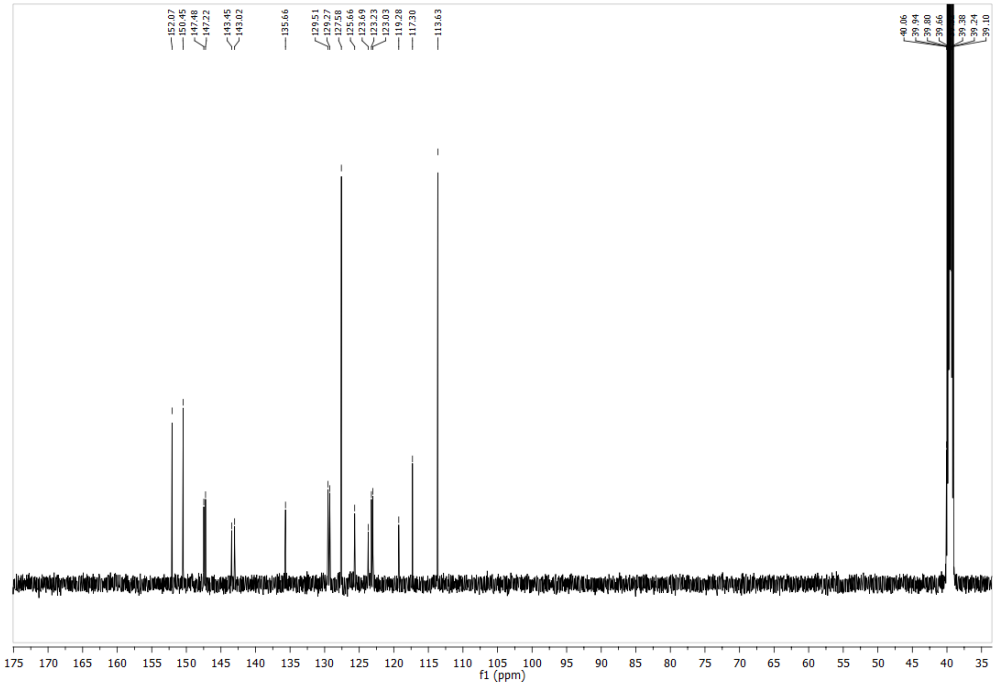

Figure A12. ^{13}C NMR spectrum (151 MHz) for compound **3** in DMSO-d_6.

Ligand B:

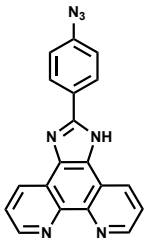

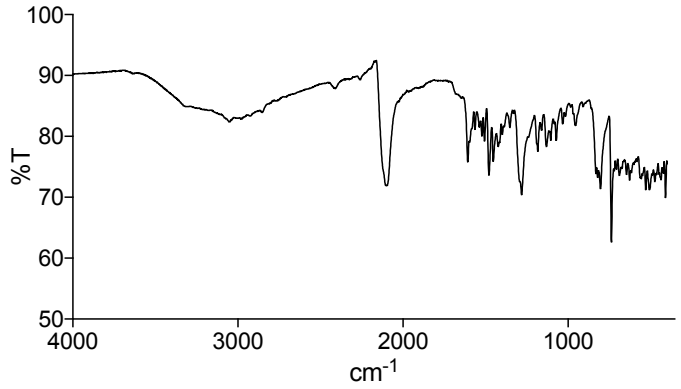

Figure A13. FTIR-ATR for ligand **B**.

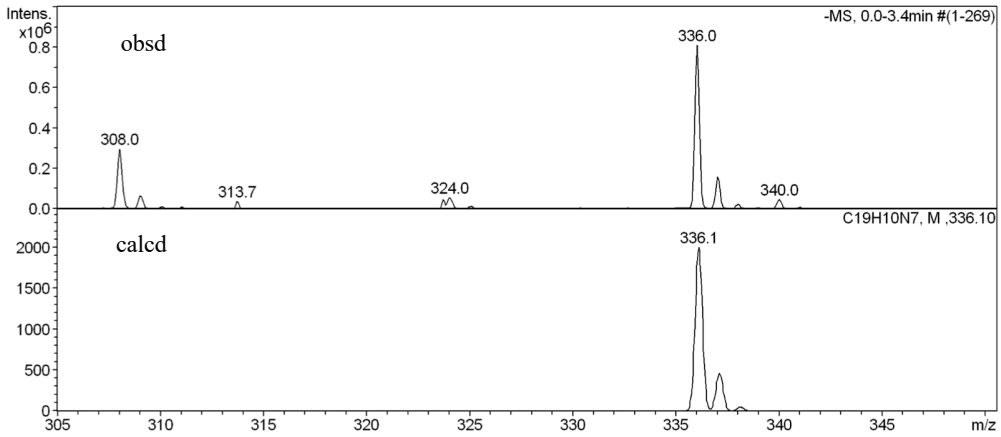

Figure A14. ESI-MS for ligand **B**.

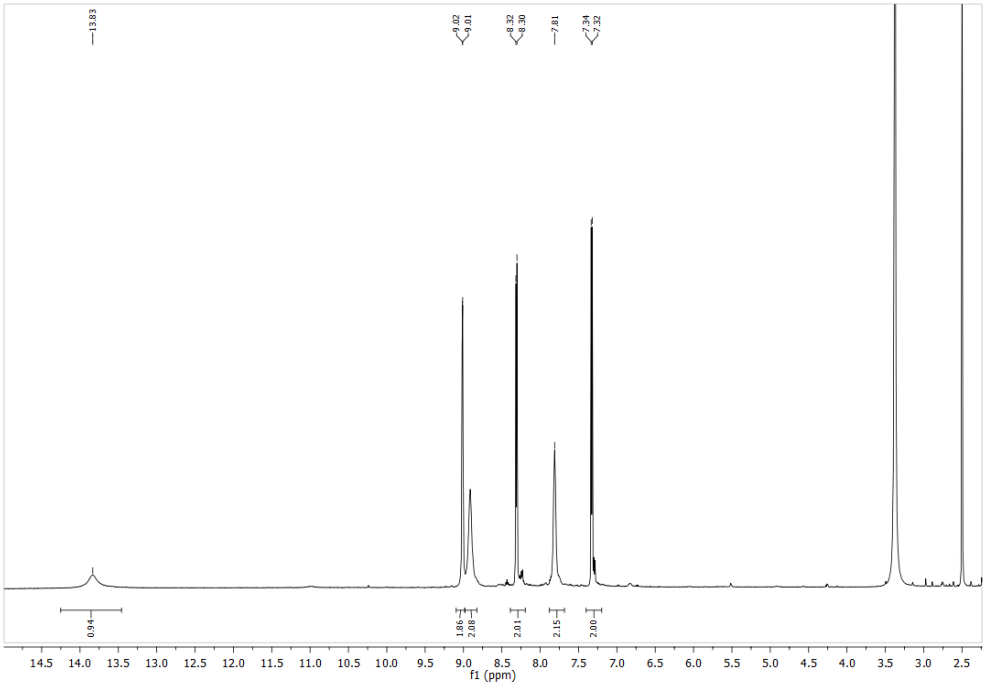

Figure A 15. ^{1}H NMR spectrum (600 MHz) for ligand **B** in DMSO-*d*$_6$.

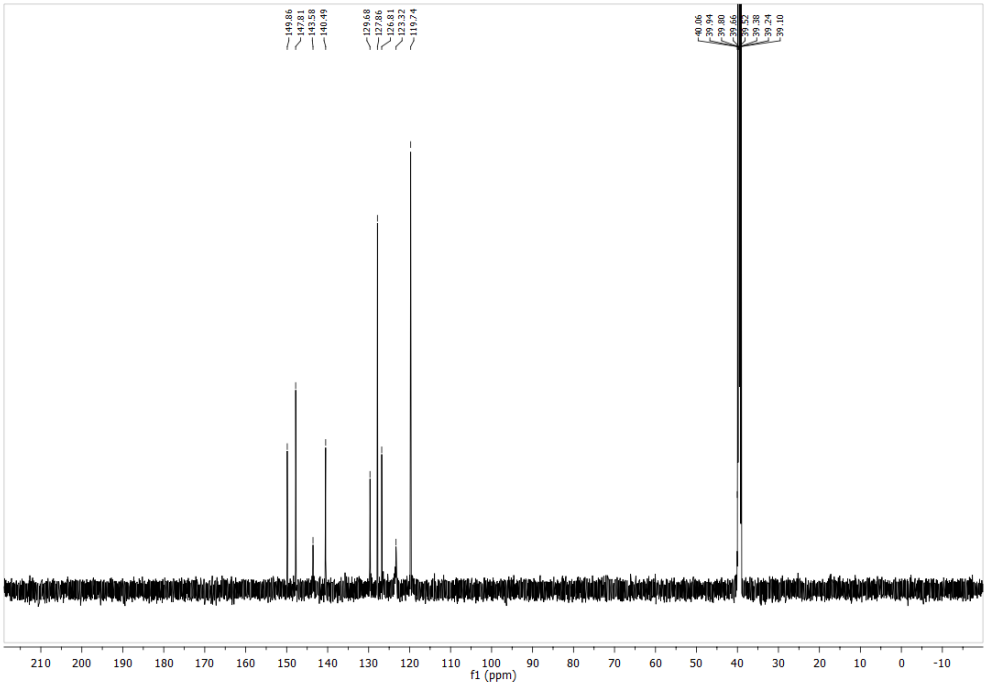

Figure A16. ^{13}C-NMR spectrum (151 MHz) for ligand **B** in DMSO-d_6.

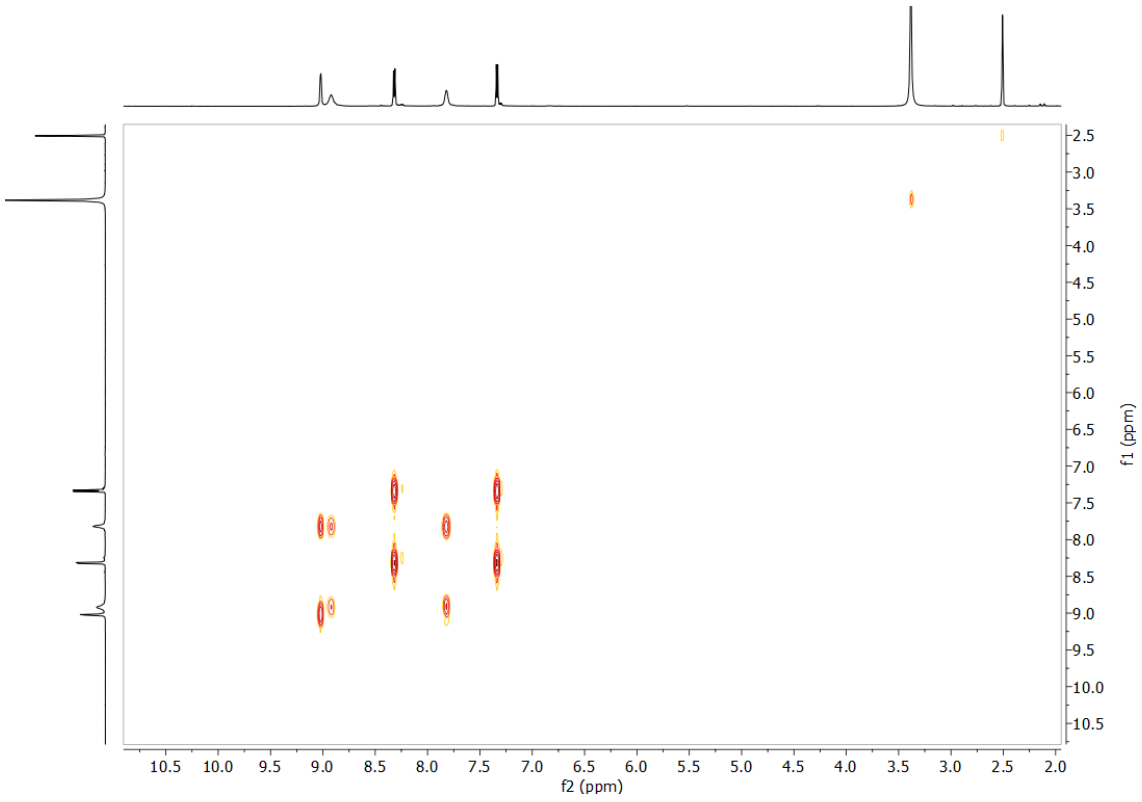

Figure A17. COSY spectrum (151 MHz) for ligand **B** in DMSO-d_6.

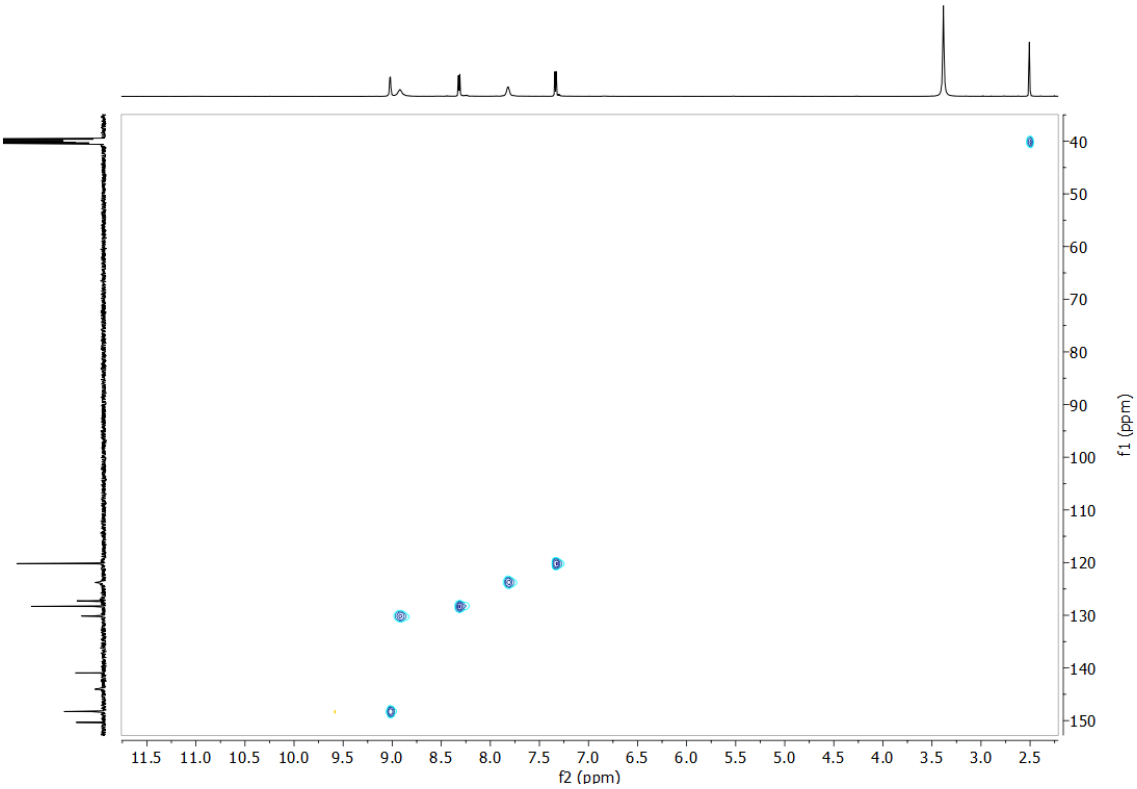

Figure A18. HSQC spectrum (151 MHz) for ligand **B** in DMSO-d_6.

Compound 4:

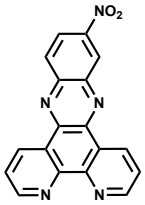

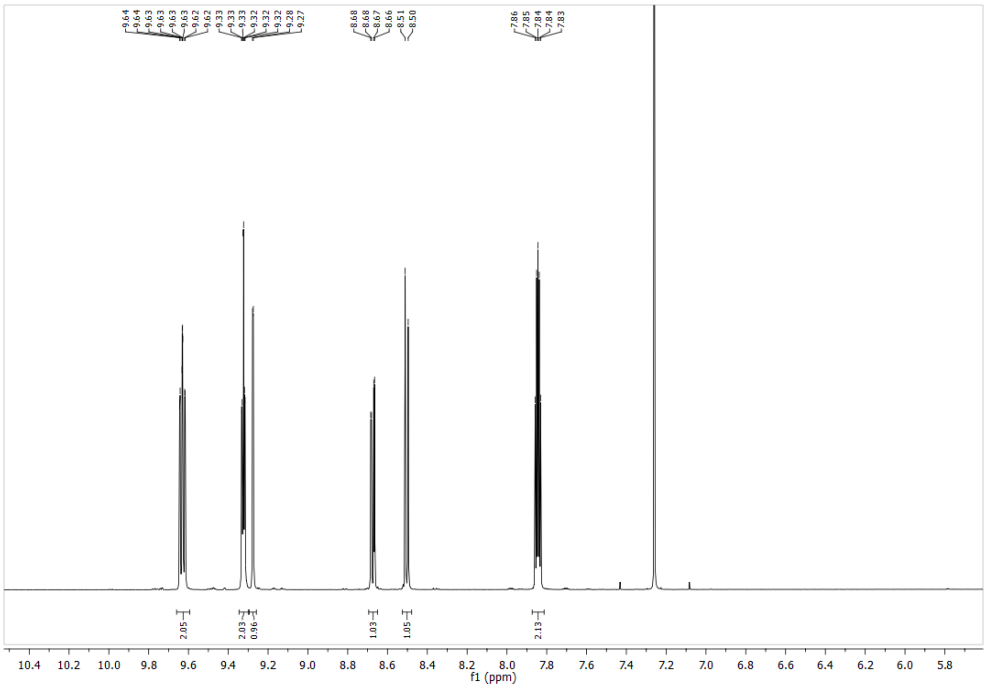

Figure A19. ^{1}H NMR (600 MHz) spectrum for compound **4** in $CDCl_3$.

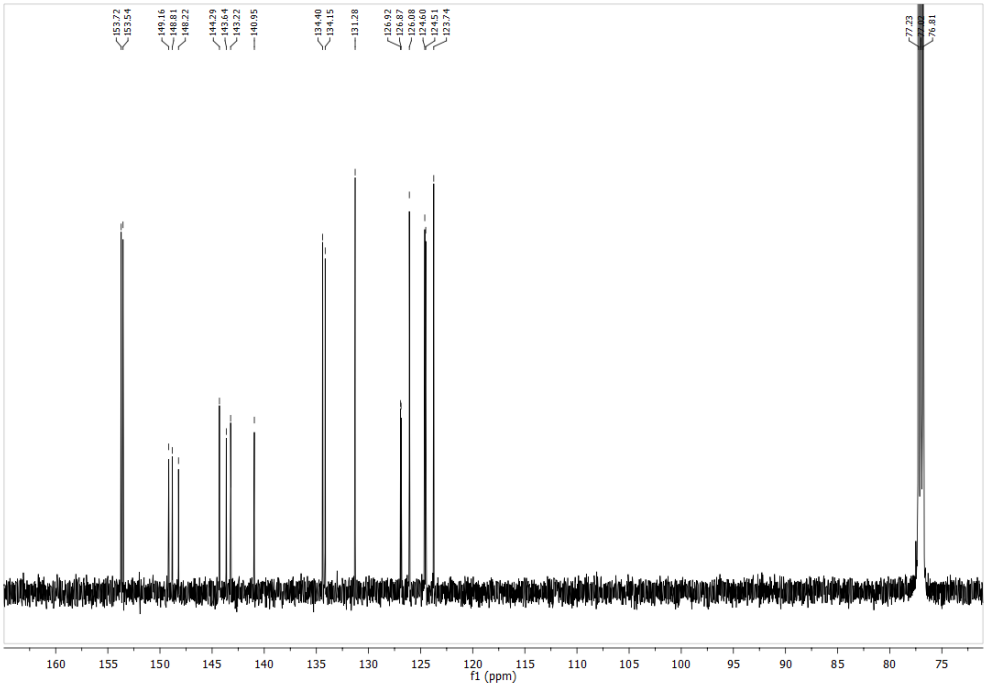

Figure A20. ^{13}C NMR spectrum (151 MHz) for compound **4** in $CDCl_3$.

Compound 5:

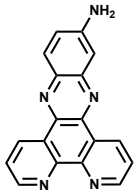

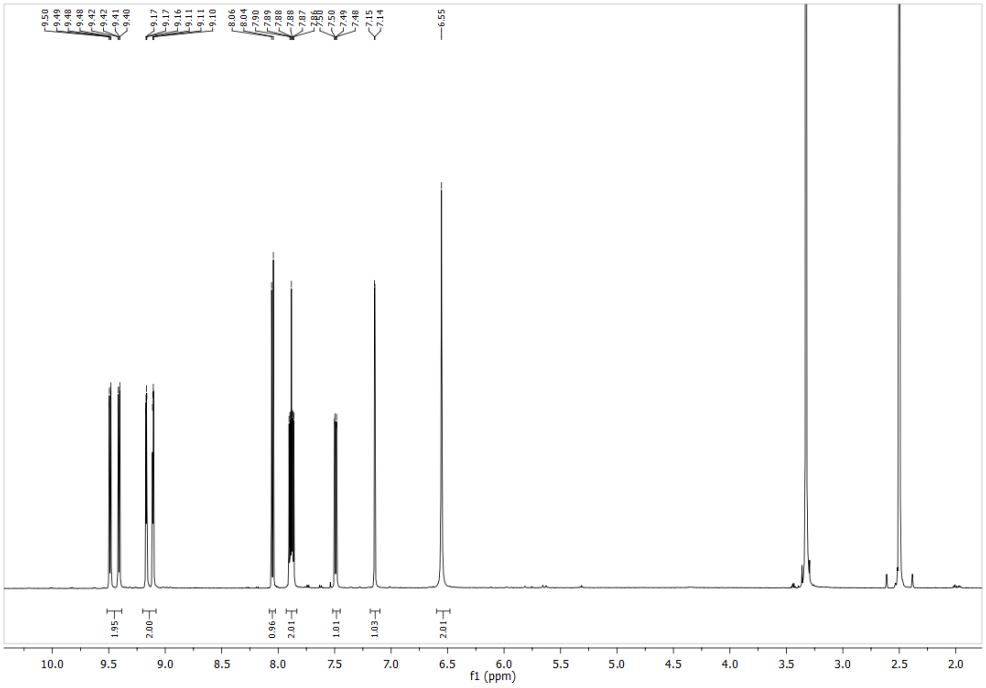

Figure A21. ^{1}H NMR spectrum (600 MHz) for compound **5** in DMSO-d_6.

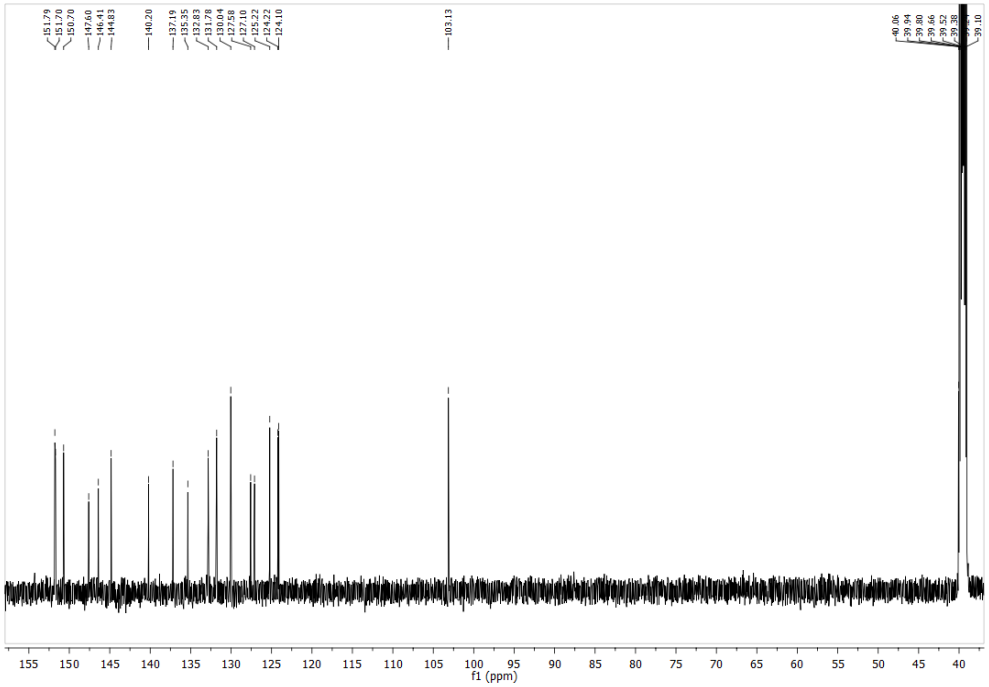

Figure A22. ^{13}C NMR spectrum (151 MHz) for compound **5** in DMSO-d_6.

Ligand C:

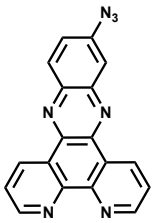

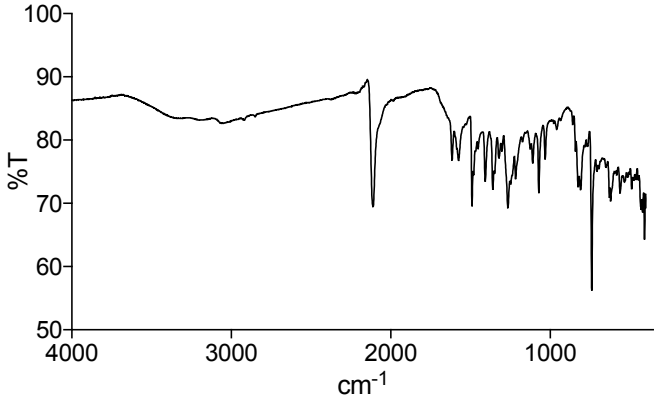

Figure A23. FTIR-ATR for ligand **C**.

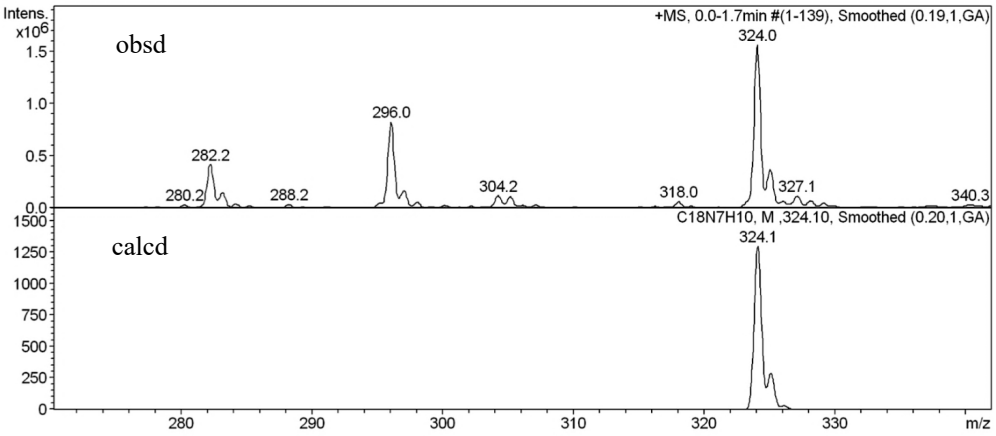

Figure A24. ESI-MS for ligand **C**.

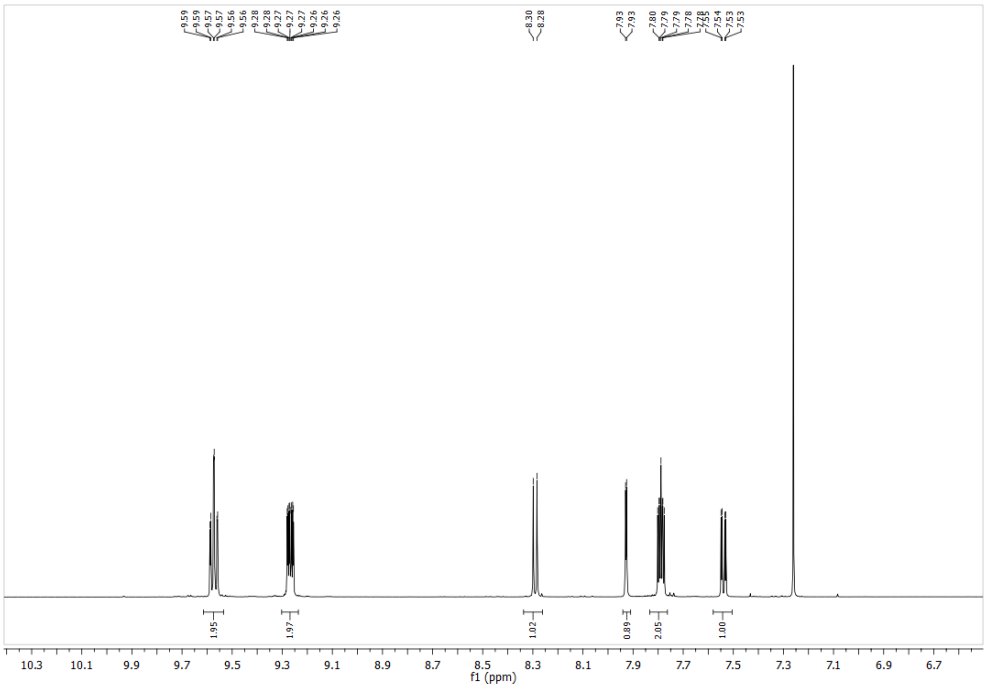

Figure A25. ^{1}H NMR spectrum (600 MHz) for ligand **C** in $CHCl_3$.

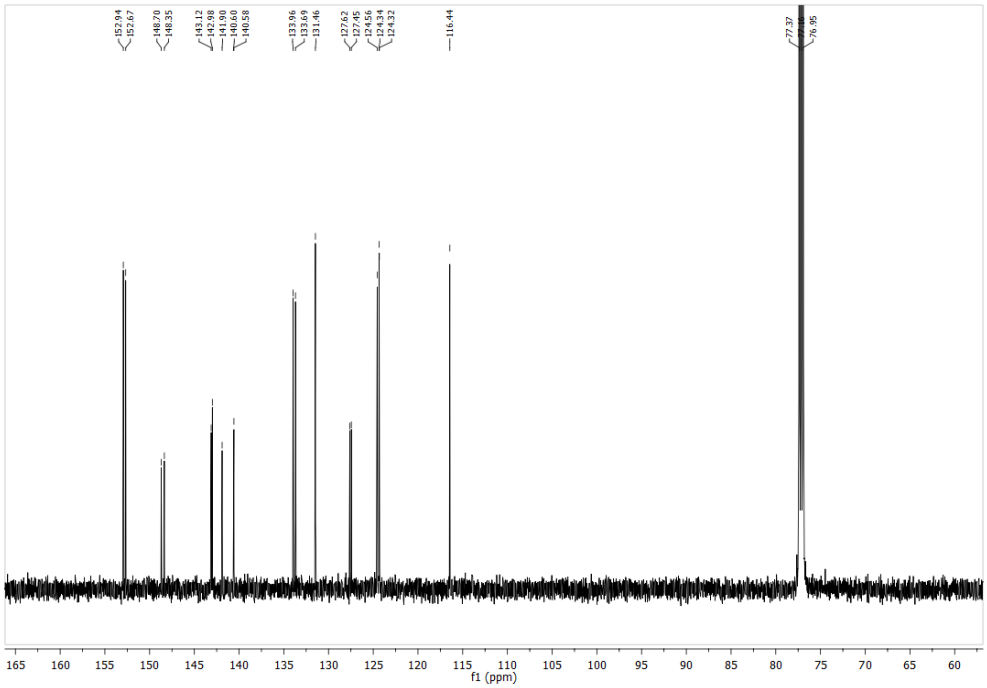

Figure A26. ^{13}C NMR spectrum (151 MHz) for ligand **C** in in $CHCl_3$.

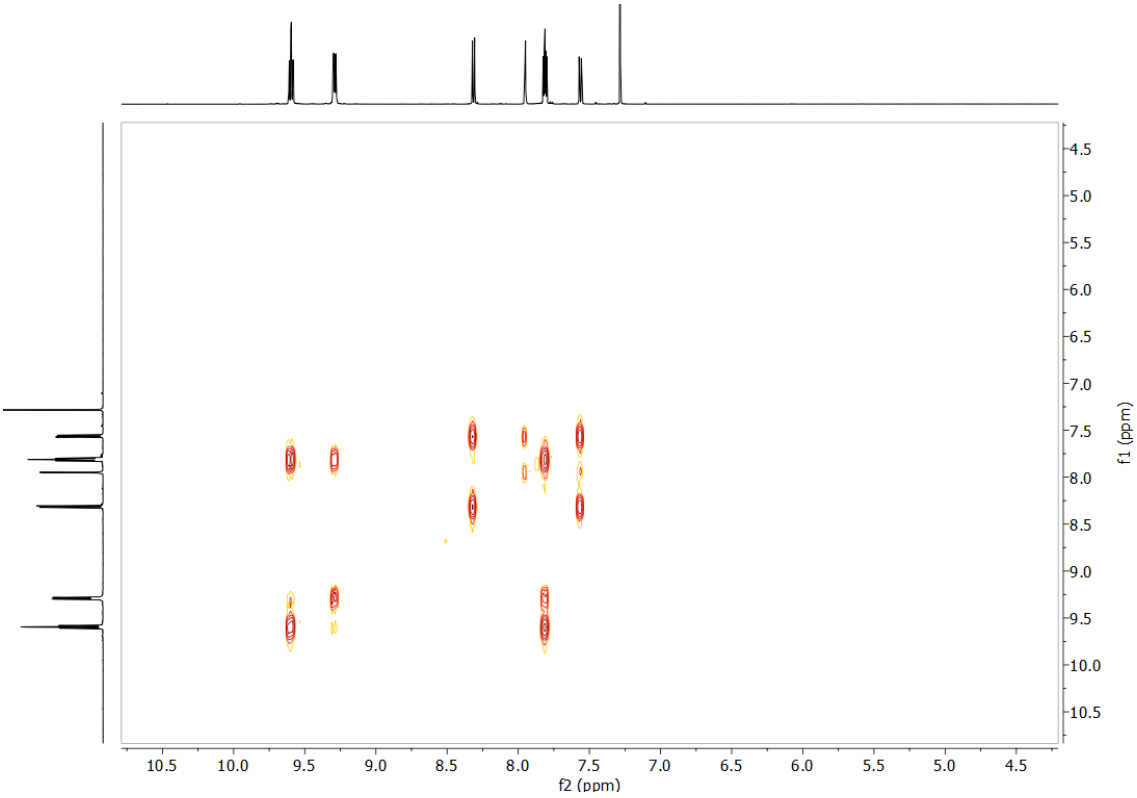

Figure A27. COSY NMR spectrum for ligand **C** in in $CHCl_3$.

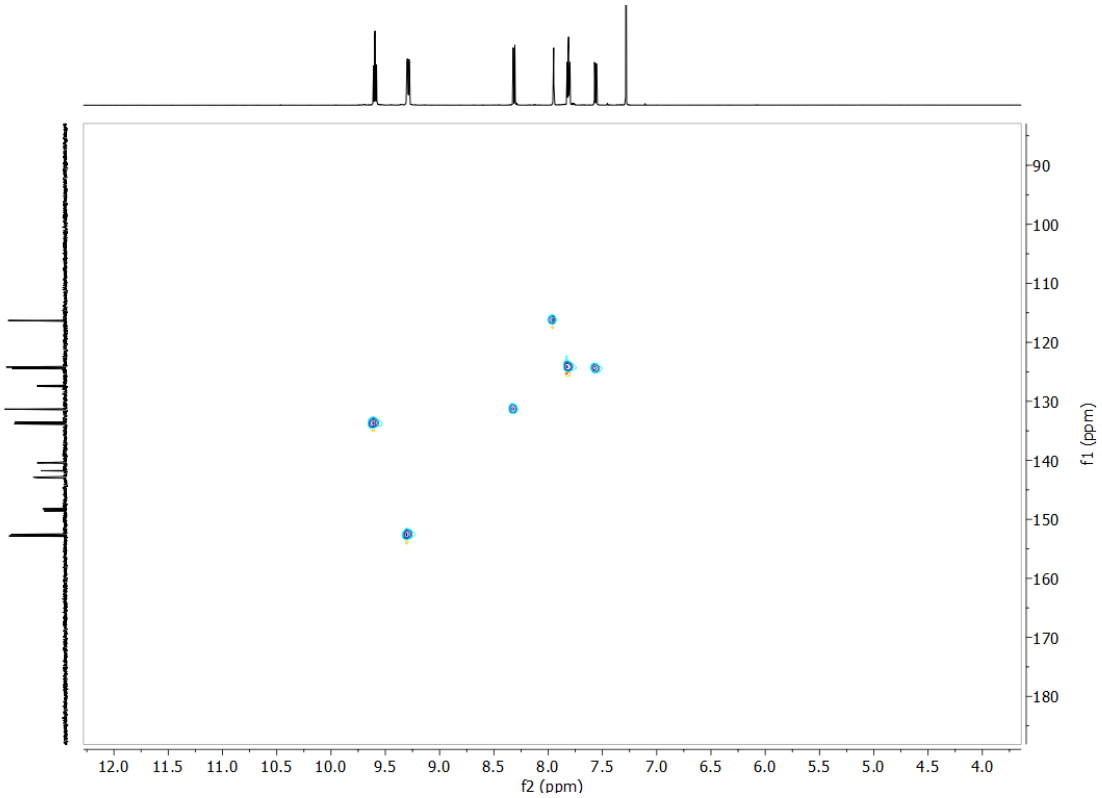

Figure A28. HSQC NMR spectrum for ligand **C** in in $CHCl_3$.

Compound 7:

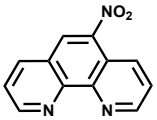

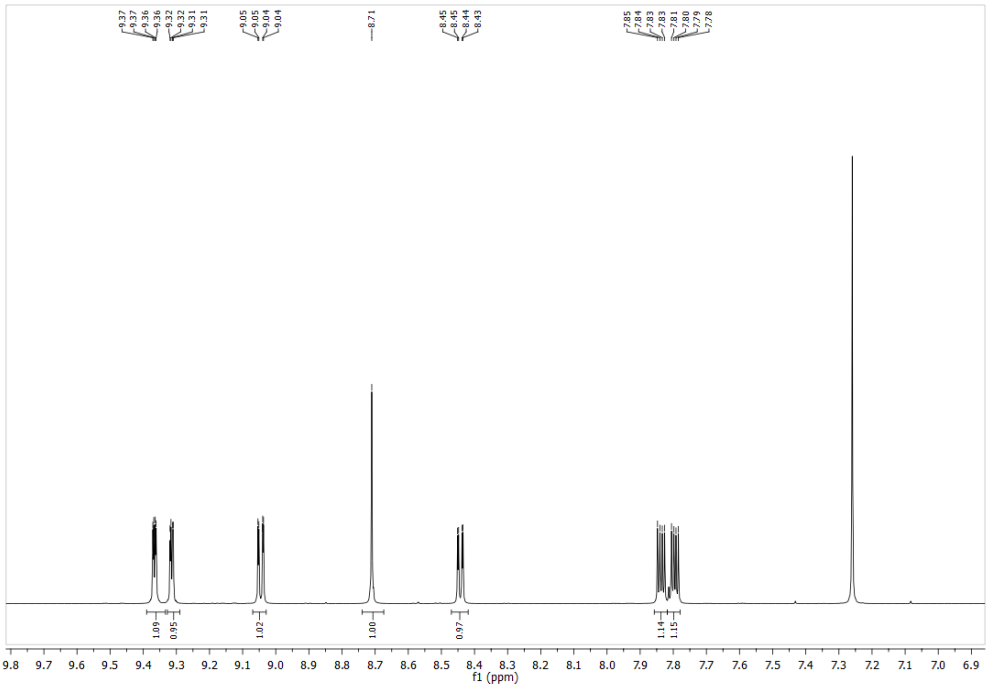

Figure A29. ^{1}H NMR spectrum (600 MHz) for compound 7 in $CDCl_3$.

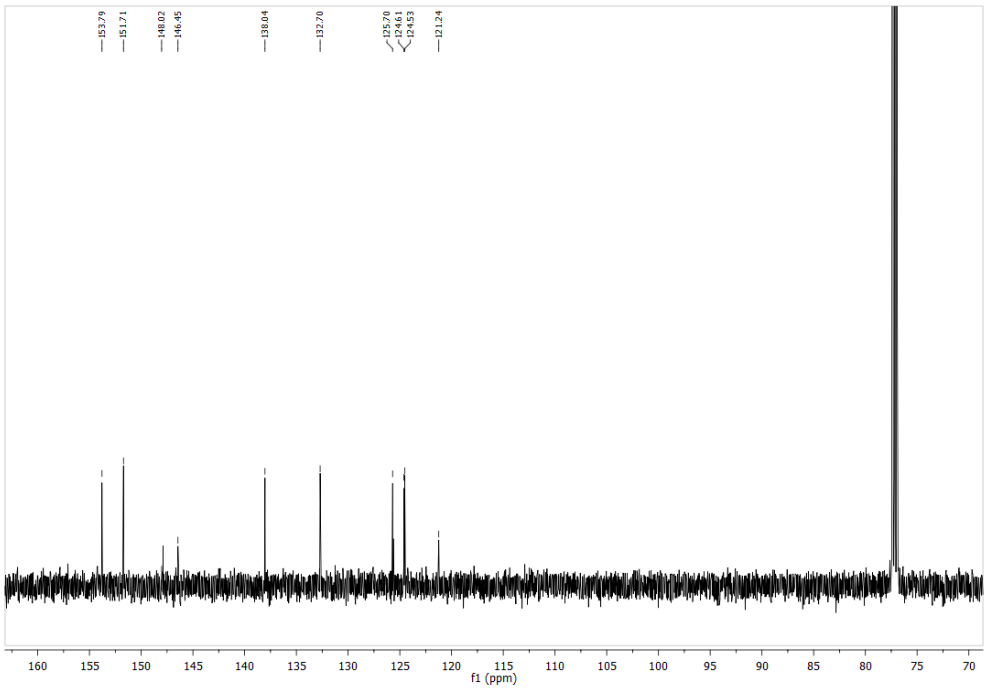

Figure A30. ^{13}C NMR spectrum (151 MHz) for compound **7** in $CDCl_3$.

Compound 8:

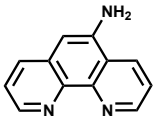

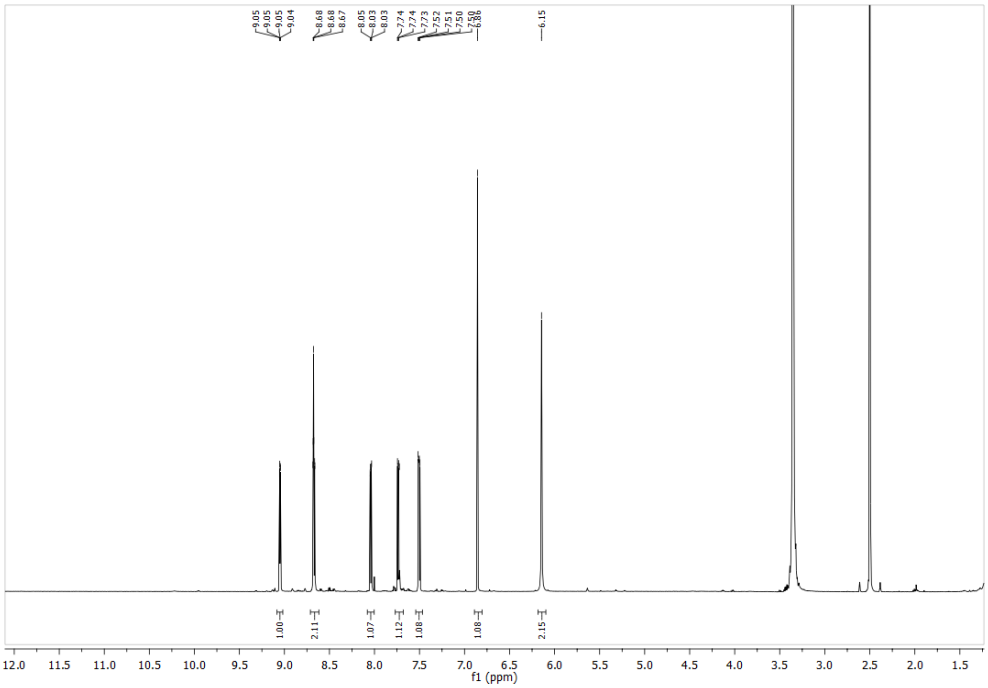

Figure A31. [1]H NMR spectrum (600 MHz) for compound **8** in DMSO-*d*$_6$.

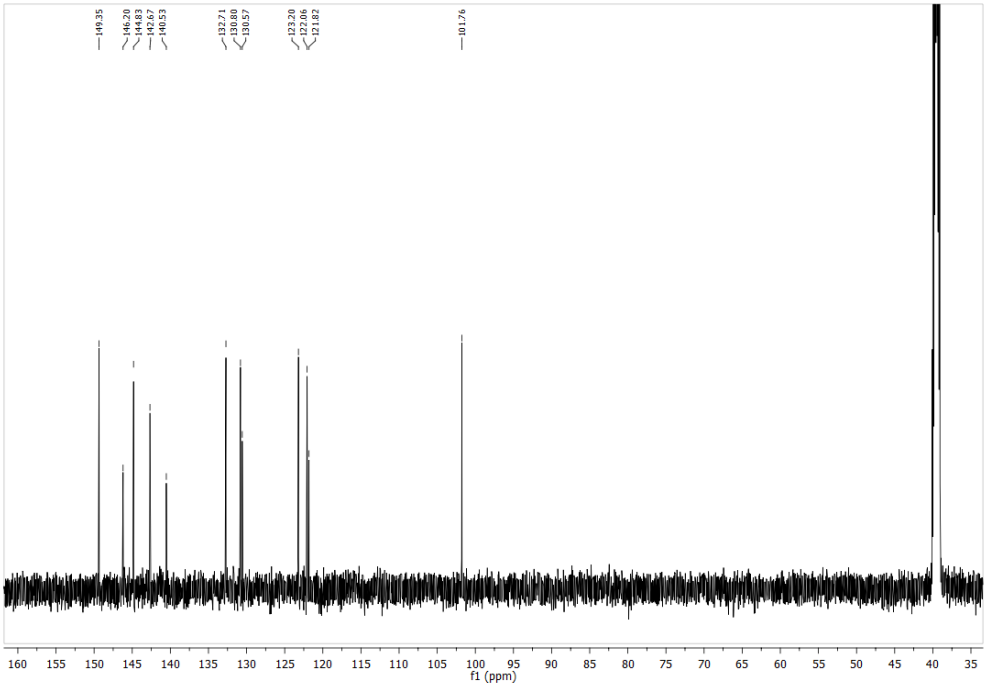

Figure A32. [13]C-NMR spectrum (151 MHz) for compound **8** in DMSO-*d*$_6$.

Compound 9:

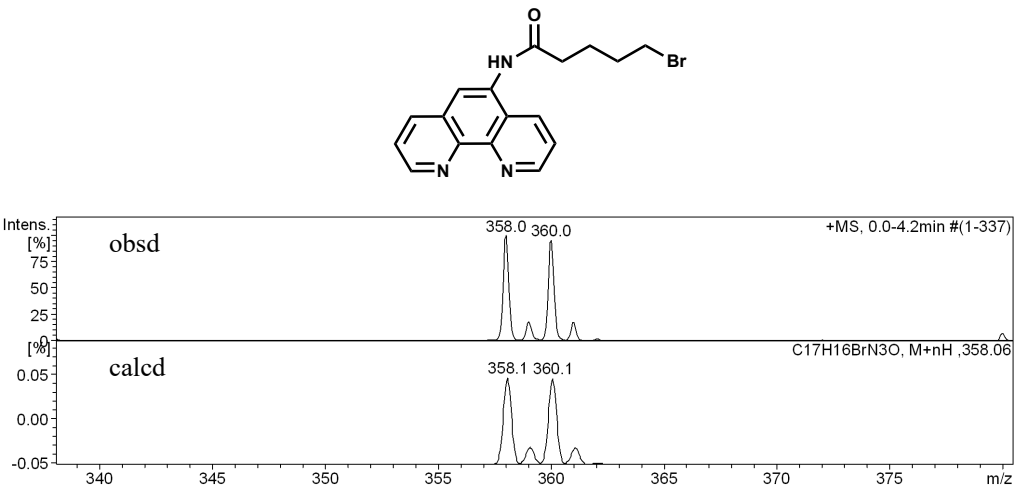

Figure A33. ESI-MS for compound **9**.

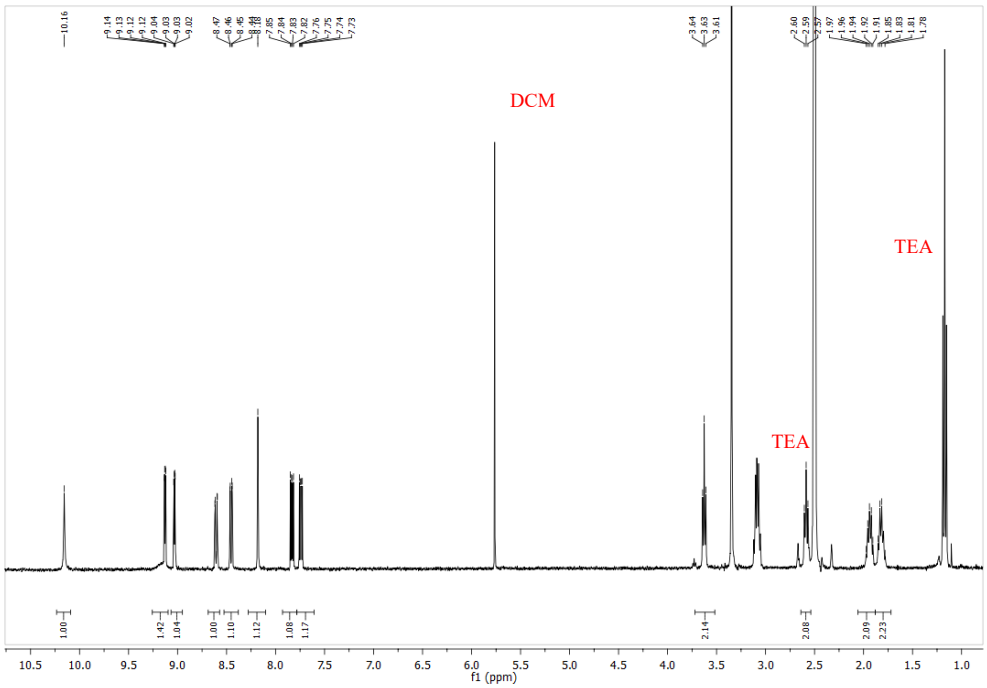

Figure A34. ^{1}H NMR spectrum (600 MHz) for compound **9** in DMSO-d_6.

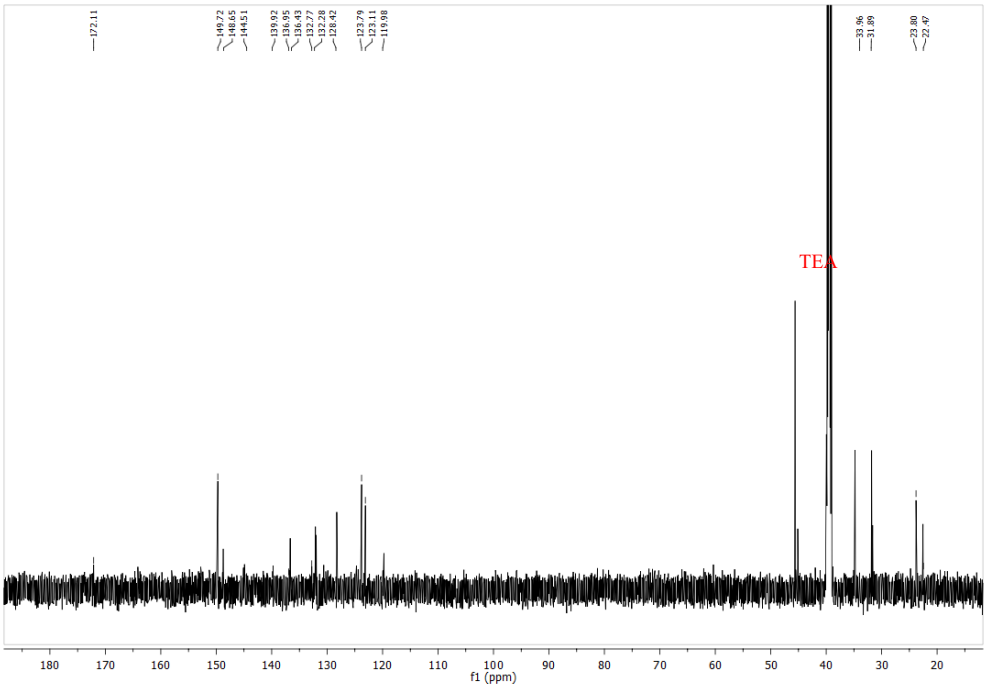

Figure A35. ^{13}C NMR spectrum (151 MHz) for compound **9** in DMSO-*d*$_6$.

Ligand D:

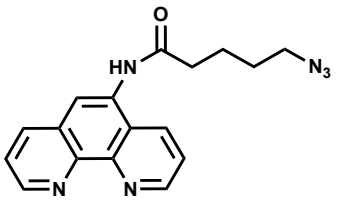

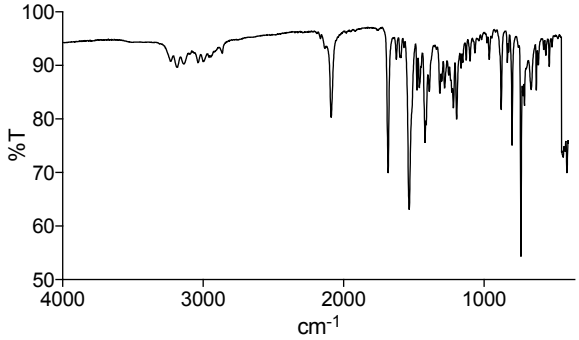

Figure A36. FTIR-ATR for ligand **D**.

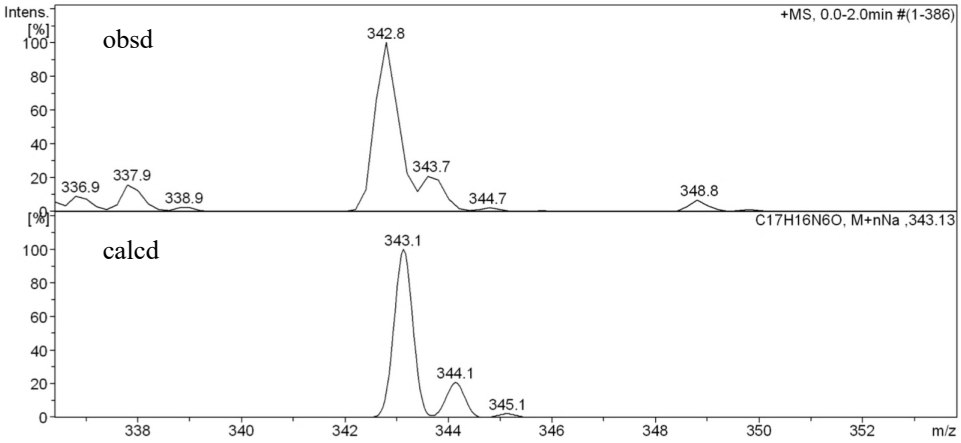

Figure A37. ESI-MS for ligand **D**.

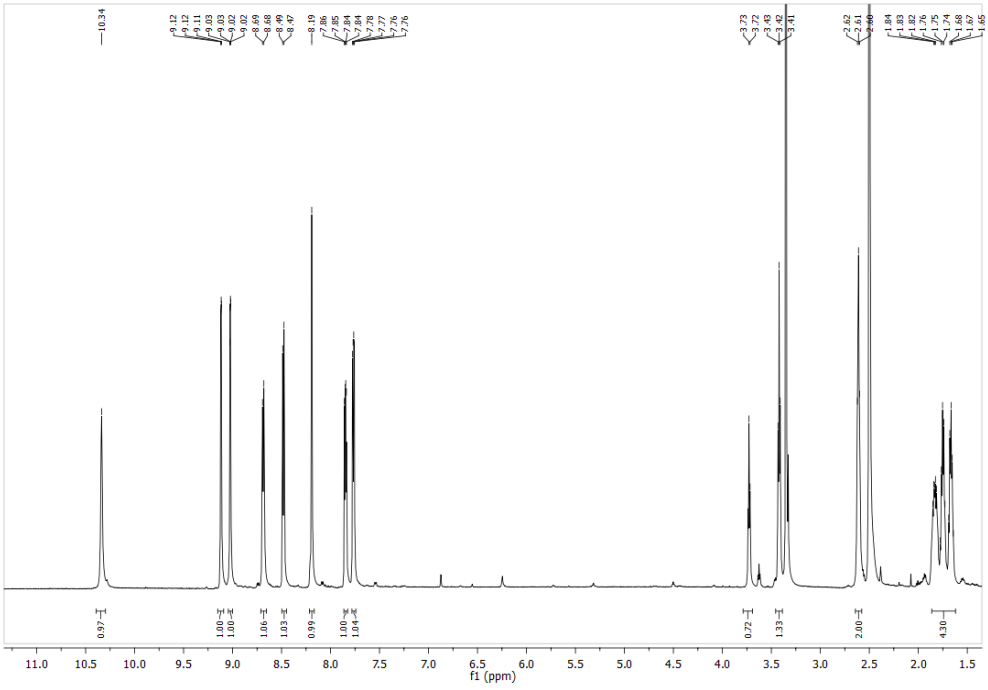

Figure A38. ^{1}H NMR spectrum (600 MHz) for ligand **D** in DMSO-*d*$_6$.

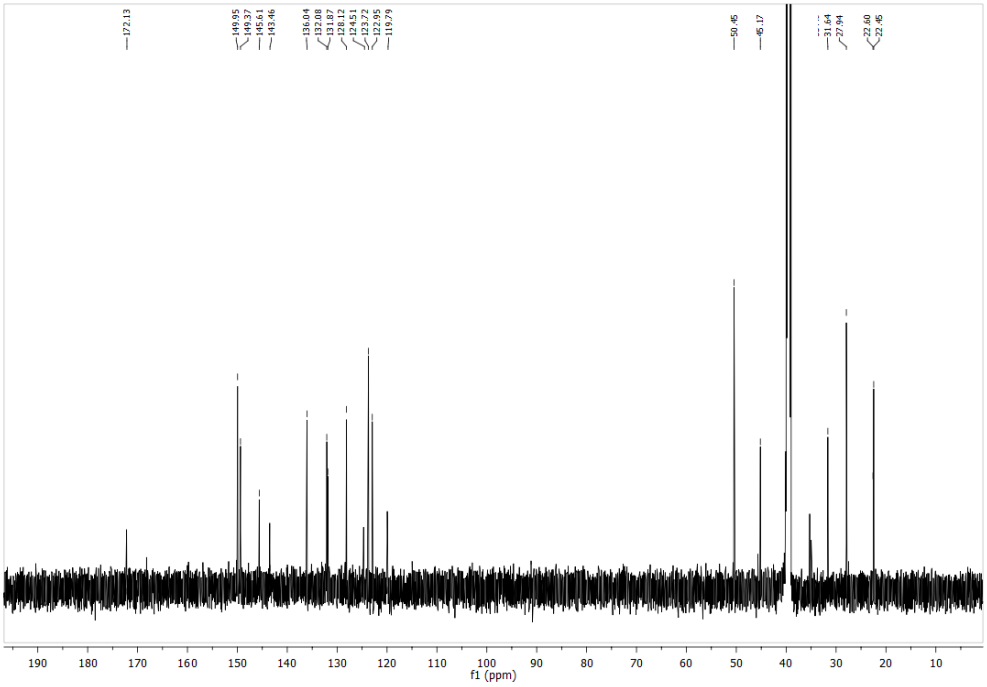

Figure A39. ^{13}C NMR spectrum (151 MHz) for ligand **D** in DMSO-d_6.

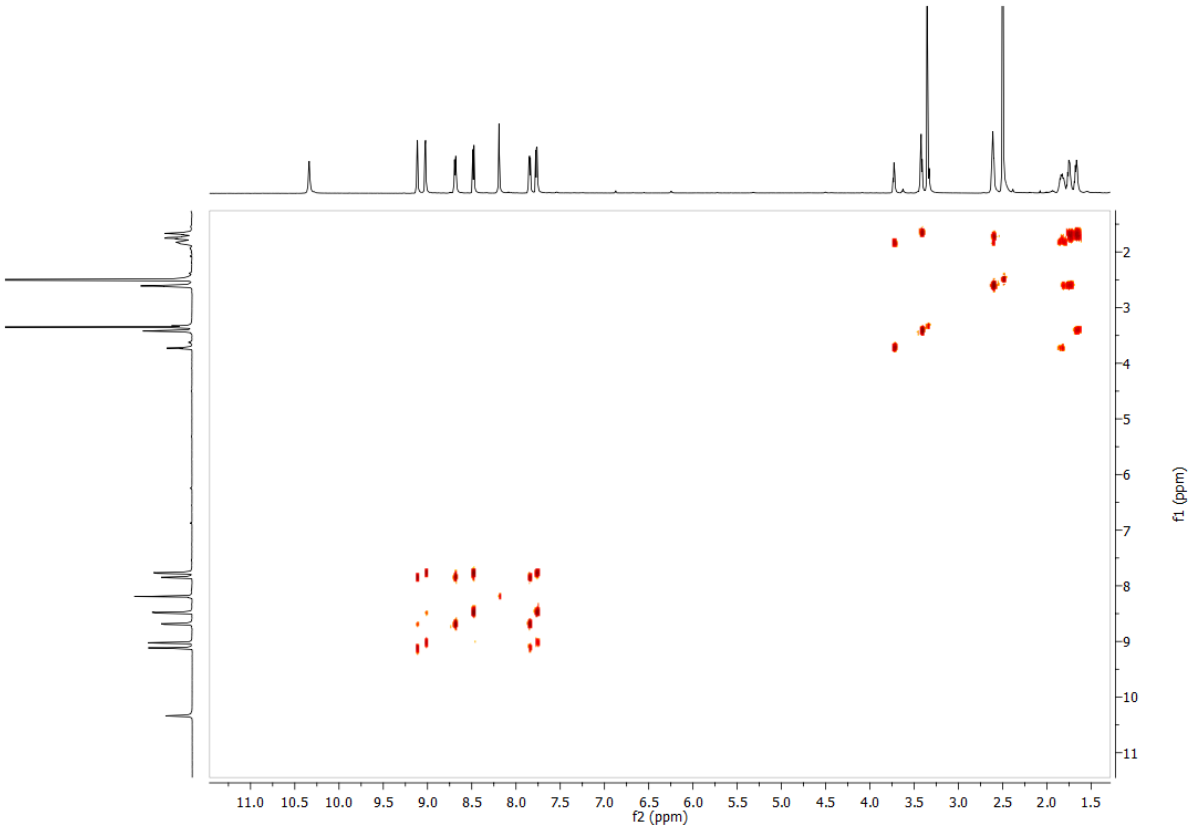

Figure A40. COSY NMR spectrum for ligand **D** in DMSO-d_6.

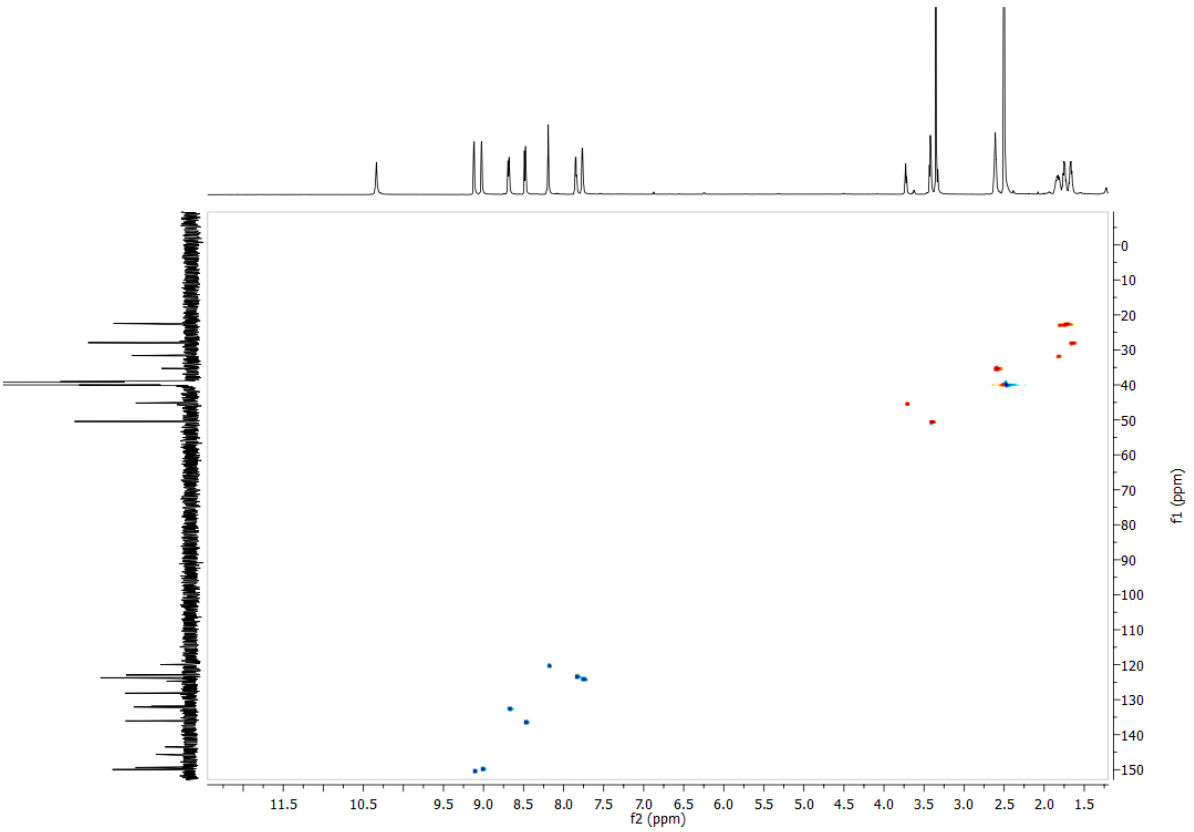

Figure A41. HSQC NMR spectrum for ligand **D** in DMSO-d_6.

Compound 11:

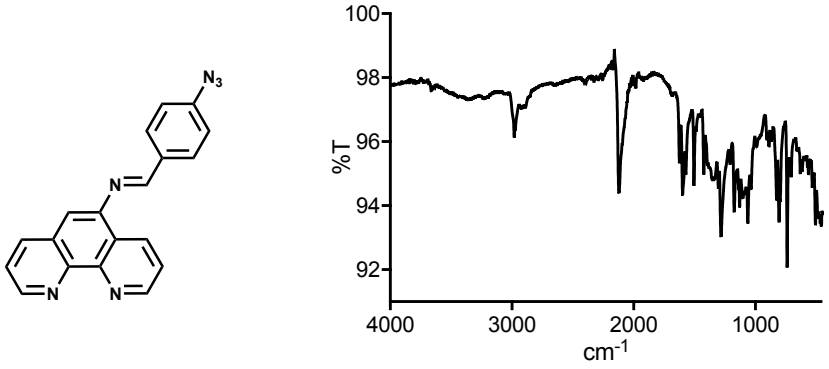

Figure A42. FTIR-ATR for compound **11**.

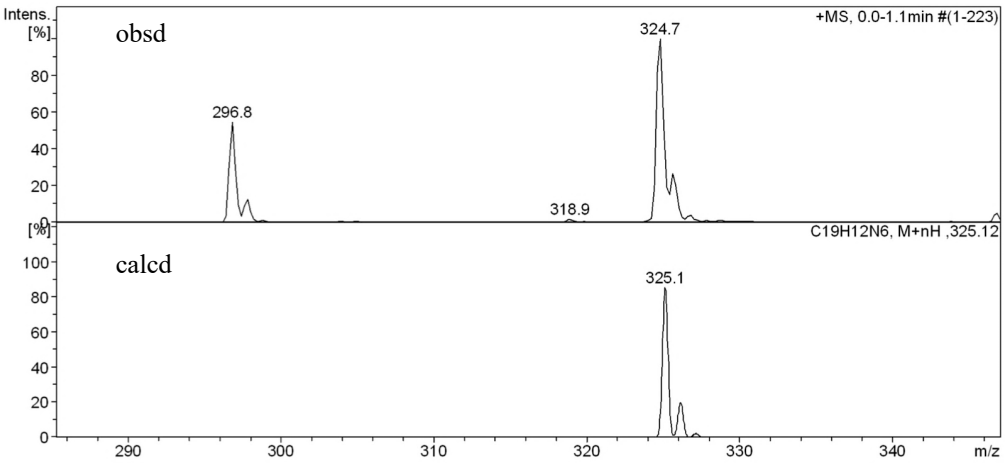

Figure A43. ESI-MS for compound **11**.

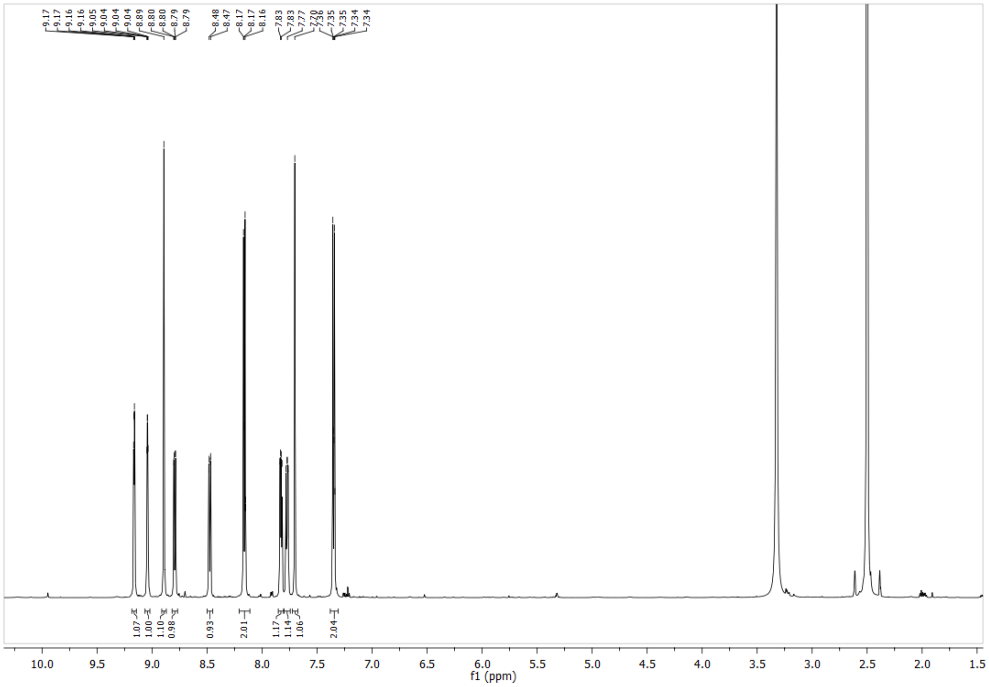

Figure A44. ^{1}H NMR spectrum (600 MHz) for compound **11** in DMSO-d_6.

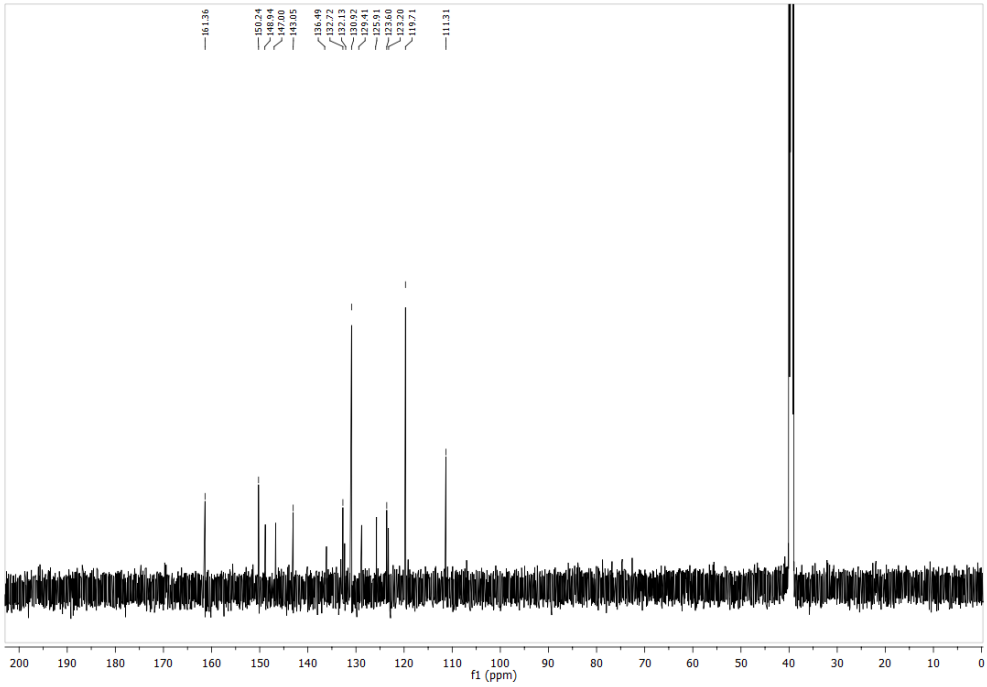

Figure A45. ^{13}C NMR spectrum (151 MHz) for compound **11** in DMSO-d_6.

Ligand E:

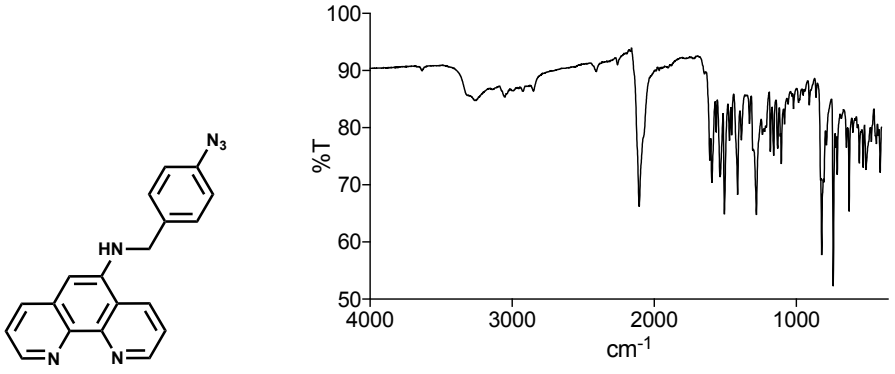

Figure A46. FTIR-ATR for ligand **E**.

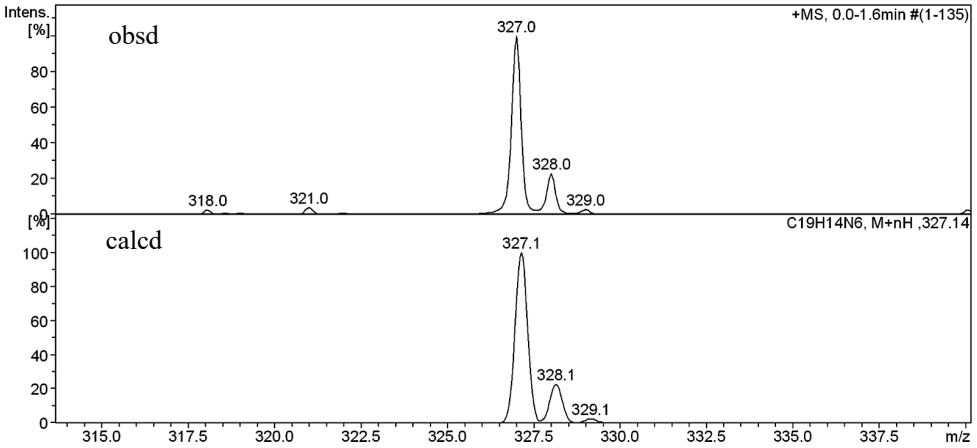

Figure A47. ESI-MS for ligand **E**.

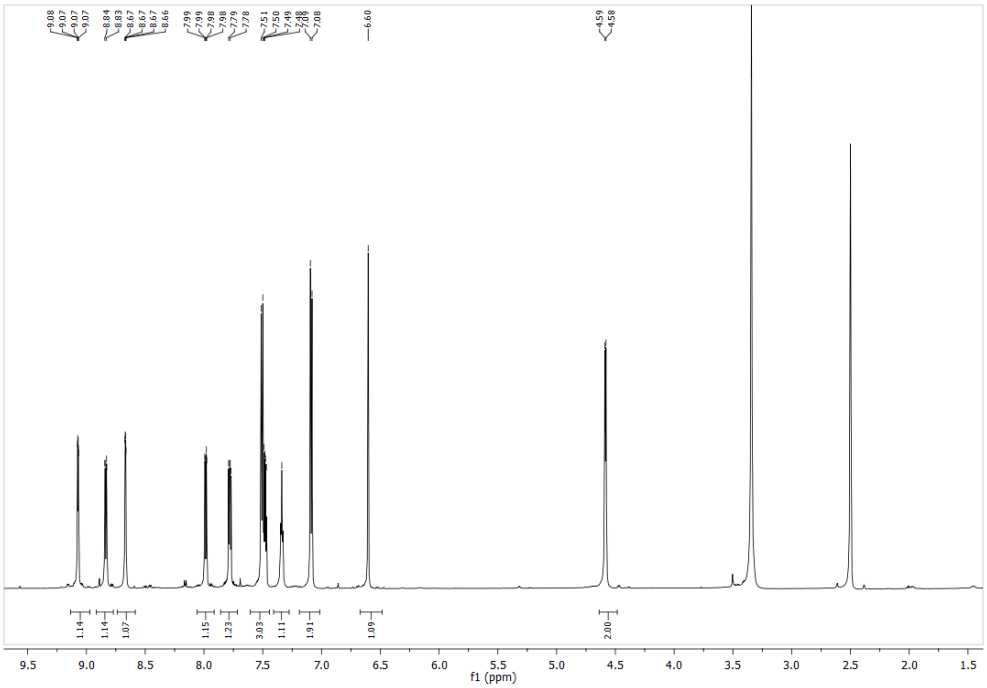

Figure A48. ^{1}H NMR spectrum (600 MHz) for ligand **E** in DMSO- d_6.

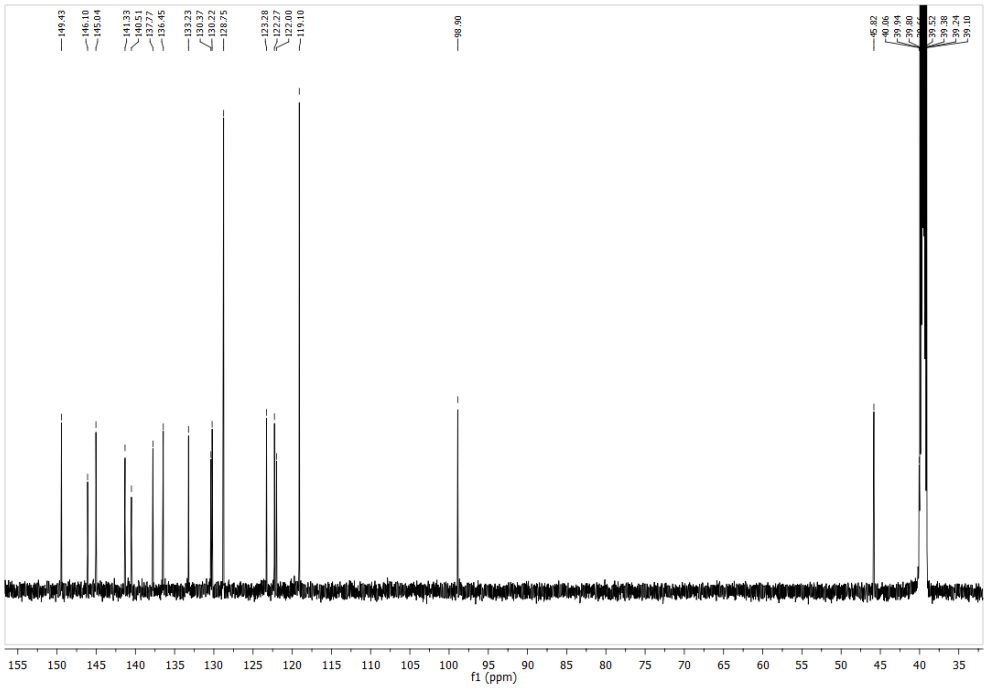

Figure A49. ^{13}C NMR spectrum (151 MHz) for ligand **E** in DMSO- d_6.

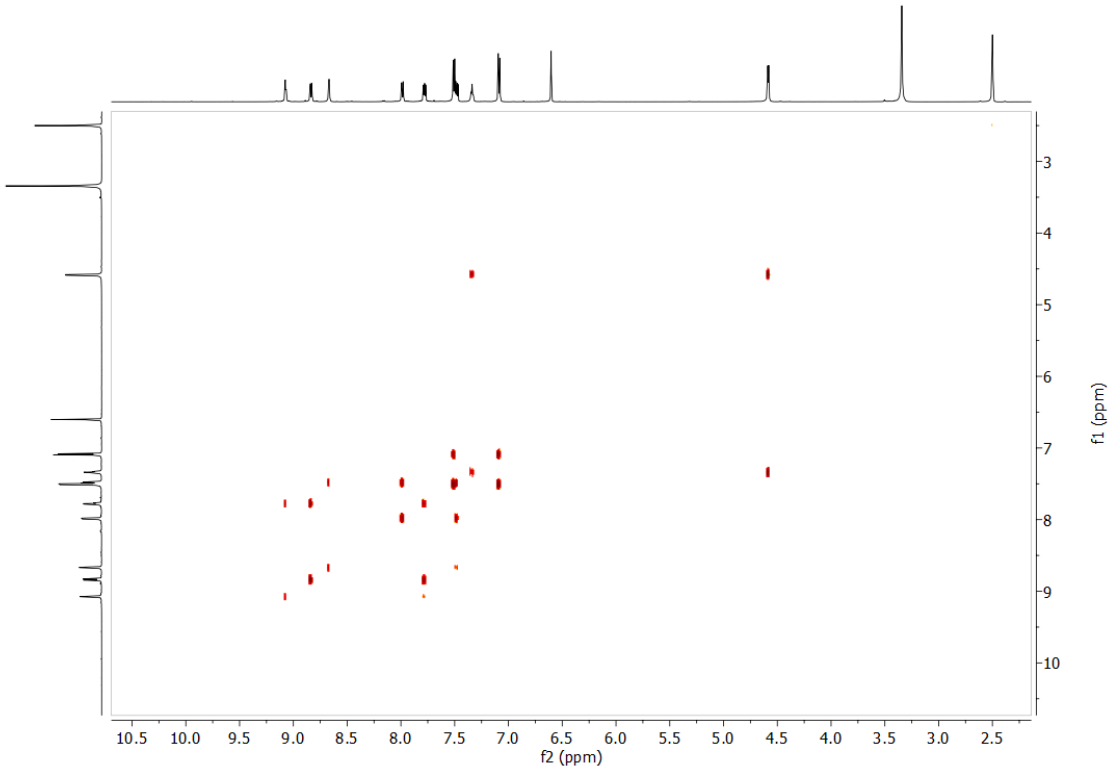

Figure A50. COSY NMR spectrum for compound ligand **E** in DMSO- d_6.

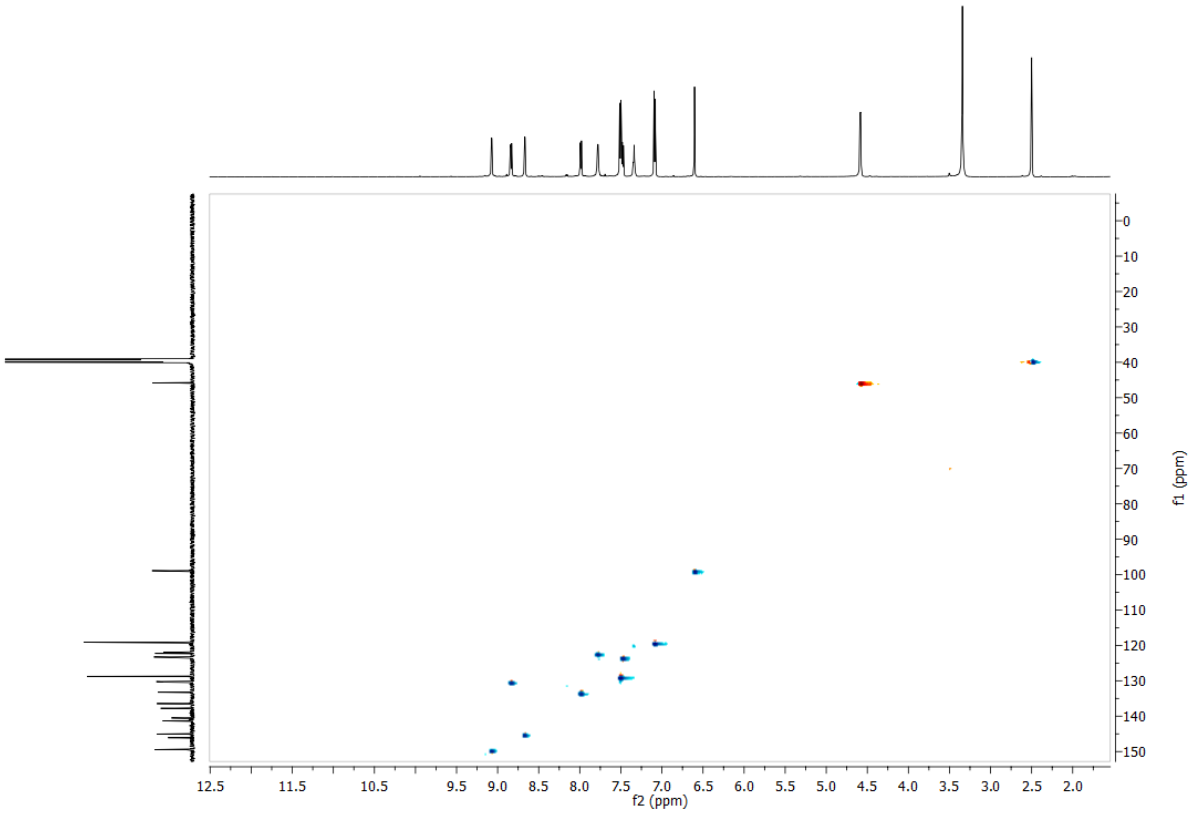

Figure A51. HSQC NMR spectrum for compound ligand **E** in DMSO-d_6.

Ligand F:

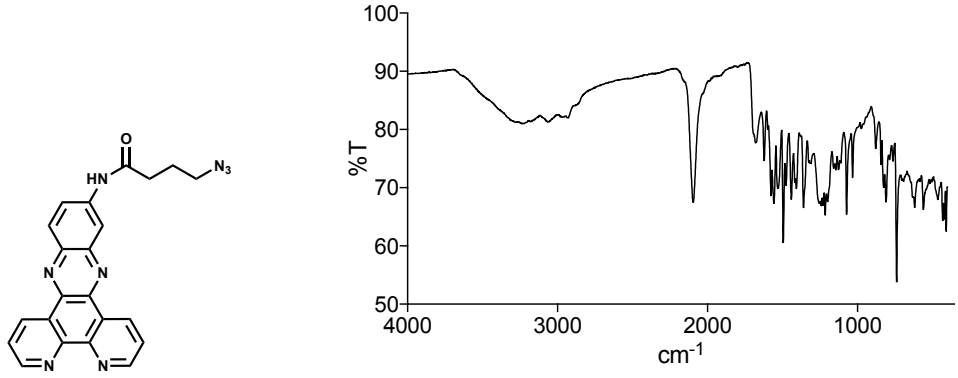

Figure A52. FTIR-ATR for ligand **F**.

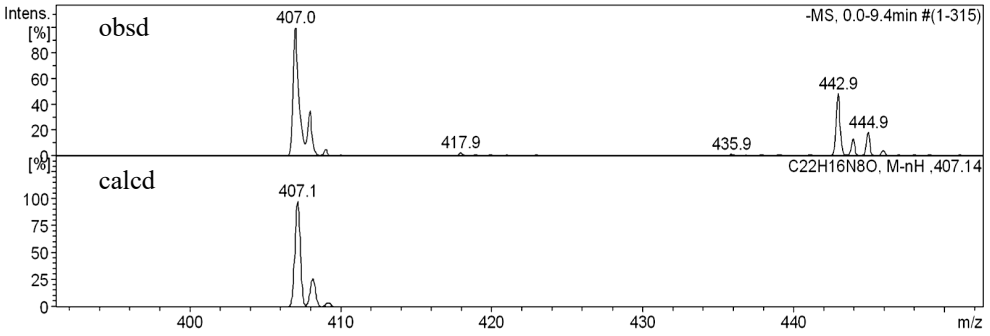

Figure A53. ESI-MS for ligand **F**.

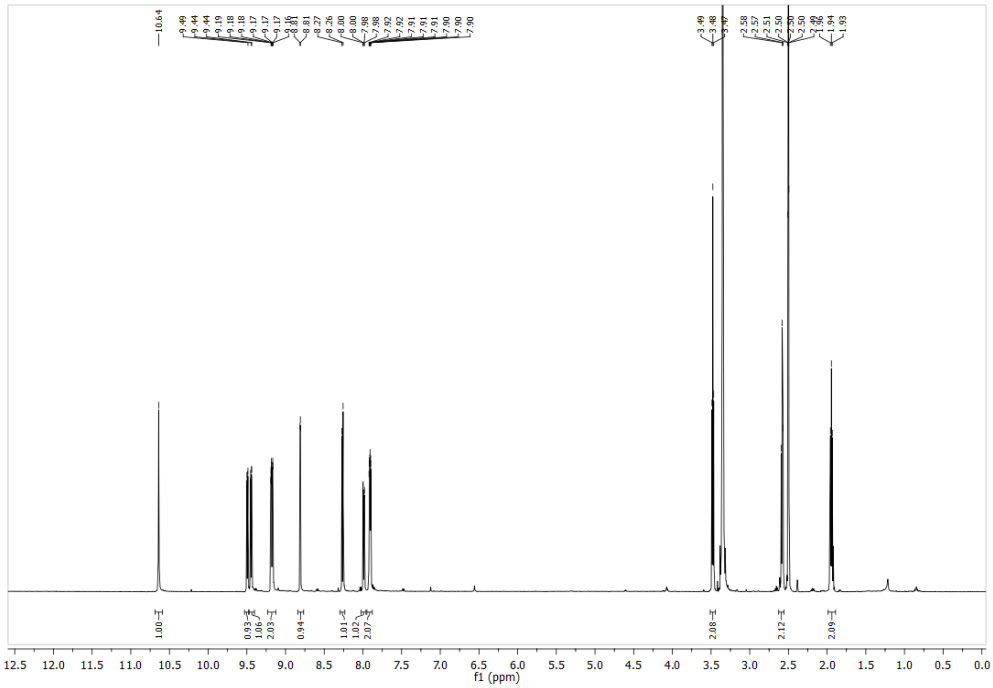

Figure A54. ^{1}H NMR spectrum (600 MHz) for ligand **F** in DMSO-d_6.

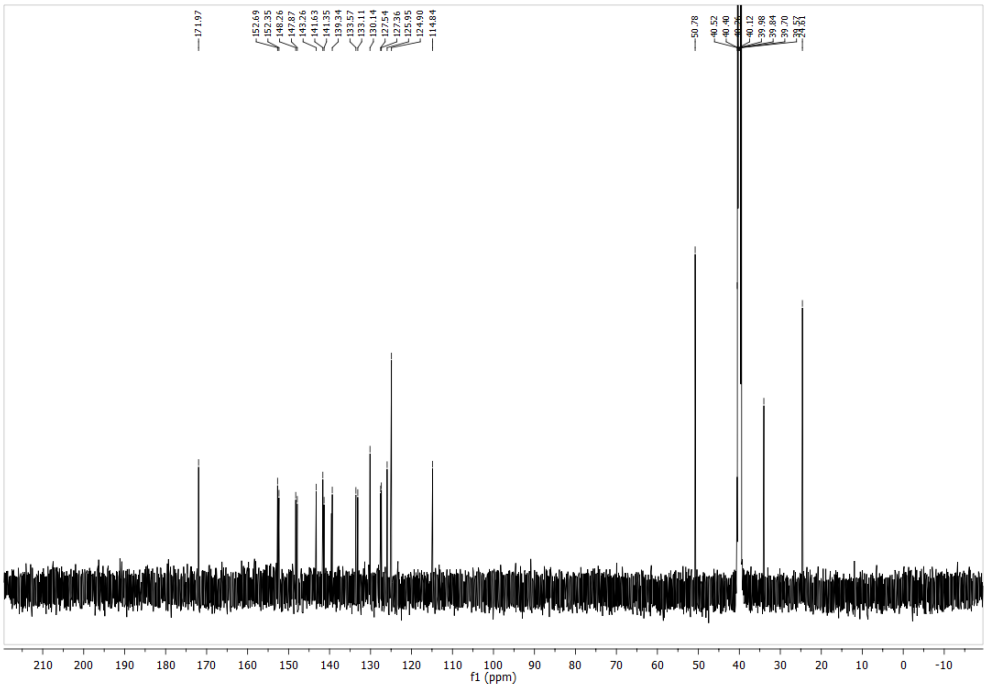

Figure A55. ^{13}C NMR spectrum (151 MHz) for ligand **F** in DMSO-d_6.

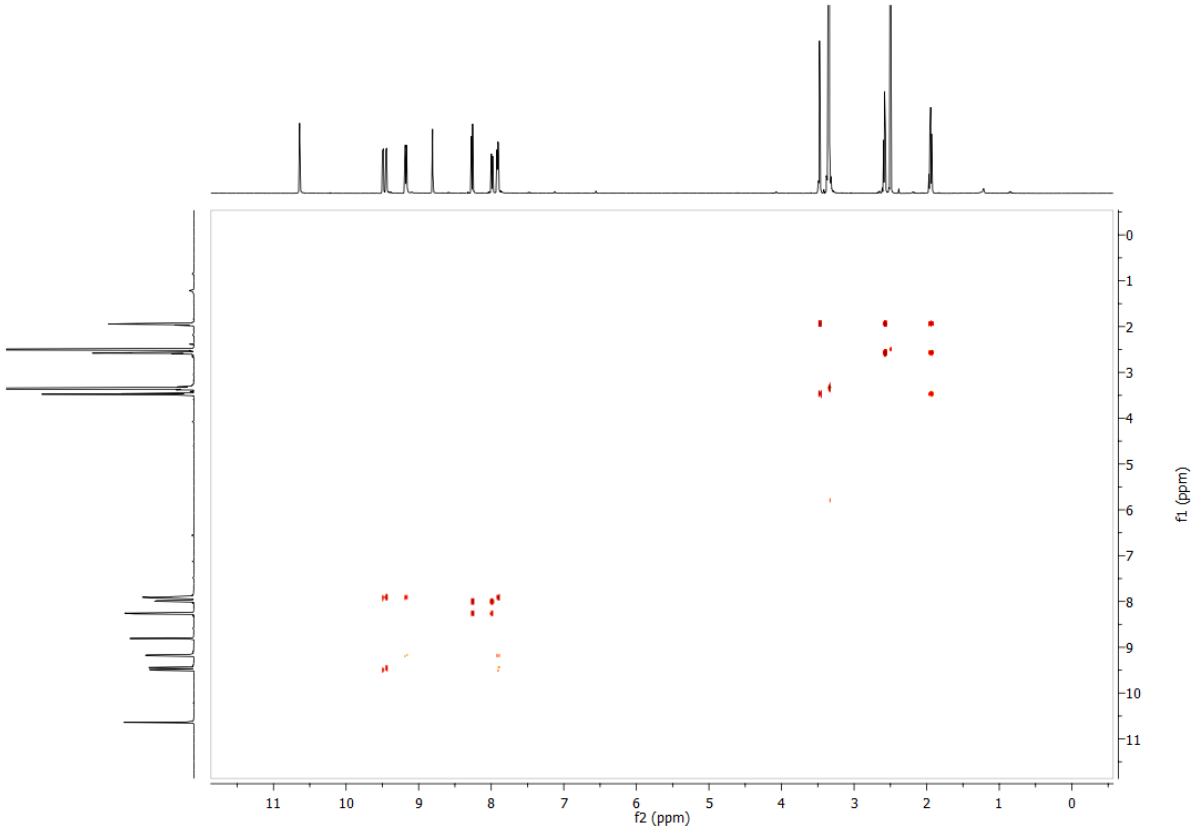

Figure A56. COSY-NMR spectrum for Ligand **F**.

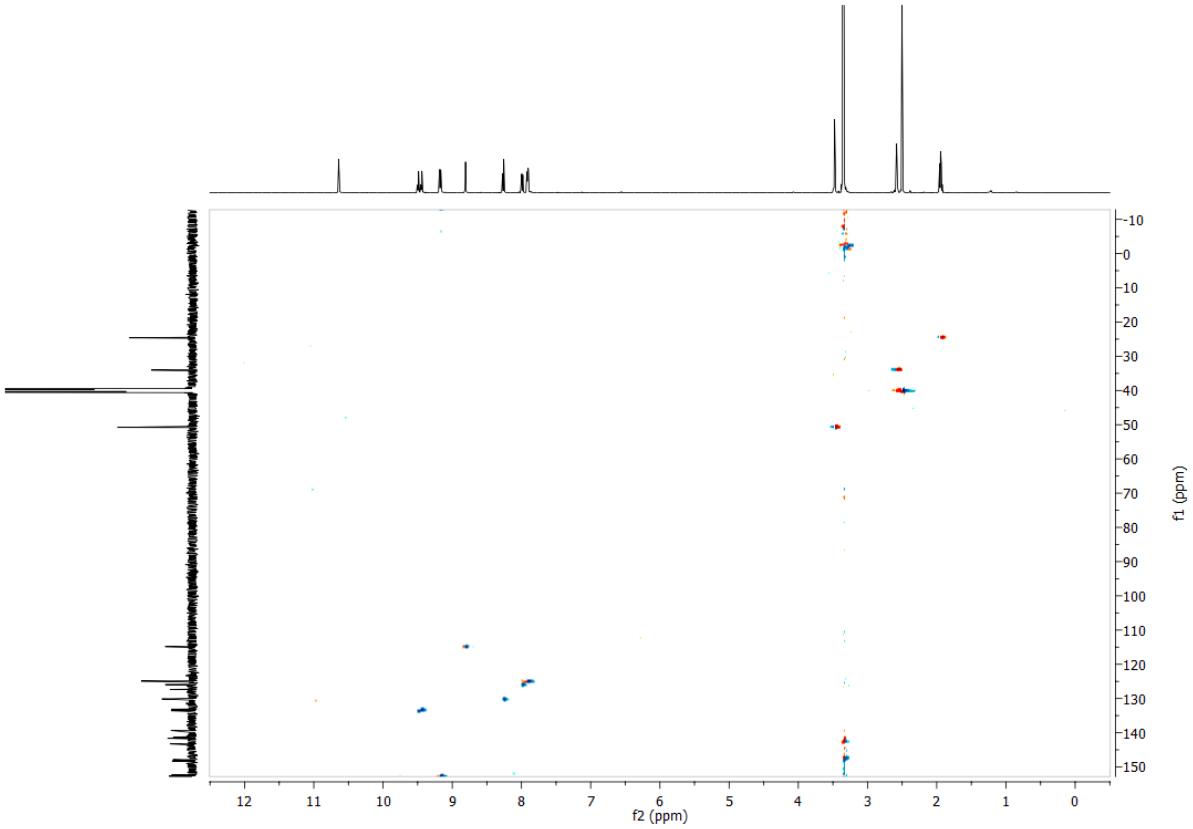

Figure A57. HSQC NMR spectrum for Ligand **F**.

APPENDIX B

Spectral characterisation of [Cu(**A**)$(NO_3)_2$]

[Cu(A)(NO$_3$)$_2$]

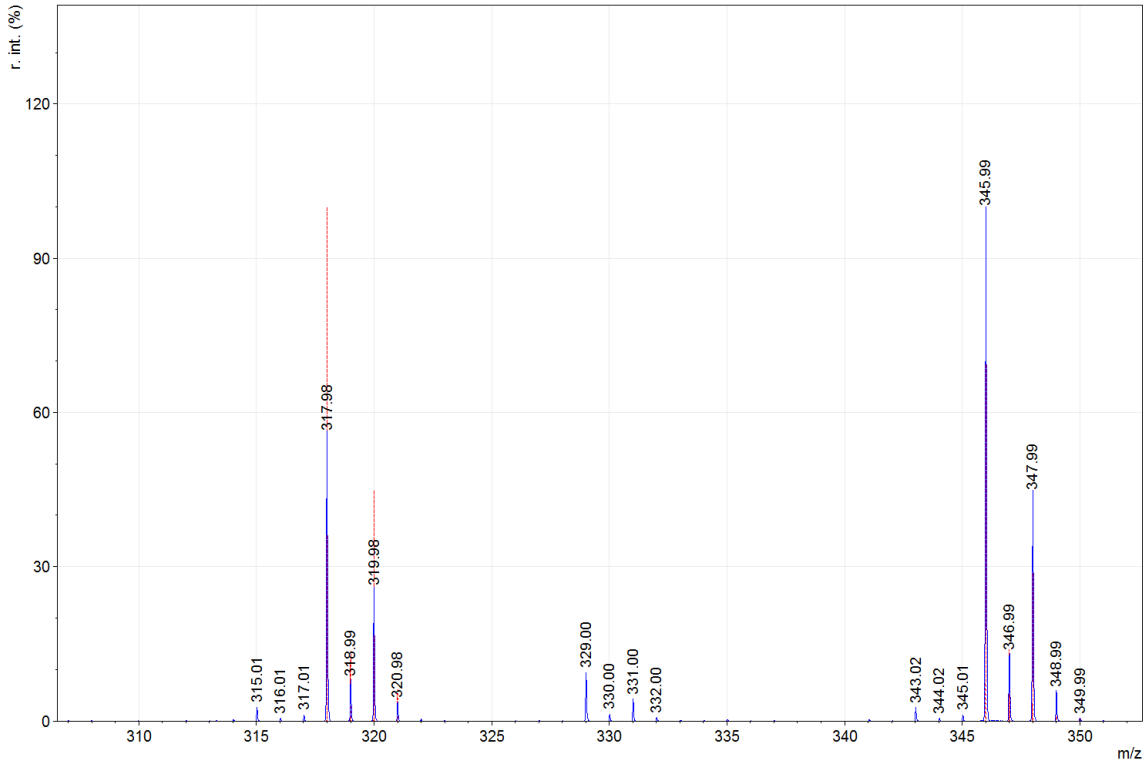

Figure B1. ESI-MS for copper complex of [Cu(**A**)NO$_3$)$_2$].

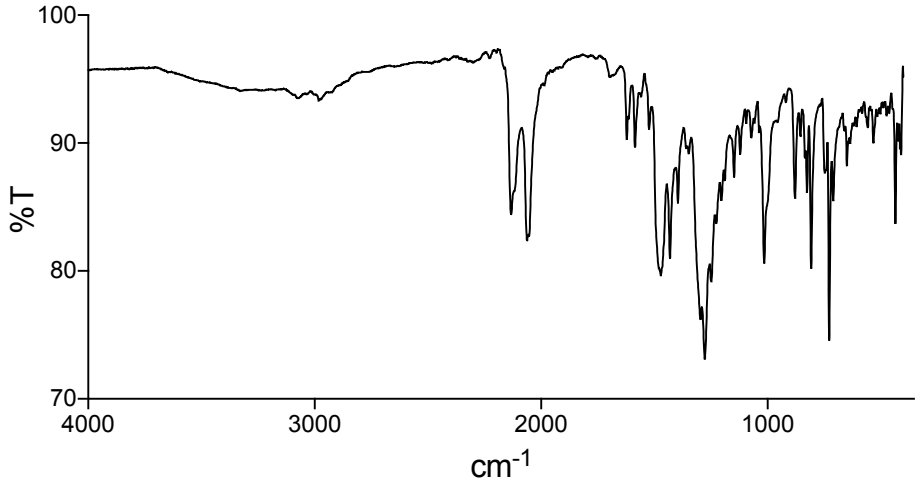

Figure B2. FT-IR spectrum of [Cu(**A**)NO$_3$)$_2$].

APPENDIX C

NMR spectra, ESI-MS and FTIR-ATR analysis of ligands **G** and $\mathbf{G_R}$ and intermediates

Compound 13:

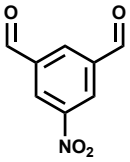

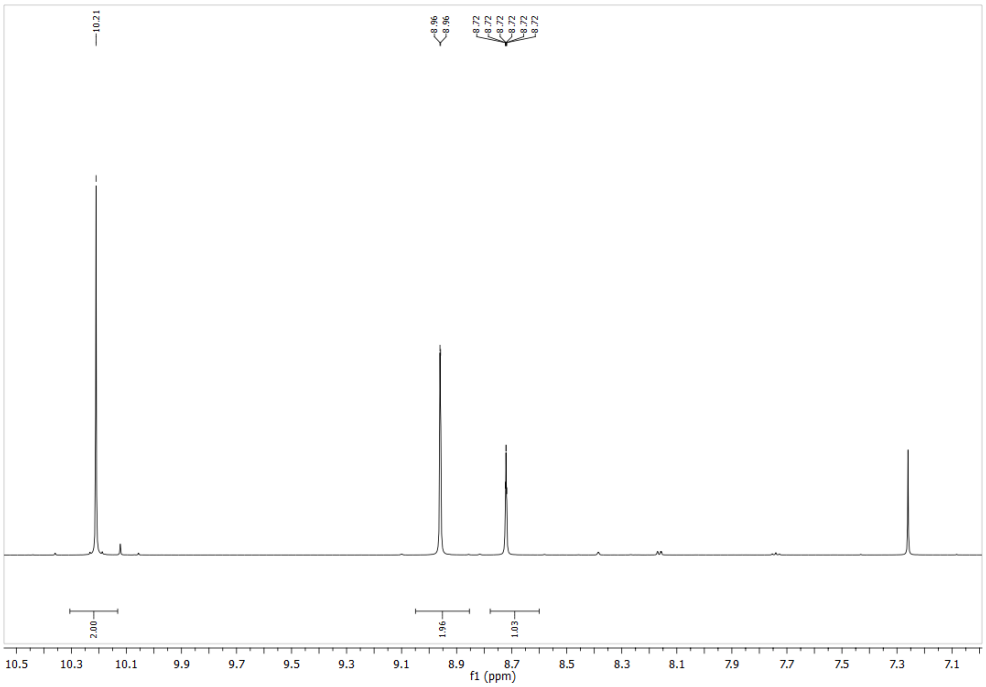

Figure C1. ^{1}H NMR spectrum (600 MHz) for compound **13** in $CDCl_3$.

Compound 14:

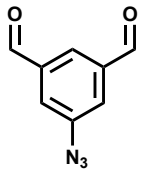

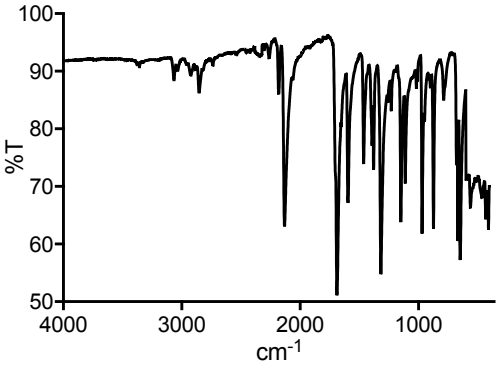

Figure C2. FTIR-ATR for compound **14**.

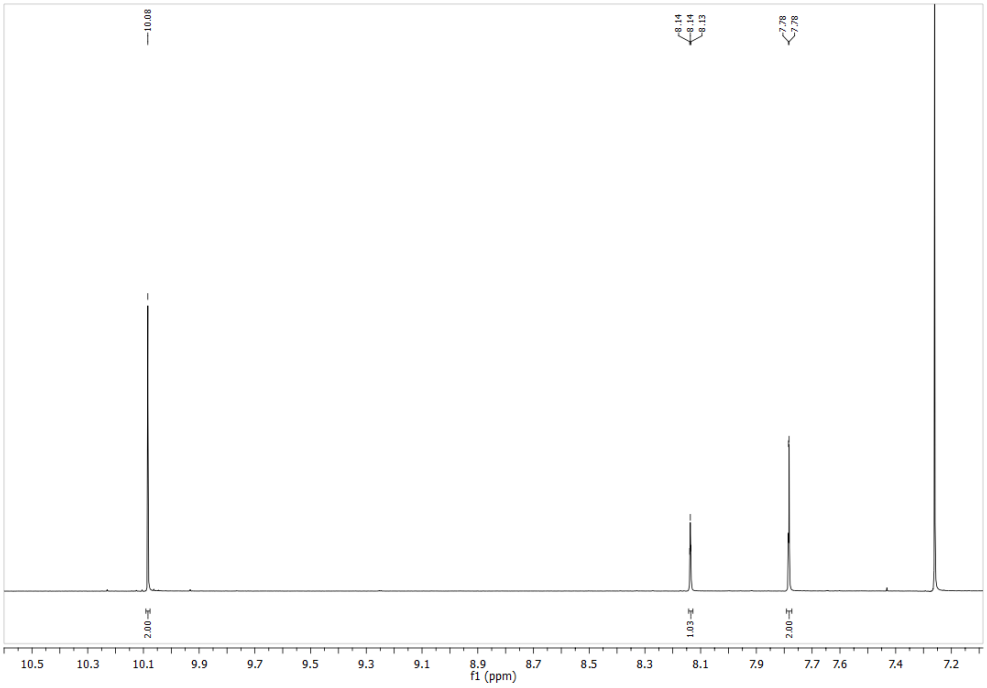

Figure C3. ^{1}H NMR spectrum (600 MHz) for compound **14** in $CDCl_3$.

Compound 15:

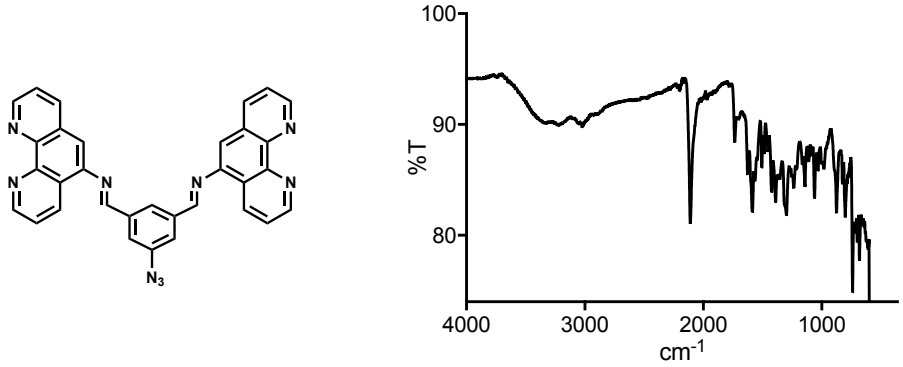

Figure C4. FTIR-ATR for compound **15**.

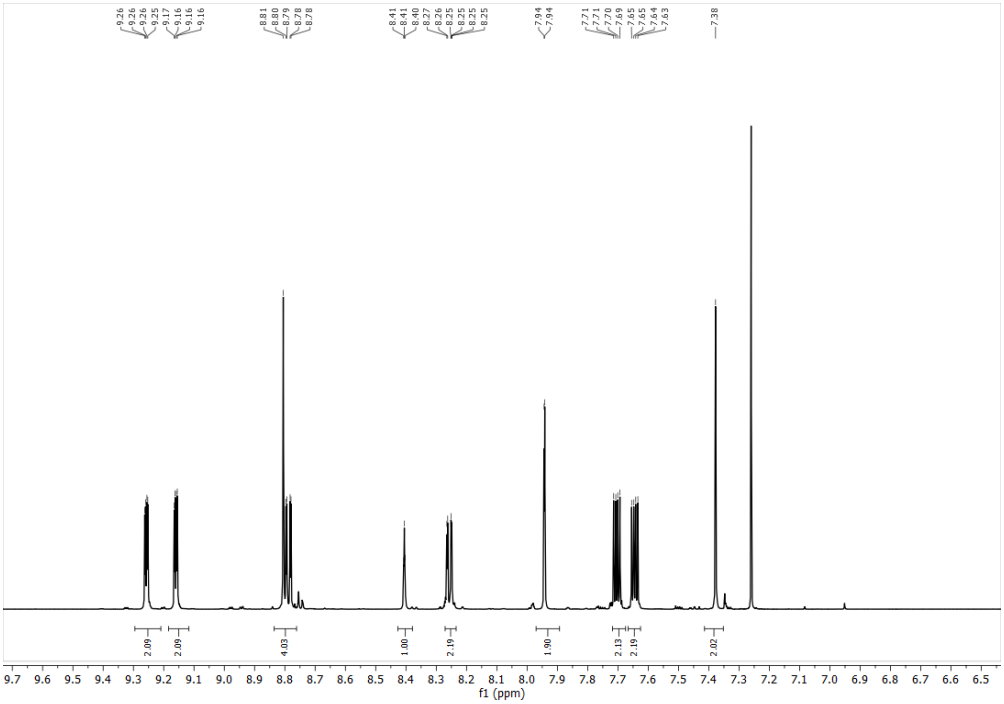

Figure C5. ^{1}H NMR spectrum (600 MHz) for compound **15** in $CDCl_3$.

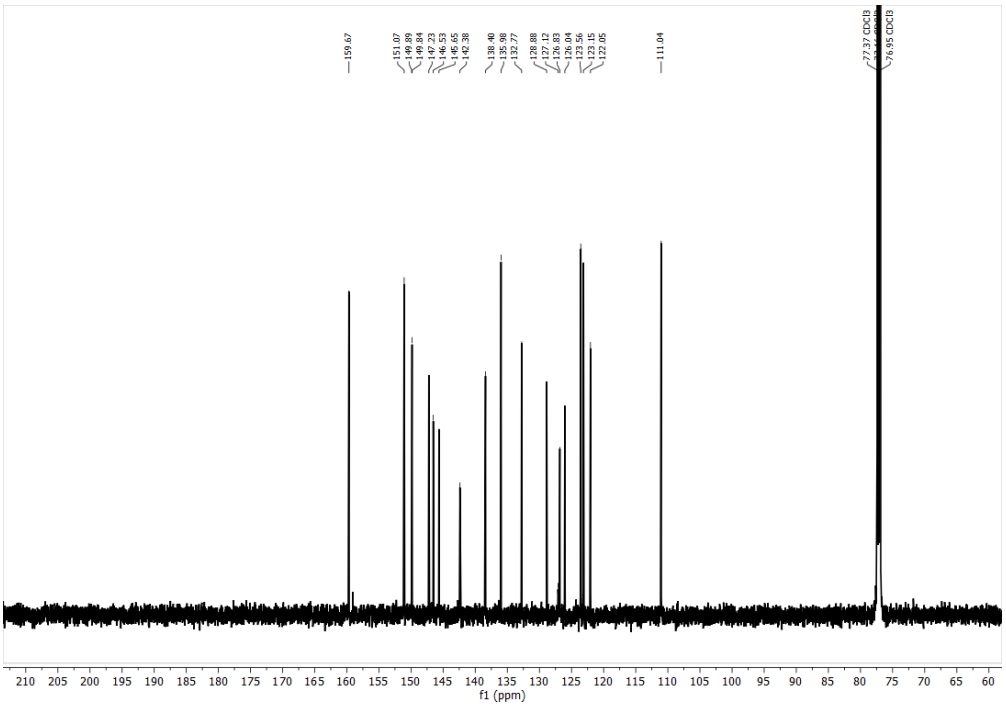

Figure C6. ^{13}C NMR spectrum (151 MHz) for compound **15** in $CDCl_3$.

Ligand G:

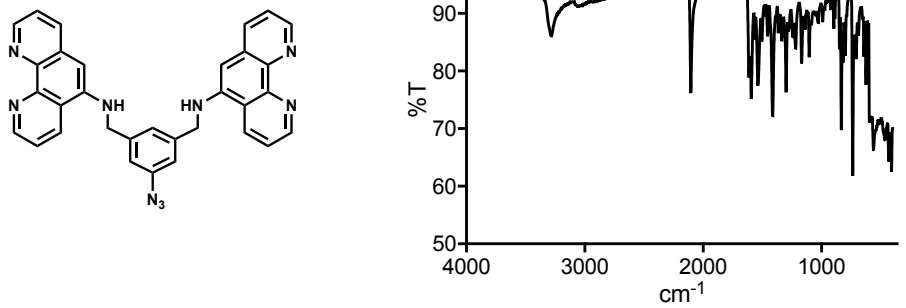

Figure C7. FTIR-ATR for ligand **G**.

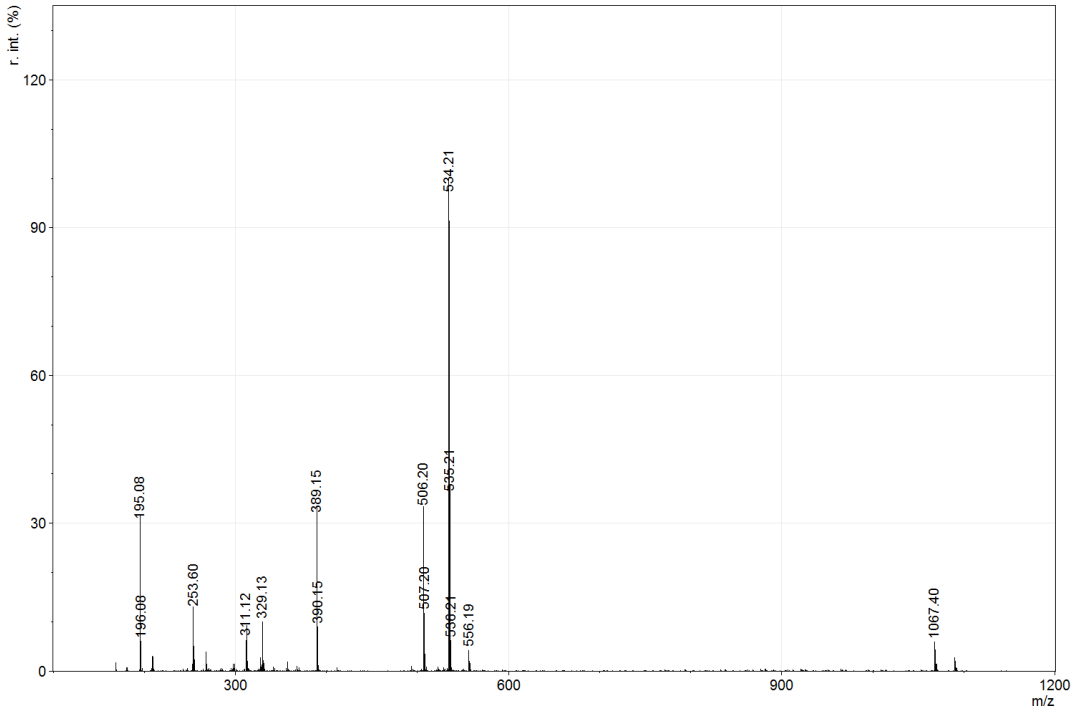

Figure C8. ESI-Ms for ligand **G**.

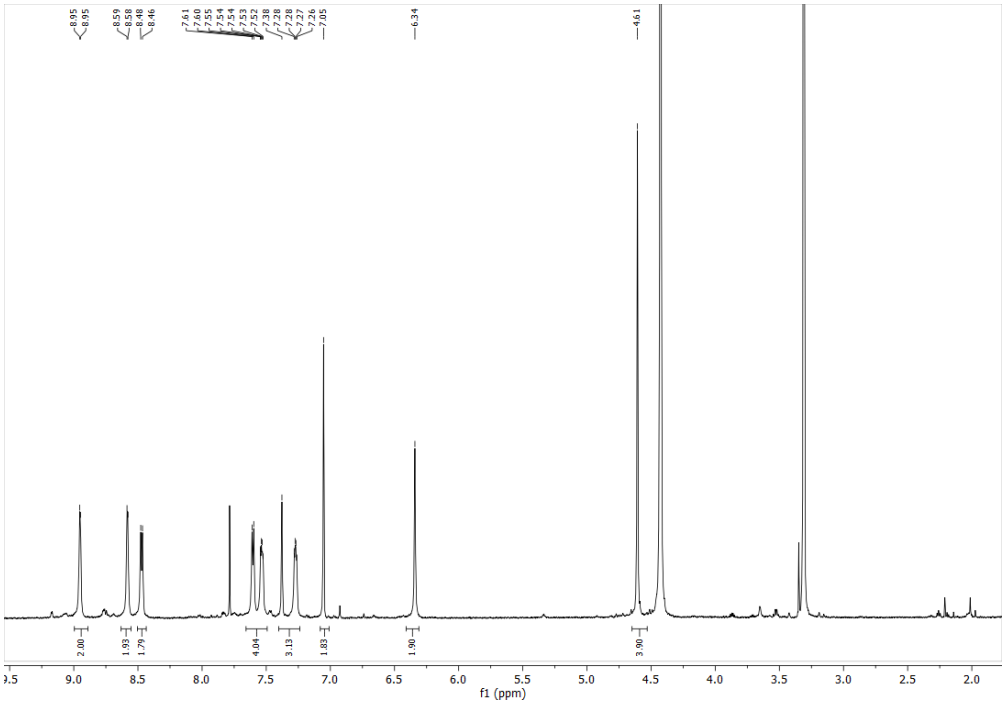

Figure C7. ^{1}H NMR spectrum (600 MHz) for ligand **G** in MeOD/$CDCl_3$.

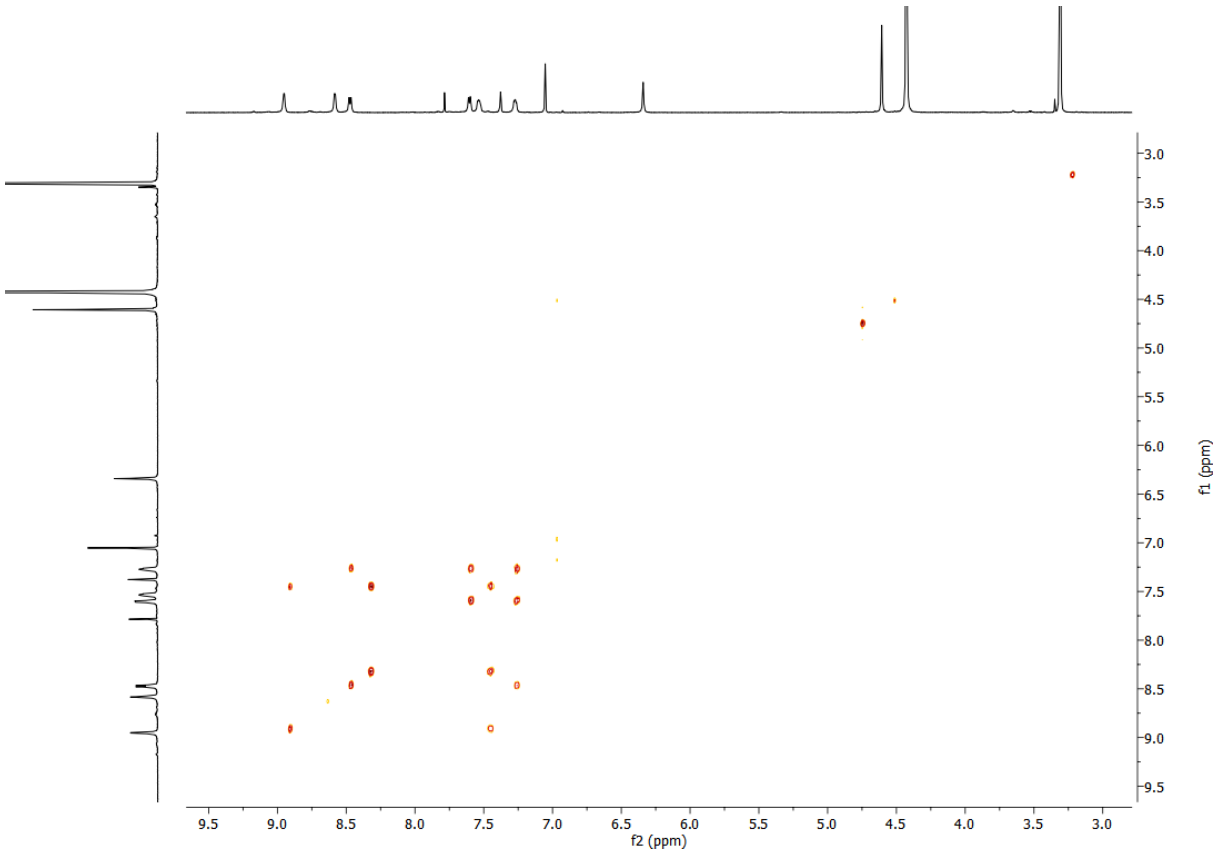

Figure C8. COSY NMR spectrum for Ligand **G** in MeOD/$CDCl_3$.

Compound 16:

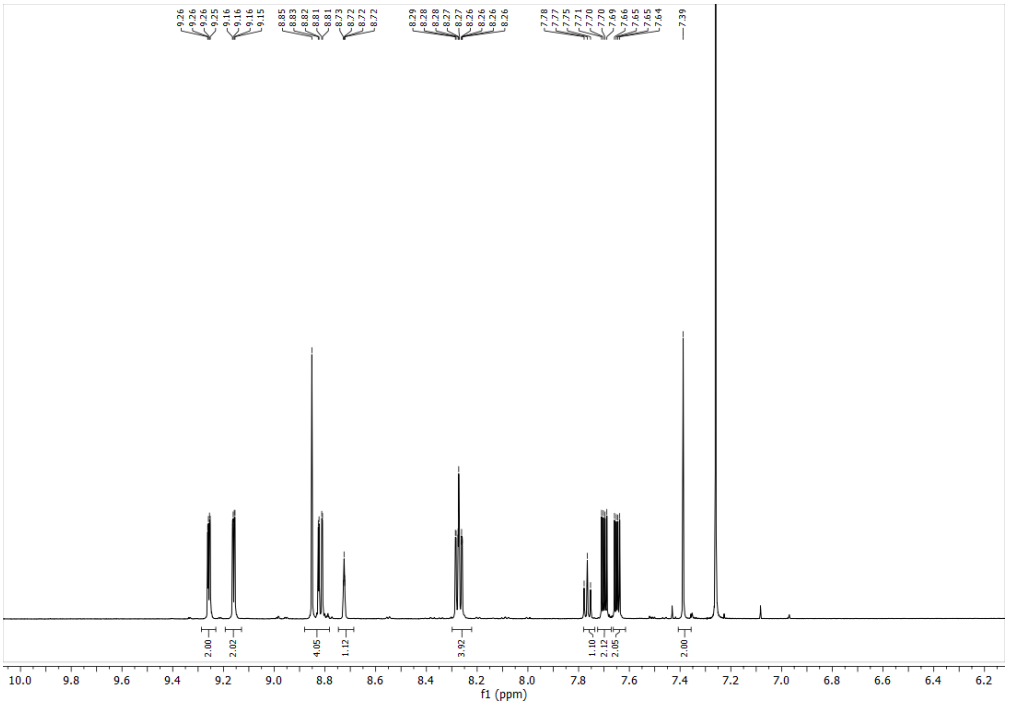

Figure C9. ^{1}H NMR spectrum (600 MHz) for compound **16** in $CDCl_3$.

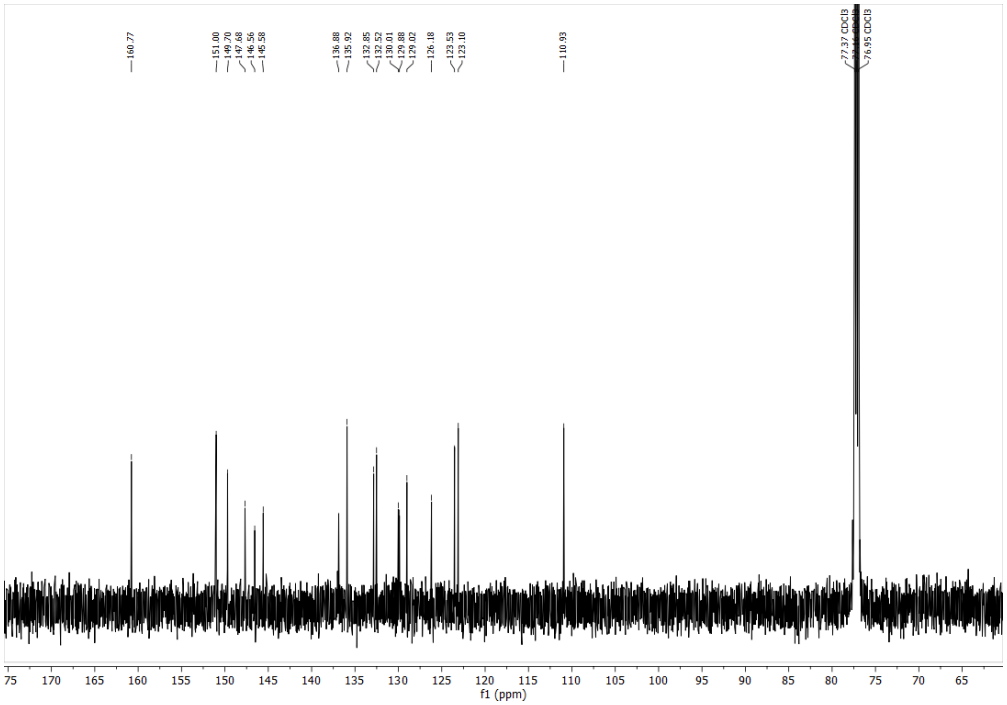

Figure C10. ^{13}C NMR spectrum (151 MHz) for compound **16** in $CDCl_3$.

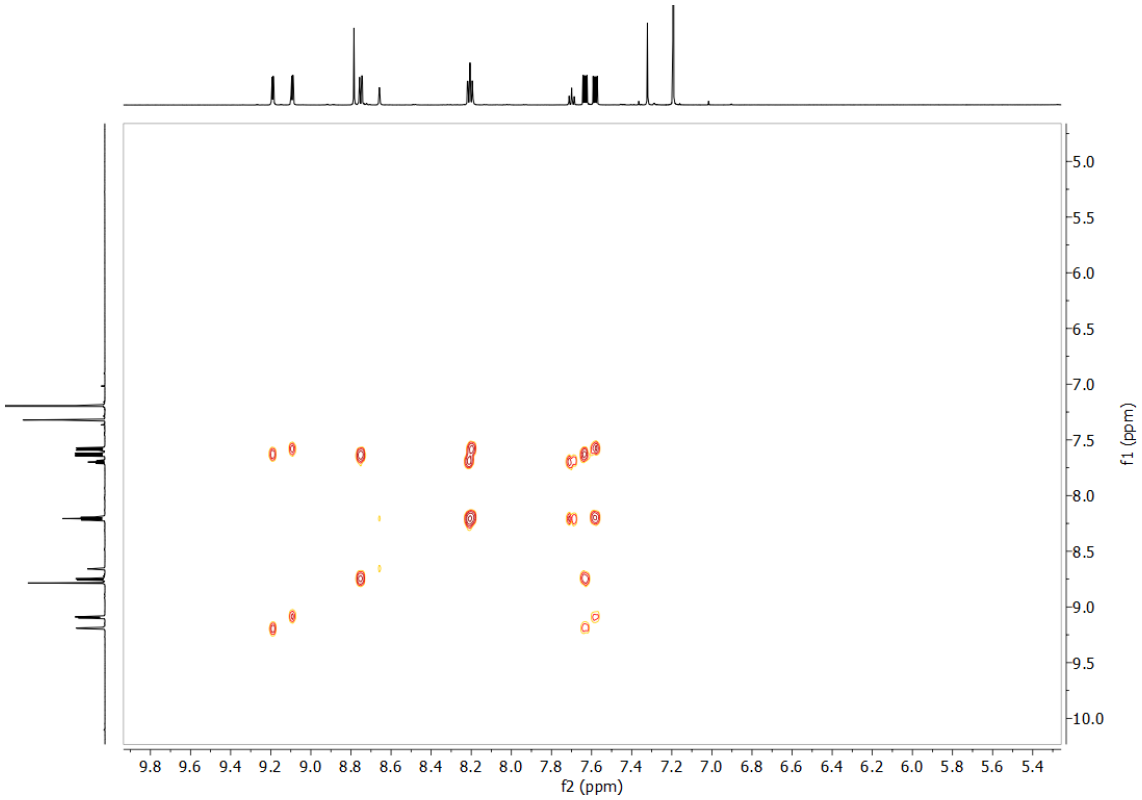

Figure C11. COSY NMR spectrum for compound **16** in $CDCl_3$.

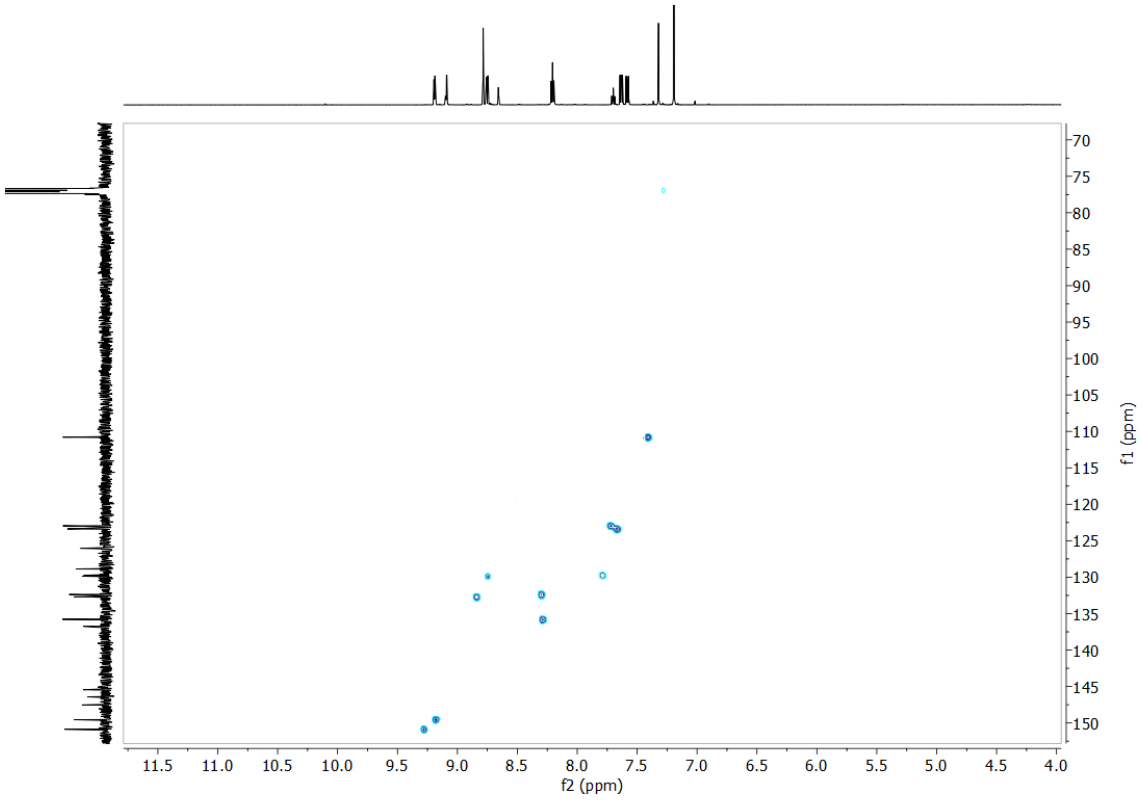

Figure C12. HSQC NMR spectrum for compound **16** in $CDCl_3$.

Ligand G_R:

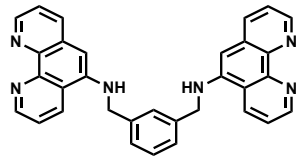

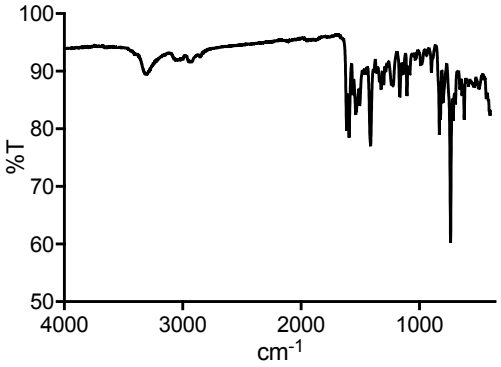

Figure C13. FTIR-ATR for ligand G_R.

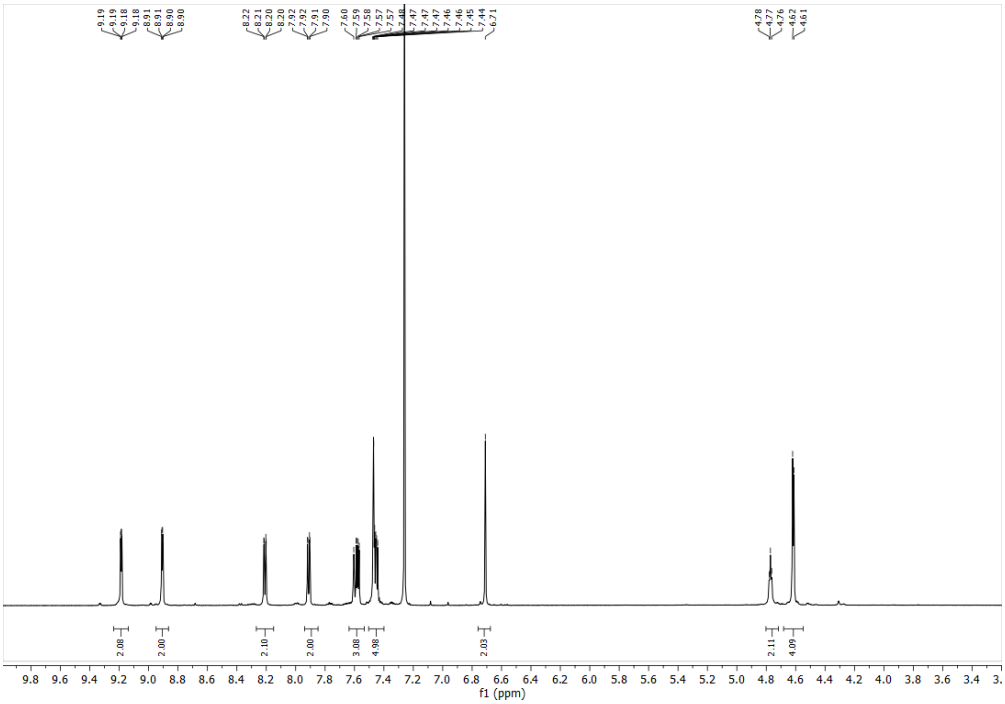

Figure C14. ^{1}H NMR spectrum (600 MHz) for ligand G_R in $CDCl_3$.

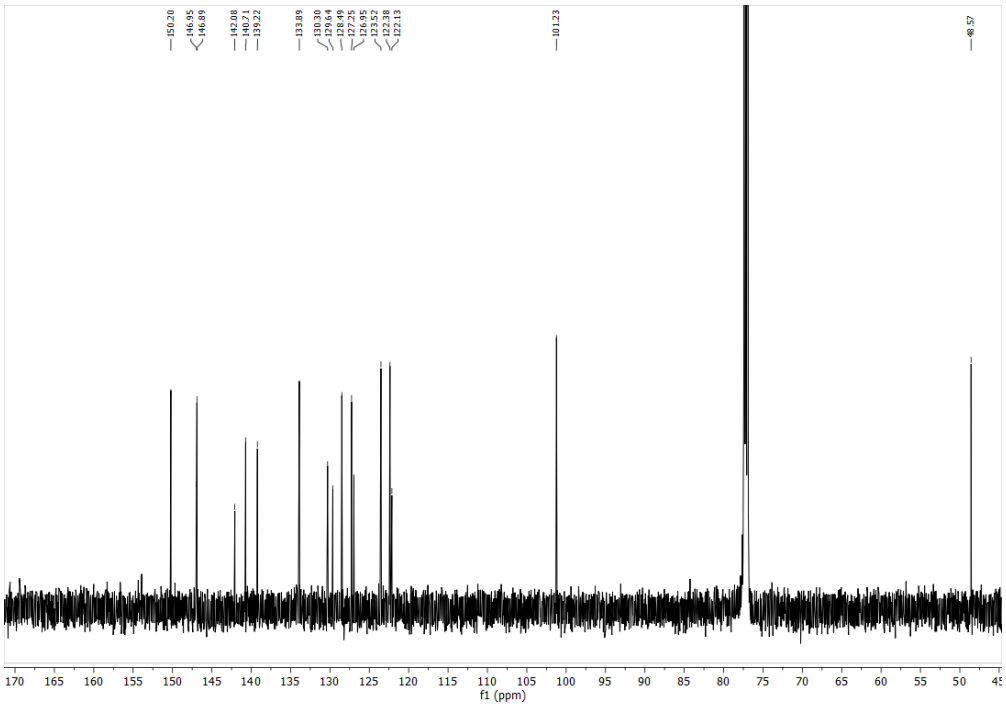

Figure C15. ^{13}C NMR spectrum (151 MHz) for ligand $\mathbf{G_R}$ in $CDCl_3$.

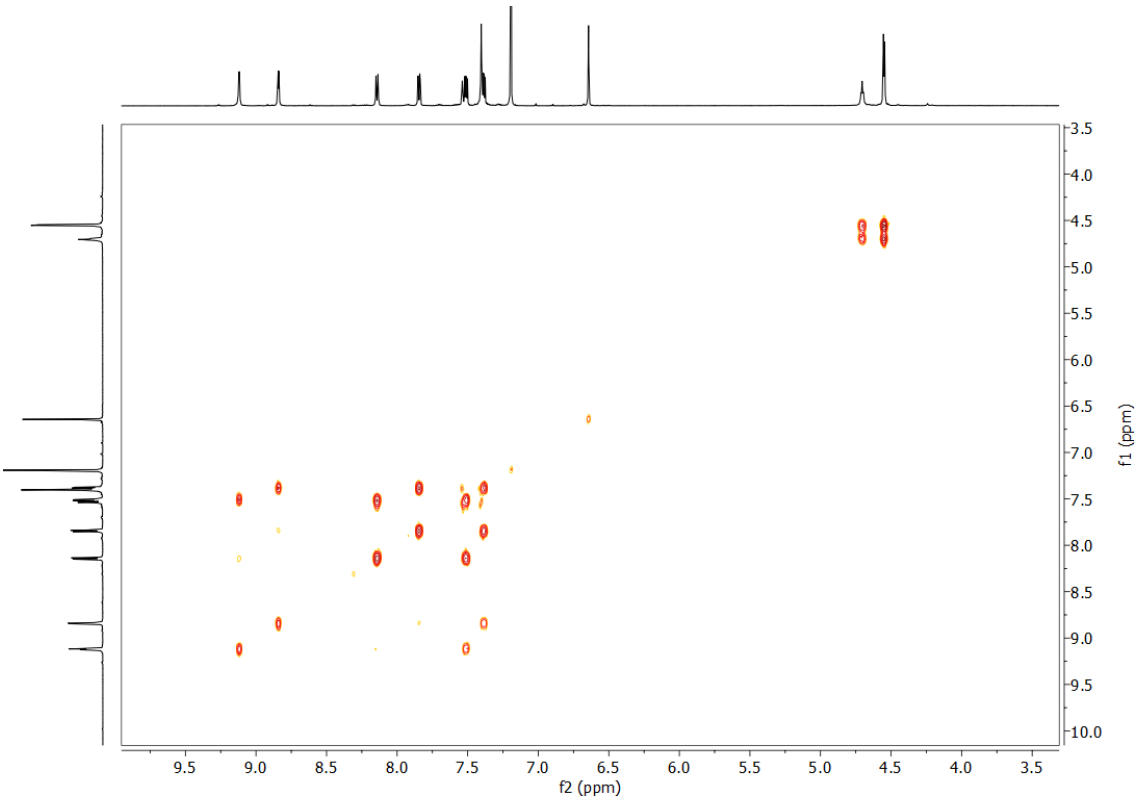

Figure C16. COSY NMR spectrum for ligand $\mathbf{G_R}$ in $CDCl_3$.

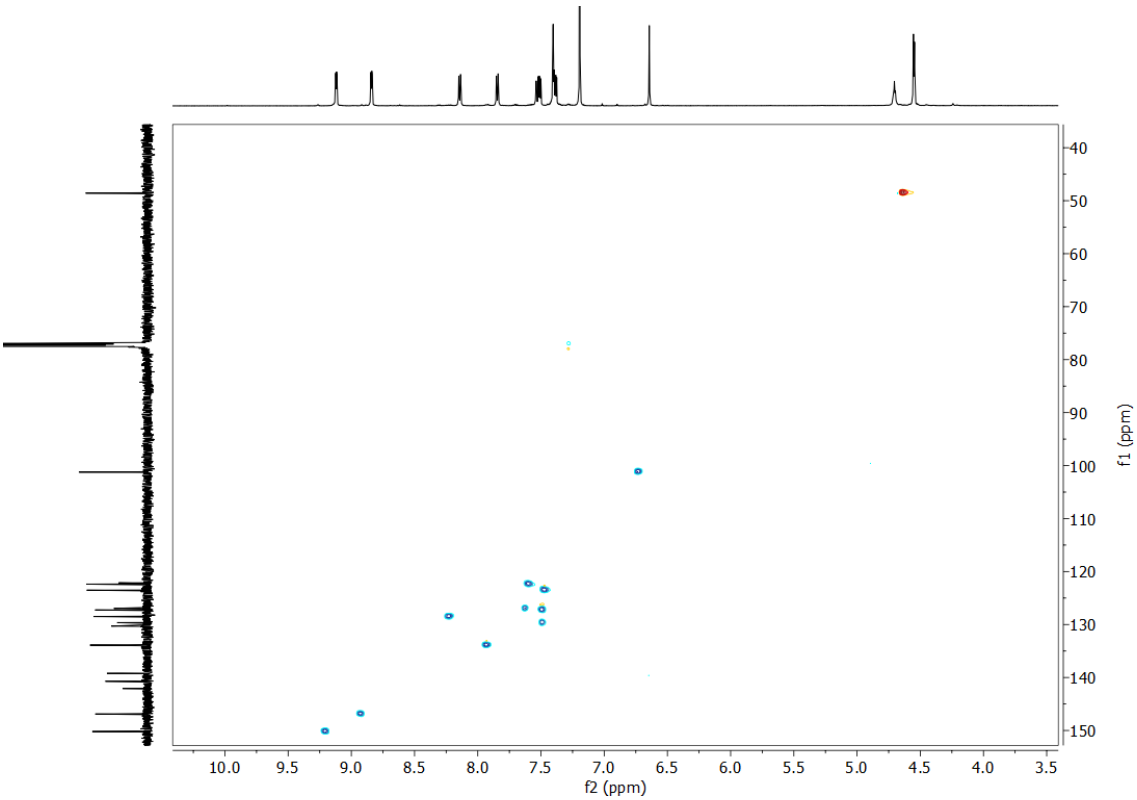

Figure C17. HSQC NMR spectrum for ligand $\mathbf{G_R}$ in $CDCl_3$.

APPENDIX D

FTIR-ATR of $[Cu_2(\mathbf{G_R})(N,N\text{-phenanthrene})_2](NO_3)_4$

$[Cu_2(G_R)(Phen)_2](NO_3)_4$:

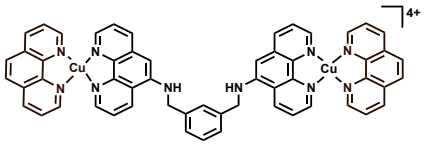

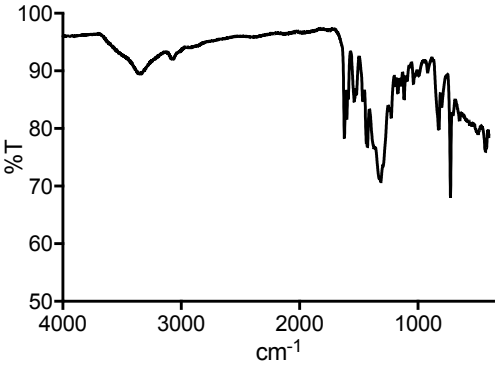

Figure D1. FTIR-ATR for $[Cu_2(\mathbf{G_R})(Phen)_2](NO_3)_4$.

$[Cu_2(G_R)(DPQ)_2](NO_3)_4$:

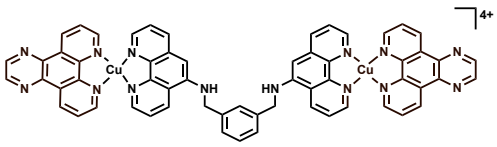

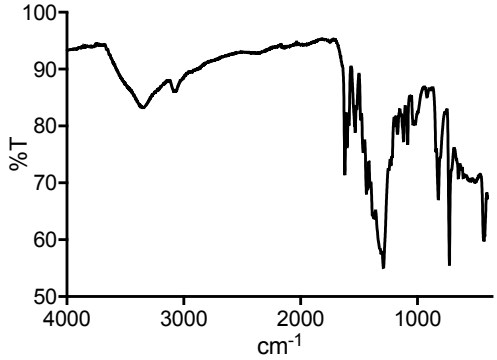

Figure D2. FTIR-ATR for $[Cu_2(\mathbf{G_R})(DPQ)_2](NO_3)_4$.

$[Cu_2(G_R)(DPPZ)_2](NO_3)_4$:

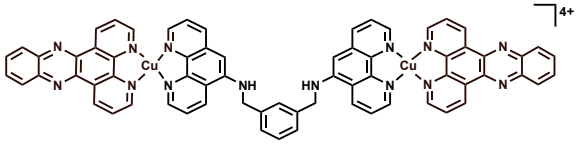

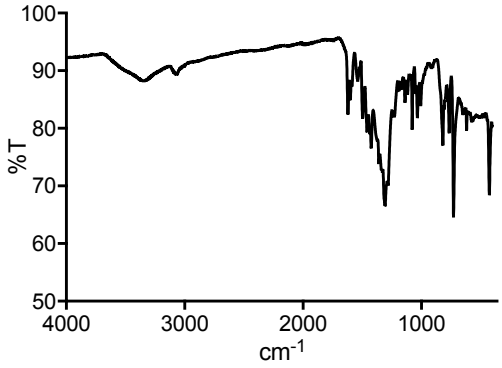

Figure D3. FTIR-ATR for $[Cu_2(\mathbf{G_R})(DPPZ)_2](NO_3)_4$.

APPENDIX E

NMR spectra, ESI-MS and FTIR-ATR of azide-functionalised Ru(II) complexes and intermediates

[Ru(1,10-phenanthroline)$_2$(5,6-epoxy-5,6-dihydro-1,10 phenanthroline)](PF$_6$)$_2$:

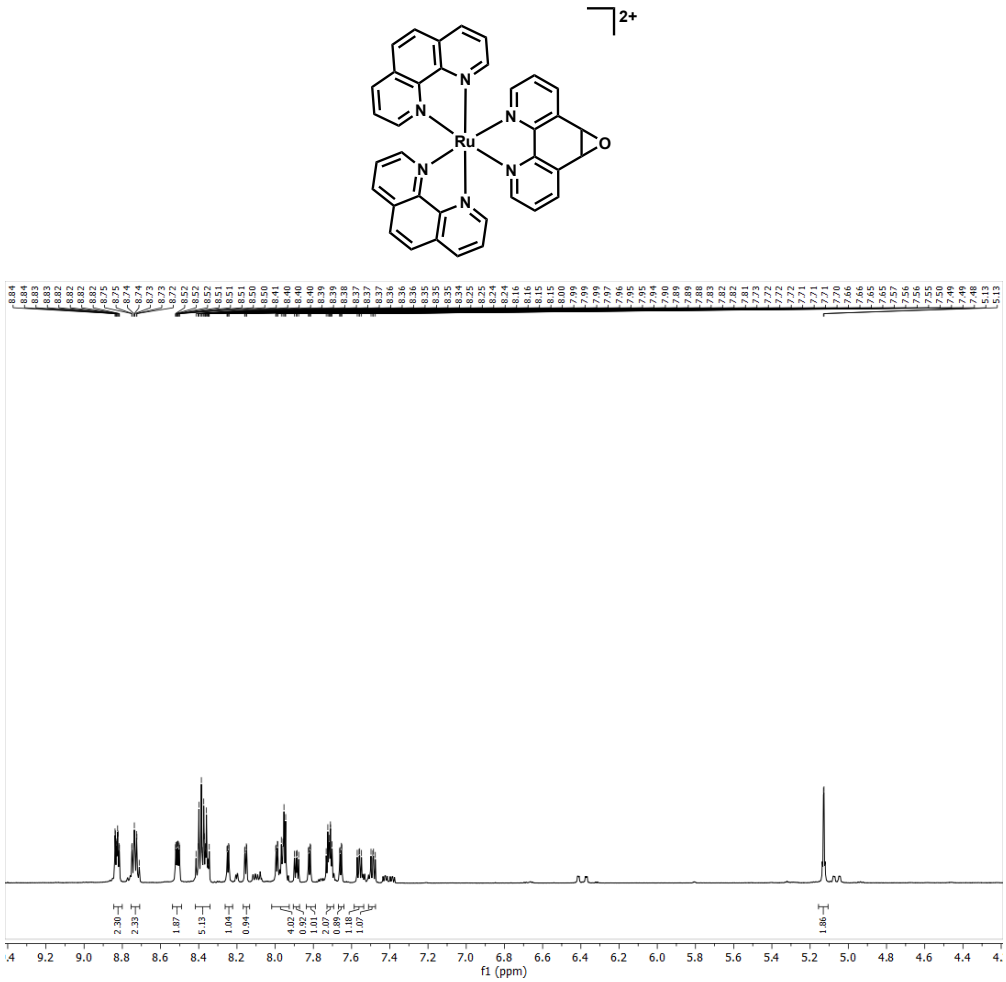

Figure E1. ^{1}H NMR spectrum (600 MHz) for [Ru(1,10-phenanthroline)$_2$(5,6-epoxy-5,6-dihydro-1,10-phenanthroline)](PF$_6$)$_2$ in DMSO-d$_6$.

[Ru(1,10-phenanthroline)$_2$(A)](PF$_6$)$_2$:

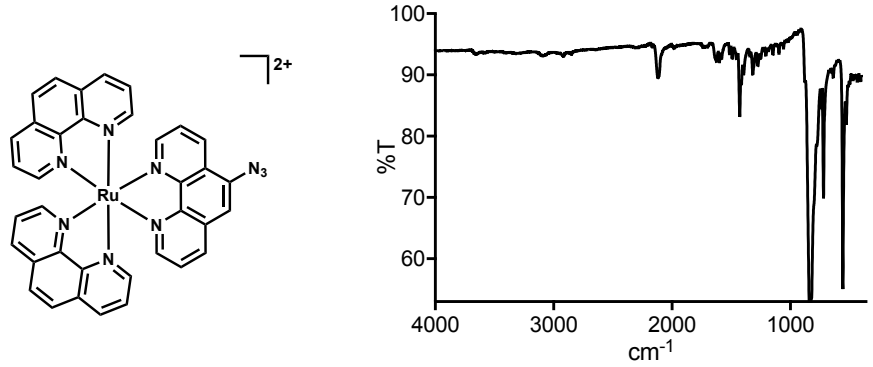

Figure E2. FTIR-ATR for [Ru(1,10-phenanthroline)$_2$(**A**)](PF$_6$)$_2$.

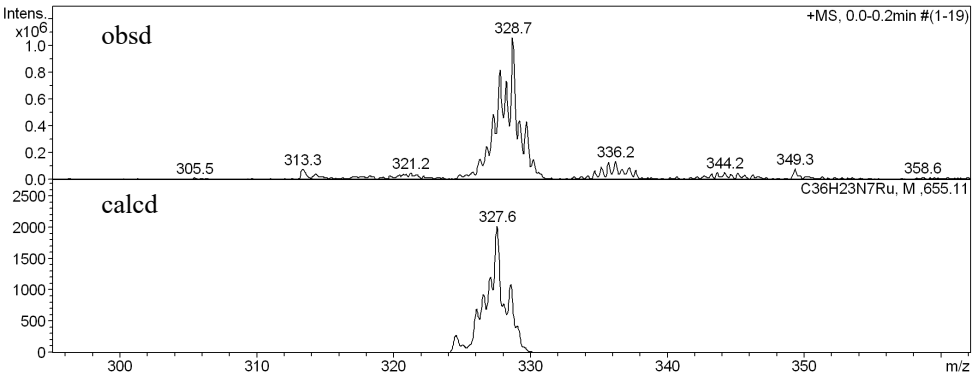

Figure E3. ESI-MS for [Ru(1,10-phenanthroline)$_2$(**A**)](PF$_6$)$_2$.

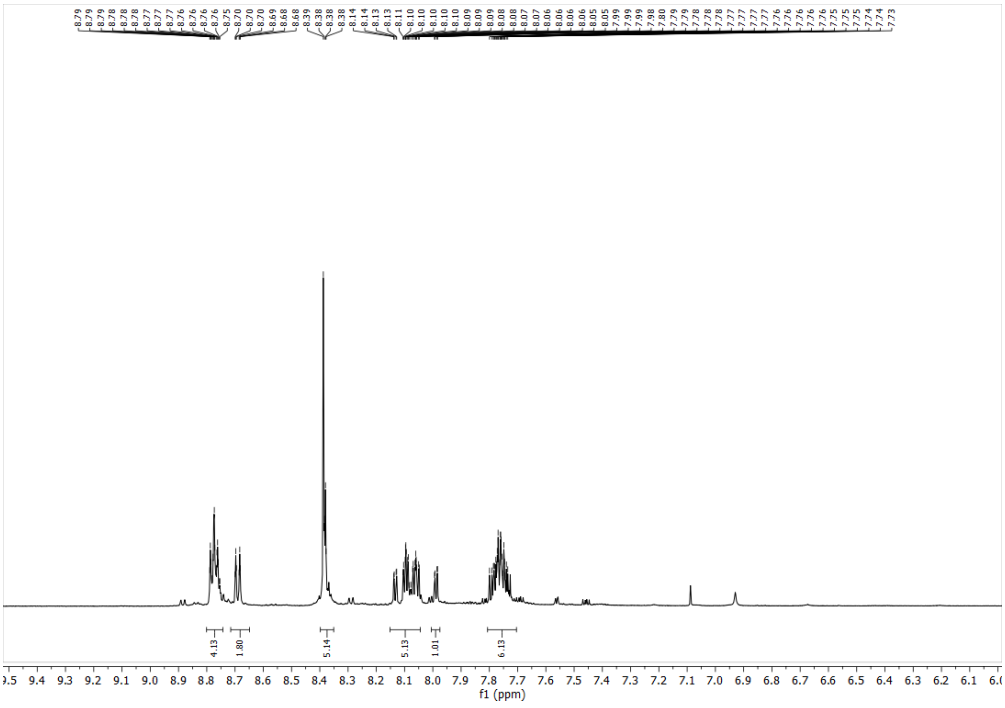

Figure E4. ^{1}H NMR spectrum (600 MHz) for [Ru(1,10-phenanthroline)$_2$(**A**)](PF$_6$)$_2$ in DMSO-*d*$_6$.

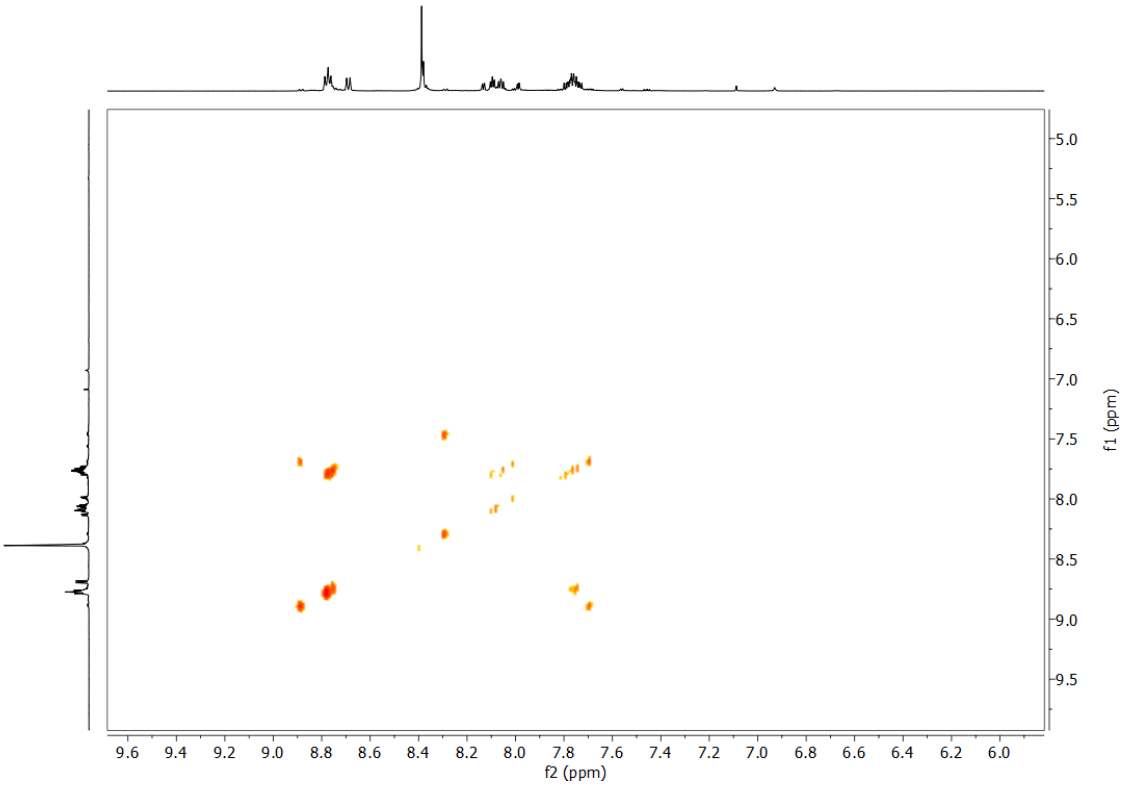

Figure E5. COSY NMR spectrum for [Ru(1,10-phenanthroline)$_2$(**A**)](PF$_6$)$_2$ in DMSO-d_6.

[Ru(1,10-phenanthroline)$_2$(3)](PF$_6$)$_2$:

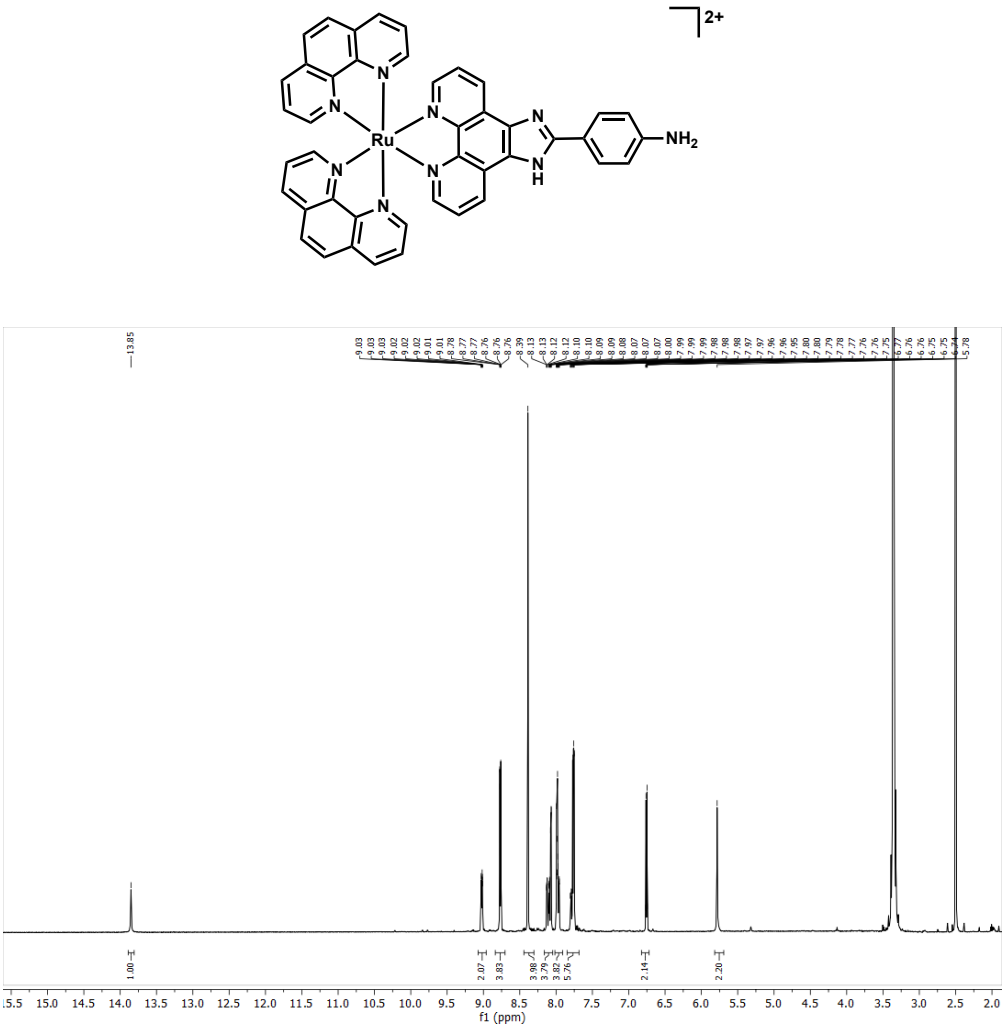

Figure E6. ^{1}H NMR spectrum (600 MHz) for [Ru(1,10-phenanthroline)$_2$(**3**)](PF$_6$)$_2$ in DMSO-d_6.

[Ru(1,10-phenanthroline)$_2$(B)](PF$_6$)$_2$:

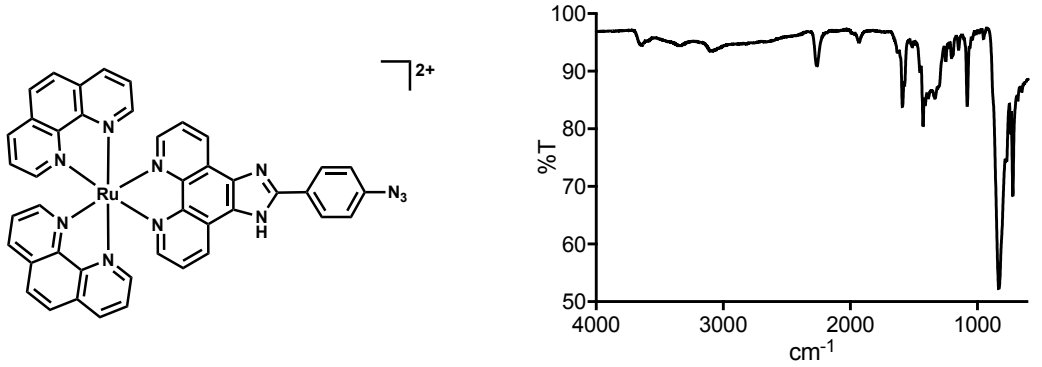

Figure E7. FTIR-ATR for [Ru(1,10-phenanthroline)$_2$(**B**)](PF$_6$)$_2$.

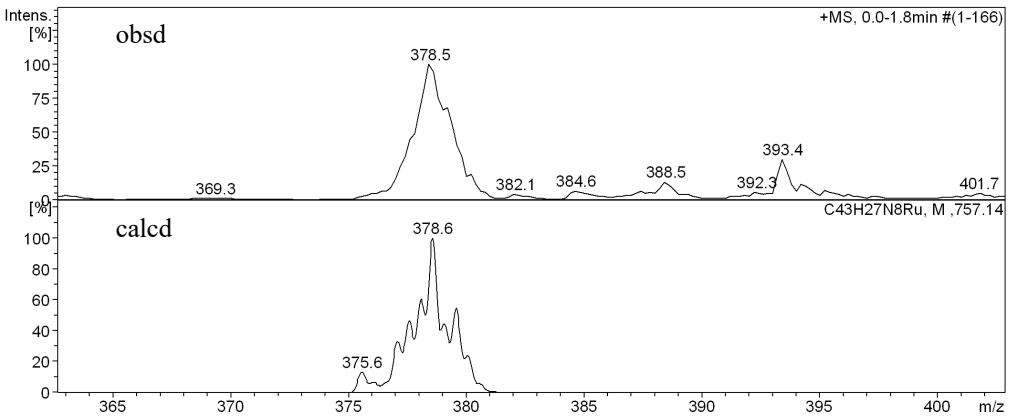

Figure E 8. ESI-MS for [Ru(1,10-phenanthroline)$_2$(**B**)](PF$_6$)$_2$.

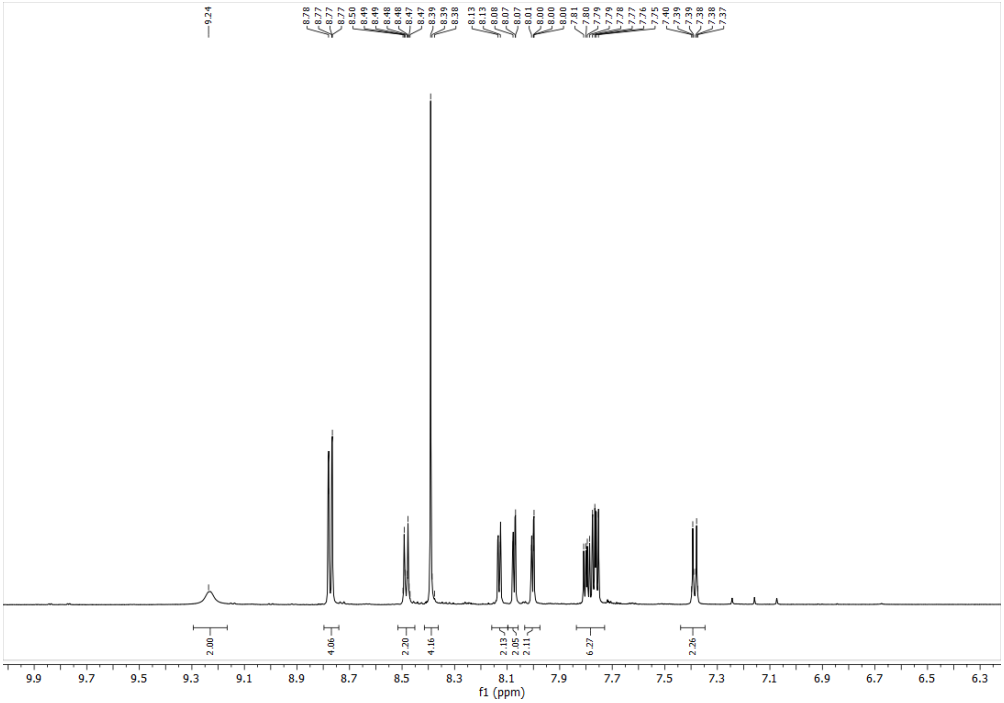

Figure E9. ^{1}H NMR spectrum (600 MHz) of [Ru(1,10-phenanthroline)$_2$(**B**)](PF$_6$)$_2$ in DMSO-d_6.

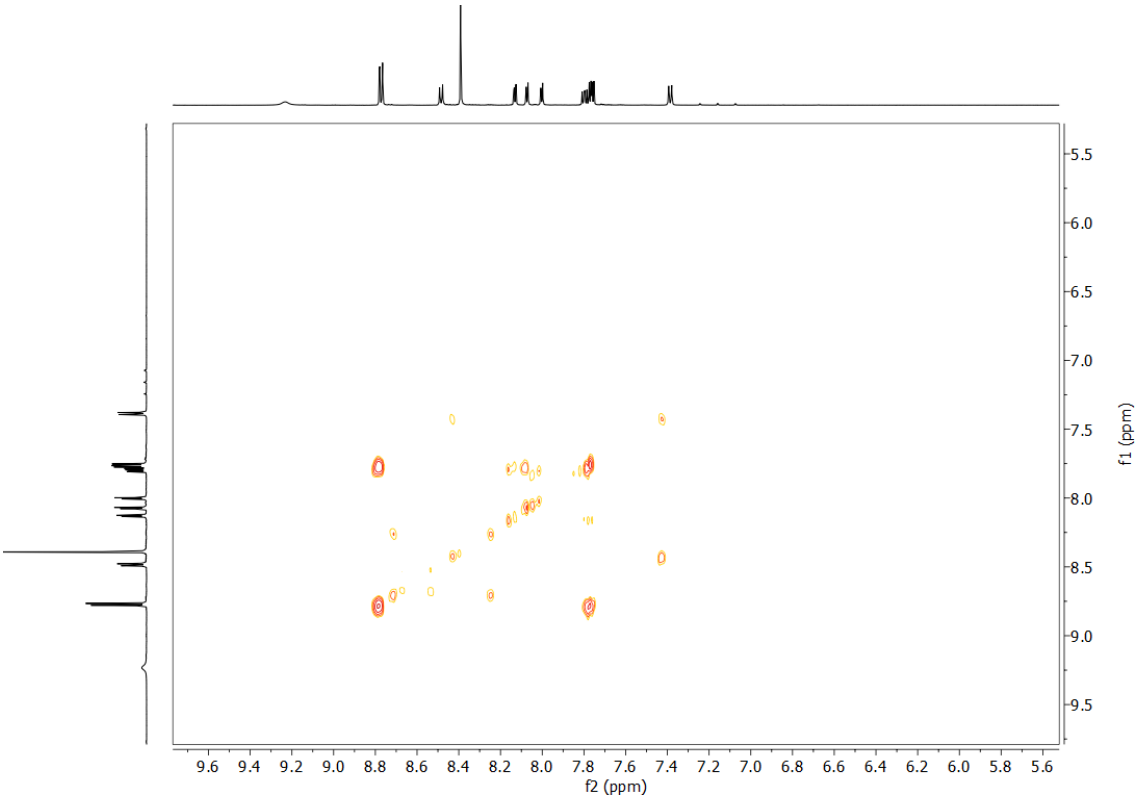

Figure E10. COSY NMR spectrum of [Ru(1,10-phenanthroline)$_2$(**B**)](PF$_6$)$_2$ in DMSO-d_6.

[Ru(1,10-phenanthroline)$_2$(5)](PF$_6$)$_2$:

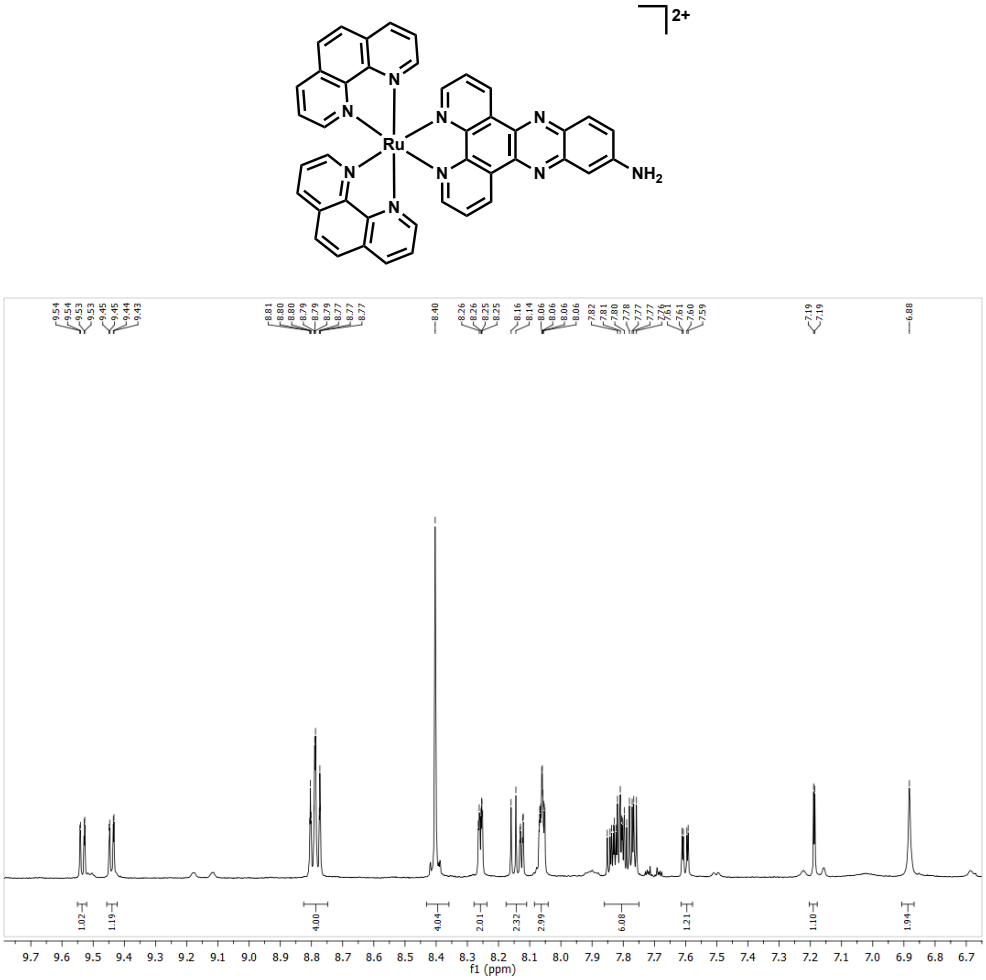

Figure E11. ^{1}H NMR spectrum (600 MHz) for [Ru(1,10-phenanthroline)$_2$(**5**)](PF$_6$)$_2$ in DMSO-*d*$_6$.

[Ru(1,10-phenanthroline)$_2$©](PF$_6$)$_2$:

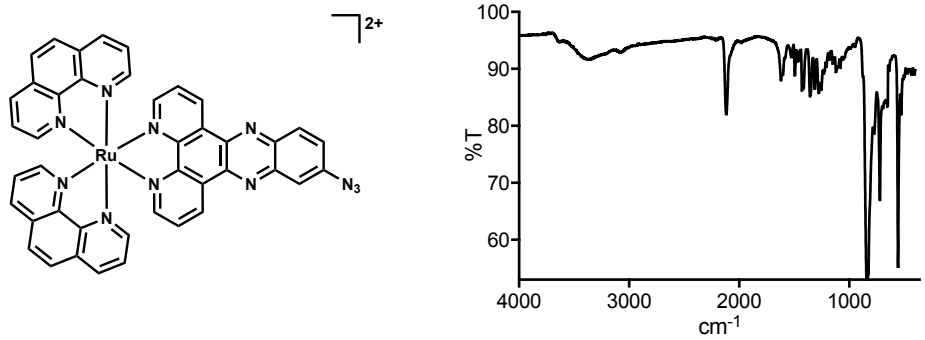

Figure E 12. FTIR-ATR for [Ru(1,10-phenanthroline)$_2$(**C**)](PF$_6$)$_2$.

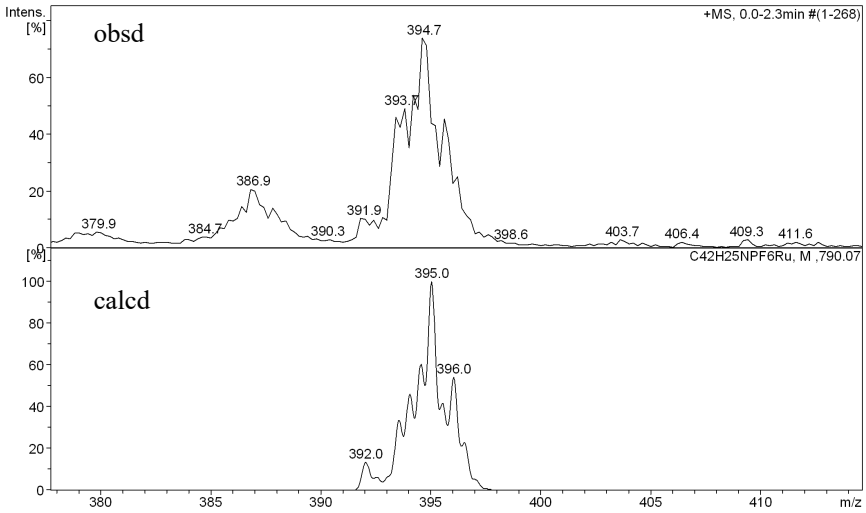

Figure E13. ESI-MS for [Ru(1,10-phenanthroline)$_2$(**C**)](PF$_6$)$_2$.

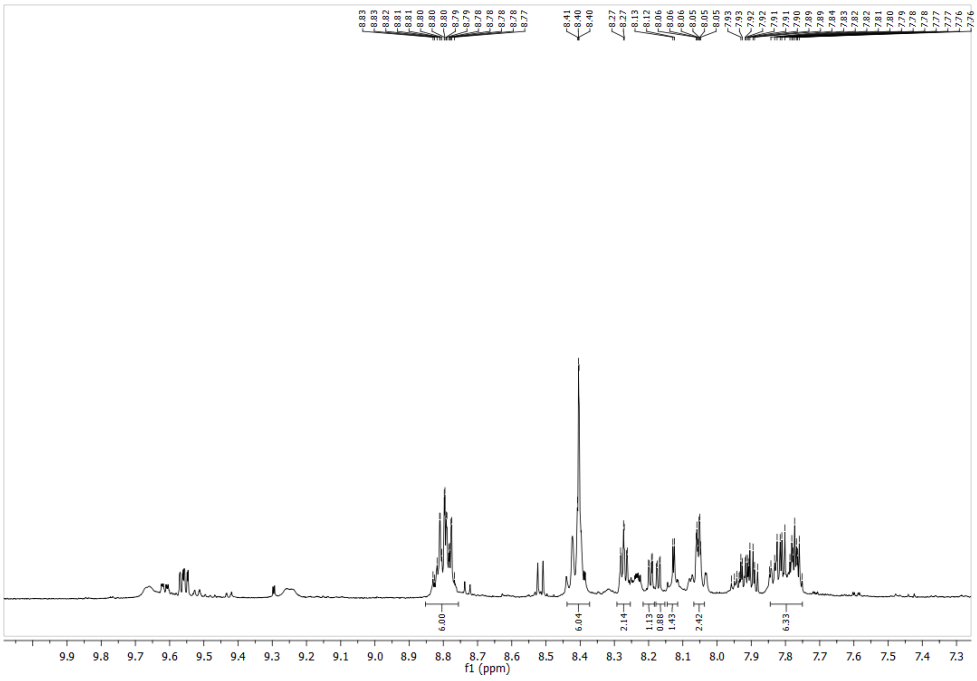

Figure E14. ^{1}H NMR spectrum (600 MHz) of [Ru(1,10-phenanthroline)$_2$(**C**)](PF$_6$)$_2$ in DMSO-d_6.

[Ru(1,10-phenanthroline)$_2$(D)](PF$_6$)$_2$:

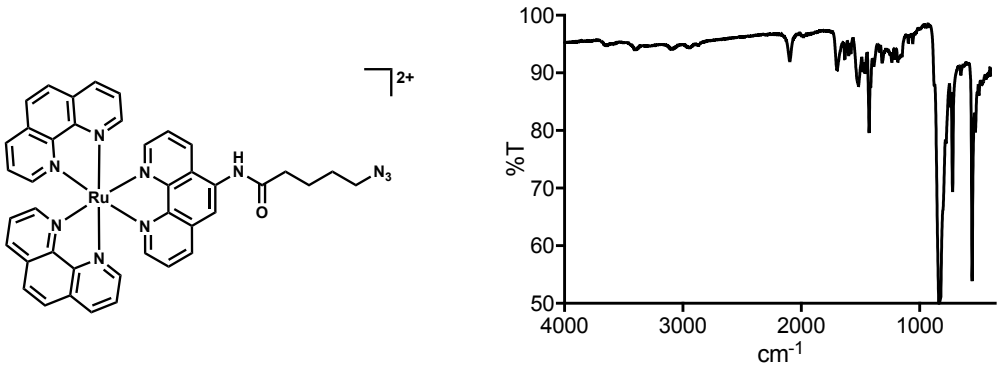

Figure E15. FTIR-ATR for [Ru(1,10-phenanthroline)$_2$(**D**)](PF$_6$)$_2$.

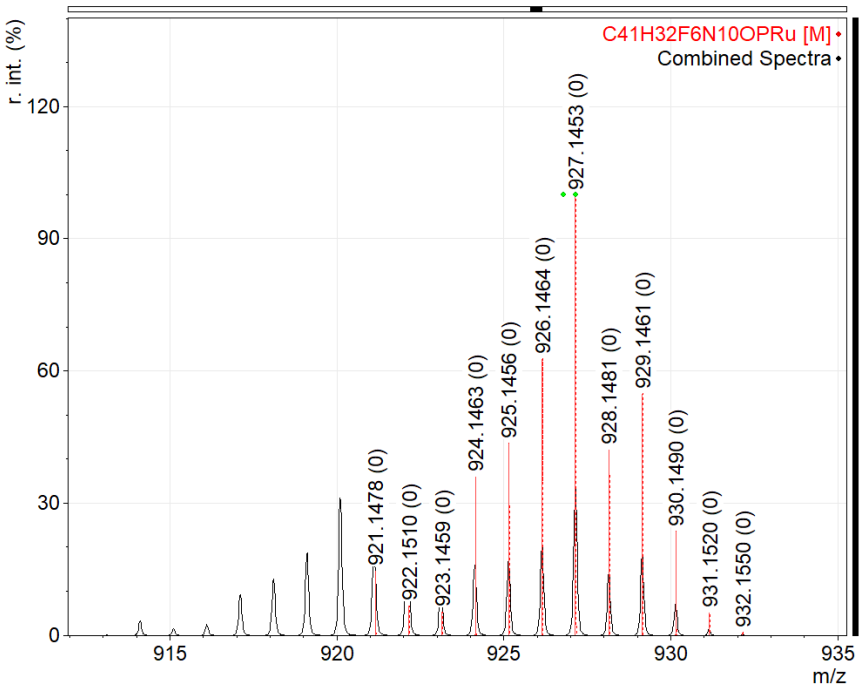

Figure E 16. ESI-MS for [Ru(1,10-phenanthroline)$_2$(**D**)](PF$_6$)$_2$.

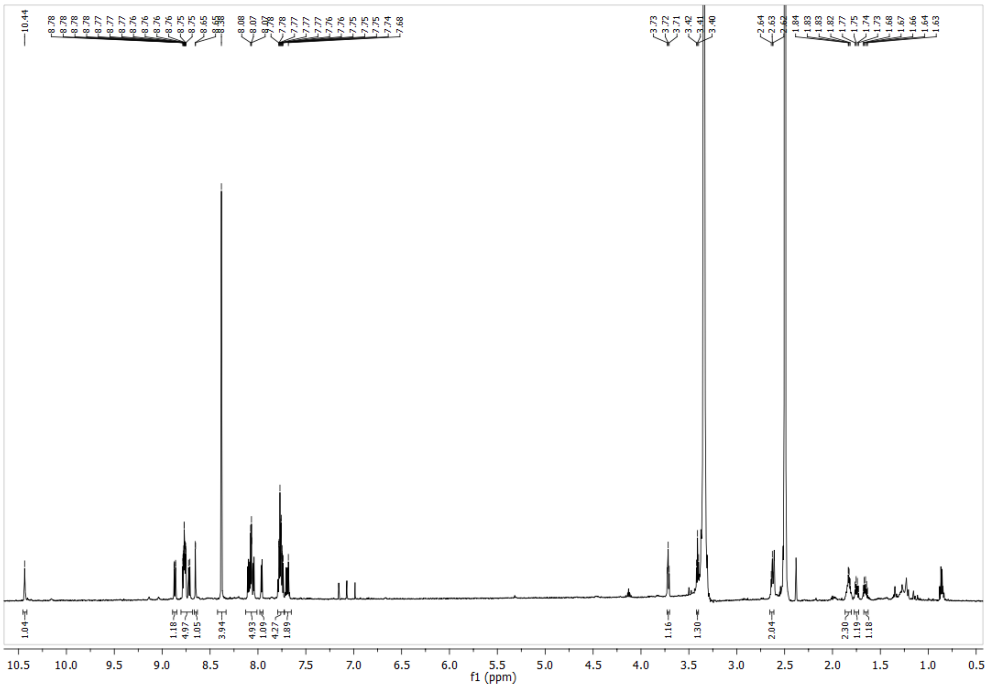

Figure E17. ^{1}H NMR spectrum (600 MHz) of [Ru(1,10-phenanthroline)$_2$(**D**)](PF$_6$)$_2$ in DMSO-d$_6$.

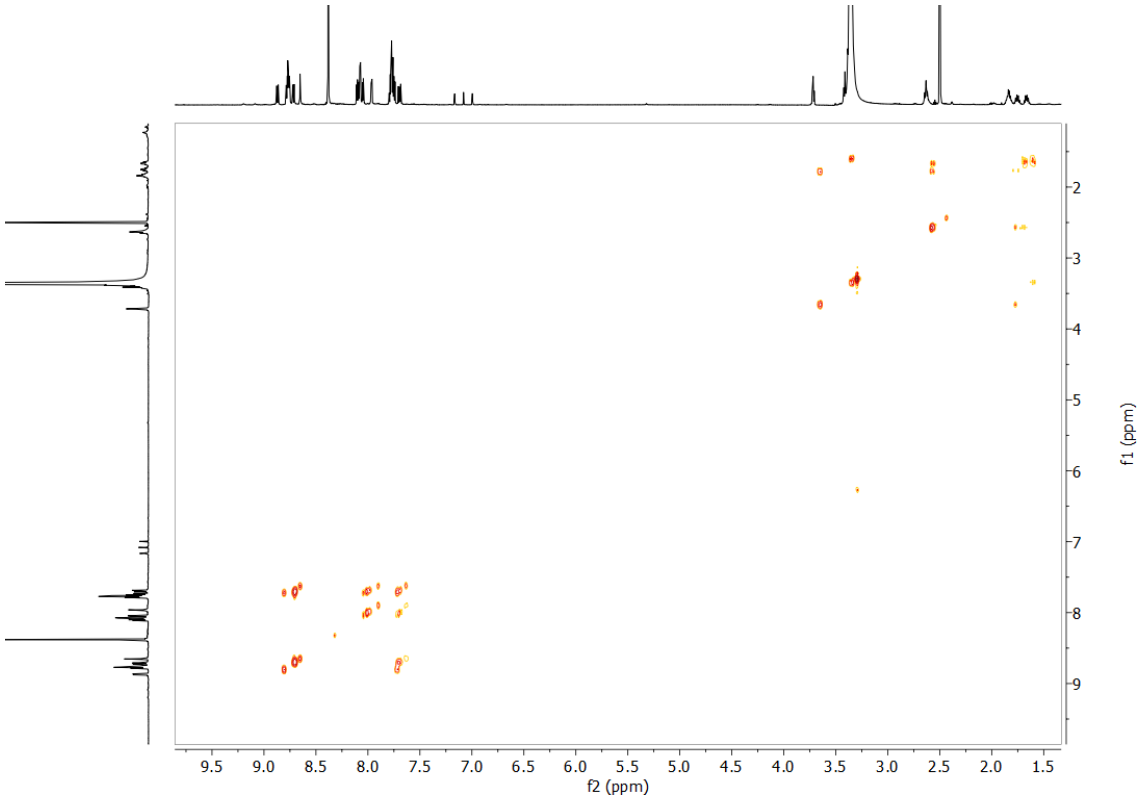

Figure E18. COSY NMR spectrum of [Ru(1,10-phenanthroline)$_2$(**D**)](PF$_6$)$_2$ in DMSO-d$_6$.

APPENDIX F

X-Ray Crystallography

Cu(A)$(NO_3)_2$

The diffraction data showed evidence of a layered structure in the crystal and the structure was refined as a 2-component pseudo-merohedral twin, twinned by rotation about the (1 0 0) axis (scales 0.686(5), 0.314(5)).[10] This is possibly an over-simplification but no attempt was made to include additional layers. The azide group is disordered between C5 and C6 with site occupancies 0.85 and 0.15, respectively. The atoms of the minor component (N3' and N4', **Figure F1**) were refined isotropically.

The copper ion is bonded to the nitrogen atoms of ligand **A** and to two nitrate ions in the basal plane and has longer axial bonds to two other nitrate ions, so it is 6-coordinate overall (**Table F1**). The nitrate anion centered on N6 acts as a monodentate ligand but the ion centered on N7 links the copper centres, via two types of bridge, to form a 1-D polymeric structure running parallel to the *c* axis. (**Figure F2**). Oxygen atom O4 bridges two copper ions (under symmetry operation -*x*+1, -*y*+1, -*z*+2), and also forms part of a 3-atom bridge to a further copper ion (under -*x*+1, -*y*+1, -*z*+1).

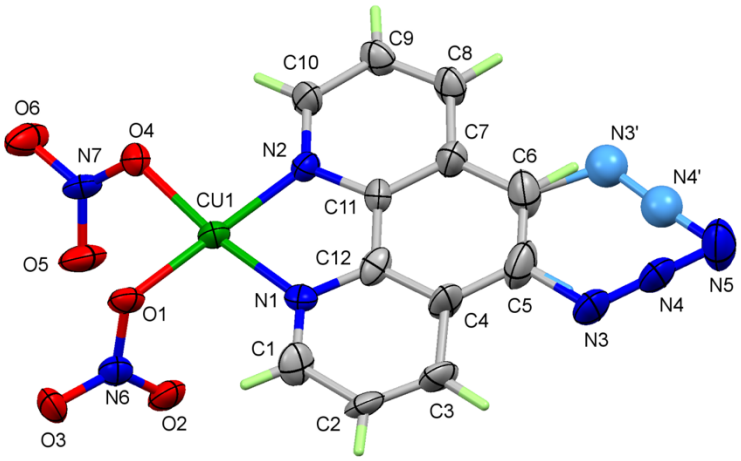

Figure F1. Structure of Cu(**A**)$(NO_3)_2$. Non-hydrogen atoms drawn with 50% displacement parameters except for the minor component of disordered azide (shown pale blue).

Table F1. Selected geometric parameters (Å, º) for Cu(**A**)$(NO_3)_2$.

Cu1—N1	1.985 (10)	Cu1—N2	1.984 (10)
Cu1—O1	1.971 (8)	Cu1—O4	1.996 (9)
Cu1—O4^{i}	2.475 (9)	Cu1—O5^{ii}	2.760 (11)
Cu1—Cu1^{i}	3.572 (4)	Cu1—Cu1^{ii}	4.670 (4)
Cu1—O4—Cu1^{i}	105.6 (4)		

Symmetry codes: (i) -*x*+1, -*y*+1, -*z*+2; (ii) -*x*+1, -*y*+1, -*z*+1.

The chains interact *via* some π-stacking involving the azide group (**Figure F3**), leading to the packing shown in **Figure F4**.

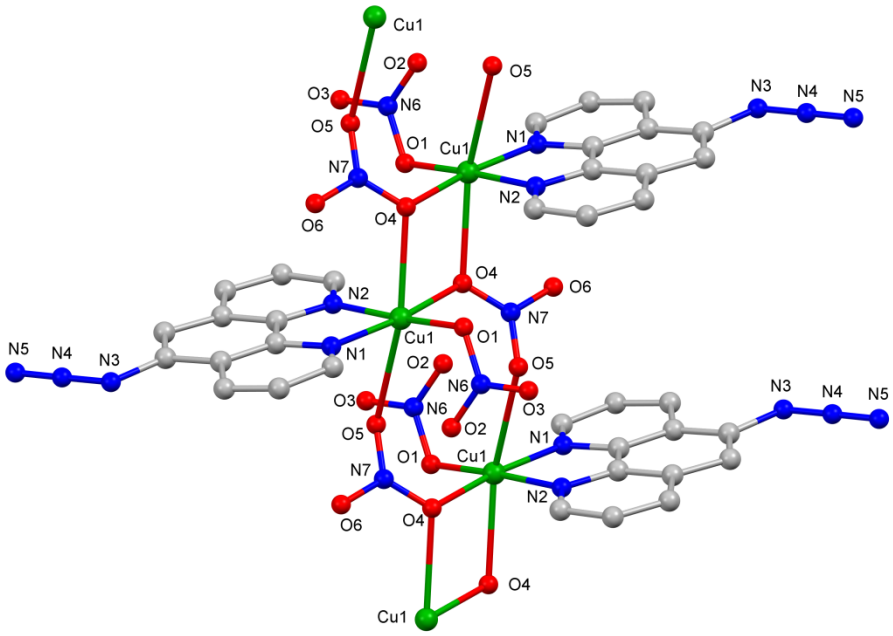

Figure F2. Polymeric structure of Cu(**A**)$(NO_3)_2$. H atoms and disorder omitted for clarity.

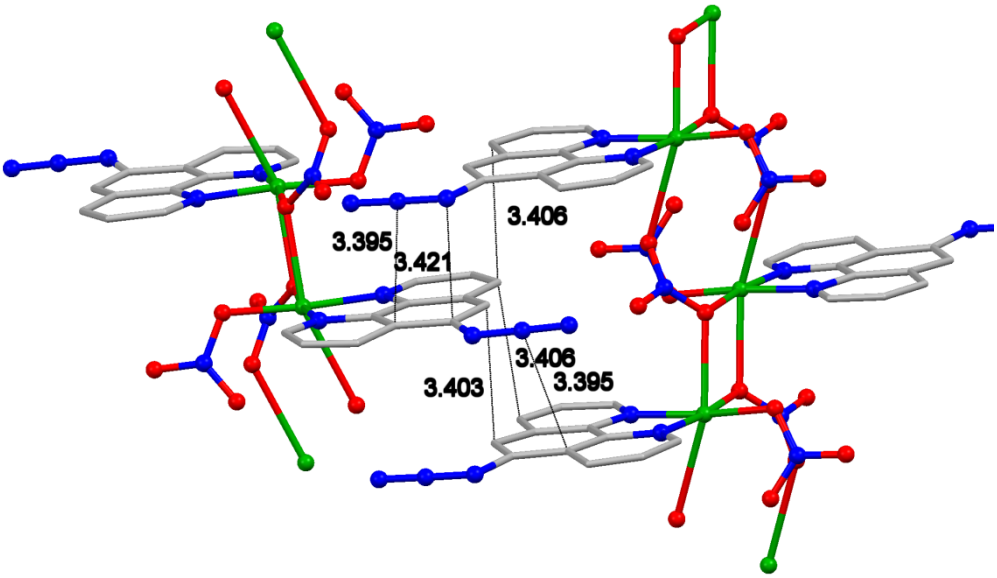

Figure F3. π-Stacking in Cu(**A**)$(NO_3)_2$.

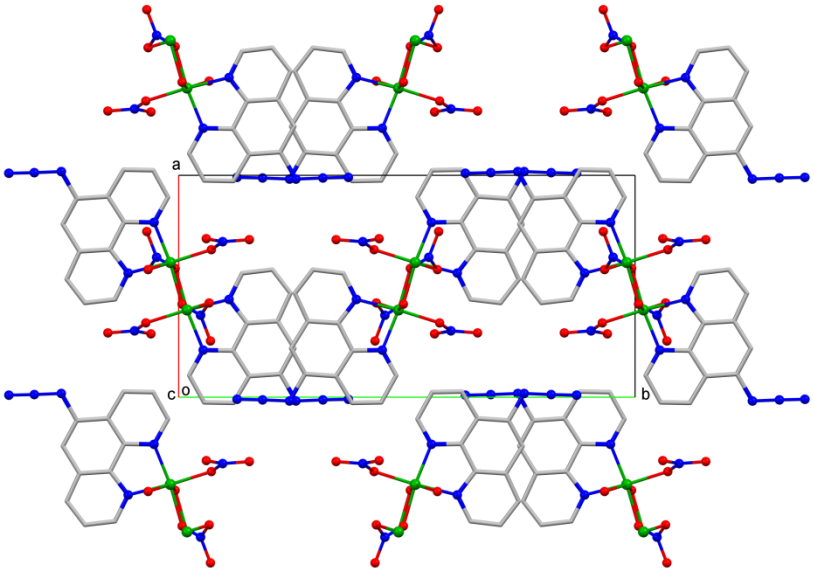

Figure F4. Packing diagram for Cu(**A**)$(NO_3)_2$ viewed down the c axis. Hydrogen atoms and disorder omitted for clarity.

(Ligand B)$_2$·2.4H$_2$O·0.8MeCN

The crystal was layered, and the structure was solved as a three-component triplet (scales 0.752(3), 0.0912(15), 0.157(3)). The compound crystallises with two independent molecules in the unit cell along with two full-occupancy water molecules and some disordered solvent (**Figure F5**). The disorder was modelled as two partial occupancy acetonitrile molecules (site occupancies 0.54 and 0.35) and two partial occupancy water molecules (both with site occupancy 0.2). The atoms of the disordered solvate were refined isotropically and the hydrogen atoms on the partial-occupancy water molecules were not located or included in the refinement.

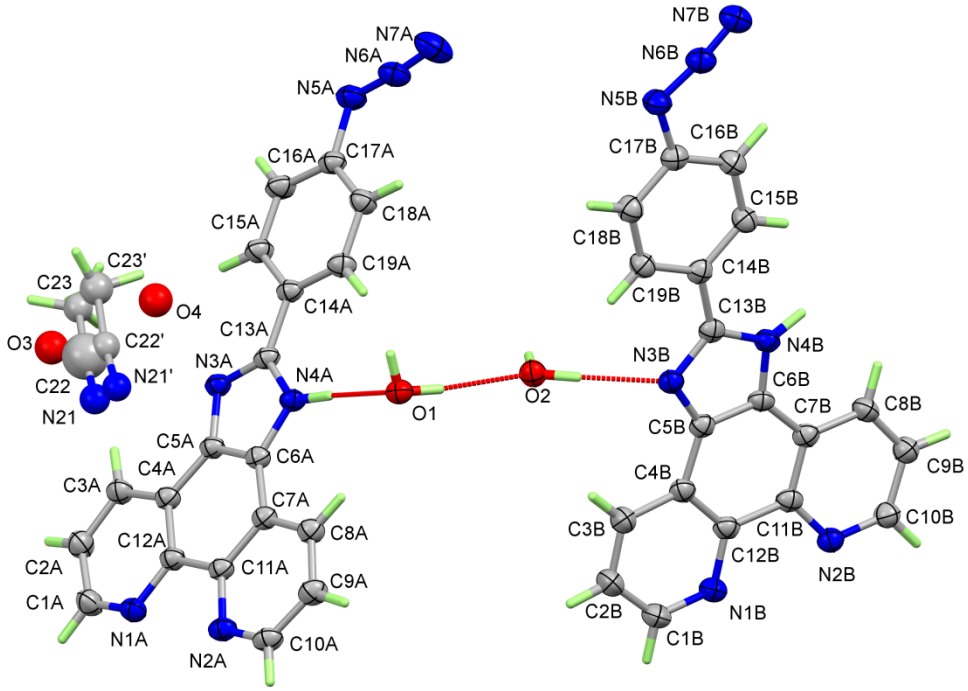

Figure F5. The asymmetric unit of (Ligand B)$_2$·2.4H$_2$O·0.8MeCN shown with 50% probability ellipsoids. Dashed red lines indicate H-bonds.

The two Ligand **B** molecules are planar (except for the azide groups) and essentially superimposable but differ in their intermolecular interactions. Hydrogen bonding *via* the full-occupancy water molecules links the molecules into 2D sheets perpendicular to *b* (**Figure F6**, **F7** and **Table F2**).

It is also evident from the packing diagram that the Ligand **B** molecules are paired by π-stacking; this is somewhat more convincing for the B molecules than for the A molecules, where the interaction is edge-to-edge (**Figure F8**).

Table F2. Hydrogen-bond geometry (Å, º) for (Ligand B)$_2$·2.4H$_2$O·0.8MeCN

D—H···*A*	*D*—H	H···*A*	*D*···*A*	*D*—H···*A*
N4*A*—H4*A*···O1	0.93 (3)	1.88 (3)	2.816 (2)	175 (2)
N4*B*—H4*B*···N1*A*^{ii}	0.92 (3)	2.21 (3)	2.890 (2)	130 (2)
N4*B*—H4*B*···N2*A*^{ii}	0.92 (3)	2.38 (3)	3.253 (3)	158 (2)
O1—H1*C*···N1*B*^{iv}	0.86 (3)	2.31 (3)	2.994 (3)	137 (3)
O1—H1*C*···N2*B*^{iv}	0.86 (3)	2.21 (3)	2.970 (2)	147 (3)
O1—H1*D*···O2	0.89 (4)	1.98 (4)	2.855 (2)	172 (3)
O2—H2*C*···N3*A*^{v}	0.95 (3)	1.95 (3)	2.861 (2)	161 (3)
O2—H2*D*···N3*B*	0.94 (4)	1.91 (4)	2.850 (3)	176 (3)

Symmetry codes: (i) -*x*+1, -*y*+1, -*z*; (ii) *x*+1, *y*, *z*-1; (iii) *x*+1, *y*, *z*; (iv) *x*-1, *y*, *z*; (v) -*x*+1, -*y*+1, -*z*+1.

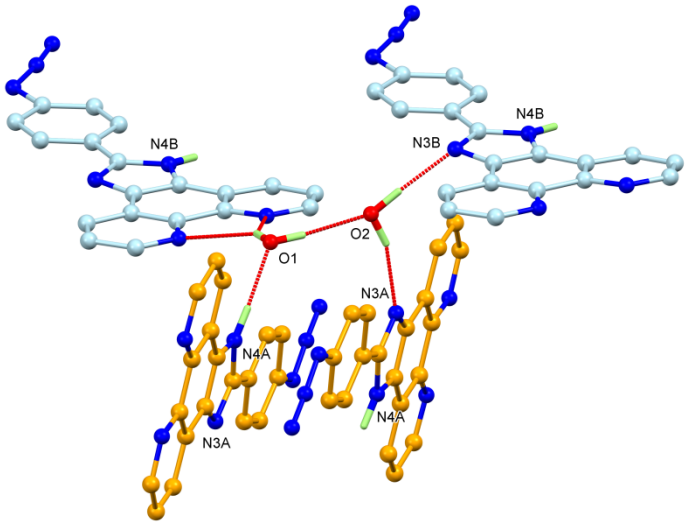

Figure F6. Hydrogen bonds (red dashed lines) linking the two independent molecules of Ligand **B**. Molecule A is drawn with orange carbon atoms and molecule **B** with pale blue carbon atoms. Hydrogen bonds not involved in H-bonding omitted.

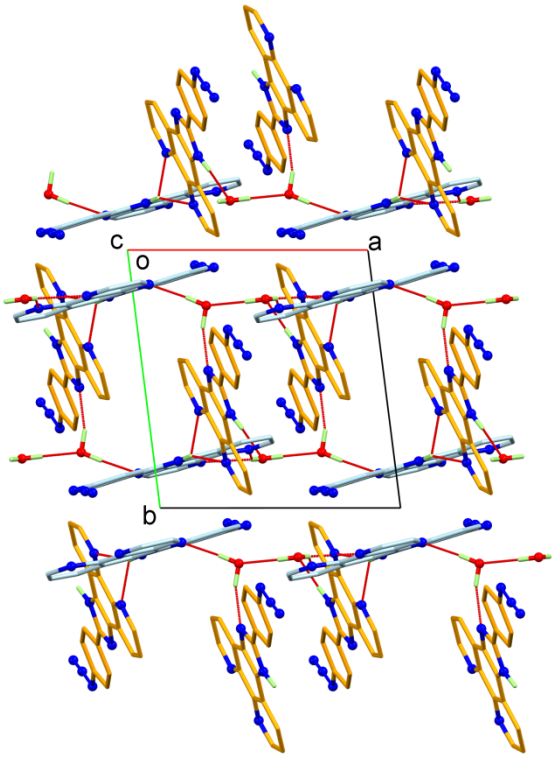

Figure F7. Packing diagram for (Ligand **B**)$_2$·2.4H_2O·0.8MeCN viewed down the c axis. Carbon atoms orange for Molecule A and pale blue for molecule **B**. Disordered solvate omitted.

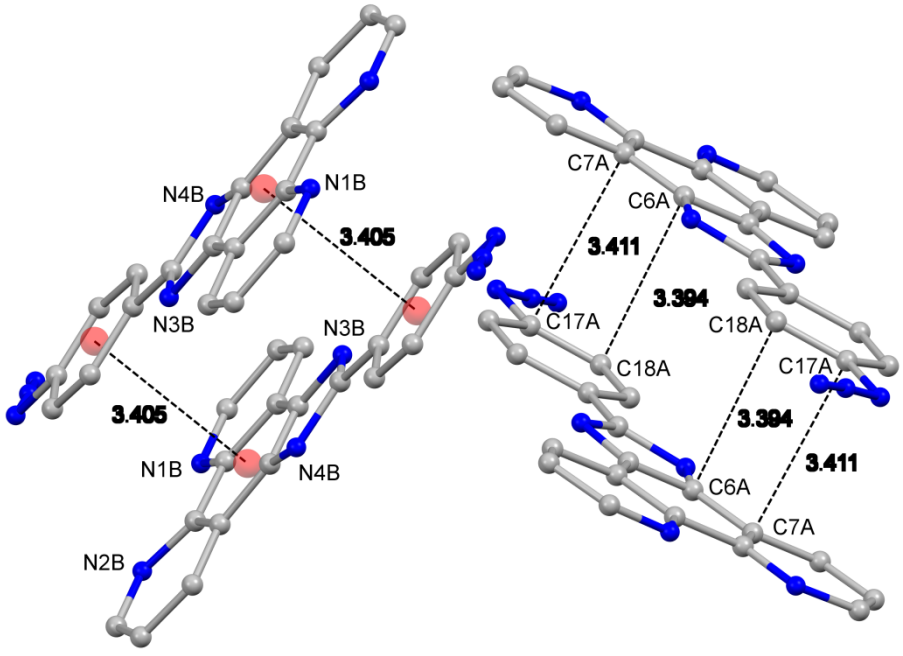

Figure F8. Dimerisation of Ligand **B** molecules by π-interactions. The figure shows centroid-centroid distances (in Å) for the B molecules and interatomic distances for the A molecules.

Ligand C·0.65MeCN

These were very poor-quality crystals, giving streaky diffraction patterns. The structure was solved and refined as the main component of a triplet using HKLF4 data (as these gave better results than HLKF5). Some solvate is present, disordered in narrow channels running parallel to the b axis. The solvent is modelled as a partial occupancy acetonitrile molecule with isotropic displacement parameters. However, its geometry is not good and it has a short interaction (2.79Å) with the neighbouring phen group. Attempts to use SQUEEZE to account for this electron density instead of modelling it was not successful. Although the data and refinement are not of high quality, the main features of the Ligand **C** molecule are clear.

The Ligand **C** molecule is shown in **Figure F9**, as expected it is planar (rms deviation from mean plane = 0.0499Å). Molecules are stacked in columns parallel to the *b* axis (**Figure F10** and **F11**).

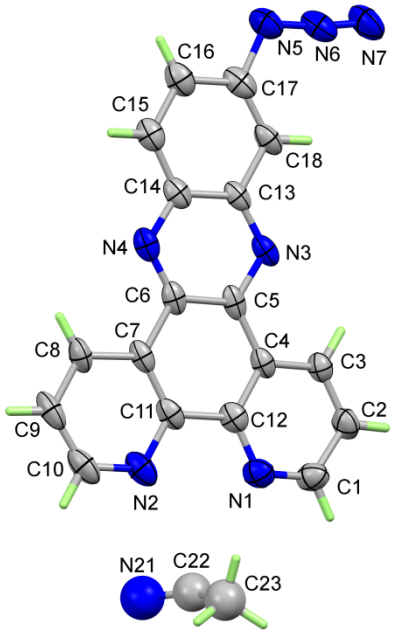

Figure F9. Asymmetric unit of Ligand C·0.65MeCN. Non-hydrogen atoms with full occupancy are shown as 50% probability ellipsoids.

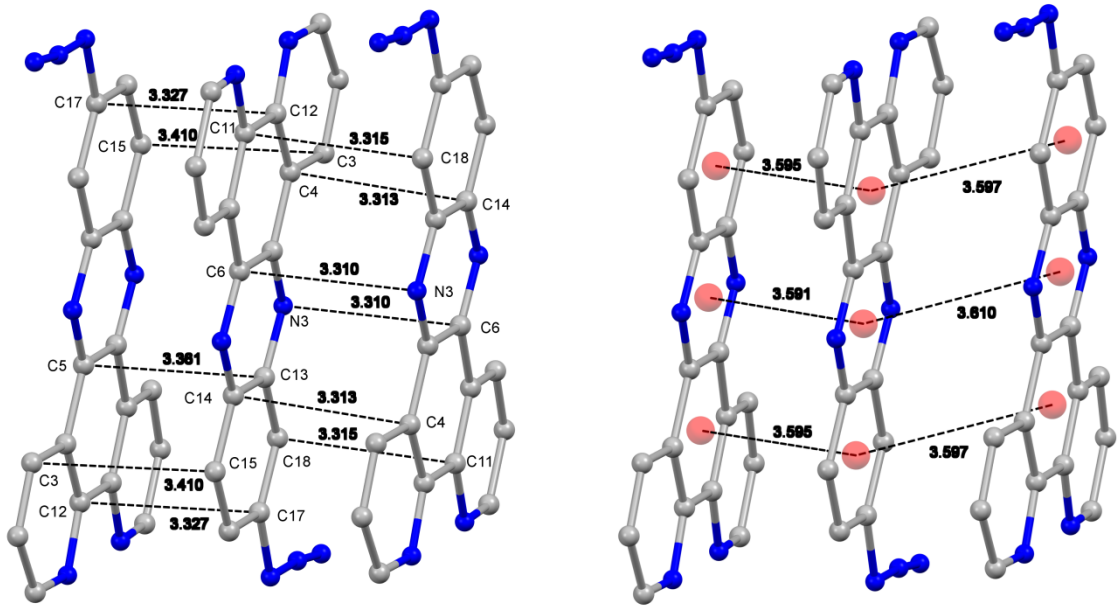

Figure F10. The π-stacking in Ligand **C**·0.65MeCN. Red spheres indicate ring centroids.

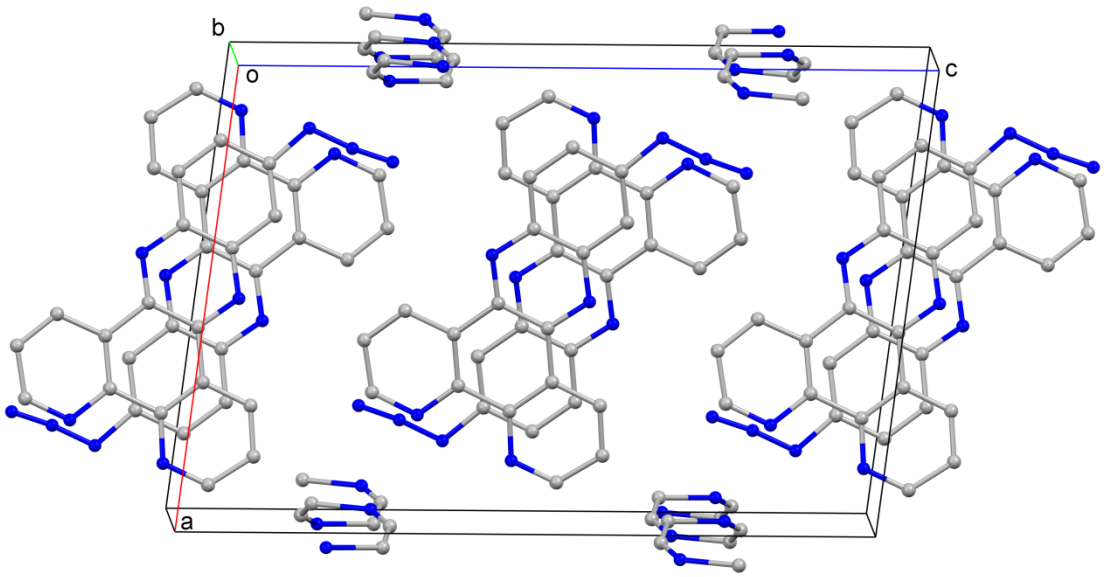

Figure F11. Packing diagram for Ligand **C**·0.65MeCN.

Ligand D·2H$_2$O

Data from the small, weakly-diffracting crystal were refined as a 2-component twin (scales 0.546(3), 0.454(3)) by rotation of 180° around [0.00 1.00 -0.00] (reciprocal) or [0.06 0.95 0.29] (direct).

The formula unit is shown in **Figure F12**; it comprises the substituted one molecule of Ligand D and two solvate water molecules. Most of the bonds in the molecule are as might be expected but the multiple bonding in the azide group, coupled with the weak diffraction and twinning, mean that the bond distances for that region are not very well defined.

The mean plane of the amide group is tilted relative to the plane of the phen in order to permit an intermolecular N-H···O=C hydrogen bonds (N3···O1 2.865 (4) Å under symmetry operation x+1, y, z), there is also some π-stacking between adjacent phen groups (**Figure F13**).

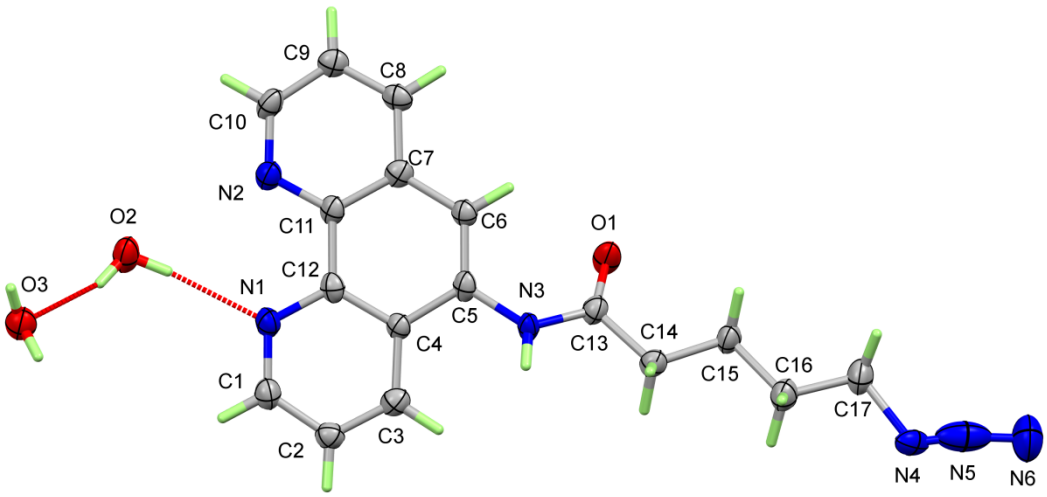

Figure F12. The asymmetric unit of Ligand **D**·2H$_2$O. Non-hydrogen atoms are shown with 50% probability ellipsoids and hydrogen bonds are shown as dashed red lines.

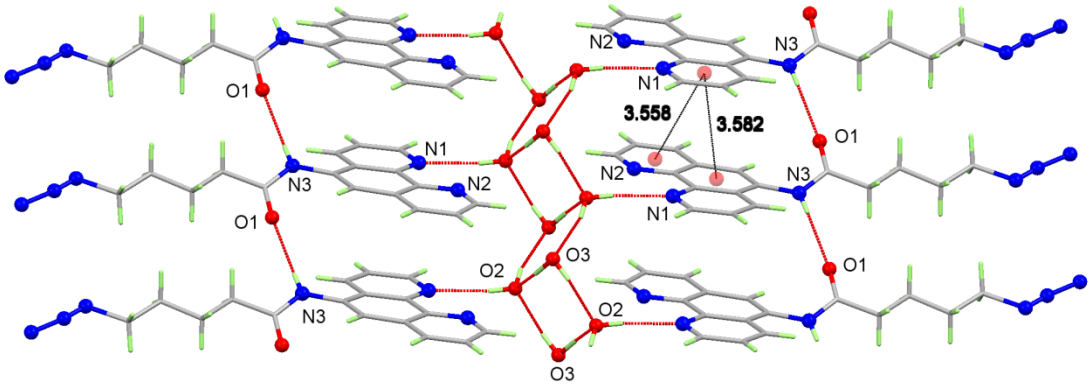

Figure F13. Hydrogen bonding (dashed red lines) and π-stacking interactions in Ligand **D**·2H$_2$O. Translucent red spheres indicate ring centroids.

These two interactions link the organic molecules into chains running parallel to the *a* axis (**Figure F12**). Additionally, the two lattice water molecules are involved in hydrogen bonding to each other and to N1 of the phen group (**Table F3**). A ladder of hydrogen bonded water molecules runs parallel to pairs of organic chains and links them into wider ribbons (**Figure F13** and **F14**).

Table F3. Hydrogen-bond geometry (Å, º) for Ligand **D**·2H$_2$O

D—H···*A*	*D*—H	H···*A*	*D*···*A*	*D*—H···*A*
N3—H3···O1^{i}	0.83 (2)	2.09 (3)	2.865 (4)	155 (5)
O2—H2*A*···N1	0.83 (2)	2.09 (2)	2.917 (5)	174 (5)
O2—H2*B*···O3	0.83 (2)	1.95 (2)	2.750 (4)	163 (5)
O3—H3*B*···O2^{i}	0.84 (2)	1.93 (3)	2.752 (5)	166 (6)
O3—H3*C*···O2^{ii}	0.86 (2)	2.07 (3)	2.914 (5)	166 (7)

Symmetry codes: (i) *x*+1, *y*, *z*; (ii) -*x*+2, -*y*+1, -*z*.

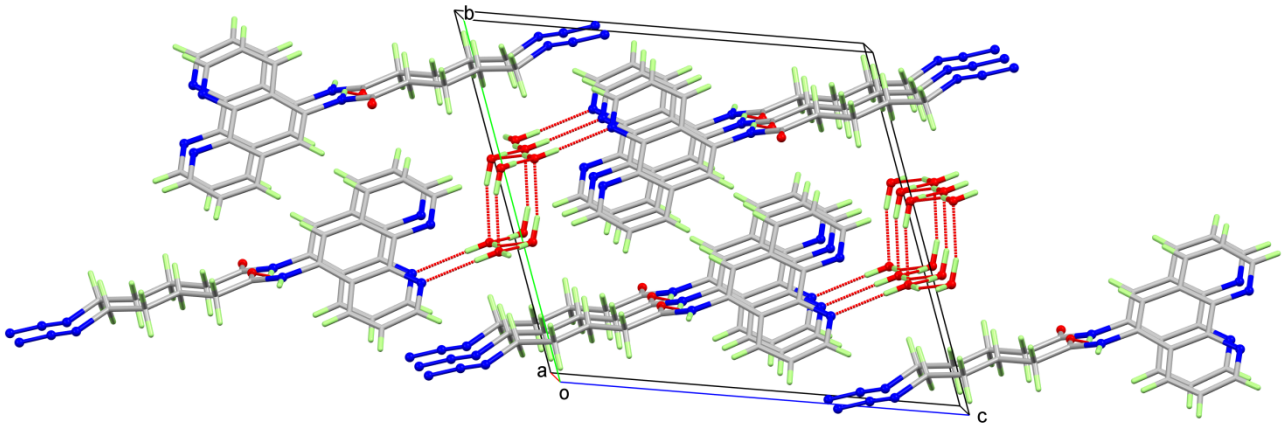

Figure F14. Packing diagram for Ligand D·2H$_2$O.

Programs used:

Olex 2. Dolomanov, O.V., Bourhis, L.J., Gildea, R.J, Howard, J.A.K. & Puschmann, H. (2009), *J. Appl. Cryst*. **42**, 339-341.

ShelXle: Hübschle, C.B., Sheldrick, G.M. & Dittrich, B. (2011) *J. Appl. Cryst*., **44**, 1281-1284.

Mercury: Macrae, C. F., Edgington, P. R., McCabe, P., Pidcock, E., Shields, G. P. Taylor, R., Towler, M. & J. van der Streek, (2006), *J. Appl. Crystallogr*., **39**, 453-457.

CrysAlisPro: Rigaku Oxford Diffraction, (2018), CrysAlisPro Software system, version 1.171.40.29a, Rigaku Corporation, Oxford, UK.

SHELXT: Sheldrick, G.M. (2015). *Acta Cryst.* **A71**, 3-8.

SHELXL: Sheldrick, G.M. (2015a). *Acta Crys*t. **C71**, 3-8.

Platon: Spek, A. L. (2009). *Acta Cryst.* D**65**, 148-155.

PublCIF: Westrip, S.P. (2010), *J. Appl. Cryst*., **43**, 920-925.

APPENDIX G

MALDI analysis of TFO hybrids

Table G1. MALDI data for all TFO hybrids generated. Standard deviation < ± 0.9%

	Calculated (m/z)							**Experimental** (m/z)						
	5'-modification			Internal modification			BCN	5'-modification			Internal modification			BCN
Ligand	**TFO 1**	**TFO 2**	**TFO 3**	**TFO 4**	**TFO 5**	**TFO 6**	**TFO 7**	**TFO 1**	**TFO 2**	**TFO 3**	**TFO 4**	**TFO 5**	**TFO 6**	**TFO 7**
A	4472.1	5908.0	8585.7	4472.1	5908.0	8585.7		4467.6	5902.5	8576.3	4439.0	5917.1	8575.7	
B	4588.3	6024.2	8701.9	4588.3	6024.2	8701.9		4585.6	6016.8	8695.8	4555.1	6031.3	8694.5	
C	4575.2	6010.1	8687.8	4574.2	6010.1	8687.8		4568.5	6002.9	8675.2	4540.0	6041.6	8702.9	
D	4571.3	6007.2	8684.9	4571.3	6007.2	8684.9		4567.8	5994.0	8671.0	4540.7	6014.8	8676.0	
E	4575.3	6011.2	8688.9	4575.3	6011.2	8688.9		4570.6	6007.7	8674.3	4543.4	6016.3	8700.0	
F	4659.3	6095.2	8772.9	4659.3	6095.2	8772.9		4650.7	6092.4	8771.8	4628.6	6106.9	8764.0	
G			8898.1			8898.1	9465.6			8902.0			8903.0	9469.0

APPENDIX H

Thermal melting analysis and electrophoresis gels

Table H1. Stabilization of triplex thermal melting induced by TFO-hybrids (**A**-**F**) in TFO1 and TFO4 when compared to unmodified TFO. T_M values for duplex D1 = 60.2 ± 0.3 °C. Samples were prepared in 10 mM phosphate buffer with 150 mM NaCl and 2 mM $MgCl_2$ (pH = 6.0).

	Ligand	**TFO 1**	**TFO 4**
T_M (°C)	TFO–≡	ND	ND
ΔT_M (°C)	A	18.4 ± 0.3	< 20
	B	30.3 ± 0.1	ND
	C	30.8 ± 0.5	23.1 ± 0.1
	D	< 20	< 20
	E	< 20	< 20
	F	32.5 ± 0.0	22.5 ± 0.2

Table H2. T_M values for highly stabilizing TFO-hybrids prepared in 1× PBS supplemented with 2 mM $MgCl_2$ (pH = 7.4)

	Ligand	**TFO2**	**TFO3**	**TFO6**
T_M (°C)	TFO–≡	ND	ND	ND
ΔT_M (°C)	A	19.9 ± 0.2	ND	ND
	B	23.1 ± 0.5	ND	22.6 ± 1.2
	C	23.2 ± 0.5	22.2 ± 0.1	ND
	D	ND	ND	ND
	E	ND	ND	ND
	F	23.7 ± 0.3	ND	ND

Table H3. T_M values for unclicked TFO3, TFO6 and TFO7 in the presence of free Cu^{2+}, Cu-Phen, Cu-DPQ, Cu-DPPZ to investigate free ancillary ligand stabilisation (pH = 6.0)

		TFO3–≡	**TFO6**–≡	**TFO7**–≡
T_M (°C)	TFO–≡	45.1 ± 0.0	44.2 ± 0.2	48.4 ± 0.4
ΔT_M (°C)	+ Cu^{2+}	-0.2 ± 0.2	0.7 ± 0.2	2.7 ± 0.2
	+ Cu-Phen	2.5 ± 0.0	1.0 ± 0.2	6.5 ± 0.7
	+ Cu-DPQ	2.3 ± 0.1	-0.2 ± 0.5	7.3 ± 0.7
	+ Cu-DPPZ	3.4 ± 0.3	1.7 ± 0.3	6.9 ± 0.6

Table H4. ΔT_M values for unclicked TFO3, TFO6, TFO7 in the presence of free Cu^{2+}, Cu-Phen, Cu-DPQ, Cu-DPPZ to investigate free ancillary ligand stabilisation for the duplex moiety compared to the thermal stabilisation of the target D3 prompted by the interaction with $\mathbf{G_R}$ and relative copper complexes (pH = 6.0).

	Ligand	TFO3–≡	TFO6–≡	TFO7–≡	D3
ΔT_M (°C)	G_R	-	-	-	2.4 ± 0.1
	+ Cu^{2+}	2.6 ± 0.1	2.4 ± 0.3	2.7 ± 0.1	3.2 ± 0.3
	+ Cu-Phen	2.8 ± 0.0	2.3 ± 0.3	3.0 ± 0.0	2.7 ± 0.0
	+ Cu-DPQ	3.3 ± 0.3	2.3 ± 0.3	2.5 ± 0.3	2.4 ± 0.0
	+ Cu-DPPZ	2.7 ± 0.1	2.2 ± 0.2	3.0 ± 0.3	3.8 ± 0.3

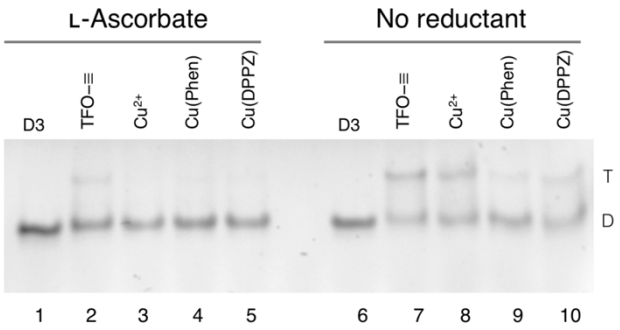

Figure H1. Investigation of unclicked hybrid components in the presence or absence of reductant. Duplex D3 (1.25 pmol) was treated with unclicked TFO3 (TFO–≡, 12.5 pmol, lane 2 and 7) in the presence of Cu^{2+} (12.5 pmol, lane 3 and 8), Cu-Phen (12.5 pmol, lane 4 and 9) or Cu-DPPZ (12.5 pmol, lane 5 and 10) with (lane 1–5) or without (lane 6–10) Na-L-ascorbate (1.25 nmol). Reactions were carried out in 10 mM phosphate buffer, 150 mM NaCl, 2 mM $MgCl_2$ (pH 6.0) in a total volume of 5.5 µL and incubated at 37 °C for 24 h. Samples were loaded onto 22% PAGE and subjected to electrophoresis for 14 h at 50 V in 50 mM tris-acetate running buffer (pH 6.0).

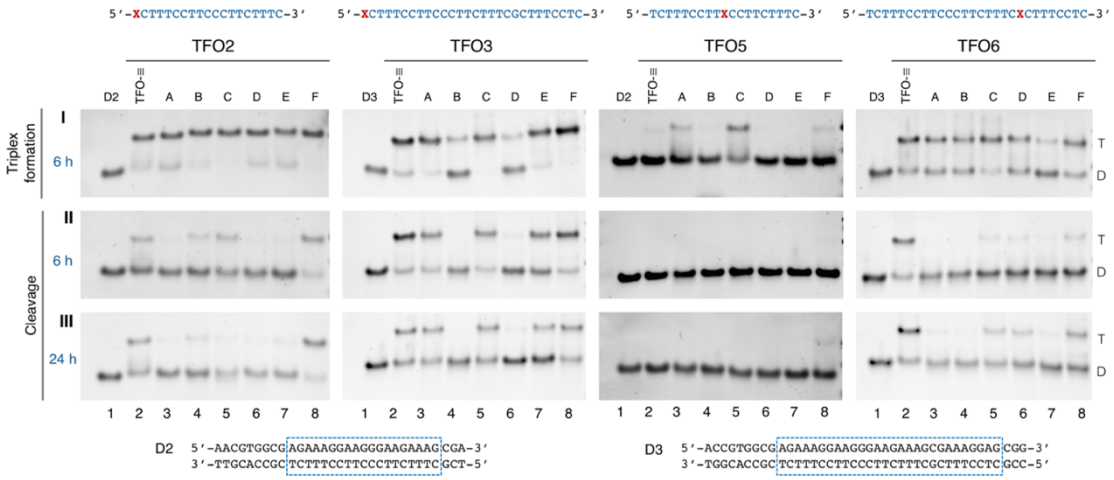

Figure H2. Triplex formation and cleavage reactions of TFO-hybrids. Target duplex (1.25 pmol, lane 1) was treated with 12.5 pmol of unclicked TFO (TFO–≡, lane 2) or TFO hybrids (A-F, lane 3-8) for **I** Triplex formation or cleavage reactions with the addition of Na-L-ascorbate (1.25 nmol) and Cu^{2+} (12.5 pmol) incubated for **II** 6 h or **III** 24 h. All samples were prepared in 10 mM phosphate buffer with 150 mM NaCl and 2 mM $MgCl_2$ (pH 6.0) in a total volume of 5.5 µL. Reactions were incubated at 37°C for either 6 or 24 h, loaded onto 22% PAGE gel and subjected to electrophoresis for 14 h at 50 V in 50 mM tris-acetate running buffer (pH 6.0).

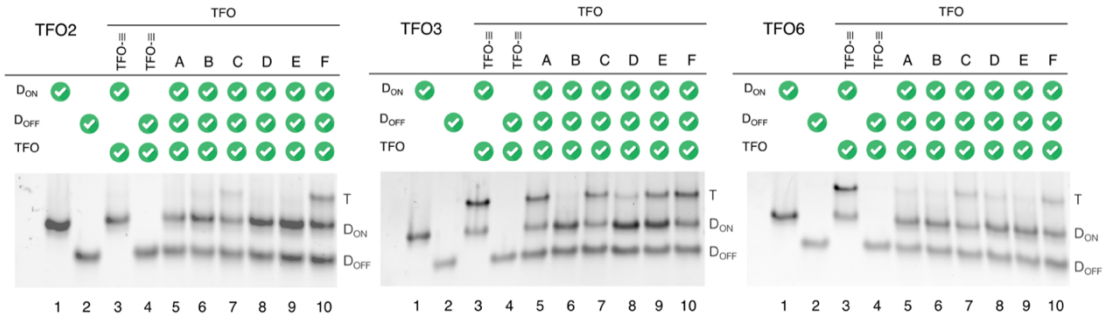

Figure H3. On/off-triplex formation with all TFO-hybrids for TFO2, TFO3 and TFO6. $D_{ON/OFF}$ (1.25 pmol, lane 1 and 2) was treated with 10 equivalents (12.5 pmol) of unclicked TFO (TFO−≡, lane 3−4) or TFO-hybrids (A−F, lane 5−10) in the presence of Cu^{2+} (12.5 pmol) and Na-ι-ascorbate (1.25 nmol). All reactions were carried out in 10 mM phosphate buffer, 150 mM NaCl, 2 mM $MgCl_2$ (pH 6.0) in a total volume of 5.5 µL and incubated for 24 h at 37 °C. Samples were loaded onto 22% PAGE and subjected to electrophoresis for 14 h at 50 V in 50 mM tris-acetate running buffer (pH 6.0).

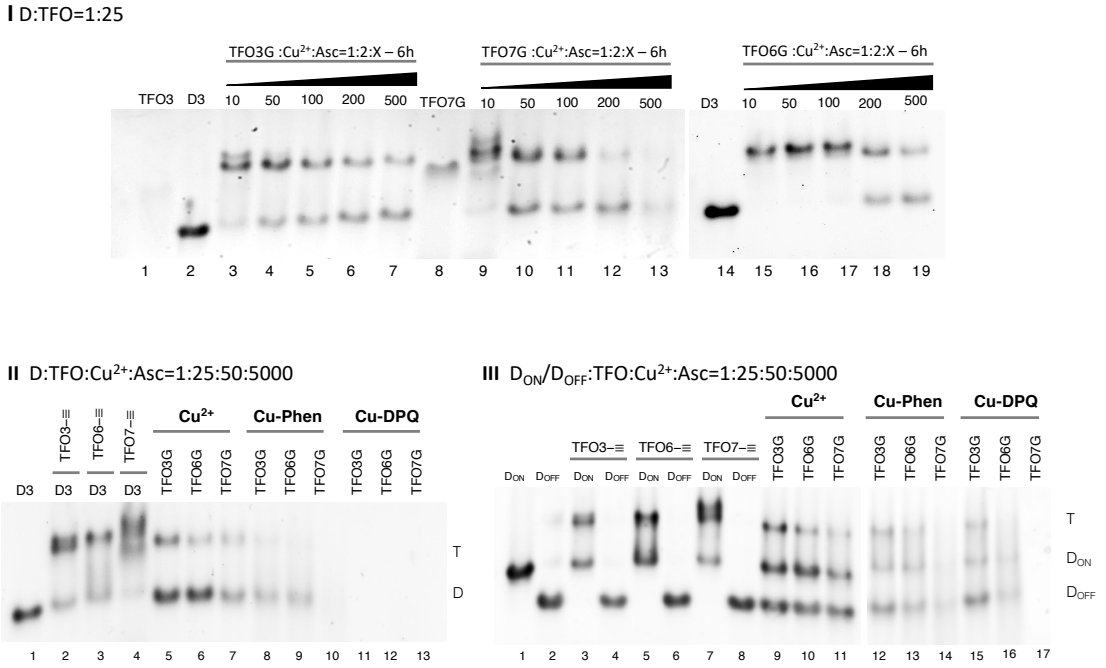

Figure H4. I Optimisation of cleavage conditions with varying amounts of ascorbate reductant at the ratio D:TFO:Cu^{2+}=1:25:50. Target duplex (1.25 pmol, lane 1) was treated with di-nuclear hybrids (31.25 pmol; TFO 3G, lane 2-7; TFO7G, lane 8-13; TFO6G, lane 14-19), Cu^{2+} (62.5 pmol) and increasing amounts of ascorbate with TFO:Cu:Asc = 1:1:X where X = 10-500 equivalents (0.313 nmol, lane 3-9-15; 1.563 nmol, lane 4-10-16; 3.13 nmol, lane 5-11-17; 6.25 nmol, lane 6-12-18; 15.63 nmol, lane 7-13-19). **II** Enhanced cleavage experiment was conducted with the ratio D:TFO:Asc=1:25:5000 with pre-treatment of the hybrids with Cu^{2+} and ancillary ligands (CuPhen, CuDPQ and CuDPPZ) with the ratio TFO:Cu(A.L.)=1:2. **III** Off-targeting experimental design with analogue method where Cu-coordinated TFO-hybrid is co-treated with recognition sequences (on-target, D_{ON}) and an indiscriminate sequence (off-target, D_{OFF}). The cleavage experiments were conducted at 37°C with the incubation time of 6 hours in 10 mM Phosphate buffer 150 mM NaCl 2 mM$MgCl_2$ in a total volume of 5.5 µL. Samples were loaded onto 22% PAGE and subjected to electrophoresis for 14 h at 50 V in 50 mM tris-acetate running buffer (pH 6.0).

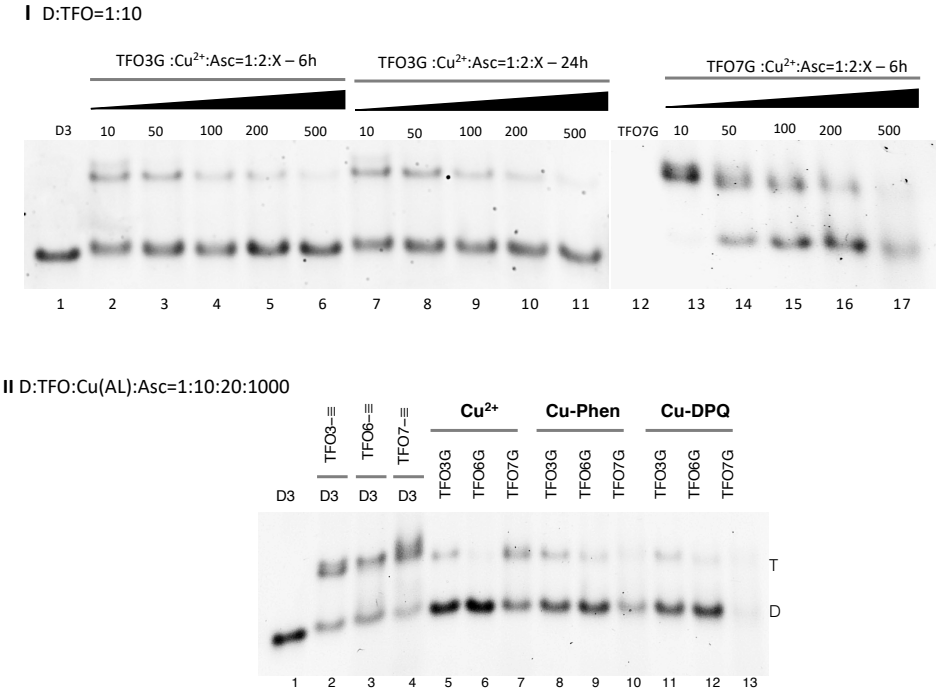

Figure H5. I Optimisation of cleavage conditions with varying amounts of ascorbate reductant at the ratio D:TFO:Cu^{2+}=1:10:20 with the incubation of 6 and 24 hours. Target duplex (1.25 pmol, lane 1) was treated with di-nuclear hybrids (12.5 pmol; TFO 3G, lane 2-11; TFO7G, lane 12-17), Cu^{2+} (25 pmol) and increasing amounts of ascorbate with TFO:Cu:Asc = 1:1:X where X = 10-500 equivalents (0.125 nmol, lane 3-7-13; 0.625 nmol, lane 4-8-14; 1.25 nmol, lane 5-9-15; 2.50 nmol, lane 6-10-16; 6.25 nmol, lane 6-11-17). **II** Enhanced cleavage experiment was conducted with the ratio D:TFO:Asc=1:10:1000 with pre-treatment of the hybrids with Cu^{2+} and ancillary ligands (CuPhen, CuDPQ and CuDPPZ) with the ratio TFO:Cu(A.L.)=1:2. The cleavage experiments were conducted at 37°C with the incubation time of 6-24 hours in 10 mM phosphate buffer 150 mM NaCl 2 mMMgCl_2 in a total volume of 5.5 µL. Samples were loaded onto 22% PAGE and subjected to electrophoresis for 14 h at 50 V in 50 mM tris-acetate running buffer (pH 6.0).

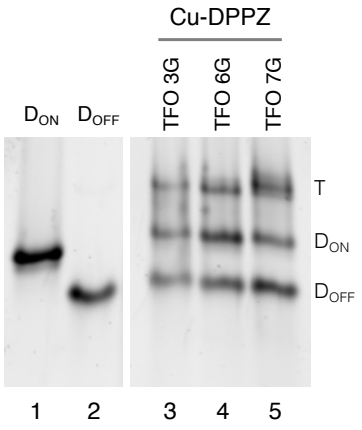

Figure H1. On/off-triplex formation with all TFO3G, TFO6G and TFO7G. $D_{ON/OFF}$ (1.25 pmol, lane 1 and 2) was treated with 25 equivalents (31.25 pmol) TFOG-hybrids, lane 3−5) in the presence of Cu^{2+} (62.5 pmol) and Na-ι-ascorbate (62.5 nmol). All reactions were carried out in 10 mM phosphate buffer, 150 mM NaCl, 2 mM $MgCl_2$ (pH 6.0) in a total volume of 5.5 µL and incubated for 24 h at 37 °C. Samples were loaded onto 22% PAGE and subjected to electrophoresis for 14 h at 50 V in 50 mM tris-acetate running buffer (pH 6.0).

APPENDIX I

Emission spectra of azide-modified Ru(II) complexes

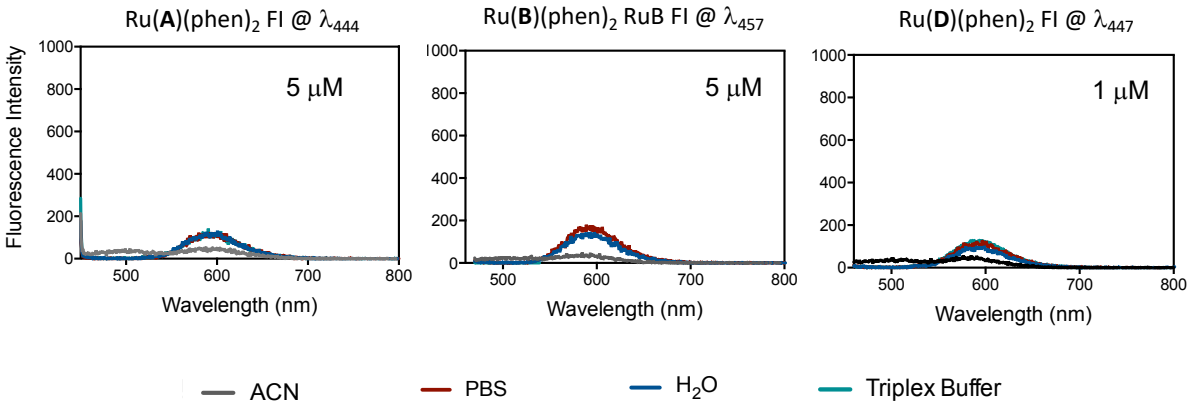

Figure I1. Fluorescent analysis of [Ru(phen)$_2$(**A**)](PF$_6$)$_2$, [Ru(phen)$_2$(**B**)](PF$_6$)$_2$5 μM and [Ru(phen)$_2$(**D**)](PF$_6$)$_2$ in ACN, H$_2$O, PBS and 10 mM Phosphate 150 mM NaCl and 2 mM MgCl$_2$ buffer (pH=6).

APPENDIX L

Emission spectra of $\mathbf{G_R}$, $[Cu_2(\mathbf{G_R})(N,N\text{-phenanthrene})_2](NO_3)_4$

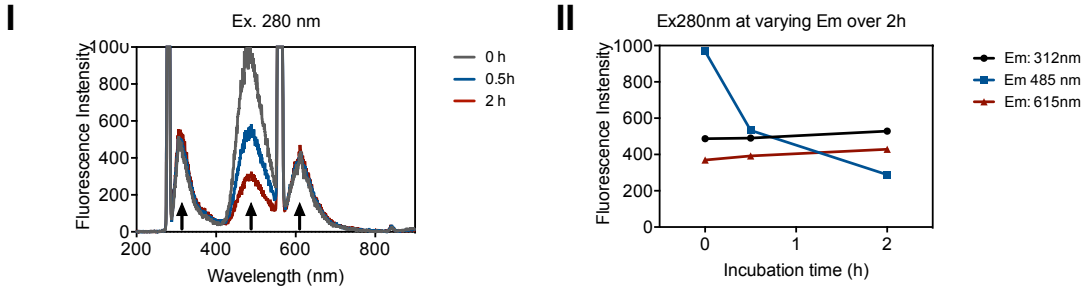

Figure L1. I Emission scans when excited at 280 nm for t = 0, 0.5 and 2 h. **II** Fluorescent intensity of the signals at 312, 485 and 615 nm at the excitation of 280 nm over 2 hours.

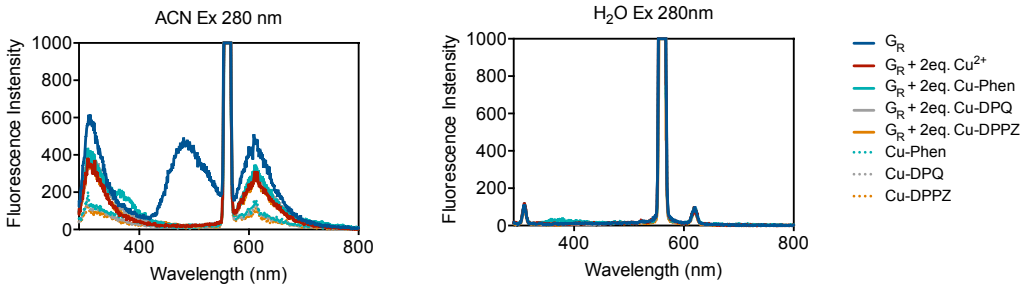

Figure L2. Comparison of the fluorescent properties of **G_R** in ACN and H_2O (1 μM) when excited at 280 nm and *in situ* complexation of 2 eq Cu(II), CuPhen, Cu-DPQ and Cu-DPPZ (scans are compared to free Cu-Phen, Cu-DPQ and Cu-DPPZ at 2 μM in ACN).